

Alma Mater Studiorum – Università di Bologna

DOTTORATO DI RICERCA IN

Chimica

Ciclo XXXII

Settore Concorsuale: 03/C1

Settore Scientifico Disciplinare: CHIM/06

Coumarins: their versatile use in photoredox catalysis and biological applications.

Presentata da: Giacomo Rodeghiero

Coordinatore Dottorato

Domenica Tonelli

Supervisore

Prof. Pier Giorgio Cozzi

Supervisore

Dott. Paul Jansen

Esame finale anno 2020

Abstract

Coumarin dyes have proven to possess unique photophysical properties thanks to the high quantum yield, and stability and an absorption and emission which cover the most part of the visible spectrum. In particular, a peculiar characteristic of this class of fluorophores is the large Stokes shift.

Thanks to these exceptional photophysical properties, coumarin dyes are widespread used in different applications including fluorescent bio-label, emitting materials in OLED and dyes in solar cells as example.

To the best of our knowledge their systematic use in photoredox catalysis has not been explored yet.

This research aimed at the design, the synthesis, the photophysical characterization of new LSS coumarin dyes and their use in different fields such as photoredox catalysis, photopolymerization and biological applications (bioconjugation and fluorescent microscopy).

The application of 3-thienyl- and 3-phenyl 7-amino coumarin derivatives as powerful photoreductants in photoredox pinacol coupling reaction of several aromatic and aliphatic aldehydes, ketones and imine was reported. The use of coumarin as photocatalyst was also extended to various organic transformations. In fact, 3-thienyl coumarin were successfully applied in ATRA reaction enantioselective α -alkylations of the tetrahydro-cinnamaldehyde, the reductive dehalogenation of bromoacetophenone and, finally the generation of trifluoromethyl radical generation for the oxytrifluoromethylation of stilbene (Figure 1).

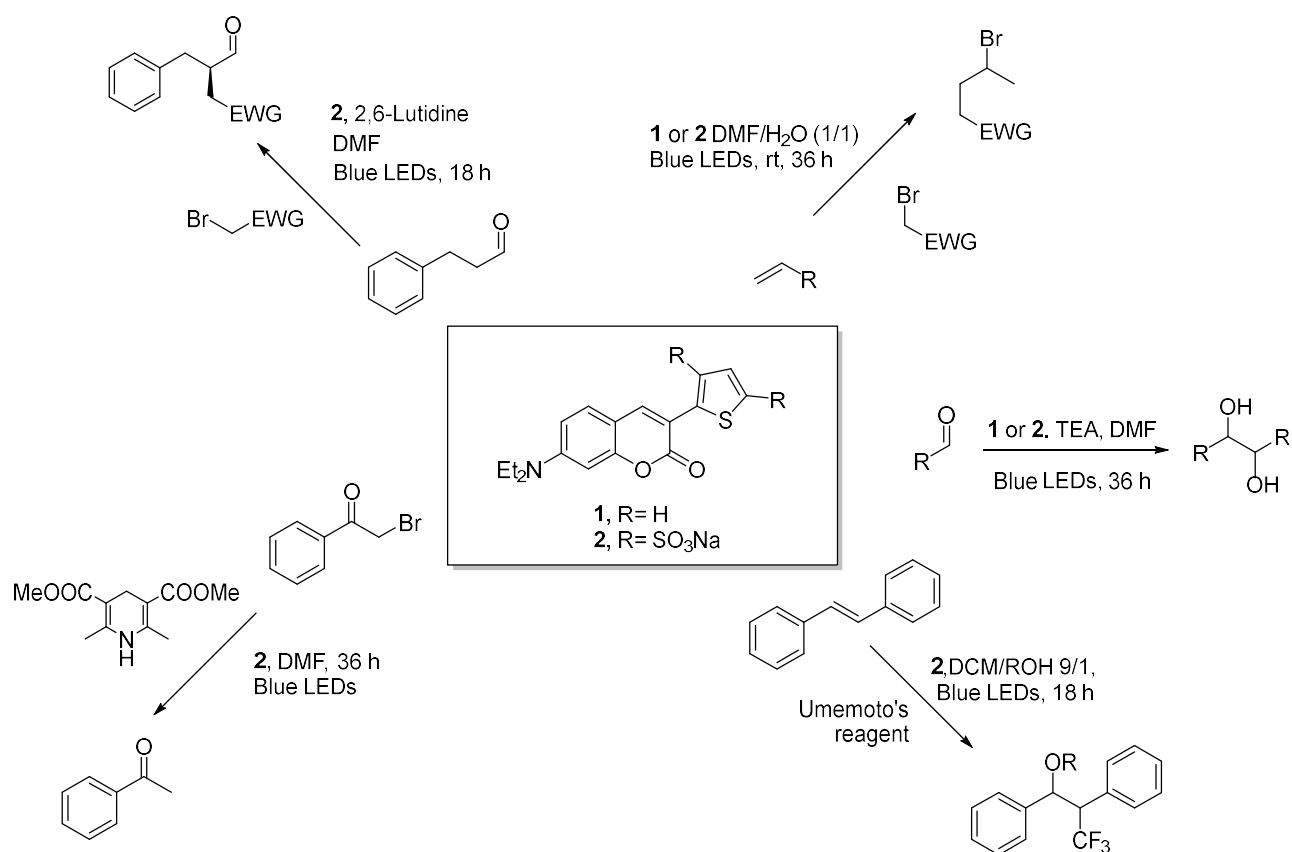


Figure 1 Use of 3-thienyl coumarin derivatives as photocatalysts of several organic reactions

As the merging of photoredox catalysis and metal catalysis is an important subject, a new method for the allylation of several aromatic and aliphatic aldehydes by a combination of of Ni(II) complex and $[\text{Ir}(\text{ppy})_2(\text{dtbbpy})](\text{PF}_6)$ or $[\text{Ru}(\text{bpy})_3]^{2+}$, in the presence of inexpensive reagents (Figure 2).

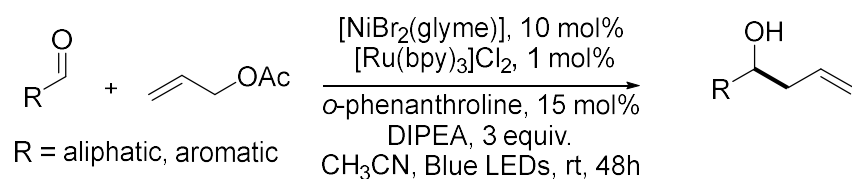


Figure 3 Allylation of aldehydes by dual nickel and photoredox catalysis

The reaction provided a broad scope obtaining the corresponding homoallylic alcohol in yields from good to excellent in the case of aromatic aldehydes. Limitations have been observed in presence of electron-withdrawing substituents such as esters, amides and nitrile in para-position. The use aliphatic aldehydes gave yields from fair to good.

In collaboration with Prof. J. Lalav e and co-workers of the Institut de Science des Mat riaux de Mulhouse, the employment as organic photocatalysts of 3-thienyl coumarin derivatives in photo polymerization was described. The applications included both the cationic polymerization of

epoxides and the free radical polymerization of (meth)acrylates, new photosensitive 3D printing and the preparation of hydrogels.

Finally, the development of a new LSS coumarin dyes for biological application was carried out. A library of several LSS dyes with photophysical properties including large Stokes shift, high quantum yield and molar extinction coefficient as well as excitability by the common available lasers was developed. Furthermore, the synthesis of different 3-thienyl coumarin derivatives for the labelling of lysosomes and mitochondria in fluorescent microscopy was reported.

List of Publications

Some of the results presented in this thesis have been published:

- Gualandi A. , Rodeghiero G., Della Rocca E. , Bertoni F. , Marchini M. , Perciaccante R. , Jansen T. P. , Ceroni P. , Cozzi P. G., “Application of coumarin dyes for organic photoredox catalysis”, *Chem Commun*, 2018, **54**, 10044.
- Gualandi A. , Rodeghiero G., Faraone A. , Patuzzo F. , Marchini M. , Calogero F. , Perciaccante R. , Jansen T. P. , Ceroni P. , Cozzi P. G.; “Allylation of aldehydes by dual photoredox and nickel catalysis”, *Chem. Commun.*, 2019, **55**, 6838 .
- Abdallah M., Hijazi A., Graff B., Fouassier, J. P., Rodeghiero G., Gualandi A., Dumur, F., Cozzi, P. G., Lalevée, J., “Coumarin derivatives as high performance visible light photoinitiators/photoredox catalysts for photosensitive resins for 3D printing technology, photopolymerization in water and photocomposites synthesis”, *Polymer Chemistry*, 2019, **10**, 872.

Table of contents

Chapter 1: General introduction	11
1.1 Introduction	11
1.1.2 Principles of photoredox catalysis	11
1.1.3 Single electron transfer (SET)	13
1.1.4 Photoredox catalysis in organic synthesis	17
1.1.5 Use of organic dyes in photoredox catalysis	22
1.1.6 Coumarin derivatives as fluorescent dyes	28
1.1.7 Large Stokes shift (LSS) in coumarin dyes	29
1.1.8 Use of coumarin dyes in SET	31
1.1.9 Outline of the thesis	31
Chapter 2: Photoredox pinacol coupling mediated by coumarins	35
2.1 Introduction	35
2.1.1 Traditional methods for the synthesis of diols	35
2.1.2 Pinacol coupling reactions by visible light photoredox catalysis	36
2.1.3 Use of coumarin dyes as photocatalysts	40
2.2 Results and discussion	42
2.2.1 Initial investigations	42
2.2.2 Synthesis of coumarin dyes 3, 4 and 5 and photophysical properties	43
2.2.3 Reaction optimization	45
2.2.4 Substrates scope	46
2.2.5 Pinacol cross coupling towards unsymmetrical diols	48
2.2.6 Pinacol coupling of ketone and imines	50
2.2.7 Mechanistic investigations	52
2.3 Conclusions	55
2.4 Experimental procedures	55
Chapter 3: Photoredox alkyl radicals generation mediated by coumarins	63
3.1 Introduction	63
3.1.1 Alkyl radicals generation by photoredox catalysis	65
3.1.2 Generation of alkyl radicals for other applications	65
3.1.3 Use of coumarin dyes as photocatalysts of several organic reactions	66
3.2 Results and discussion	67
3.2.1 Coumarin dyes for photoredox catalysis of ATRA reactions	67

3.2.2 Reaction Optimization	68
3.2.3 Substrates scope.....	69
3.2.4 Proposed mechanism	72
3.2.5 α -alkylations of cinnamaldehyde by photoredox catalysis	72
3.2.6 Photoredox catalysis of reductive dehalogenations mediated by coumarins	74
3.2.7 Photoredox oxy-trifluoromethylation mediated by coumarin.....	75
3.3 Conclusions	76
3.4 Experimental procedures	77
Chapter 4: Development of new efficient coumarin for photoredox catalysis	82
4.1 Introduction	82
4.1.1 Development of new efficient core dyes for photoredox catalysis	82
4.2 Results and discussion	85
4.2.1 Development of new dyes by computational calculations	85
4.2.2 Synthesis of coumarin 12, 14, 18 and 19.....	87
4.2.3 Use of coumarin 12, 14, 18 and 19 in photoredox pinacol coupling reactions.....	91
4.2.4 Enantioselective version of photoredox pinacol coupling using chiral acids	95
4.2.5 Development of new photocatalysts by rational design.....	96
4.2.6 Synthesis of compounds 10-12	97
4.3 Conclusions	102
4.4 Experimental procedures	103
Chapter 5: Allylation of aldehydes by dual photoredox and nickel catalysis	112
5.1 Introduction	112
5.1.1 Nozaki-Hiyama-Kishi reaction	112
5.1.2 Metallaphotoredox catalysis	113
5.1.3 Metallaphotoredox catalysis for the allylation of aldehyde	115
5.1.4 Allylation of aldehydes by dual photoredox and nickel catalysis.....	117
5.2 Results and discussion	117
5.2.1 Initial investigations.....	117
5.2.2 Reaction optimization	118
5.2.3 Substrates scope.....	120
5.2.4 Use of different alkylating agents	123
5.2.5 Photoredox allylation of ketones	125
5.2.6 Mechanistic investigations	126
5.3 Conclusions	130
5.4 Experimental procedures	131

Chapter 6: Use of coumarins in photoredox polymerization processes.....	148
6.1 Introduction.....	148
6.1.1 Photocatalysis in polymerization processes.....	148
6.1.2 Organophotocatalysis based systems	150
6.1.3 Use of coumarin as photoinitiators	151
6.2 Results and discussion	152
6.2.1 Light absorption properties of the investigated compounds.....	152
6.2.2 Cationic photopolymerization (CP) of epoxides.....	153
6.2.3 Free radical photopolymerization of acrylates (TMPTA).....	155
6.2.4 Free radical photopolymerization of methacrylates (BisGMA/TEGDMA).....	158
6.2.5 3D printing experiments using coumarin/Iod & coumarin/Iod/NPG systems	160
6.2.6 Photopolymerization in water for hydrogel synthesis using 2/MDEA	161
6.2.7 Near-UV conveyor experiments for access to photocomposites.....	162
6.2.8 Chemical mechanism.....	163
6.2.9 Coumarin derivatives as Photoredox Catalysts in Three-Component System.....	166
6.3 Conclusions	167
6.4 Experimental procedures	167
Chapter 7: Use of coumarins in biological applications	172
7.1 Introduction.....	172
7.1.1 Development of new LSS dyes for biological applications.....	172
7.2 Results and discussion	176
7.2.1 Development of a library of LSS coumarins	176
7.2.2 Extension of the π -system in the C3 position	177
7.2.3 Insertion of a heteroatom in position C6.....	179
7.2.4 Synthesis of 7-methoxy coumarins	182
7.2.5 Synthesis of LSS dyes for fluorescent microscopy	185
7.2.6 Cell staining of lysosomes and mitochondria	186
7.3 Conclusions	190
7.4 Experimental procedures	190
Summary	195

List of abbreviations

4CzIPN dicyanobenzene	Fc ferrocene
AIBN azobisisobutyronitrile	FL fluorescein
AMCA 7-amino 4-methylcoumarin acetate	FRP free radical polymerization
ATPR atom transfer radical polymerization	HAT hydrogen atom transfer
ATRA Atom Transfer Radical Reaction	HEA 2-(hydroxyethyl) acrylate
ATRP atom transfer radical reaction	HEMA 2- (Hydroxyethyl) methacrylate
BIH 1,3-dimethyl-2-phenyl-2,3-dihydro-1H-benzo[d]imidazole	HIV human immunodeficiency viruses
BINOL 1,1'-Bi-2-naphthol	HOMO highest occupied molecular orbital
BisGMA bisphenol α -glycidyl methacrylate	IC internal conversion
BNAH nicotinamide	ICT internal charge transfer
BODIPY boron-dipyrromethene	IP ionization potential
BOX bisoxazoline	ISC inter system crossing
CFL compact fluorescent lamp	JAK2 janus kinase
CP cationic polymerization	K_{SV} Stern-Volmer constant
DBMM 2-bromo-2-methylmalonate	LBM leuco methylene blue
DCA 9,10-dicyanoanthracene	LDI laser direct imaging
DCC N^N - dicyclohexylcarbodiimide	LEDs light emitting diodes
DCE dichloroethane	LiHMDS Lithium bis(trimethylsilyl)amide
DCM dichloromethane	LSS large Stokes shift
DFT density functional theory	LUMO lowest unoccupied molecular orbital
DH Hydrogen Donor	MB ⁺ methylene blue
DMAP 4-dimethylaminopyridine	MDEA <i>N</i> -Methyldiethanolamine
DMF dimethylformamide	MeCN acetonitrile
DMSO dimethylsulfoxide	MLTC metal-to-ligand-charge-transfer
DSSC dye sensitized solar cells	N.A. not available
EA electron affinity	NLO nonlinear optics organic
EBP α -ethylbromoacetate	NMR nuclear magnetic resonance
EDA electron donor acceptor complex	NMR nuclear magnetic resonance
EPOX (3,4-Epoxy cyclohexane)methyl 3,4-epoxycyclohexylcarboxylate	NPG <i>N</i> -Phenylglycine
ESI-MS electrospray ionization – mass spectrometry	OFETs organic field effect transistors
ESIPT intramolecular proton transfer	OLED organic light emitting diode
ET electron transfer	OPC organic photocatalyst
EY eosin Y	OSLs solid state lasers
	PBN phenyl- <i>N</i> - <i>tert</i> -butylnitron

PC photocatalyst
PHT phenothiazine
PI photoinitiator
PIS photoinitiating system
PMB *p*-methoxy benzyl
PPP poly(*p*-phenylene)
Q quencher
RB rose bengal
SCE saturated calomel electrode
SET single electron transfer
TBAP tetrabutylammonium hydrogen phosphate
TD-DFT time dependent density functional theory
TEA triethylamine
TEAPF₆ tetraethylammonium hexafluorophosphate
TEGDMA bisphenol α -glycidyl methacrylate
TGA thermo gravimetric analysis
THF tetrahydrofuran
TICT twisted intramolecular charge transfer
TMS trimethylsilane
TMSCl trimethylsilyl chloride
TMTPA trimethylolpropane triacrylate
Tr-Ad truxene-acrinedione
UV ultra-violet

General introduction

1.1 Introduction

1.1.1 Photoredox catalysis

In the recent years, the development of more efficient and sustainable processes in chemistry has become a hot topic of research in industrial field as well as in academia.

Over the last four decades, photoredox catalysis has undergone a significant renaissance thanks to its facility to generate active radical species under controlled and mild conditions. This sustainable approach has found widespread application in the fields of water splitting,¹ carbon dioxide reduction,² solar cell materials³ and more recently in the catalysis of organic reactions.⁴ The rapid growth of photoredox catalysis may be also attributed to the technological progress and broad commercial availability of light-emitting diodes as energy efficient sources for the photocatalysts. Furthermore, the use of transparent flow reactors helped to overcome challenges in the upscaling and reproducibility of photochemical reactions, an important aspect for any larger-scale industrial application.

1.1.2 Principle of the photoredox catalysis

Photoredox catalysis is based on a visible light-absorbing catalyst (photocatalyst) which, upon excitation by a light source, evolves in a variety of processes. The pathway associated to the light absorption of a photocatalyst are illustrated by the Jablonsky diagram that reports the electronic states of a molecule and the transitions between them (Figure 1).⁵

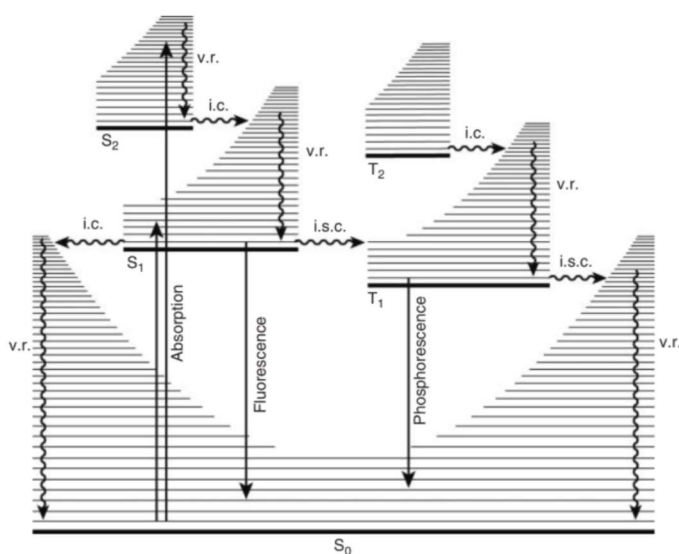


Figure 1 Jablonsky diagram.

The absorption is the promotion of an electron from a ground state singlet (S_0) to vibrational state of the singlet excited states (S_1, S_2) (line pointing up). The capacity of a molecule to absorb light at certain wavelength is measured by the molar extinction coefficient (ϵ). This value is calculated by the Lambert-Beer law where A is the absorbance, c is the concentration, expressed in $M\ dm^{-1}$ and l is the pathlength in cm (Equation 1).

$$1) \epsilon = \frac{A}{c l}$$

After the light absorption, the photocatalyst undergoes to vibrational relaxation, a very fast process (between 10^{-14} and 10^{-11} seconds) to the lowest vibrational level of S_1 . Afterwards, the molecule decay through three possible pathways, to S_0 .

A radiative pathway is the *fluorescence*, a slow (between 10^{-9} and 10^{-7} seconds) transition from S_1 to S_0 ($S_1 \rightarrow S_0$) characterized by the emission of a photon. The internal conversion (IC), instead, is a non-radiative vibrational relaxation between two electronic states of the same multiplicity ($S_1 \rightarrow S_0$). An alternative pathway is the non-radiative transition from S_1 to a triplet state T_1 ($S_1 \rightarrow T_1$) through a spin forbidden process called Inter System Crossing (ISC). The following decaying $T_1 \rightarrow S_0$ is also spin forbidden and it takes place through slow radiative (phosphorescence) or non-radiative deactivations. All these processes are regulated by kinetic constants k_w which influence the quantum yield and the lifetime of the excited state.

The quantum yield (ϕ_i)⁶ is expressed by the ratio between the kinetic constant of the process i and the sum j of the kinetic constants of every event (Equation 2). The lifetime τ_{A^*} is the time elapsed between the activation of the photocatalyst and its emission of a photon. The usual τ_{A^*} for a photocatalyst is from the nanosecond to the millisecond (Equation 3).

$$2) \phi_i = \frac{k_i}{\sum_j k_j} \quad 3) \tau_A = \frac{1}{\sum_j k_j}$$

Different events can occur when the photocatalyst in the excited state (PC^*) encounters a second species B (Figure 2).

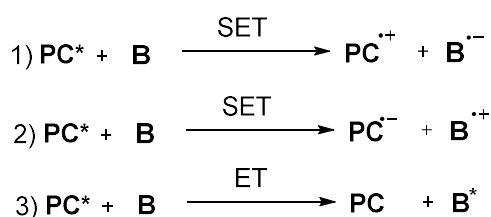


Figure 2 Processes between PC^* and B.

In this case, PC^* can accept or donate an electron to the other species, behaving respectively as an oxidizing or reducing agent. This process is called single electron transfer (SET) or photo-induced electron transfer (PET). In alternative, PC^* can do energy transfer (ET) to B promoting its excitation in the state B^* .

In general, SET and ET processes are influenced by several parameters of the photocatalyst including the wavelengths of absorption (λ_{max}) and emission (λ_{em}), the lifetime of fluorescent (τ_f), the quantum yield and the excited state energy of S_1 ($E^{S1_{0,0}}$) and T_1 ($E^{T1_{0,0}}$).

1.1.3 Single Electron Transfer (SET)

SET events are on the basis of the photoredox catalysis and they occurs by the interaction of the species B with the electronic states of the PC^* . Single electron transfer relies on the property of the photocatalysts to be both more easily reduced as well as more easily oxidized in their excited states than their corresponding ground states, a assertion that can be easily recognized by considering the ionization potential (IP) and the electron affinity (EA) of the excited and ground states (Figure 3).

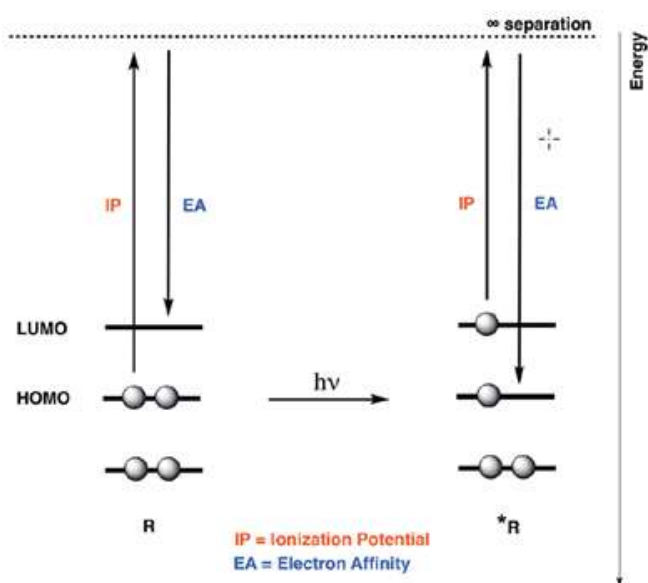


Figure 3 Ionization potential and electron affinity.

The term IP (ionization potential) is the energy necessary to remove an electron from a molecule. This value is inversely proportional to the energy and facility to remove an electron from an orbital. The term EA (electronic affinity) is the energy released by a process in which an electron is added to a vacant orbital present in the molecule.

When we consider the photocatalyst in its excited state, PC^* , in a very simplified view, the transition of an electron from HOMO to LUMO level of the molecule leads to a lower ionization potential and,

equally, a higher electron affinity than respect to its ground state. Therefore, the oxidation process and reduction of the photocatalyst in the excited state will be favoured. The process in which the specie B is able to receive or donate electrons by ET with the photocatalyst is denominated quenching.

The excited state of the photocatalyst must have sufficiently long lifetime leading to encounter the species B before relaxing back to the ground state, in what is called dynamic quenching. It is also possible a static quenching, if in the ground state, the specie B is interacting with the photocatalyst.

The kinetic of the SET events can be rationalized by the Marcus theory,⁷ and will be not discussed in this introduction. The thermodynamic of the ET, in other words if the oxidation or reduction of the PC in its excited state, can be rationalized by what is called Rehm-Weller formalism.⁸ In first approximation, and neglecting the difference in entropy between the ground and the excited state and the contribution of the Coulombic interactions, i.e. the electrical work due to the separation of charges, it is possible to estimate the oxidation and reduction potential of the photocatalyst in its excited state. (Equations 4-5).

$$4) E(\text{PC}^*/\text{PC}^-) = E(\text{PC}/\text{PC}^-) + E_{0,0}(\text{PC}^*/\text{PC})$$

$$5) E(\text{PC}^+/\text{PC}^*) = E(\text{PC}^+/\text{PC}) - E_{0,0}(\text{PC}^*/\text{PC})$$

$E(\text{PC}^*/\text{PC}^-)$ and $E(\text{PC}^+/\text{PC}^*)$ are the reduction and the oxidation state potential of the photocatalyst, respectively. $E(\text{PC}/\text{PC}^-)$ represents the ground state reduction potential and it is commonly shortened to $E_{1/2}(\text{PC}/\text{PC}^{\bullet-})$ and the half reaction is $\text{PC} \rightarrow \text{PC}^{\bullet-}$. This value is negative (<0 V) for the most ground state species since the reduction is thermodynamically unfavourable. $E(\text{PC}^+/\text{PC})$ is referred to the oxidation potential and it can be written as $E_{1/2}(\text{PC}^{\bullet+}/\text{PC})$ describing the reduction half reaction $\text{PC}^{\bullet+} \rightarrow \text{PC}$. In this case, $E_{1/2}(\text{PC}^+/\text{PC})$ is positive value because the reduction of PC species is energetically favourable. $E_{0,0}$ is the

energy gap between the ground state and the excited state, or energetic content after the excitation process. $E_{0,0}$ can be assigned spectroscopically, and is in general approximate with the energy corresponding the wavelength at the tail of the absorption spectra of the PC, although can be also estimate at the crossing point of the absorption and emission profile of the PC (if the PC is emitting). $E_{0,0}$ is measured in eV.

During a SET process, the excited state of the photocatalyst PC^* is quenched by a substrate B following two possible interactions (Figure 4).

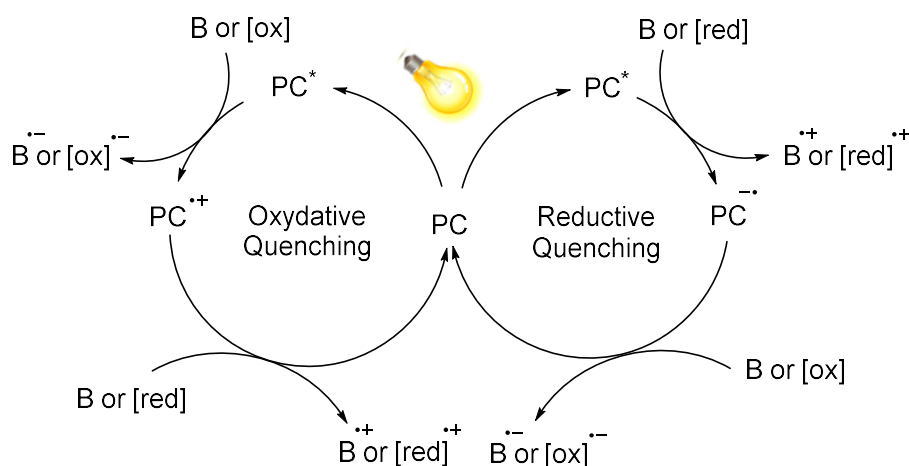


Figure 4 Oxidative and reductive quenching.

In the *oxidative quenching*, the excited state PC* gives an electron to the specie B or to an oxidant [ox] present in the reaction mixture generating the specie radical cation PC^{•+} and the reduced species B^{•-} or [ox]^{•-}. Instead, in what is called *reductive quenching*, PC* is reduced by B or a reducing species [red] to provide the corresponding radical anion PC^{•-} with the subsequent formation of B^{•+} and [red]^{•+}. In both the processes, the photocatalyst needs to be restored in its ground state, and this is important for catalytic processes. In the oxidative quenching, the restore of the photocatalyst PC involves the reduction of PC^{•+}, while in the reductive quenching, the re-generation of the PC in its ground state involves the oxidation of PC^{•-} by a substrate (B or a different substrate) or by a sacrificial compound. There are other possible interactions between excited states and molecules in solution, that do not involve the transfer of electrons. The process of energy transfer is the physical energy transfer from the photoexcited states to acceptors, and there are different processes that were designed in photocatalysis that are effectively promoted by these pathways.⁹ Excited-state energy in PC can be transferred directly to molecules without changing their oxidation or reduction states. The processes are called productive sensitization. For example, the triplet energy transfer from an electronically excited photosensitizer (Ru(bpy)₃(PF₆)₂), is 46 kcal/mol, and when this energy is transferred to an acceptor molecule, electrons are promoted to the excited state and the diradical species can undergo interesting reactions.

The effective quenching of the excited state PC* by a species B can be governed by the Stern-Volmer equation, which relates the intensity of emission to the concentration of the quencher. It is important that the PC is able to emit, or more sophisticated experiments and analysis need to be performed. As a second instance, a truly Stern-Volmer analysis is performed by considering in the equation the lifetime of the excited states in the absence and in the presence of the quencher. The use of the intensity of the emission is a useful and practical approximation that is generally possible, but not in all cases. The use of the

Stern-Volmer emission-quenching experiments can shed some light about the interaction of excited-state species with other reaction components. It is also quite important to remark that the experiment cannot discriminate between energy-transfer and electron-transfer manifolds, and normally, other studies about the reaction mechanism, are necessary. Considering the lifetime of the excited state in absence or in the presence of a quencher B, τ_0 and τ , it is possible to verify the following equation (Stern-Volmer) (Equation 6).

$$6) \tau^0/\tau = 1 + K_{SV}[B] = 1 + k_q\tau^0[B]$$

The constants K_{SV} and k_q (Stern-Volmer and quenching constants, respectively) can be calculated by the linear correlation between τ/τ_0 and the concentration of B, obtained by a Stern-Volmer plot (Figure 5).

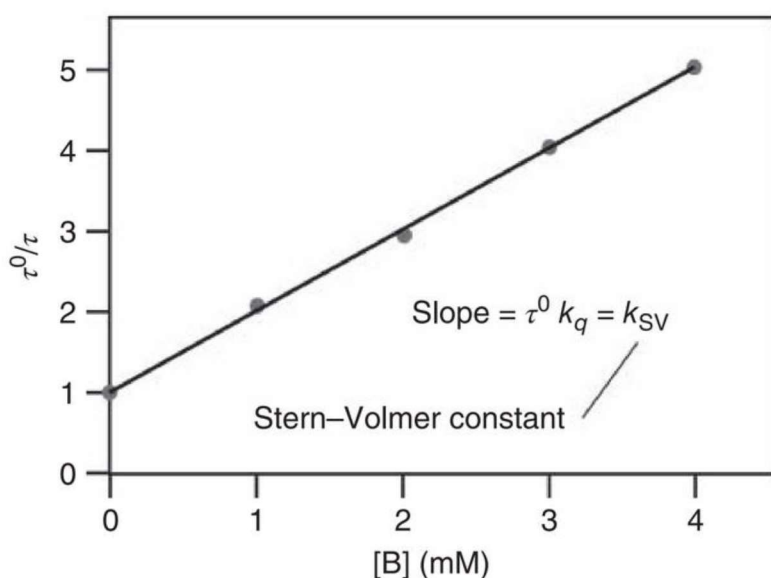


Figure 5 Stern-Volmer plot.

The progress of the Stern-Volmer equation is linear in the case of the dynamic quenching which is due to collisional encounters between the photocatalyst PC and quencher B. Otherwise, a deviation in the linearity, generates a static quenching obtained by the formation of a non-fluorescent complex between PC and B in the reaction mixture.

As photoredox reaction are radical reactions, photoredox reactions can follow other mechanistic schemes as the case of the radical-chain mechanism (Figure 6).

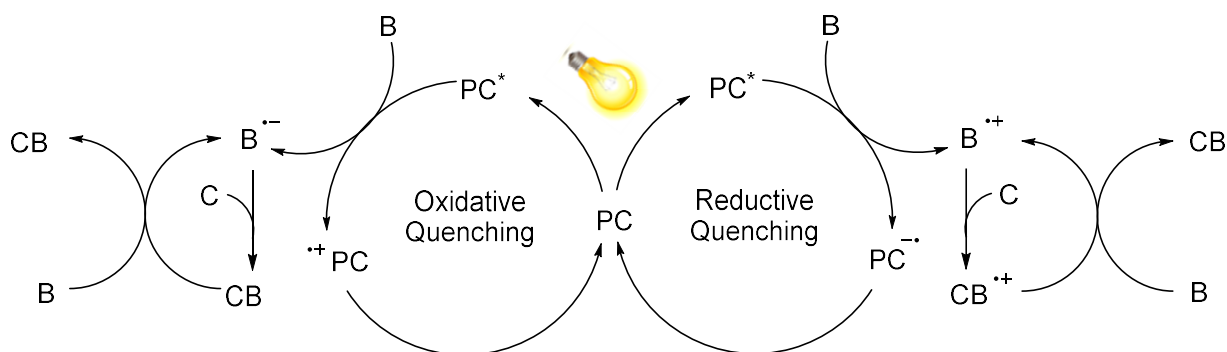


Figure 6 Chain reaction mechanism.

A single electron transfer from the excited state PC^* to the substrate B generates the radical anion $B^{\bullet-}$, in the case of the oxidative quenching, and the radical cation $B^{\bullet+}$ in the reductive quenching. The compounds $B^{\bullet-}$ and $B^{\bullet+}$ interact with a second substrate C giving the radical species $CB^{\bullet-}$ and $CB^{\bullet+}$. The subsequent oxidation of $CB^{\bullet-}$ and reduction $CB^{\bullet+}$ by the substrate B generates the final product CB . In this case, the photocatalyst acts as an initiator triggering the reaction and the process does not require the restore of the photocatalytic cycle.

In the end, the photoredox reactions can be also driven by EDA complexes or exciplexes,¹⁰ without the presence of a photocatalyst. The electron donor-acceptor EDA is a complex formed by the association of two reactants at the ground state through a charge transfer. Normally, a bathochromic shift arose from the formation of a visible-light absorbing electron donor-acceptor (EDA) complex is observed. Irradiation of the coloured EDA complex can induce an SET event, allowing access to radical species that trigger the desired reaction. In the case of exciplexes, the association of two reactants takes place in their excited state. This process leads to catalyst-free photolytic transformations using visible light, enabled by the fact that EDA complexes, as well as exciplexes, cooperatively absorb a photon at a lower energy (longer wavelength) than either reactant.

1.1.4 Photoredox catalysis in organic synthesis

Photoredox catalysis of organic transformations has been mainly focused on the application of transition metals complexes as photocatalyst. In particular, Ruthenium and Iridium polypyridyl complexes stand at the forefront of this class (Figure 7).¹¹

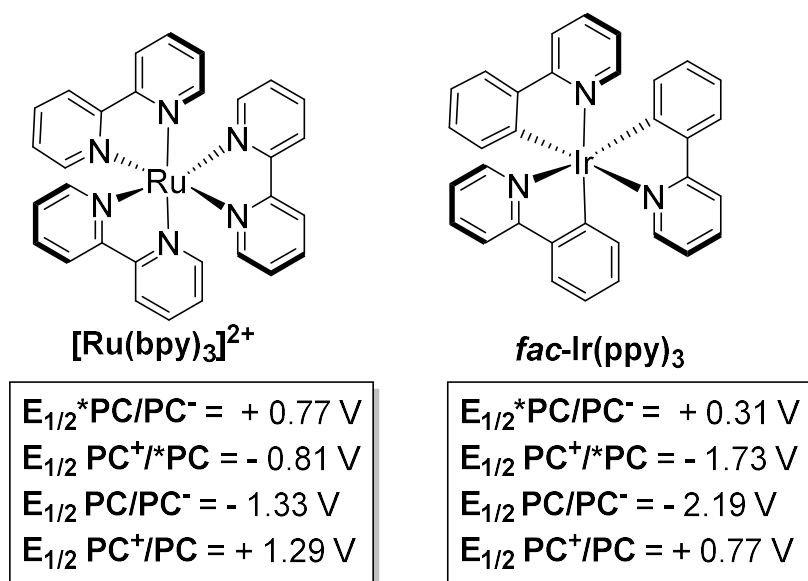


Figure 7 $[Ru(bpy)_3]^{2+}$ and $Ir(ppy)_3$ molecular structures and electrochemical properties (potential in V vs SCE).

These complexes show exceptional properties as photocatalysts including long excited-state lifetimes, originating from metal-to-ligand-charge-transfer (MLCT), high redox potential in the excited state, reversible oxidation and reduction in their ground states, and an excellent chemical stability. The absorbance in the visible range allows the excitation of these photocatalysts by irradiation with LEDs, CFL (Compact Fluorescent Light) household bulb and in some cases with solar light.

Furthermore, the ability to tune the properties of such metal complexes through modification of the ligands has significantly expanded the repertoire of synthetic transformations that can be accomplished using photoredox catalysis, thereby enhancing further interest in the field (Figure 8). This trend was demonstrated by the exponential increase in the number of publications over the last two decades.

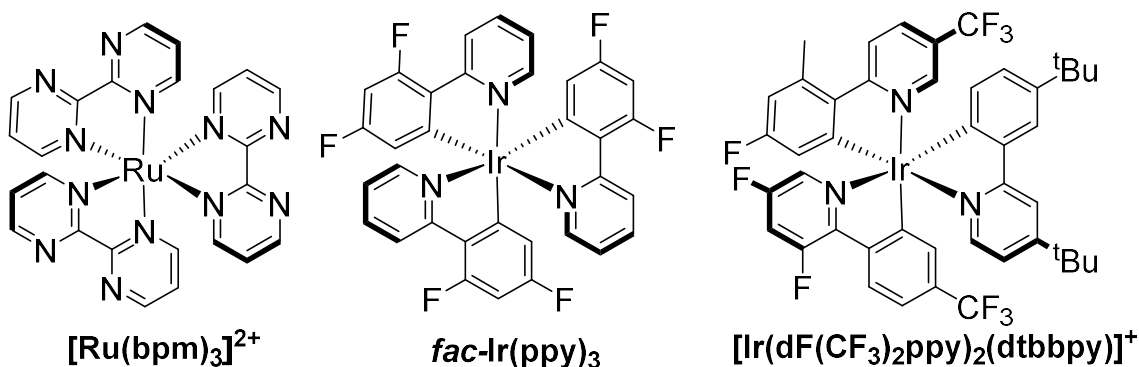


Figure 8 Molecular structure of several Ir(III) Ru(II) complexes used in photoredox catalysis.

The origin of the photoredox catalysis are attributed to Giacomo Ciamician an Italian chemist who, together with his colleague Paul Siber, at the beginning of the last century developed new reactions promoted by visible light.¹²

In 1978, the first example of photoredox catalysis applied to the organic synthesis was reported by Kellogg who demonstrated the reduction of sulfonium ions to the corresponding alkanes **1**, accelerated by the addition of a catalytic amount of $[\text{Ru}(\text{bpy})_3]\text{Cl}_2$ under irradiation of light (Figure 9).¹³

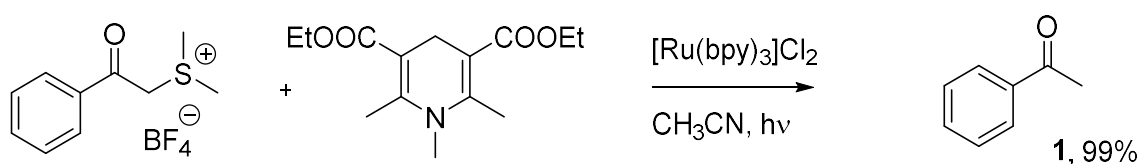


Figure 9 Photoredox reduction of sulfonium ion mediated by $[\text{Ru}(\text{bpy})_3]\text{Cl}_2$.

In the following years other organic transformations photocatalyzed by ruthenium complexes were carried out: in 1984 DeRonzier¹⁴ disclosed a Pschorr cyclization induced by $[\text{Ru}(\text{bpy})_3]\text{Cl}_2$ to give the corresponding phenanthrene **2** in quantitative yields. The first example of photoredox catalysis mediated by almost visible light (395 nm) is the cyclization of the α - β unsaturated ketone derivative to the keto-ester derivatives **3a** and **3b** reported by Pandey.¹⁵ In this case, the reaction relies on the presence of 9,10-dicyanoanthracene (DCA) as photocatalyst and triphenylphosphine (Figure 10).

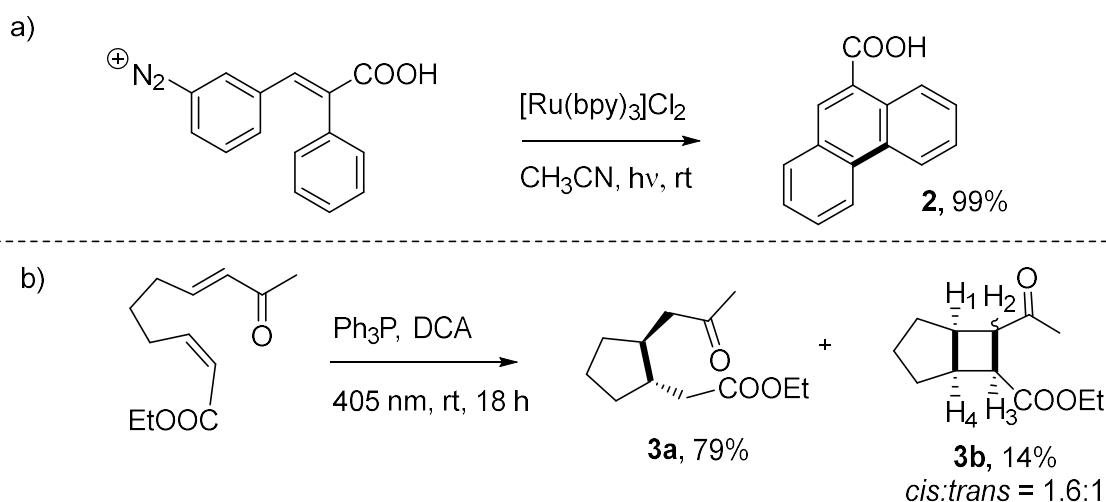


Figure 10 a) Pschorr cyclization reported by DeRonzier b) Cyclization visible light mediated developed by Pandey.

The tremendous growth in the last ten years is attributed to the investigations of Albini (Pavia),¹⁶ Balzani (Bologna),¹⁷ Cossy (Paris)¹⁸ and Lewis (Northwestern University, Illinois) on the use of single electron transfer processes applied to the organic transformations.

Thanks to these studies, the photoredox catalysis has led to the development of mild protocols for a wide range of organic transformations. Oxidation¹⁹ and reduction²⁰ reactions, formation of C-C bonds in sp^2 - sp^2 ,²¹ sp^2 - sp^3 ²² and sp^3 - sp^3 ²³ hybridizations and C-heteroatom bonds including C-S,²⁴ C-N,²⁵ C-O²⁶ and C-P²⁷ bond formations are some well-known examples (Figure 11).

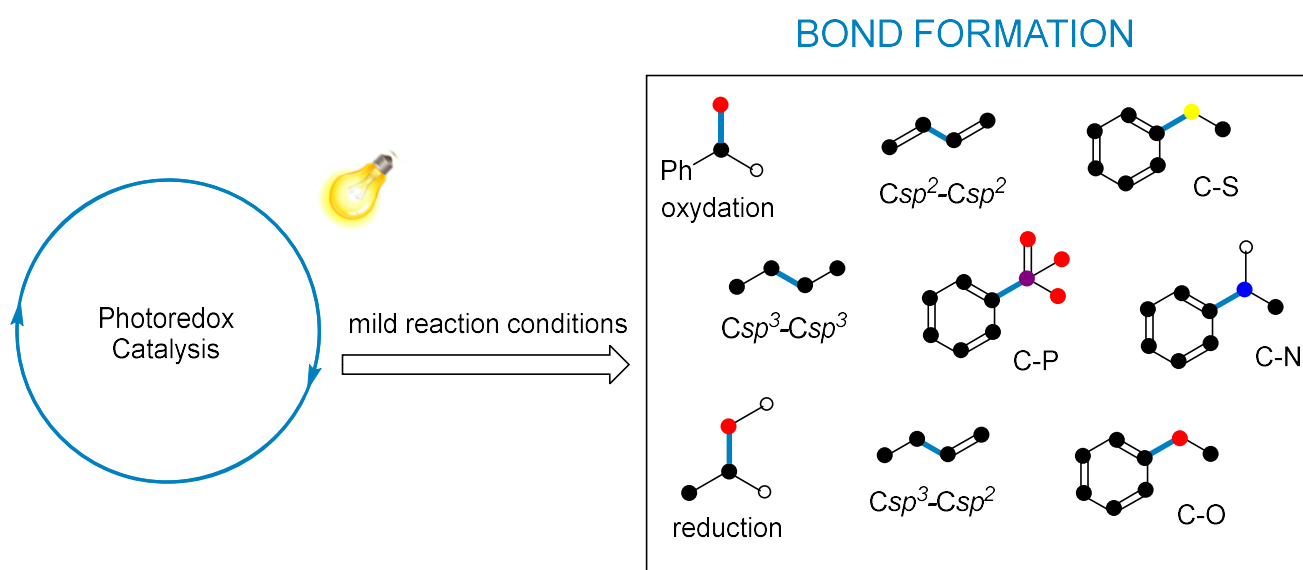


Figure 11 Various organic transformations mediated by photoredox catalysis.

The promotion of enantioselective reactions by the use of $[Ru(bpy)_3]Cl_2$ was demonstrated by MacMillan and co-workers.²⁸ The α -alkylation of aldehydes obtained by a combination of photoredox and organocatalysis represents a milestone among chemists working in organic synthesis and catalysis (Figure 12).

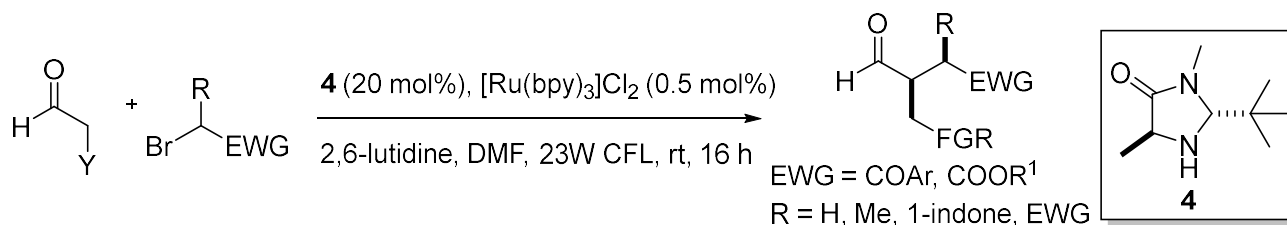


Figure 12 Enantioselective α -alkylation of aldehydes promoted by $[Ru(bpy)_3]Cl_2$.

In view of the remarkable impact in the organic synthesis field, photoredox catalysis was applied to the development of more complex, drug-like compounds. Among the various example, the

conjugate addition of α -amino radicals for the racemic synthesis of baclofen promoted by $[\text{Ir}(\text{dF-CF}_3\text{-ppy})(\text{dtbpy})]\text{PF}_6$ was reported by Koike and Akita (Figure 13).²⁹

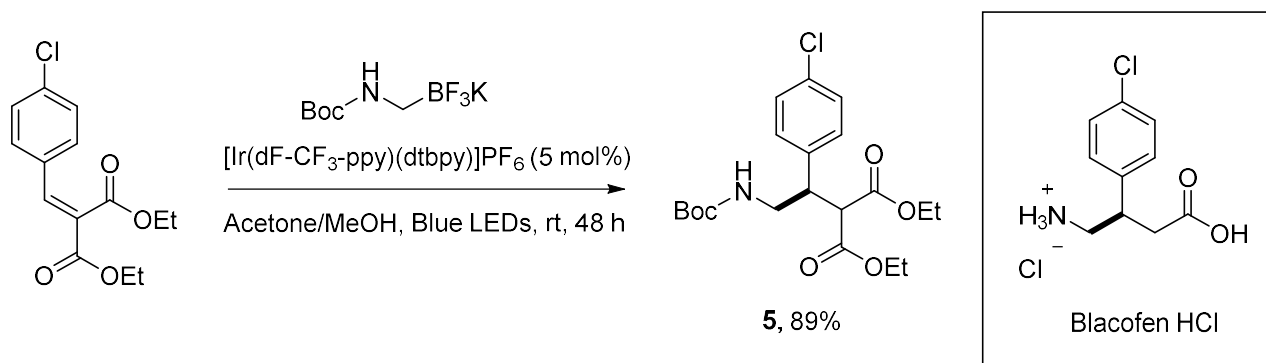


Figure 13 Alkylation of Michael acceptors by α -amino radicals in the total synthesis of Baclofen HCl.

Stephenson and co-workers demonstrated that $\text{Ir}(\text{ppy})_3$ mediated coupling of *N*-methylmorpholine with pyridazine derivatives provides rapid access to an intermediate in the total synthesis of the Gandotinib, a JAK2 (Janus kinase) inhibitor (Figure 14).³⁰

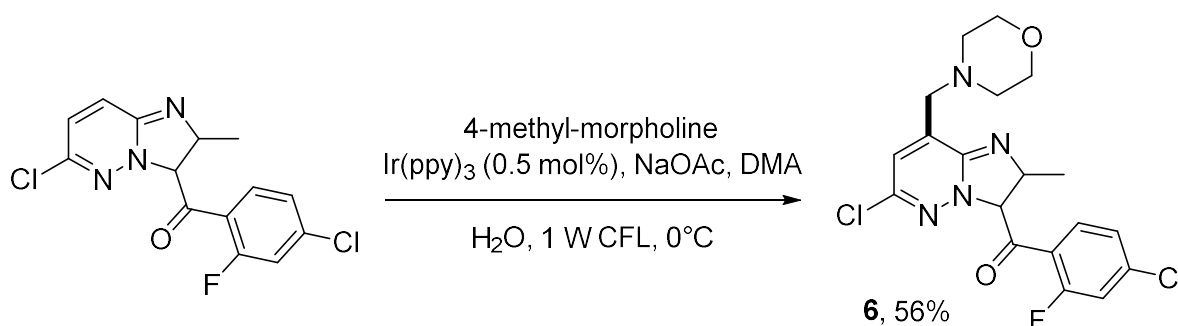


Figure 14 Coupling of *N*-methylmorpholine with pyridazine mediated by $\text{Ir}(\text{ppy})_3$.

Di Rocco *et al.*, scientists at Merck Research Laboratories, developed an optimized C–H alkylation, achieved by $[\text{Ir}(\text{ppy})_2(\text{dtbpy})]\text{PF}_6$, for the methylation, ethylation and cyclopropanation of a wide range of medicinal and agrochemical agents. In the last step of the synthesis, the camptothecin was obtained with a 77% of yield (Figure 15).³¹

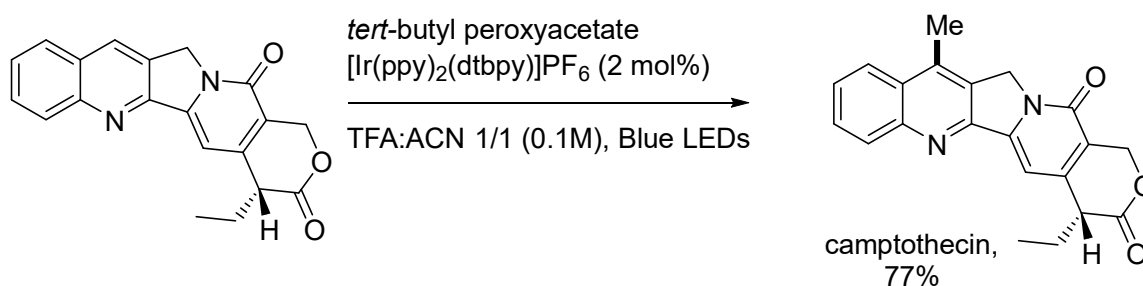


Figure 15 Last step in the total synthesis of camptothecin.

1.1.5 Use of organic dyes in photoredox catalysis

Ir(III) and Ru(II) complexes, and more in general of gold, platinum and palladium catalysts, lack in availability due to the growing demand in other applications, including displays for smart phones, televisions and renewable energy systems (fuel cells, wind energy, and photovoltaics).³²The development of more sustainable synthetic protocol represents the next step in the evolution of photoredox catalysis as green process.

Given the low price and toxicity, the employment of organic dyes as photocatalysts could be a valuable alternative to the transition metal complexes. Methylene blue, acridinium-type compounds and xanthene derivatives (rhodamine and fluorescein) are only some example of the organic photocatalyst used in photoredox catalysis (Figure 16).³³

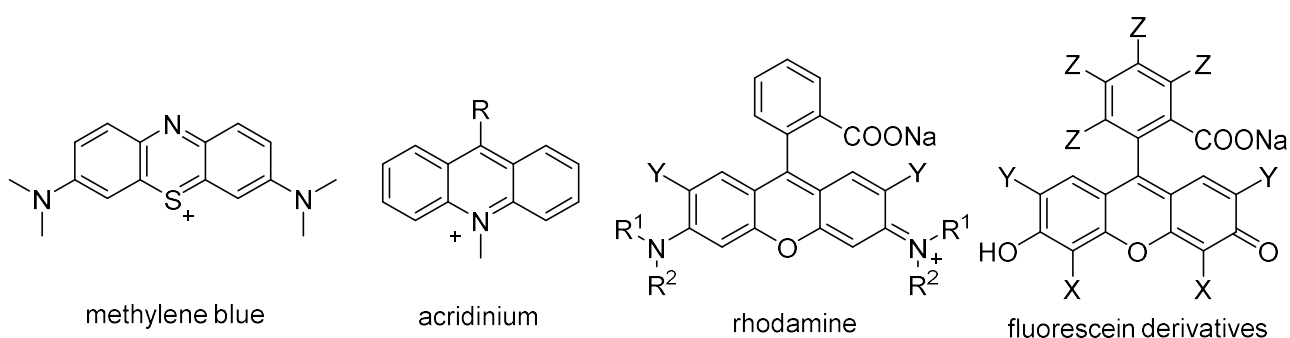


Figure 16 Molecular structure of the most employed organic dyes.

The diversity of the organic dyes, and the simple synthesis can allow interesting discovery and optimization of new synthetic methodologies. Furthermore, organic dyes can be accessible to a lower price and compare the transition-metal counterparts allowing the access to new scenarios in organic synthesis. By contrary, normally lifetimes of the excited states are quite reduced compared to metal photocatalyst, but some classes of organic dyes are showing quite remarkable lifetime, as in the case of dicyanobenzene 4CzIPN which exhibits a lifetime of 5.1 μ s.³⁴

In view of above, the limited use, so far, of these photocatalysts is rather surprising and it is probably due to the missing of an exhaustive collection of photophysical data for this type of compounds. On the other hand, the availability of photophysical and electrochemical properties has made Ru(II) and Ir(III) complexes very popular and extensively employed in photoredox catalysis.

Prototypical examples of organic dyes are the N-alkylated acridinium salt derivatives (Figure 17).

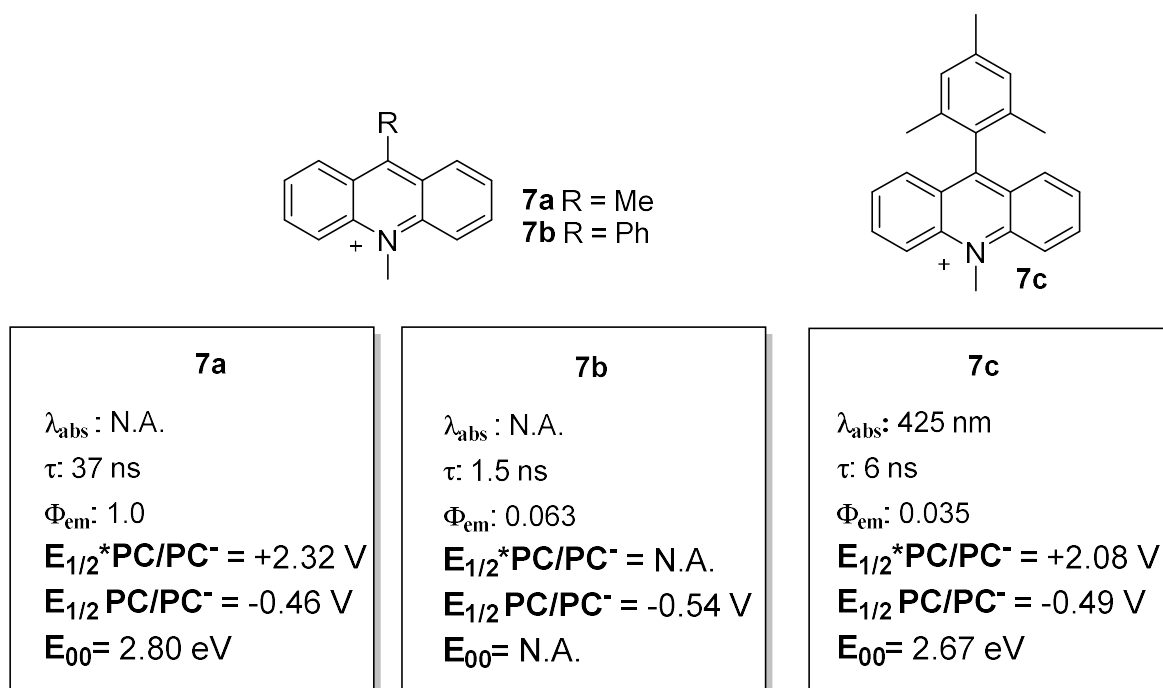


Figure 17 Molecular structure of acridinium dyes **7a**, **7b** and **7c**.

Thanks to their strong oxidizing ability in the lowest singlet excited state ($E_{1/2} = +2.32$ and $+2.08 \text{ V}$ vs. SCE, in MeCN, respectively), acridinium dyes were largely exploited in oxidative quenching processes.³⁵

Unfortunately, compounds **7a** and **7b** have found limited use in photocatalysis because of the susceptibility to nucleophile addition and, in the case of **7b**, the low lifetime of the excited state ($\tau=1.5 \text{ ns}$ and $\phi_i=0.06$)

The 9-aryl-substituted acridinium derivative **7c**, known as Fukuzumi catalyst, was employed as photocatalyst of wide range of photoredox reactions including oxidation of alkyl and aromatic compounds, dehydrogenative couplings, C-H functionalization of arenes and alkenes and cycloadditions (Figure 18).

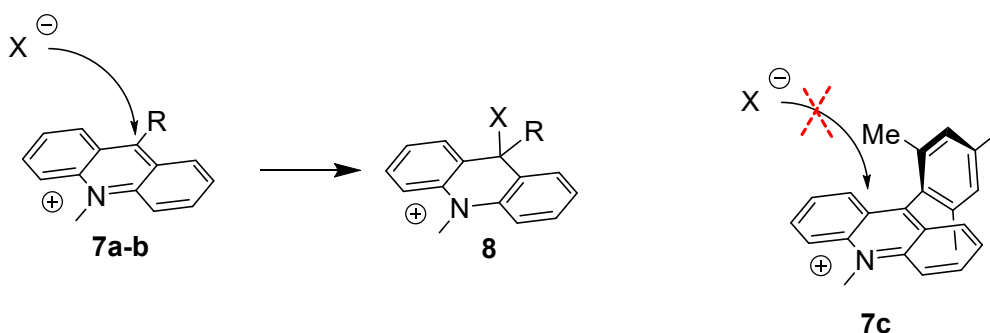


Figure 18 Deactivation pathway of compounds **7a** and **7b**.

The success of the acridinium salt **7c** is due to the protective effect of the methyl substituents on the mesityl group which prevents the nucleophile or radical addition to the acridinium/acridinyl radical which would generate a dihydroacridines **5** deactivating the photocatalyst.

A remarkable example of Fukuzumy catalyst applied to the photoredox catalysis is the anti-Markovnikov addition of strong Brønsted acids to styrene derivatives in the presence of a redox-active thiol as hydrogen donor (Figure 19).

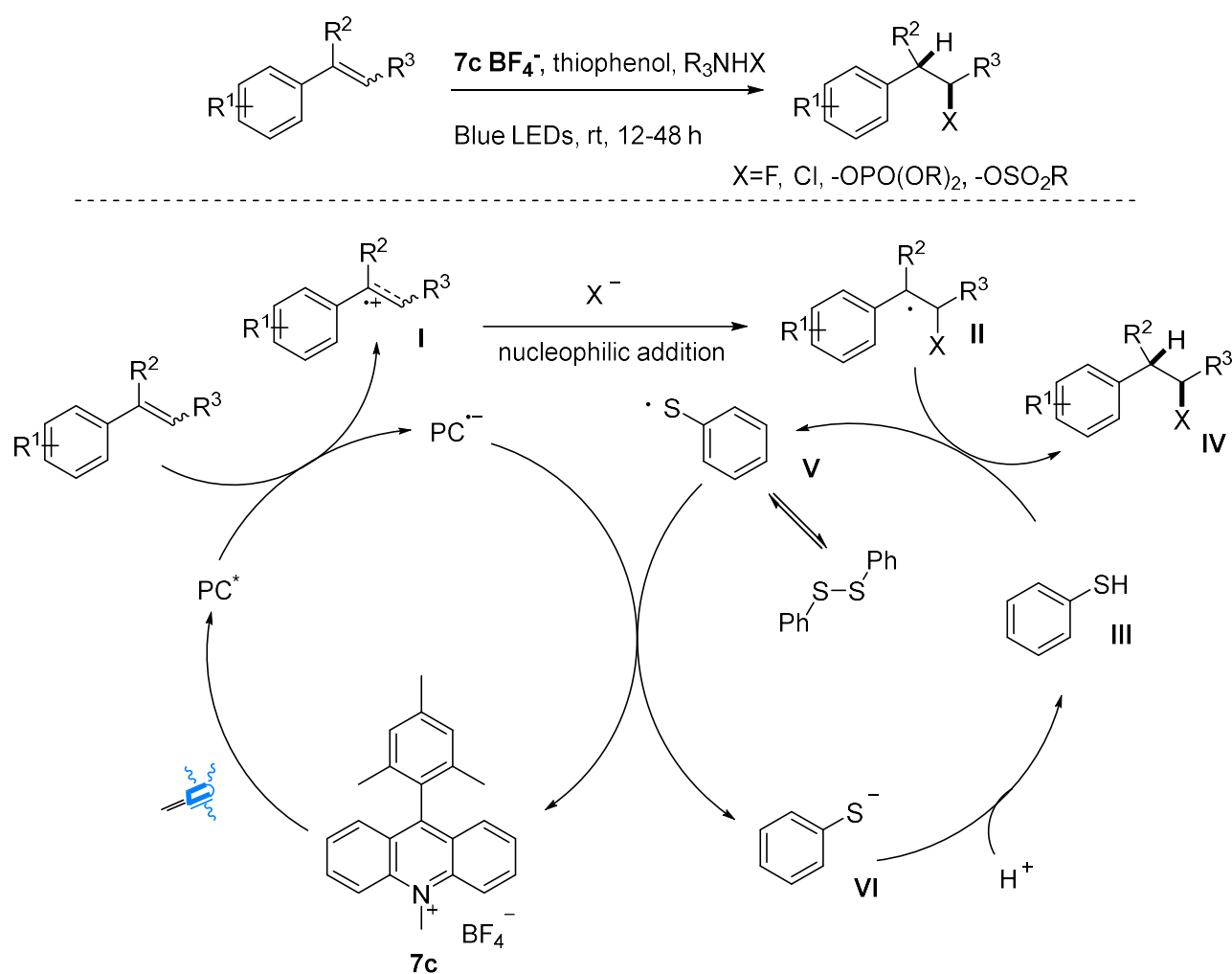


Figure 19 Photoredox anti-Markovnikov addition of strong Brønsted acids to styrene derivatives.

The reaction proved efficient for the addition of low nucleophile conjugate bases of HCl, HF, phosphoric and sulfonic acids showing a complete regioselectivity and excellent yields in the most part of the cases. The SET from the excited state PC^* and the alkene generates the carboanion $PC^{\bullet+}$ and the electrophilic species **I**. The nucleophilic attack of the nucleophiles X^- to the species **I** give the radical **II**. The hydrogen atom transfer (HAT) from the thiol **III** to **II** provides the final product **IV** and the thiol radical **V**. The turnover of the photocatalyst is obtained by the oxidation of the

carboanion PC^{*-} by the compound **V**. The formed thiolate **VI** undergoes protonation to regenerate the thiol **III**.

Another class of organic dyes are the fluorescein derivatives (fluorescein FL, eosin y EY, rose Bengal RB) (Figure 20).

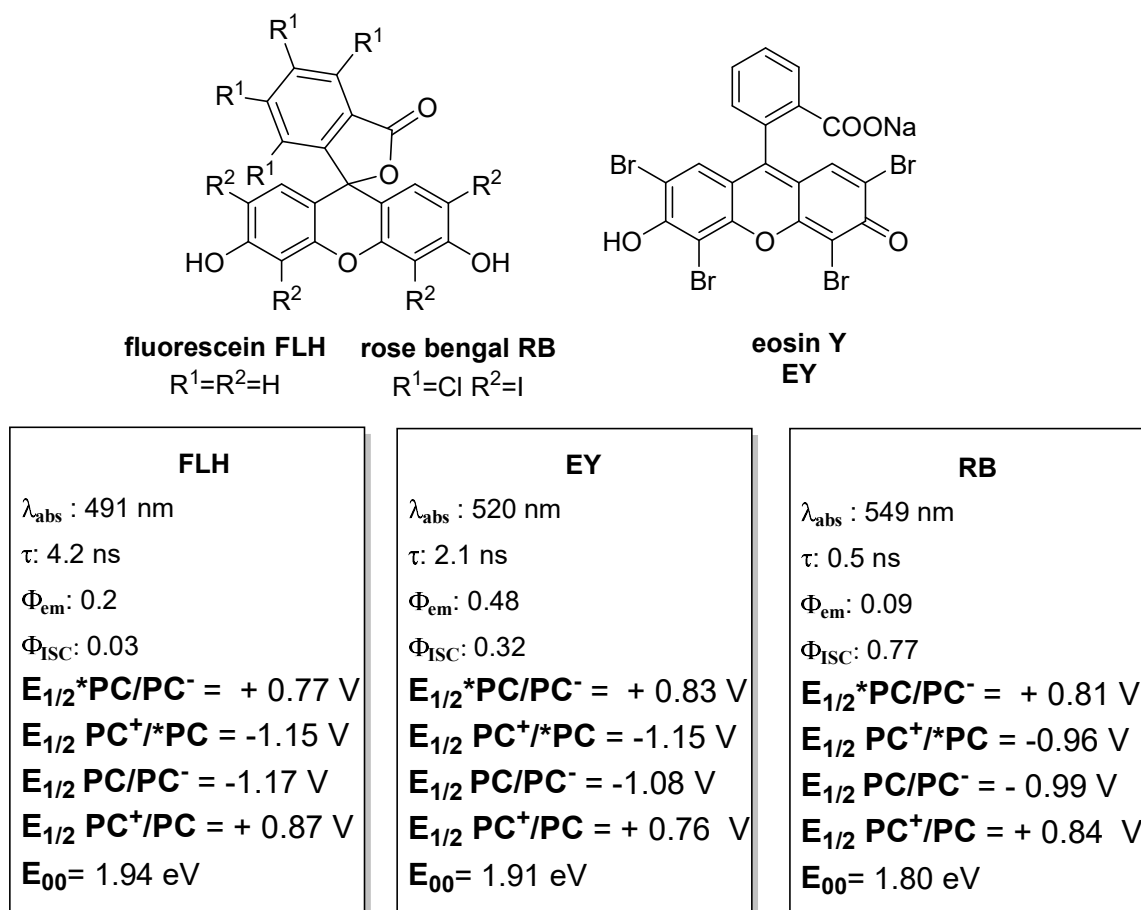


Figure 20 Molecular structures of fluorescein FL, eosin y EY and rose Bengal RB.

The excited state $^3FL^*$ is formed with low efficiency ($\Phi_{ISC} = 0.03$) showing a moderate oxidizing and reducing character. Eosin Y and rose bengal exhibit fast ISC ($\Phi_{ISC} = 0.32$ and 0.77 , respectively) to triplet state corresponding to a very short singlet lifetime. The excited state $^3EY^*$ and $^3RB^*$ are considered the most relevant excited state in the photoredox reactions. The excited state reduction potentials are fairly similar (0.85V) while the oxidation potentials of $^3RB^*$ is roughly 0.2V than respect to $^3EY^*$.

As in the case of acridinium salts, these compounds are largely used in photocatalyzed oxidative reactions (Figure 21).

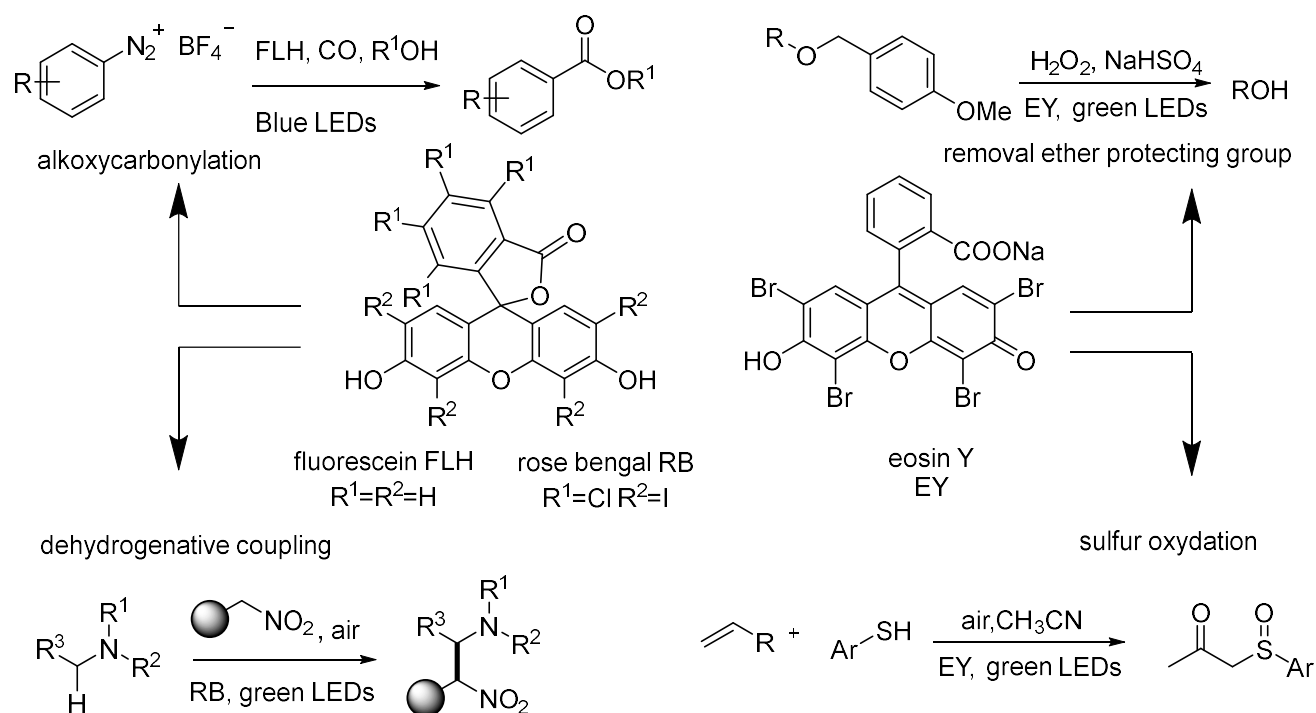


Figure 21 Use of fluorescein derivatives in photoredox catalysis of several organic transformations.

In particular, eosin Y was widespread used, as neutral EYH_2 or ionic species EY^{2-} , in the photoredox catalysis of several oxidation processes including the conversion of benzylic bromide to aldehyde,³⁶ the removal of PMB protecting group³⁷ and in the synthesis of β -keto sulfoxide from alkene.³⁸ Rose Bengal was used in dehydrogenative couplings between tetrahydroquinoline and several partners including nitroalkanes,³⁹ nitrile,⁴⁰ alkynes and CF_3 .⁴¹ Fluorescein is less employed as photocatalyst. The photoredox alkoxy carbonylation of aridazonium salts mediated by FLH was described by Xiao and workers.⁴²

Albeit the strong oxidizing ability of several organic dyes is deeply reported in literature, examples of strong reductants are much less common and in the most part of the cases the use of UV-light was required.

Murphy described a class of super electron donor (SED) organic reductants, derived by the tetrakis(dimethylamino)ethene, with reduction potentials ≤ -1.5 V (vs. SCE). These dyes are capable to reduce unactivated benzene derivatives to the corresponding radical anion and promote the cleavage of $ArC-X$, $ArX-C$ bond (with $X = N, O$ and S) and $ArC-C$ when irradiated by UV light (Figure 22).⁴³

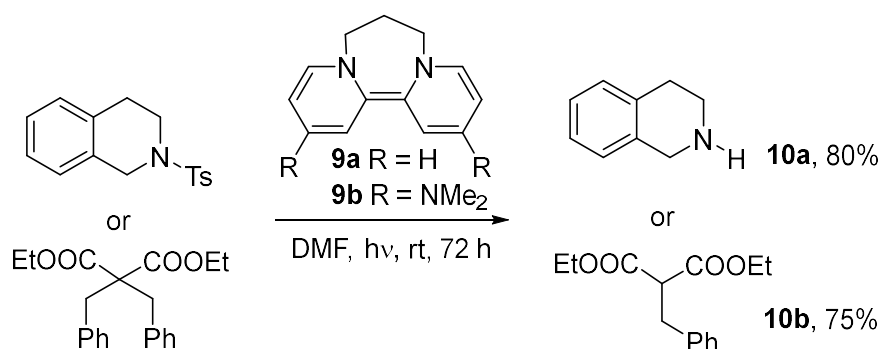


Figure 22 Reduction of un-activated benzene derivatives promoted by photoredox catalysis.

Other organic photocatalysts with a reduction potential in a range of -1.5 to -2.1 V (vs. SCE) are phenoti- and phenox- azine derivatives and perylene. These molecules contain electron-rich motifs which stabilize the radical cation formed in the photocatalytic process.⁴⁴ An example is the 10-phenothiazine (PHT) which was employed by DeAlaniz *et al.* for the reduction of carbon-halogen bonds⁴⁵ (Figure 23).

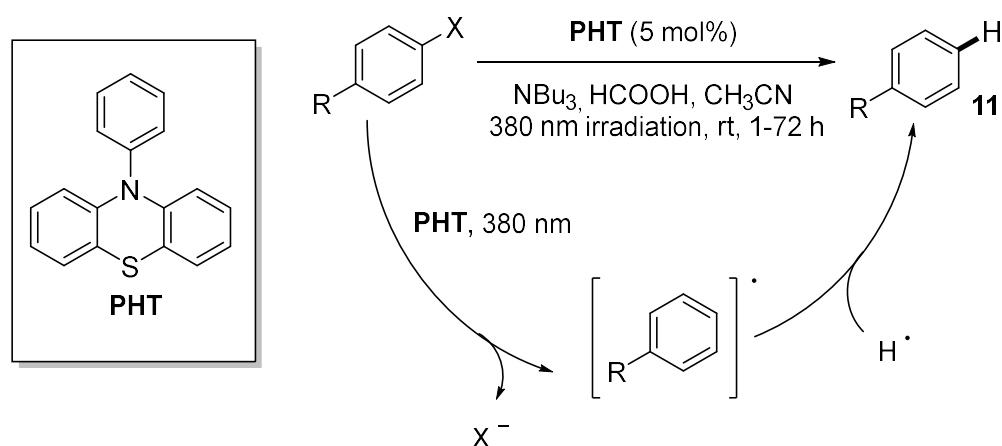


Figure 23 Reductive dehalogenation mediated by PHT.

The reaction was applied to various aryl halogenate including iodide, chloride and bromide giving the reduced product in almost quantitative yields in the most part of the cases.

As last example, a photoredox atom transfer radical polymerization (ATPR) mediated by perylene,⁴⁶ phenoxazines⁴⁷ and dihydrophenazines⁴⁸ was reported by Miyake (Figure 24).

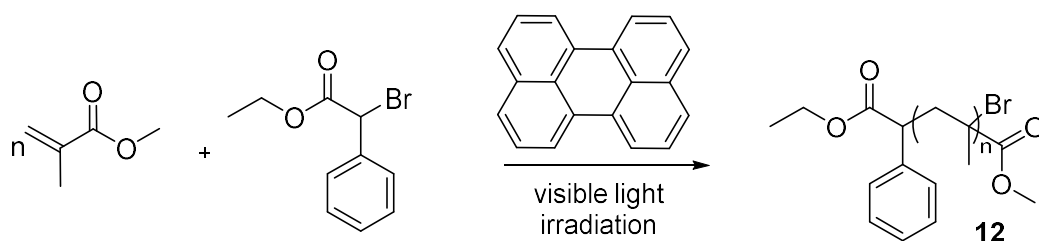


Figure 24 Photoredox ATRP mediated by perylene.

Remarkably, polymerization of methyl methacrylate, using perylene as photocatalyst takes place under visible light. As the best of our knowledge, this is the first example of organic dye which did not require an UV irradiation during the photoredox process.

1.1.6 Coumarin derivatives as fluorescent dyes

Coumarin derivatives are phenolic substances composed of fused benzene and α -pyrone rings which show different kinds of biological activities. The pharmacological profile of coumarin derivatives includes anticancer, antidiabetic, antiHIV, antioxidant, antimicrobial, anti-inflammatory, vasodilator, anticoagulant and other bioactivities⁴⁹ (Figure 25).

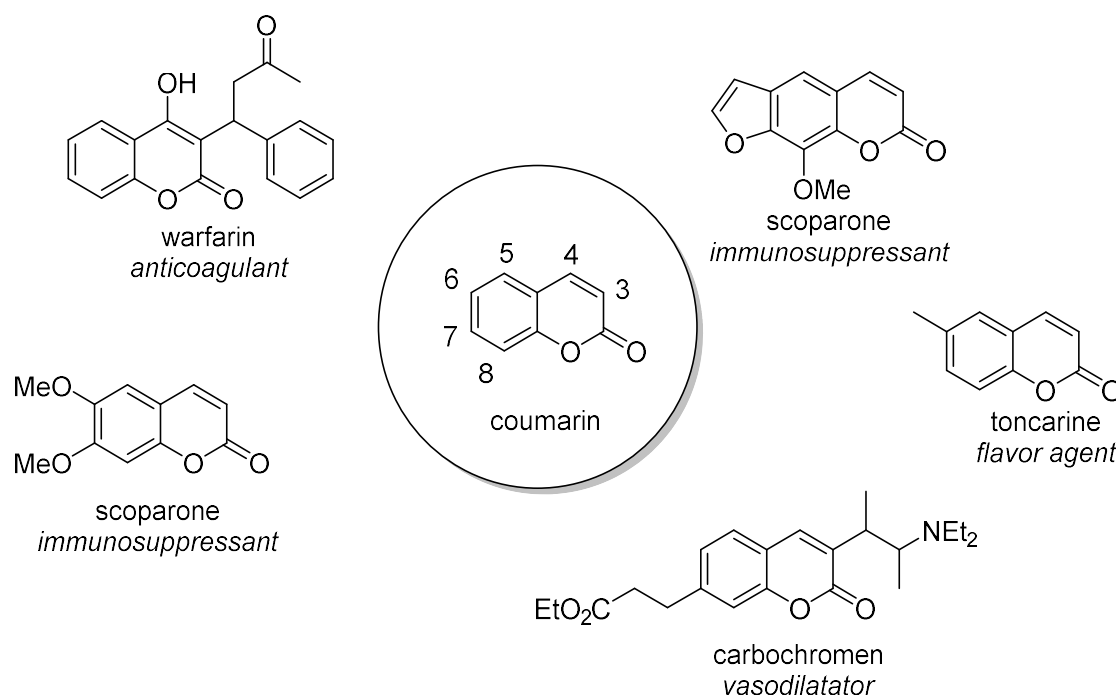


Figure 25 Coumarin core structure (and its numbering). Molecular structure of coumarin derivatives and their application.

They also have found application as starting material or intermediate in the agrochemical, food, and cosmetic industries as aroma enhancers, flavorants, and additives.

Among the various applications, coumarin derivatives are also employed as fluorescent material in fluorescent bio labelling,⁵⁰ laser device,⁵¹ organic light-emitting diodes (OLED)⁵² and solar cells.⁵³ The employment of coumarins as fluorescent dye is due to presence of electron donating substituents (including amino and hydroxy groups) in position 6-7 of the core structure (Figure 26).

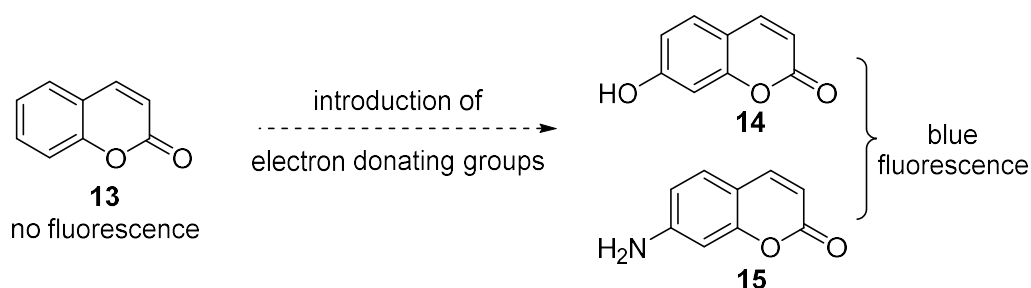


Figure 26 Insertion of electron donating group on the coumarin core.

Insertion of amino and hydroxy group in position 7 generates a “push and pull” effect between the electron donor groups and the electron withdrawing lactone moiety. As results, coumarin **13** is not fluorescent while 7-substitued coumarin **14** and **15** show an intense blue emission.

The emission spectra of 7-hydroxy coumarin is sensitive to pH, as well as the solubility in water, because of the ionizable hydroxy group ($pK_a=7.8$). On the other hand, the fluorescence of 7-aminocoumarin derivatives is not dependent to pH. In the case of no alkylated or partially alkylated amino groups, the corresponding dyes are slightly soluble in water thanks to the formation of hydrogen bond with water.

1.1.7 Large Stoke Shift (LSS) of coumarin dyes

Introduction of acceptor aroyl groups at C-3 or trifluoromethyl at C-4 of 7-hydroxy- or 7-aminocoumarins provides bathochromic and bathofluoric shifts thanks to the extension the conjugation system of the dye. Furthermore, values of Stokes shift (the difference between positions of the band maxima of the absorption and emission spectra) higher than 50 nm were observed making the 7-amino- and 7-hydroxy-coumarin derivatives large Stokes shift (LSS) dyes (Figure 27).

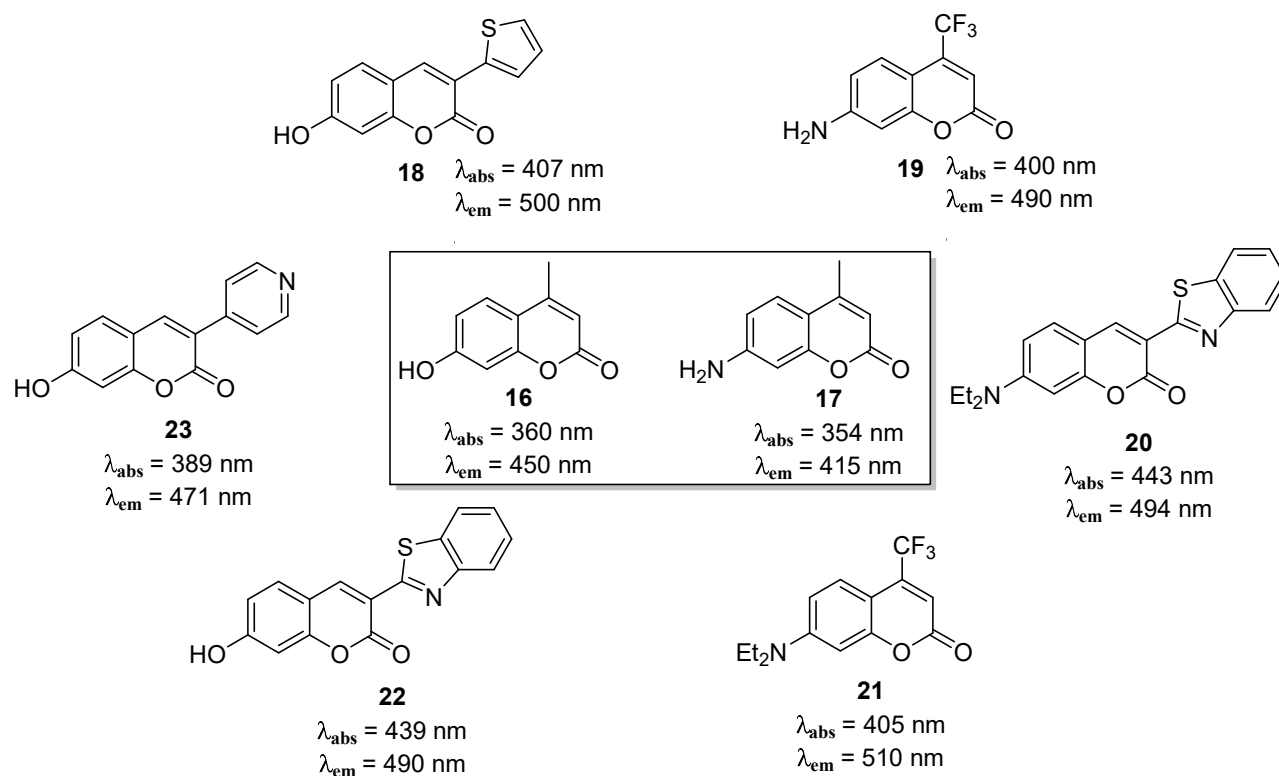


Figure 27 Insertion of electron withdrawing group on 7-hydroxy- and 7-amino coumarins.

The high stoke shift values are generally attributed to geometrical relaxation in the excited state and rearrangement of the solvent dipoles (relaxation of the solvent media). In particular, intramolecular charge transfer ICT, twisted ICT (TICT) and, rarely, intramolecular proton transfer (ESIPT) mechanism are considered the main responsible for the large Stokes shift (Figure 28).⁵⁴

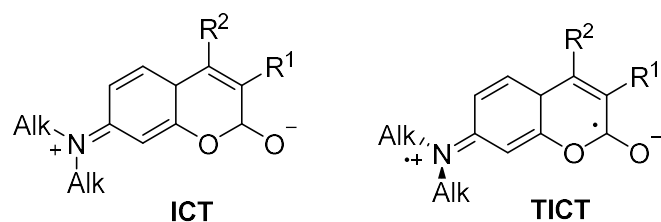


Figure 28 ICT and TICT relaxation mechanisms.

All the processes are associated with low emission intensity of the dye. In particular, the formation of non-emissive TICT-state dramatically affect the fluorescent quantum yield. This reduction is particularly sharp for the dialkylated aminocoumarin in highly polar solvent due to the rotation of the amino group which favour an internal conversion from the ICT to a non-emissive TICT state with a full charge separation. The incorporation of amino group in one or two six- membered rings, fused

with the π system, does not allow the TICT relaxation. Thus, the excited state molecule relaxed through a planar ICT with a consequent improvement in the fluorescent efficiency (Figure 29).

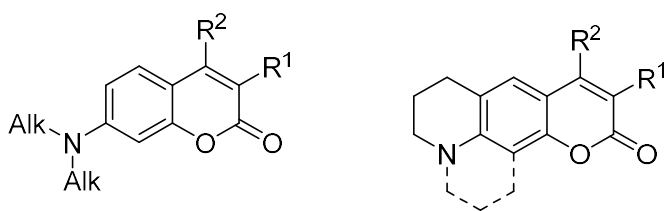


Figure 29 Incorporation of amino group in one or two six- membered rings.

The rigidized amino groups have lone electron pairs which overlap efficiently with the π -electron system of the dye. These ‘planar’ amino groups are stronger electron-donors than ‘twisted’ dimethyl- or diethylamino groups. Therefore, they are directly conjugated with an electron-acceptor part of the coumarin fluorophore, and the fully developed ‘push–pull’ effect shifts the absorption and emission bands further to longer wavelengths.

1.1.8 Use of coumarin dyes in SET

Although the employment of coumarin dyes in SET processes is not widely described in literature, the ability of coumarin to promote single electron transfer, generating radical species, was disclosed for the first time by Bergmark and co-workers.⁵⁵ In the case of 7-aminocoumarin, SET takes place more efficiently in the presence of freely rotating 7-dialkylamino groups, capable to give TICT, than respect to rigidized structures, as demonstrated by Ramakrishna *et al.*,⁵⁶ and through the formation of a charge separation in the excited state.⁵⁷

1.1.9 Outline of the thesis

The goal of the thesis was the employment coumarin dyes in different application including photoredox catalysis, biological labelling and photopolymerization. Furthermore, the development of new synthetical approaches in metallaphotoredox catalysis was investigated.

In **Ch2**, photoredox pinacol coupling reaction of several aldehydes, ketones and immines, mediated by coumarin dyes as photocatalysts, was described.

In **Ch3**, the use of coumarin as photocatalyst was extended to various transformations including ATRA reactions, α -alkylation of aldehydes, reductive protonation of bromoketones and trifluoromethylations of alkenes.

In **Ch4**, the development of more efficient coumarin dyes as photocatalysts of photoredox pinacol coupling reactions was reported.

In **Ch5**, a new protocol for the allylation of aromatic and aliphatic aldehydes through the nickel photoredox catalysis was described.

In **Ch6**, the photopolymerization mediated by coumarin dyes was described.

In **Ch7**, the design, synthesis, characterization and evaluation of new fluorescent LSS dyes excitable by UV, violet and blue lasers for biological multiplex assays was reported.

References

- ¹ a) M. Gratzel, *Acc. Chem. Res.*, 1981, **14**, 376; (b) T. J. Meyer, *Acc. Chem. Res.*, 1989, **22**, 163.
- ² H. Takeda, O. Ishitani, *Coord. Chem. Rev.*, 2010, **254**, 346.
- ³ K. Kalyanasundaram, M. Gratzel, *Coord. Chem. Rev.* 1998, **177**, 347.
- ⁴ For selected recent reviews on photoredox catalysis, see: (a) K. L. Skubi, T. R. Blum and T. P. Yoon, *Chem. Rev.*, 2016, **116**, 10035; (b) X. Lang, J. Zhao and X.-d. Chen, *Chem. Soc. Rev.*, 2016, **45**, 3026; (c) M. Parasram and V. Gevorgyan, *Chem. Soc. Rev.*, 2017, **46**, 6227; (d) K. N. Lee and M.-Y. Ngai, *Chem. Commun.*, 2017, **53**, 13093; (e) Y.-Q. Zou, F. M. Hoermann and T. Bach, *Chem. Soc. Rev.*, 2018, **47**, 278; (f) J.-R. Chen, X.-Q. Hu, L.-Q. Lu and W.-J. Xiao, *Acc. Chem. Res.*, 2016, **49**, 1911; (g) D. Ravelli, M. Fagnoni, A. Albini, *Chem. Soc. Rev.*, 2013, **42**, 97.
- ⁵ V. Balzani, P. Ceroni and A. Juris, *Photochemistry and Photophysics*, Wiley, 2014.
- ⁶ IUPAC. *Compendium of Chemical Terminology*, 2nd ed. (the "Gold Book"). Compiled by A. D. McNaught and A. Wilkinson. Blackwell Scientific Publications, Oxford (1997).
- ⁷ R. A. J. Marcus, *Phys. Chem.*, 1968, **72**, 891.
- ⁸ Rehm, Weller, *Isr. J. Chem.*, 1970, **8**, 834.
- ⁹ Q.-Q. Zhou, Y.-Q. Zou, L.-Q. Lu, W.-J. Xiao, *Angew. Chem. Int. Ed.*, 2019, **58**, 1586.
- ¹⁰ C. G. S. Lima, T. d. M. Lima, M. Duarte, I. D. Jurberg, and M. W. Paixão, *ACS Catalysis* 2016, **6**, 1389.
- ¹¹ C. K. Prier, D. A. Rankic, D. W. C. MacMillan, *Chem. Rev.*, 2013, **113**, 5322.
- ¹² G. Ciamician, *Science*, 1912, **36**, 385.
- ¹³ D. M. Hedstrand, W. M. Kruizinga and R. M. Kellogg, *Tetrahedron Lett.*, 1978, **19**, 1255.
- ¹⁴ H. Cano-Yelo and A. Deronzier, *J. Chem. Soc., Perkin Trans. 2*, 1984, 1093.
- ¹⁵ G. Pandey, S. Hajra, M. K. Ghorai and K. R. Kumar, *J. Am. Chem. Soc.*, 1997, **119**, 8777.
- ¹⁶ E. Fasani, M. Fagnoni, D. Dondi and A. Albini, *J. Org. Chem.*, 2006, **71**, 2037.
- ¹⁷ *Photoinduced energy and electron transfer processes*, in: *The Exploration of Supramolecular Systems and Nanostructures by Photochemical Techniques*, HEILDEBERG, Springer, 2012, 21–38.
- ¹⁸ J. Cossy, *Photoinduced electron transfer in radical reactions*, in: *Radicals in Organic Synthesis*, P. Renaud and M. P. Sibi, 2008.
- ¹⁹ R. Lechner and B. König, *Synthesis*, 2010, **10**, 1712.
- ²⁰ T. Slanina, T. Ghosh and B. König, *Chem. Sci.*, 2015, **6**, 2027.
- ²¹ I. Ghosh, L. Marzo, A. Das, R. Shaikh and B. König, *Acc. Chem. Res.*, 2016, **49**, 1566.
- ²² a) C. Tellis, D. N. Primer and G. A. Molander, *Science*, 2014, **345**, 433; b) C. Lévêque, L. Chenneberg, V. Corcé, J.-P. Goddard, C. Ollivier and L. Fensterbank, *Org. Chem. Front.*, 2016, **3**, 462; c) M. Jouffroy, D. N. Primer and G. A. Molander, *J. Am. Chem. Soc.*, 2016, **138**, 475; d) P. Zhang, C. C. Le, and D. W. C. MacMillan, *J. Am. Chem. Soc.*, 2016, **138**, 8084.
- ²³ C. P. Johnston, R. T. Smith, S. Allmendinger and D. W. C. MacMillan, *Nature*, 2016, **536**, 322.

- ²⁴ M. Majek and A. J. von Wangelin, *Chem. Commun.*, 2013, **49**, 5507.
- ²⁵ E. B. Corcoran, M. T. Pirnot, S. Lin, S. D. Dreher, D. A. DiRocco, I. W. Davies, S. L. Buchwald and D. W. C. MacMillan, *Science*, 2016, **353**, 279.
- ²⁶ J. A. Terrett, J. D. Cuthbertson, V. W. Shurtleff and D. W. C. MacMillan, *Nature*, 2015, **524**, 330.
- ²⁷ R. S. Shaikh, S. Düsel and B. König, *ACS Catal.*, 2016, **6**, 8410.
- ²⁸ D. A. Nicewicz and D. W. C. MacMillan, *Science*, 2008, **322**, 77.
- ²⁹ K. Miyazawa, T. Koike and M. Akita, *Adv. Synth. Catal.*, 2014, **356**, 2749.
- ³⁰ J. J. Douglas, K. P. Cole and C. R. J. Stephenson, *J. Org. Chem.*, 2014, **79**, 11631.
- ³¹ D. A. DiRocco, K. Dykstra, S. Krska, P. Vachal, P., D. V. Conway, and M. Tudge, *Angew. Chem., Int. Ed.*, 2014, **53**, 4802.
- ³² British Geological Survey, "Risk list 2012: An updated supply risk index for chemical elements or element groups which are of economic value".
- ³³ A. N. Romero and D. A. Nicewicz, *Chem. Rev.*, 2016, **116**, 10075.
- ³⁴ T.-Y. Shang, L.-H. Lu, Zhong Cao, Y. Liu, W.-M. He and B. Yu, *Chem. Commun.*, 2019, **55**, 5408.
- ³⁵ a) N. A. Romero, K. A. Margrey, N. E. Tay and D. A. Nicewicz, *Science*, 2015, **349**, 1326; b) N. A. Romero and D. A. Nicewicz, *J. Am. Chem. Soc.*, 2014, **136**, 17024; c) D. J. Wilger, J.-M. Grandjean, T. R. Lammert and D. A. Nicewicz, *Nat. Chem.*, 2014, **6**, 720.
- ³⁶ a) N. Kornblum, J. W. Powers, G. J. Anderson, W. J. Jones, H. O. Larson, O. Levand and W. M. A. Weaver, *J. Am. Chem. Soc.*, 1957, **79**, 6562; b) N. Kornblum, W. J. Jones and G. J. Anderson, *J. Am. Chem. Soc.*, 1959, **81**, 4113.
- ³⁷ Z. Liu, Y. Zhang, Z. Cai, H. Sun and X. Cheng, *Adv. Synth. Catal.*, 2015, **357**, 589.
- ³⁸ T. Keshari, V. K. Yadav, V. P. Srivastava and L. D. S. Yadav, *Green Chem.*, 2014, **16**, 3986.
- ³⁹ Y. Pan, C. W. Kee, L. Chen and C.-H. Tan, *Green Chem.*, 2011, **13**, 2682.
- ⁴⁰ Y. Pan, S. Wang, C. W. Kee, E. Dubuisson, Y. Yang, K.P. Loh and C.-H. Tan, *Green Chem.*, 2011, **13**, 3341.
- ⁴¹ W. Fu, W. Guo, G. Zou and C. Xu, *J. Fluorine Chem.*, 2012, **140**, 88.
- ⁴² W. Guo, L.-Q. Lu, Y. Wang, Y.-N. Wang, J.-R. Chen and W.-J. Xiao, *Angew. Chem., Int. Ed.*, 2015, **54**, 2265.
- ⁴³ J. A. Murphy, *J. Org. Chem.*, 2014, **79**, 3731.
- ⁴⁴ Quite recently, a number of phenoxazine derivatives have been developed as visible light-absorbing, organic photoredox catalysts (PCs) with high reduction potentials (-1.42 V up to -2.01 vs. SCE); see: B. McCarthy, R. Pearson, C. -H. Lim, S. M. Sartor, N. H. Damrauer and G. M. Miyake, *J. Am. Chem. Soc.*, 2018, **140**, 5088.
- ⁴⁵ E. H. Discekici, N. J. Treat, S. O. Poelma, K. M. Mattson, Z. M. Hudson, Y. Luo, C. J. Hawker and J. R. de Alaniz, *Chem. Commun.*, 2015, **51**, 11705.
- ⁴⁶ G. M. Miyake and J. C. Theriot, *Macromolecules*, 2014, **47**, 8255.
- ⁴⁷ Y. Du, R. M. Pearson, C. -H. Lim, S. M. Sartor, M. D. Ryan, H. Yang, N. H. Damrauer and G. M. Miyake, *Chem. – Eur. J.*, 2017, **23**, 10962.
- ⁴⁸ J. C. Theriot, C.-H. Lim, H. Yang, M. D. Ryan, C. B. Musgrave and G. M. Miyake, *Science*, 2016, **352**, 1082.
- ⁴⁹ R. Bhatia, S. Pathania, V. Singh and R. K. Rawal, *Chem. Heterocycl. Comp.*, 2018, **54**, 280.
- ⁵⁰ H. Li, L. Cai, J. Li, Y. Hu, P. Zhou and J. Zhang, *Dyes Pigm.*, 2011, **91**, 309.
- ⁵¹ B. B. Raju and T. S. Varadarajan, *Laser Chem.*, 1995, **16**, 109.
- ⁵² M. Fujiwara, N. Ishida, M. Satsuki and S. Suga, *J. Photopolym. Sci. Technol.*, 2002, **15**, 237.
- ⁵³ K. Hara, Z.-S. Wang, T. Sato, A. Furube, R. Katoh, H. Sugihara, Y. Dan-oh, C. Kasada, A. Shinpo and S. Suga, *J. Phys. Chem. B*, 2005, **109**, 15476.
- ⁵⁴ M. Sednev, V. Belov and S. Hell, *Methods Appl. Fluoresc.*, 2015, **3**, 042004.
- ⁵⁵ a) G. Jones, W. R. Jackson, C. Y. Choi and W. R. Bergmark, *J. Phys. Chem.*, 1985, **89**, 294, b) G. Jones, S. F. Griffin, W. R. Jackson, C. Y. Choi and W. R. Bergmark, *J. Org. Chem.*, 1984, **49**, 2705.

⁵⁶ G. Ramakrishna and H. N. Ghosh, *J. Phys. Chem. A*, 2002, **106**, 2545.

⁵⁷ M. Murakami, K. Ohkubo, T. Nanjo, K. Souma, N. Suzuki, S. Fukuzumi, *ChemPhysChem.*, 2010, **11**, 2594.

Photoredox pinacol coupling reactions mediated by coumarins

2.1 Introduction

2.1.1 Traditional methods for the synthesis of diols

Diols, diamines and amino alcohols are important motifs in natural products, pharmacologically active compounds,¹ ligands and auxiliaries.² In particular, the traditional procedure for the synthesis of diols requires the use of a metal catalyst M (Cp_2TiCl_2 , SmI_2 or other lanthanides) and a co-reducing metal Co-Red (metallic manganese, zinc, or aluminium) as the stoichiometric reducing agent.³ These catalysis are driven by a catalytic redox-cycle in which the active metal complex, for example Cp_2TiCl_2 is reduced to the active state, $\text{Cp}_2\text{Ti(III)Cl}$ by the stoichiometric reducing agent (Mn or Zn). In the new oxidation state $\text{Cp}_2\text{Ti(III)Cl}$ is able to promote ET reaction, going back to Ti(IV). Normally, to liberate Ti(IV) and allowing the turn-over of the catalyst scavengers are used. When the $\text{Cp}_2\text{Ti(III)Cl}$ is applied in promoting pinacol coupling, strong Ti-O bonds are formed, and, in the presence of silylating agent such as Me_3SiCl , the strong Ti-O bond is cleaved by the formation of a new silylated species containing the fragment OSiMe_3 . The silylating agent is a scavenger of the reaction and is able to make possible to the active metal to restart a reduction. The stoichiometric metals employed in the reaction are not interfering and are, generally not able to induce fast pinacol coupling. Instead, the reduction of the active metal complexes is more rapid. It is possible to use other scavengers for catalytic redox reactions, such as lutidium hydrochlorides, Cp_2ZrCl_2 , or acylating agents. In the presence of a scavenger the Cp_2TiCl_2 molecule is restored and can undergoes a new reduction by the metal present in the reaction conditions. In Figure 1 the process is illustrated in general.

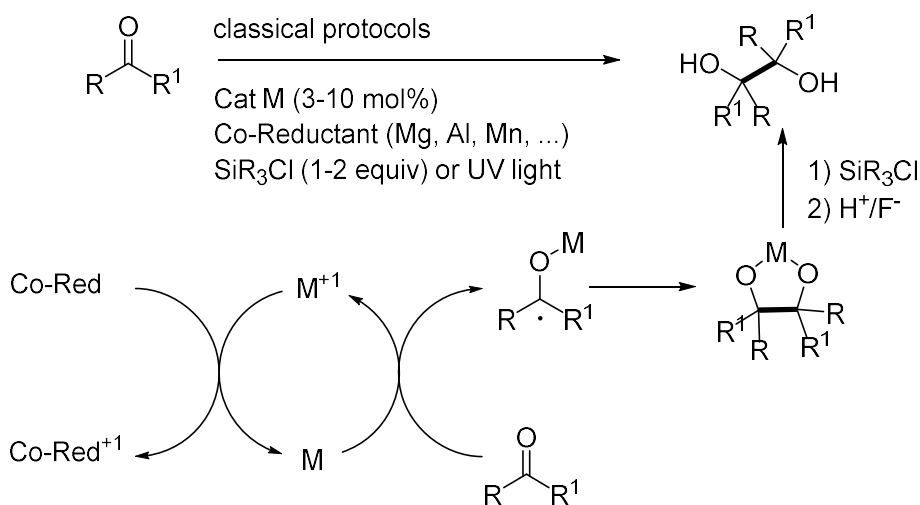


Figure 1 Classical protocols for the reductive dimerization of aldehyde and ketones.

Considering the cost of metal catalysts, by the employment as co-reducing metals in stoichiometric amount and the use of a scavenger, these classical protocol for the synthesis of diols are not sustainable anymore, as the production of waste.

2.1.2 Pinacol coupling reactions by visible light photoredox catalysis

As the pinacol coupling is produced from the corresponding ketyl radicals, a possible solution of the synthesis of pinacol can consist in the formation of the ketyl radical and its dimerization. Ketyl radicals are accessible by photoredox catalysis.⁴ Various photoredox methodologies were developed to produce and react ketyl radicals by the use of photoredox conditions: the generation of ketyl radical anions through a photoredox catalysed reduction of aldehydes, imines and ketones allows a straightforward access to the synthesis of diols, diamines and amino alcohols (Figure 2).

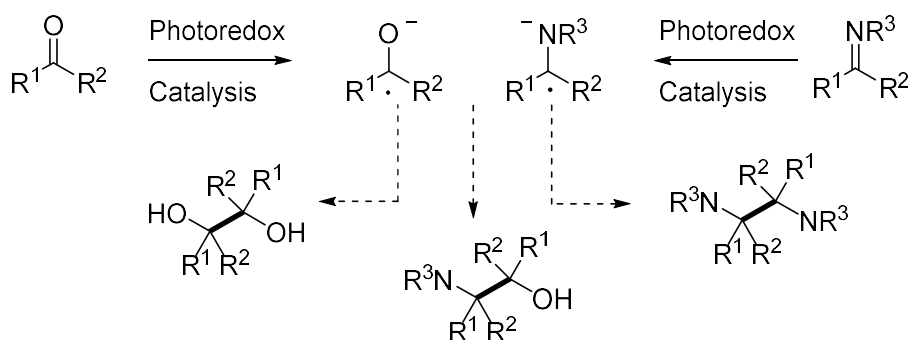


Figure 2 Synthesis of diols, imines and amino alcohols using the photoredox catalysis.

The first attempts of ketyl radical formation by photocatalysis were conducted on benzaldehyde derivatives and concerned the reduction to the corresponding alcohol mediated by $Ru(bpy)_3^{2+}$ and the dimerization of benzaldehyde employing poly(p-phenylene) (PPP) as an effective photocatalyst and the nicotinamide derivate BNAH (Figure 3).⁵

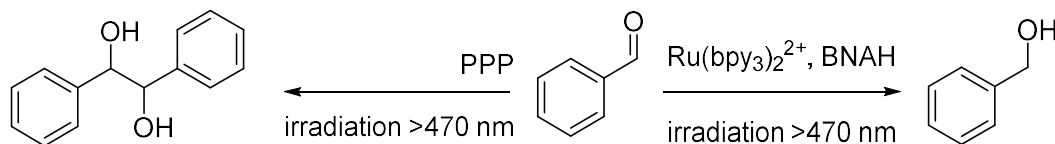


Figure 3 Reduction and dimerization processes of benzaldehyde mediated by photoredox catalysis.

In the last decades, ketyl radical anions obtained through photoredox catalysis were efficiently exploited in intra- and intermolecular coupling reactions with other functional groups and radical

species. For instance, Ollivier *et al.* generated ketyl radical anions from epoxides and aziridines to create a new C-C bond through a tandem radical-opening⁶ and allylation reaction, while efficient [2+2] cycloadditions of enones using Ru(bpy)₃²⁺ as photocatalyst were reported by Yoon.⁷ More recently, Rueping *et al.* reported the first example of a pinacol coupling reaction mediated by photoredox catalysis for a wide range of aldehydes, ketones, and imines (Figure 4).⁸

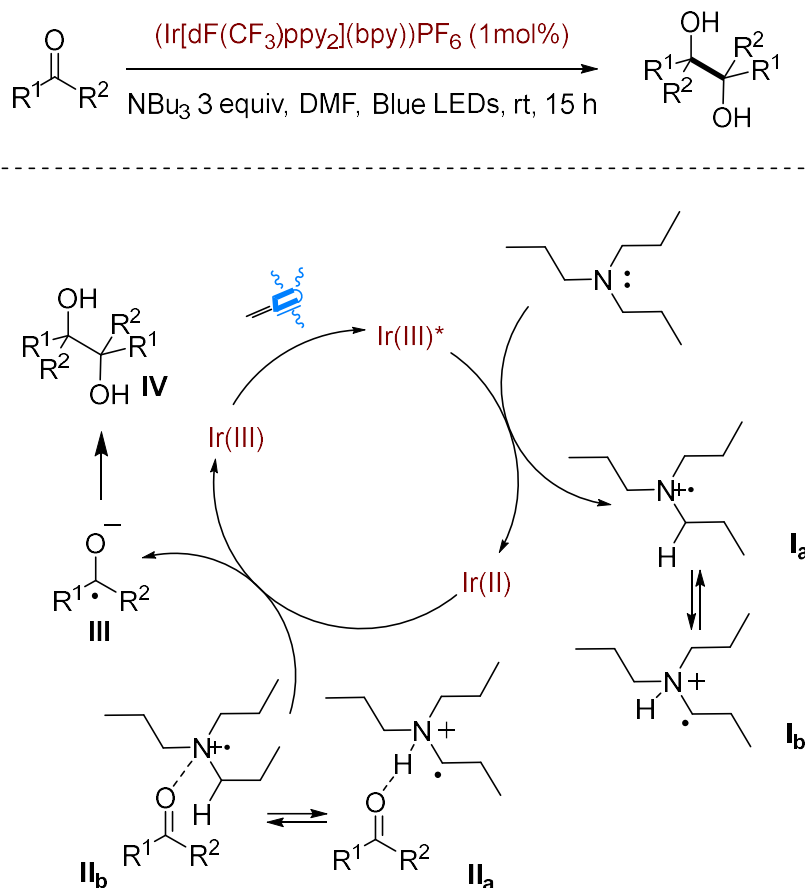


Figure 4 Photoredox catalysis of pinacol coupling reactions of aldehydes mediated by Iridium complexes.

The Ir(III)* species, generated by photoexcitation of an Ir(III) complex, is reduced by the presence of Et₃N as a sacrificial agent to give the Ir(II) and radical cation **I_{a-b}**. The Ir(II) species is responsible for the reduction of carbonyl groups **II_{a-b}** generating the radical **III** which undergoes a dimerization to achieve the diol **IV**. Interestingly, in order to explain the effective coupling of aromatic substrates with a reduction potential close to -2 V, Rueping have demonstrated that the carbonyl compounds are activated for the reduction by the coordination with the so-formed radical cation Et₃N^{•+} (**I_{a-b}**). This specie is acting as a Lewis acid and by a coordination with the carbonyl oxygen (species **II_{a-b}**) is making the process exoergonic lowering the reduction potential of the carbonyl. In this reactions, the

presence of Brønsted or Lewis acids is fundamental to activate the carbonyl compounds considering the reduction potential of Ir(II) species ($E_{1/2}^{\text{red}} = -1.69 \text{ V vs Fc}$) compared with the reduction potentials of aldehydes, ketones and imines ranging from -1.66 to -2.5 V as reported by Nicewicz and co-workers (Figure 5).⁹

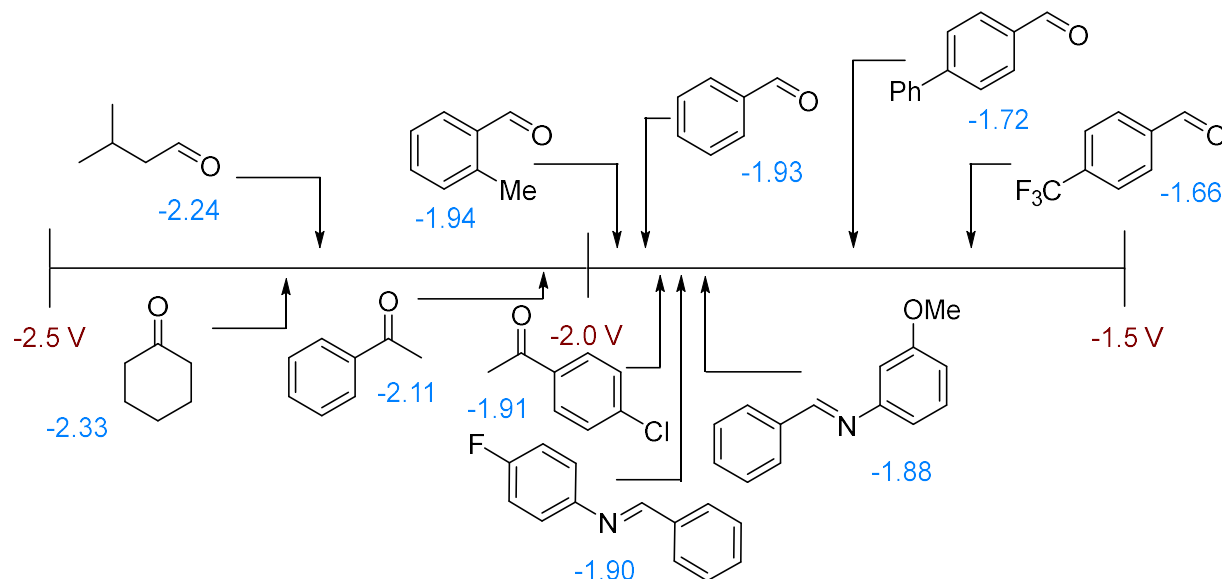


Figure 5 Electrochemical series of aldehydes, ketones and imines; potentials are reported against SCE.

A metal free version of photoredox pinacol coupling of carbonyl compounds is described by Sudo *et al.*¹⁰ In this work, the coupling of several aromatic aldehydes and imines, mediated by perylene, a simple polyaromatic hydrocarbon, was carried out using visible light emitted by a white LEDs energy source (Figure 6).

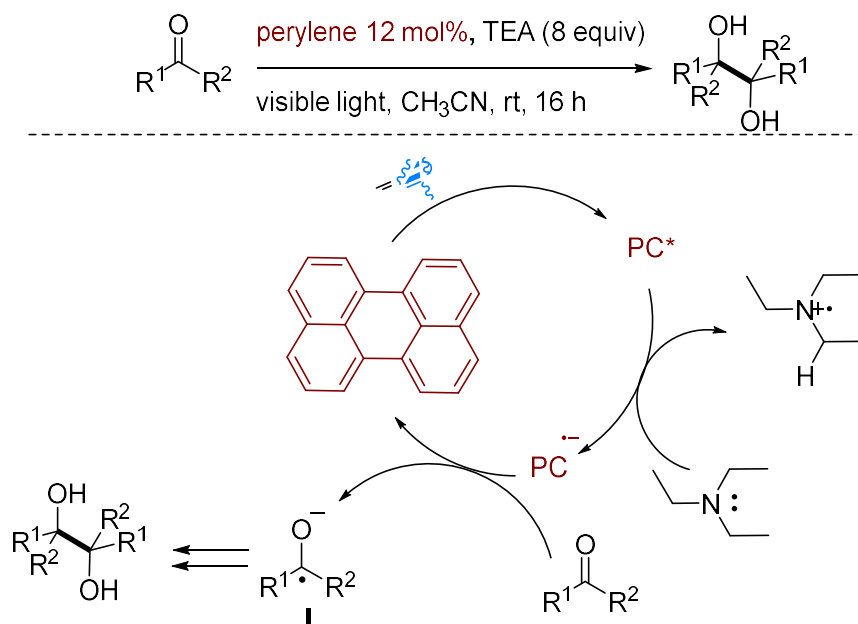


Figure 6 Metal free version of photoredox catalysis using aldehydes as substrates.

After the reduction of PC* in the excited state with Et₃N as the sacrificial agent, the radical anion PC^{•-} ($E_{1/2}^{\text{red}} = -2.23 \text{ V vs Fc}$)¹¹ is capable of single electron transfer to the carbonyl species yielding the ketyl radical anion I intermediate. Pinacol coupling products are obtained in fair yields (67% at best) while ketones did not react because of their high reduction potential (acetophenone $E_{1/2}^{\text{red}} = -2.48 \text{ V vs Fc}$).¹² In the end, further studies by Rueping and co-workers have demonstrated a new photocatalytic method for the synthesis of unsymmetric 1,2-diamines. Generation of intermediary ketyl and α -amino radical anions by visible light photoredox catalysis allowed coupling of a wide range of aldimines with aniline derivatives (Figure 7).

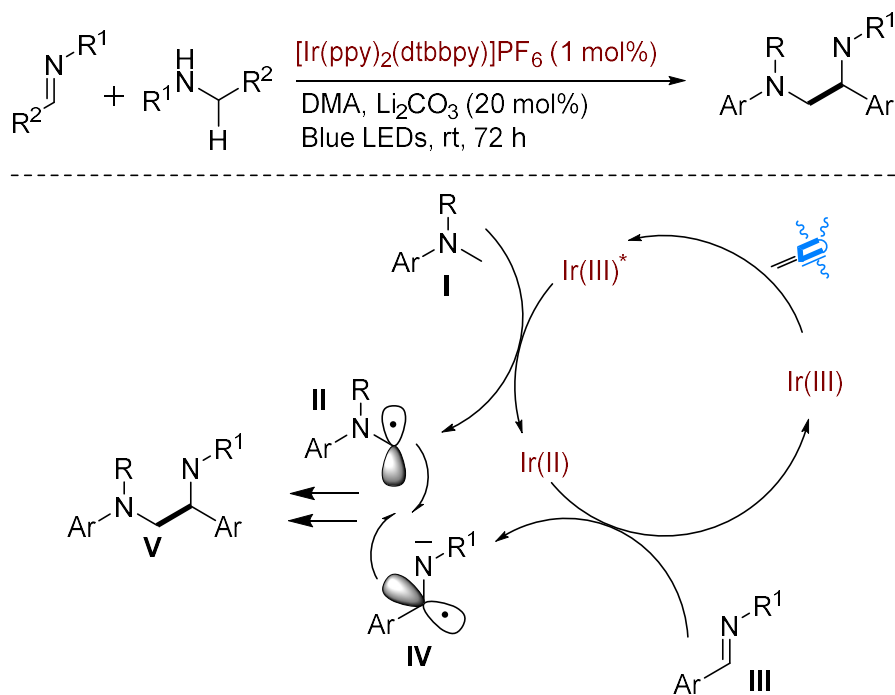


Figure 7 Photoredox catalysis of unsymmetric 1-2 diamines mediated by iridium complexes.

Single electron transfer (SET) oxidation of the alkyl amine **I** to Ir(III)^* in the excited state generates the α -amino radical anion **II** and the reduced Ir(II) species. The SET from Ir(II) to the imine **III** gives the ketyl radical anion **IV** which undergoes radical recombination with α -amino radical anion **II** achieving the unsymmetric 1,2-diamines **V**.

This methodology has also successfully provided 1,2-amino alcohols in good yields by the coupling of several benzaldehyde derivatives with *N,N*-dimethyl-4-methylaniline. Unfortunately, this approach cannot be applied to cyclic and aryl ketones.¹³

2.1.3 Use of coumarin dyes as photocatalysts

In order to develop new alternatives to the expensive but widely used Ru(II) - and Ir(II) - complexes, we focused our attention on organic dyes and in particular coumarins. As reported in chapter 1, coumarin dyes have been largely employed in several fields such as fluorescent labeling of biomolecules,¹⁴ laser dyes,¹⁵ emitting materials in organic light-emitting diodes (OLED)¹⁶ and solar cell applications.¹⁷ To the best of our knowledge, their systematic employment in photoredox reactions has not been explored yet. In addition, their low molecular weight and their straightforward synthesis gives the possibility of varying their photophysical and redox properties, allowing a wide range of photoredox potentials to be covered. With all these potentialities, the coumarin class attracted our interest for photoredox catalytic applications.

Numerous synthetic approaches have been reported for the synthesis of coumarin derivatives. Pechmann condensation,¹⁸ Knoevenagel condensation¹⁹ and Perkin reaction²⁰ are the most classical synthetic methods (Figure 8).

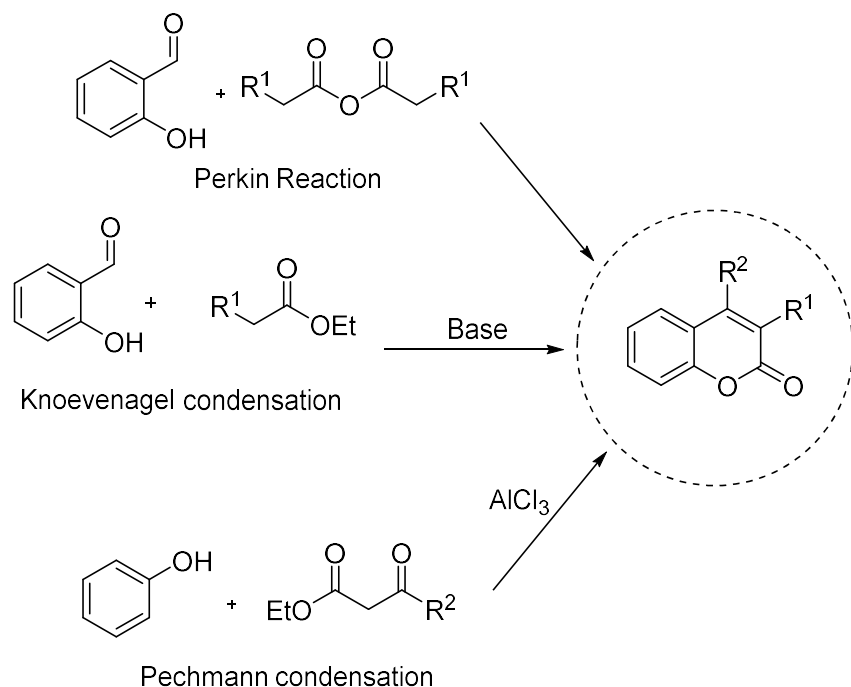


Figure 8 Different approaches for the synthesis of the coumarins

Perkin reaction for the synthesis of coumarin is carried out through the heating of the 2-hydroxybenzaldehyde with an acetic anhydride derivative at a high temperature and subsequent irradiation or treatment with iodine to promote the cyclization. The yields are generally poor. The Knoevenagel condensation, between benzaldehydes with activated methylene compounds in the presence of an amine, is used to overcome the inherent difficulties associated with the Perkin reaction. Instead, the Pechmann condensation is a widely used method for the synthesis of 4-substituted coumarin. The reaction takes place in the presence of phenol, a β -oxo ester and a catalyst such as aluminium trichloride.

In this chapter, we will discuss the application of coumarin dyes as photocatalyst in the pinacol coupling reaction using several aromatic aldehydes, ketones and imines as the substrates.

2.2 Results and discussion

2.2.1 Initial investigations

For this initial investigation, we decided to employ commercially available and readily synthesized coumarin dyes capable of absorbing in the visible light region dyes in the pinacol coupling of 4-chlorobenzaldehyde, as the model substrate. These test-reactions were conducted overnight in the presence of triethylamine as a sacrificial reducing agent, dry DMF and under Blue LEDs irradiation. Among the coumarin dyes tested in the model reaction, only few were active, with compounds **3**, **4** and **5** being the best performing photocatalysts (Figure 9).

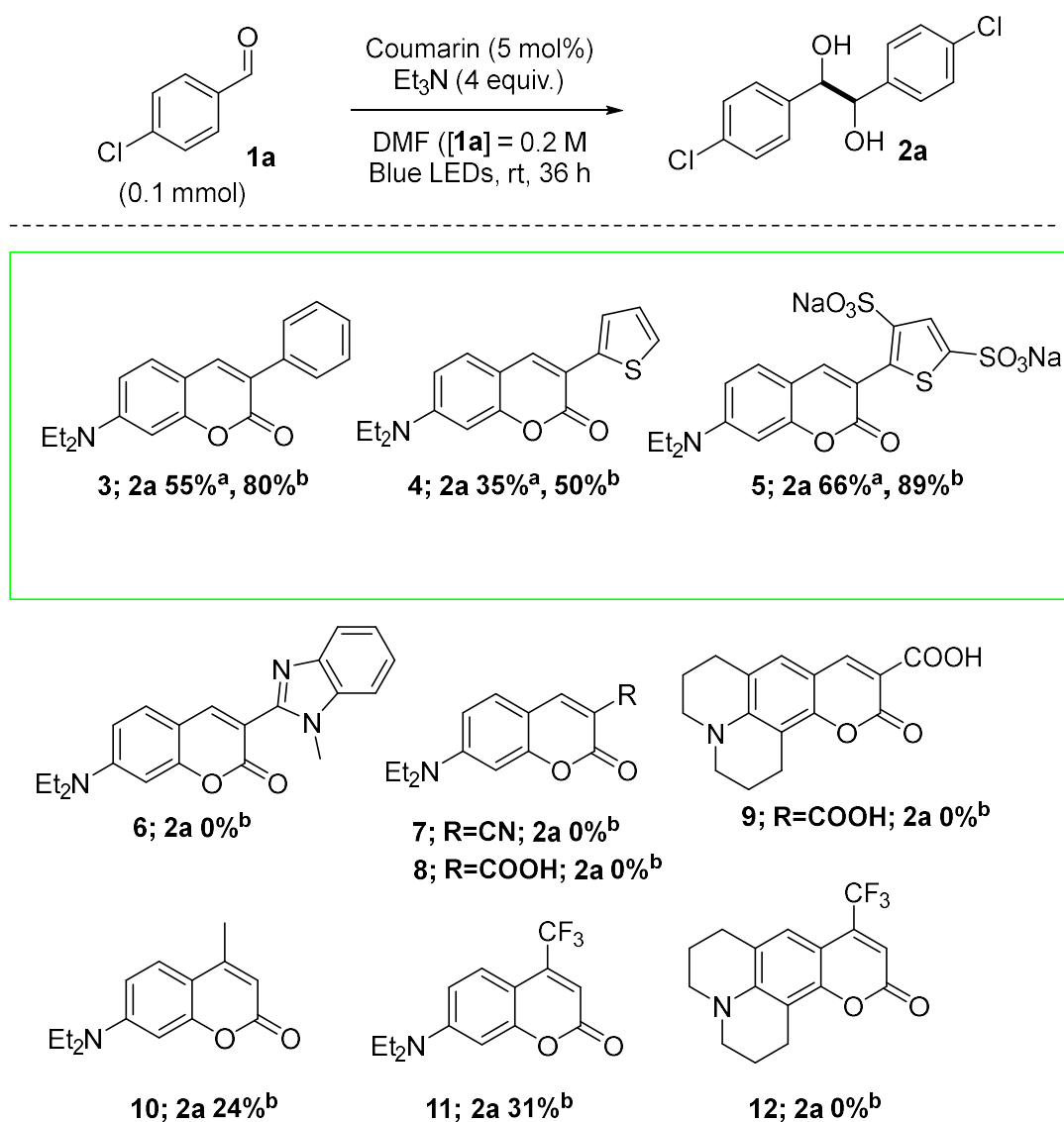


Figure 9 Screening of coumarin derivatives in the photocatalytic pinacol coupling reaction. ^a Yield after chromatographic purification ^b Conversion ratio determined by ¹H-NMR analysis.

The molecular structure of the active coumarin photocatalysts is characterized by the presence of a diethylamino group in position 7 and phenyl (**3**) or thienyl (**4-5**) groups in position 3 of the coumarin core. In particular, 7-amino-3-thienyl coumarin derivate **5** gave the product **2a** in a 66% isolated yield. Photocatalysts differently substituted including 3-imidazolyl (**6**), 3-cyano (**7**) and 3-carboxylic acid (**8**) coumarin derivatives proved to be completely inactive while the presence of methyl and trifluoromethyl substituents in position 4 gave poor yields (**10-12**) or no trace of products (**11**).

2.2.2 Synthesis of coumarin dyes **3,4,5** and photophysical properties

Compounds **3**, **4** and **5** are readily prepared. The synthesis of compound **3** was carried out by a palladium catalyzed decarboxylative arylation of commercially available 7-(diethylamino)coumarin-3-carboxylic acid with phenyliodide in a 57% yield (Figure 10).²¹

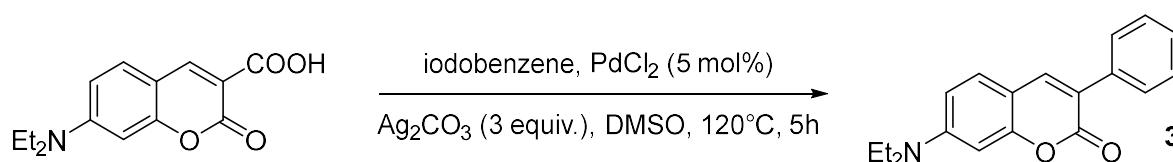


Figure 10 Synthesis of compound **3**.

3-thienyl coumarin **4** was obtained in 46% isolated yield by reaction of (diethylamino)-salicylaldehyde with thiophene acetic acid, performing the reaction with acetic anhydride and triethyl amine. A straightforward sulfonation of **4** with a sulfur trioxide N,N-dimethylformamide complex in DMF gave the desired product **5** in 33% yield after purification by reverse phase chromatography (Figure 11).

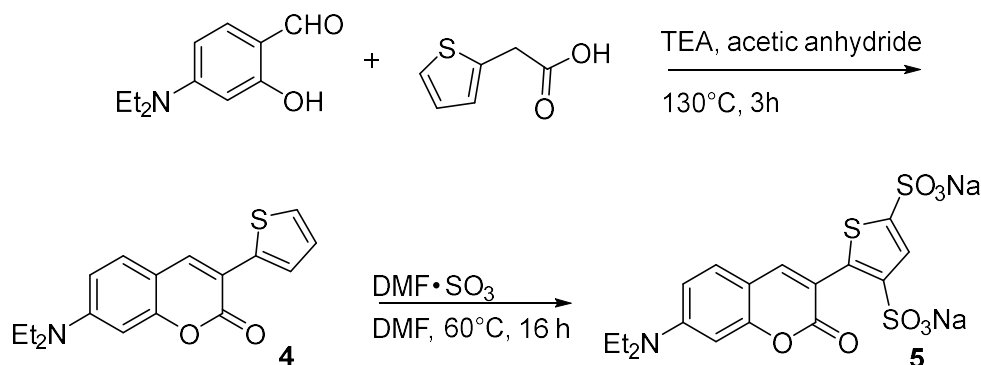


Figure 11 Synthesis of compounds **4** and **5**.

Because of the promising results as photoreductants, the photophysical and electrochemical properties of compounds **3**, **4** and **5** were determined.

From a photophysical point of view, coumarin dyes **3**, **4** and **5** are fairly similar. They are good light absorbers (molar extinction coefficient of $30000 \text{ M}^{-1} \text{ cm}^{-1}$ in DMF), show absorption maxima near 400 nm and strongly emit around 500 nm with good quantum yields and lifetimes of 3.0 ns circa (Figure 12).

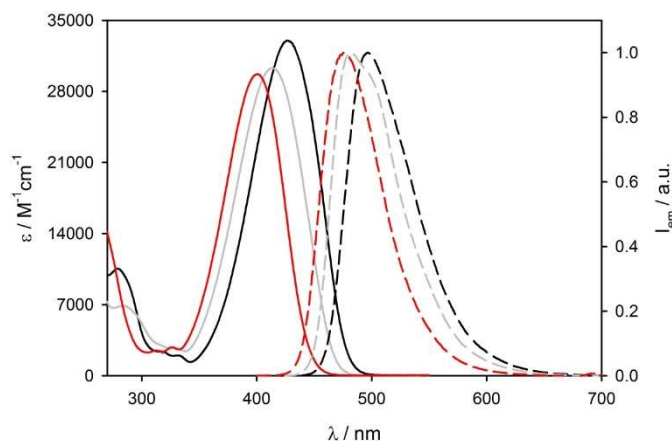


Figure 12 Absorption (left, solid lines) and emission spectra (right, dashed lines) of **3** (red line), **4** (black line) and **5** (gray line) in DMF solution at 298 K. $\lambda_{\text{ex}} = 400 \text{ nm}$.

Regarding the electrochemical aspects, cyclic voltammetry studies were carried out and provided data about ground state and excited state potentials. The greater stability of the oxidized species of **5** compared to that of **4** may be responsible for the better efficiency of the catalyst. Interestingly, excited state reduction potentials ($E(\text{A}^+/\text{A}^*)$) of about -1.88 V vs SCE more negative respect to $\text{Ir}[\text{dF}(\text{CF}_3)\text{ppy}_2](\text{bpy})\text{PF}_6$ (-1.69 V vs SCE) used by Rueping in his studies previously discussed in section 2.1.2 (Table 1).

ENTRY	ABSORPTION		EMISSION			ELECTROCHEMISTRY		
	λ (NM)	ϵ ($\text{M}^{-1} \text{ CM}^{-1}$)	λ (NM)	Φ_{EM}	τ (NS)	E_{00} (EV)	$E(\text{A}^+/\text{A})$ (V)	$E(\text{A}^+/\text{A}^*)$ (V)
3	400	2.97	476	0.82	3.0	2.79	+0.92	-1.87
4	427	3.30	497	0.50	3.3	2.66	+0.79	-1.87
5	413	3.03	482	0.57	2.9	2.72	+0.83	-1.89

Table 1 Photophysical and electrochemical properties ($E_{1/2}$ in V vs. SCE) of coumarins **3**, **4** and **5** in DMF solution at 298 K.

Examples of organic photocatalysts with comparable reduction potentials were reported by Miyake, but not used in pinacol coupling.²² In the introduction, we have reported the interesting studies of Murphy with strong organic photoreductant.²³ It is worth adding that the strong organic reductant introduced by Murphy has in most of cases lower reduction potential compared to coumarins, and are quite unstable and difficult to handle.

2.2.3 Reaction Optimization

Subsequently, optimization of the reaction conditions was carried out. Due to superior in the coupling of chlorobenzaldehyde, we chose coumarin **5** in the optimization attempts.

The reaction conditions were optimized by screening several parameters including solvents, sacrificial agents, presence of additives, and reaction times (Table 2).

Entry ^[a]	Sacrificial Agent	Solvent	Additives	Conversion (%) ^b
1	TEA	DMF	-	89
2	Bu ₃ N	DMF	-	67
3	N,N-Dimethylaniline	DMF	-	6
4	4-Methoxy aniline	DMF	-	0
5	Sodium Ascorbate	DMF/H ₂ O	-	0
6	TEA	CH ₃ CN	-	37
7	TEA	DCE	-	0
8	TEA	THF	-	0
9	TEA	DMSO	-	66
10	TEA	EtOH	-	0
11	TEA	DMF/H ₂ O	-	0
12	TEA	DMF	TMSCl ^c	29
13	TEA	DMF	Colloidine HCl ^c	30
14	TEA	DMF	Oxalic Acid ^d	49
15 ^e	TEA	DMF	-	65
16 ^f	TEA	DMF	-	69
17	TEA	DMF	-	52

Table 2 Screening of parameters (bases, solvents, additives, photocatalyst loading and reaction times in the photocatalytic pinacol coupling of aldehyde **1a**. ^aReaction conditions: **1a** (0.1 mmol), sacrificial agent (4 equivalents), **5** (5 mmol%), [**1a**]=0.2M, Blue LEDs, room temperature, 36h; ^b Determined by ¹H-NMR analysis; ^c Additive (1 equivalent); ^dAdditive (20 mol%); ^e Reaction performed using 1 mmol% of **5** ^f Reaction performed using 2.5 mmol% of **5**.

Triethylamine proved to be the best base as sacrificial agent (Entry 1) giving an excellent 89% conversion while tributylamine, previously used in photoredox catalysis mediated by iridium complexes, showed a conversion of 67% (Entry 2) in our hands. Use of other bases including aromatic amines (Entry 3-4) and inorganic salts such as sodium ascorbate (Entry 5) did not give any reaction. Particularly, cheap and available ascorbate salts were proven to be quite insoluble in the reaction media. Despite several aprotic polar solvents gave good results (Entry 6-9), none of them reach the level of DMF; in other types of solvents no reaction (Entry 10-11) was observed. The addition of Brønsted acids such as oxalic acid (Entry 12), used by Rueping to increase the yield or trimethylsilyl chloride (Entry 13) and collidine (Entry 14), employed as carbonyl activators, also did not afford any improvement. Studies on the effect of the photocatalyst loading (Entry 15-16) and reaction times (Entry 17) demonstrated that the best conversion was obtained using 5 mmol% of photocatalyst conducting the reaction over 36 hours.

Among the performed attempts, the conditions shown in entry 1 proved to be the best. These reaction conditions were further used in the screening of other carbonyl substrates.

2.2.4 Substrates scope

Next, substrate scope was investigated by screening a wide range of aromatic aldehydes on a 0.2 mmol substrate scale (Figure 13).

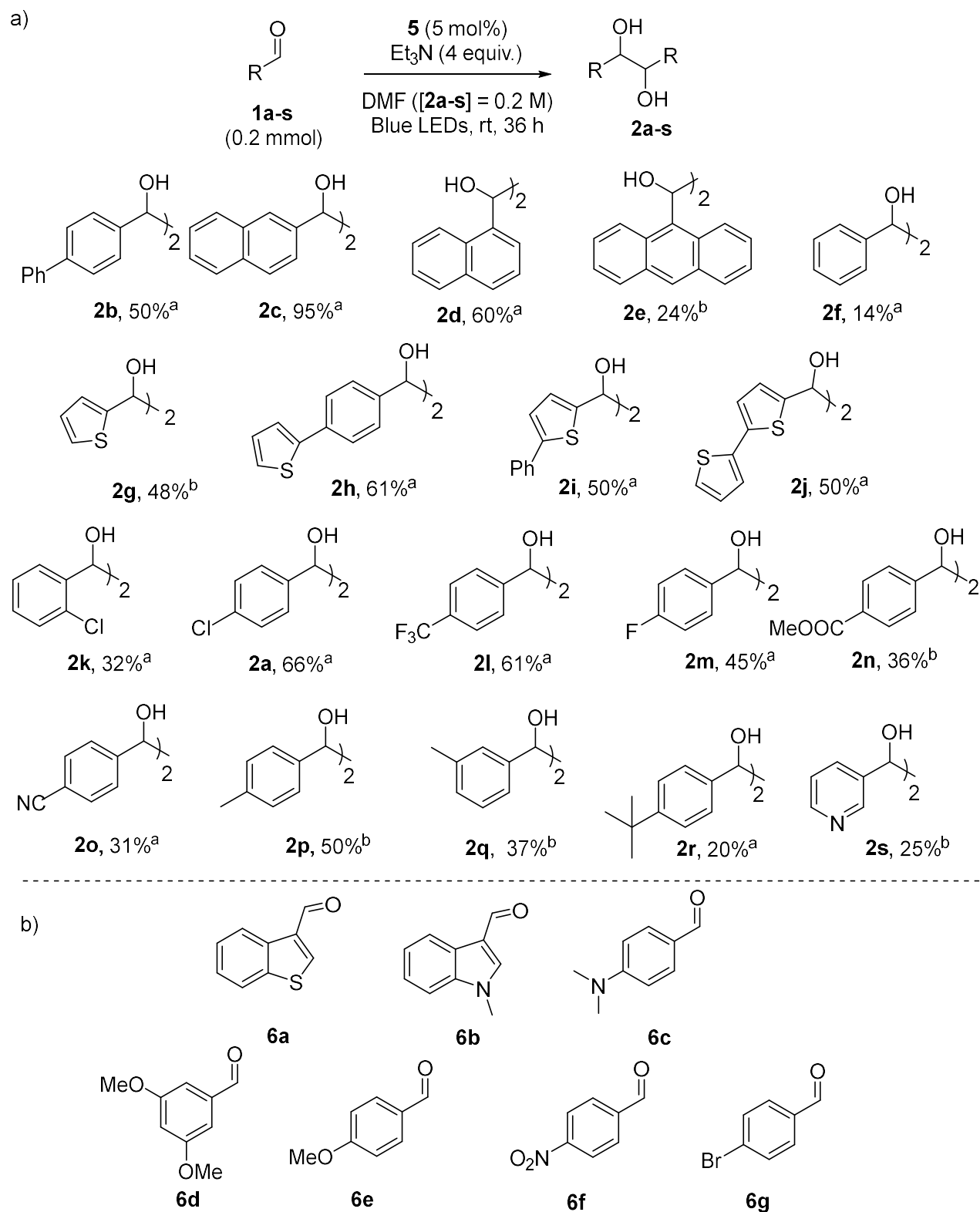


Figure 13 a) Pinacol coupling of selected aldehydes (yields after chromatographic purification) b) Non reactive substrates tested in the photocatalytic pinacol coupling reaction. ^a Yield after chromatographic purification ^b Determined by ¹H-NMR analysis.

The best results were achieved using 2-naphthaldehyde **1c**. The desired product was isolated in an excellent yield of 97%. Good yields were obtained in the presence of biphenyl (**2b**) and 1-naphthyl (**2d**) substituents. This is probably due to a better stabilization of the ketyl radical intermediate that does not allow back electron transfer processes. The poor yield for anthranyl (**2e**) and phenyl (**2f**) derivatives is presumably attributed to steric hindrance (**2e**) and high reduction potential (**1f** -1.93 V vs SCE), respectively. The presence of thienyl group is well tolerated (**2g-j**). Substrates bearing withdrawing groups including chlorine (**2a-2k**), trifluoromethyl (**2l**), fluorine (**3m**), ester (**3n**) and cyano (**3o**) provided moderate to good yields. In the case of isomers **2a** and **2k**, *para*- position of chlorine atom on the aromatic ring influences the reaction efficiency probably because it lowers the reduction potentials with respect to *ortho*- substituted ones. This reason could also explain the different performance of 4-methyl (**1p**) and 3-methyl (**1q**) aldehyde derivatives. Unfortunately, this methodology cannot be extended to a widespread class of aromatic aldehydes: benzothienyl (**6a**) and indolyl (**6b**) groups were completely unreactive. The presence of electron donating substituents including alkylamine (**6c**) and methoxy (**6d-e**) is not tolerated. The use of *p*-nitrobenzaldehyde (**6f**) gave the formation of side-products which were not further investigated. *p*-bromobenzaldehyde (**6g**) furnished products of dehalogenation in accordance to the literature.²⁴

Considering the good results obtained, we tested the developed methodology on the synthesis of unsymmetrical diols.

2.2.5 Pinacol cross coupling towards unsymmetrical diols

We attempted to perform the pinacol cross coupling reaction of 4-chloro benzaldehyde (**2a**) with other aromatic aldehydes. We decided to employ 2-naphthyl (**2c**) and diphenyl (**2b**) aldehydes which gave good results in the homo-coupling reactions and less reactive aldehydes including *p*-cyano (**2o**) and *p*-methoxy (**6e**) benzaldehydes. Substrates **2o** and **6e** were used in excess because of their observed low reactivity in the homo-coupling reaction (Figure 14).

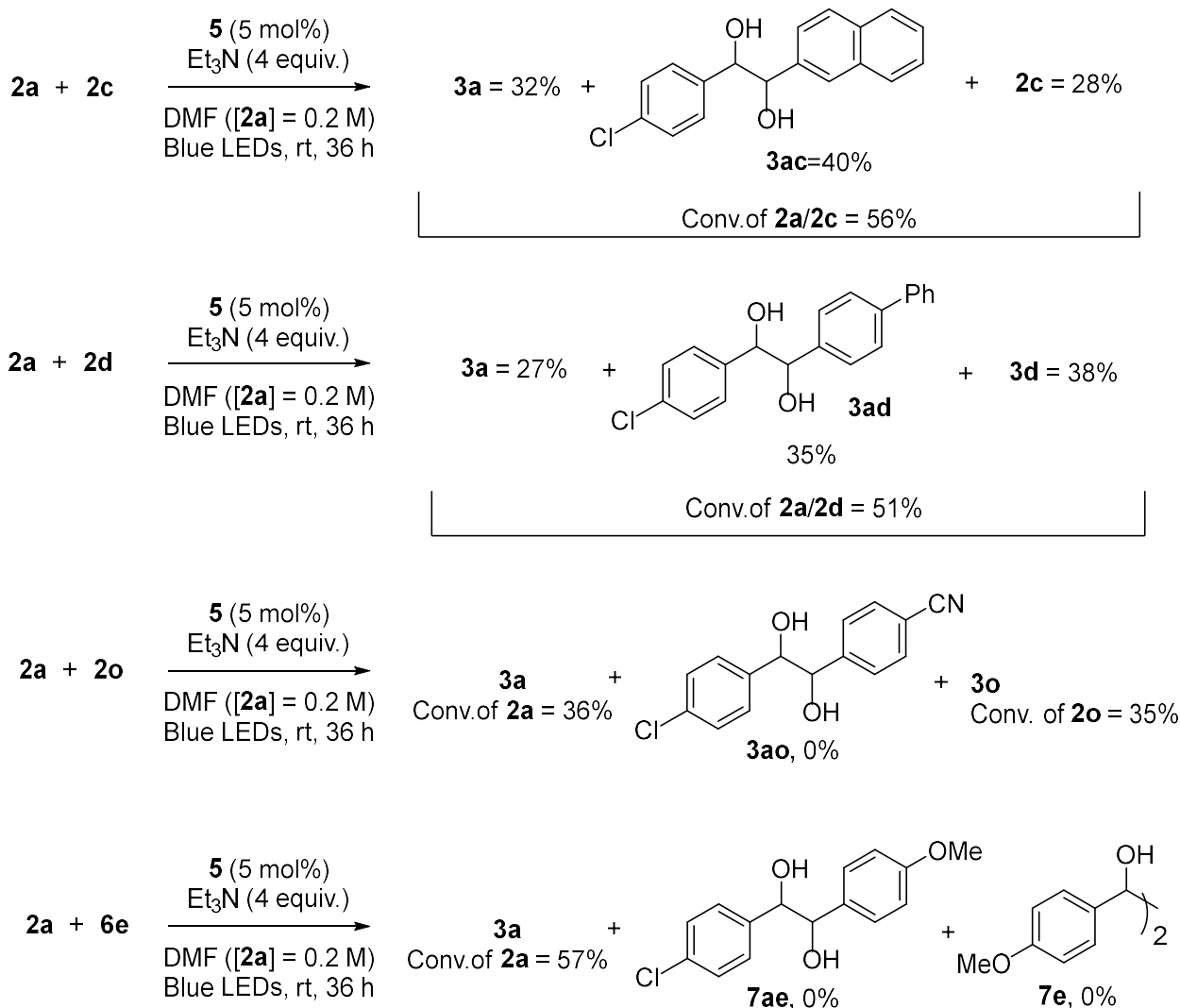


Figure 14 Attempts to perform cross pinacol coupling reaction; Reactions were performed using 0.1 mmol of aldehydes. Substrates **2o** and **6e** were used in excess (0.3mmol). Conversions and ratios determined by ^1H - NMR analysis.

In the first two cases cross coupling products **3ac** and **3ad** were obtained as inseparable mixtures with homo-coupling products while in the latter two cases compounds **3ao** and **7ao** were not observed. Despite the products **3ac** and **3ad** were achieved in moderate conversions, the unsymmetrical synthesis of diols was not further investigated because of the tedious processing to isolate these cross coupled products.

Finally, we investigated the photoredox catalyzed pinacol coupling reaction of other carbonyl species including ketones as well as imines.

2.2.6 Pinacol coupling of ketones and imines

Using the optimized conditions, the pinacol coupling of ketones and imines were attempted.

We were pleased to find that the reaction worked well with benzophenone, a substrate with a particularly high reduction potential (-1.87 V vs SCE) as well as some of its derivatives. The corresponding 1,2-diols were formed in moderate yield (Figure 15). To the best of our knowledge, the pinacol coupling of benzophenone reported by Sudo²⁵ in unsatisfactory yields is the only reported organic photocatalyst mediated example.

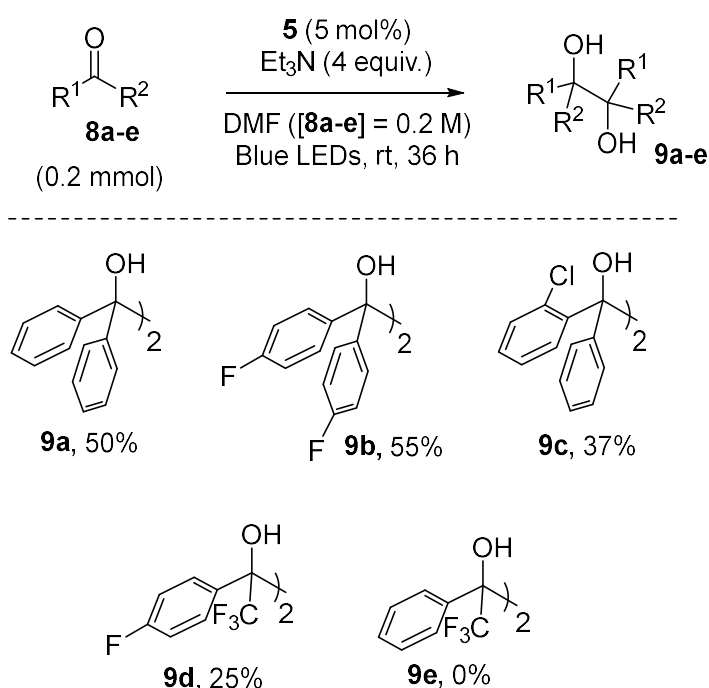


Figure 15 Pinacol coupling of selected ketones, yields after chromatographic purification.

Concerning substrates **9d** and **9e**, ¹⁹F-NMR analysis showed the presence of byproducts **9da** and **9ea** resulting from epoxide formation. In fact, after formation of the ketyl radical anion **I** presumably, ring closure onto the trifluoromethyl carbonatom (**II**) occurs (Figure 16).

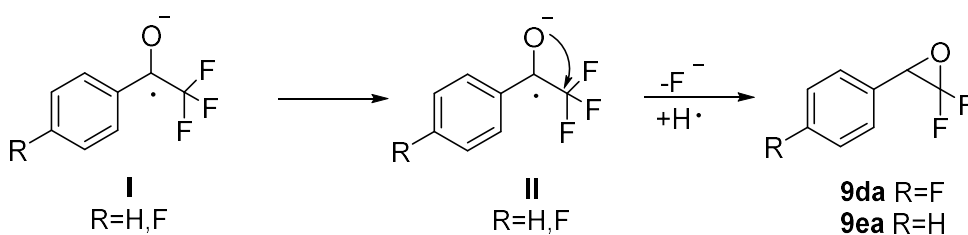


Figure 16 Formation of side-products **9da** and **9ea**.

Imines were also suitable substrates and under the standard reaction conditions, different benzyl and aryl imines reacted in satisfactory yields. Not only was possible to use a cleavable benzyl - protecting group, but chiral benzylimines also were suitable substrates and give access to chiral protected 1,2-diamines (Figure 17).²⁶

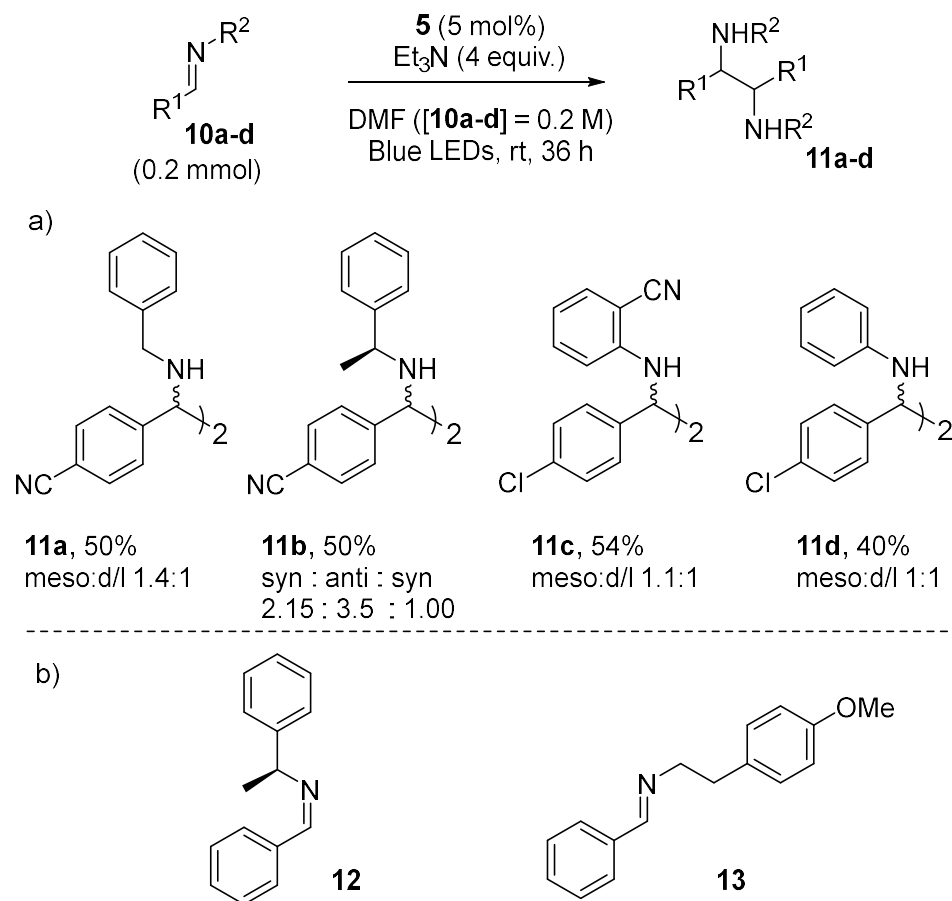


Figure 17 a) Pinacol coupling of selected imines, yields after chromatographic purification b) Non reactive substrates tested in the photocatalytic pinacol coupling reaction.

The presence of electron withdrawing groups including cyano (**11a-b**) and chlorine (**11c-d**) in *para*-position of the aromatic ring is indispensable to decrease the reduction potential of the compound **12** which results completely non-reactive as well as the benzeneethanamine derivative **13**.

The obtained 1-2 diamines gave a diastereomeric ratio of 1:1, in the case of compound **11a** the meso form is slightly favourable. The presence of a stereocenter on compound **11b** gave the formation of three diastereoisomers in a ratio 2.15: 3.50: 1.00.

In the end, investigations about mechanism of the photoredox pinacol coupling reaction mediated by coumarin dye were performed.

2.2.7 Mechanistic investigations

Photochemical studies about the behaviour of the photocatalyst **5** in the pinacol coupling of aldehyde **1a** allowed getting an insight about the role of the coumarin dyes and the mechanism of the process. Absorption spectra of the compound **5** recorded at different times showed an excellent photostability of the photocatalyst during the reaction; only 1% of degradation at the end of irradiation was observed (Figure 18).

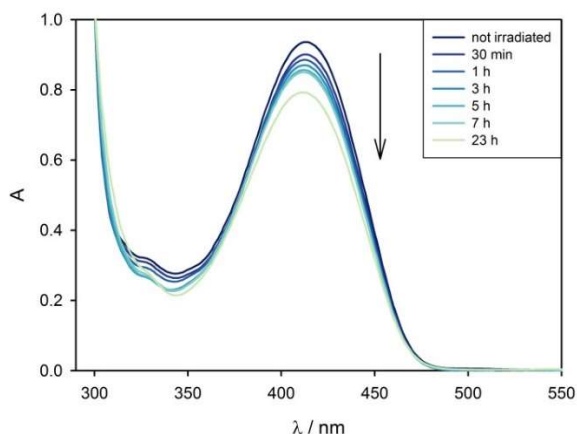


Figure 18 Absorption spectra of coumarin **5** 3.1×10^{-4} M (0.15 mol%) in degassed DMF solution in the presence of aldehyde **1a** 0.21 M and Et₃N 0.8 M upon irradiation at 450 in the time interval 0 – 23 h (left). Optical pathlength = 0.1 cm.

Intensity decay, upon irradiation at 405 nm, in presence and in absence of TEA (0.8 M) showed the independency of the coumarin dye by the sacrificial agent, but it is quenched by aldehydes as it is demonstrated by the Stern-Volmer analysis conducted at different concentrations of aldehydes **1a** and **1c** in the presence of tertiary amine (Figure 19a).

These analyses showed a direct correlation between concentration and quenching process.

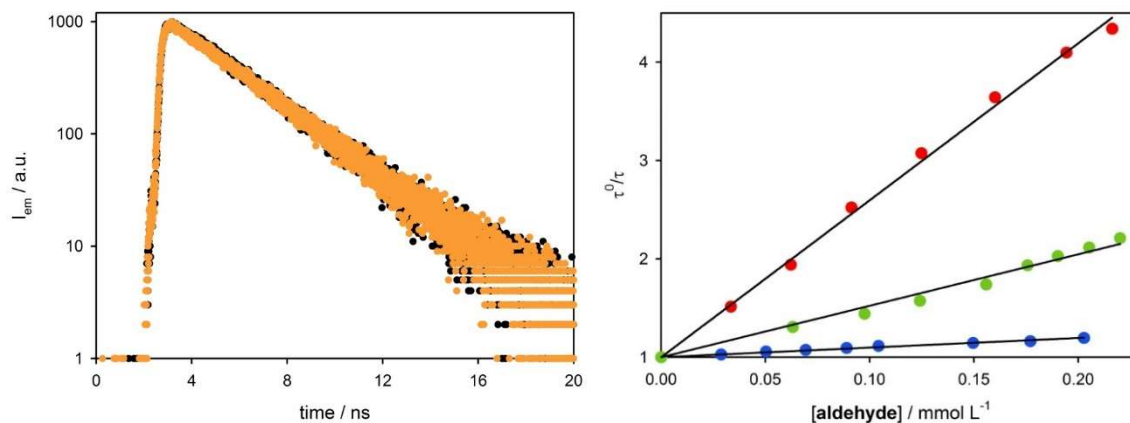


Figure 19 a) Emission intensity decays of **5** in DMF solution in absence (black dots) and in presence of Et₃N 0.8 M (orange dots) upon excitation at 405 nm. b) Emission intensity decays of **10** in DMF solution containing Et₃N 0.8M in the absence (τ^0) and in the presence (τ) of increasing amount of aldehyde **1a** (blue dots) and **1c** (green dots). The slopes represent the Stern-Volmer constant (KSV), i.e. the product of the quenching constant (k_q) and τ .

The Stern-Volmer plots (Figure 19b) show a linear correlation between the ratio τ^0 / τ and the aldehyde concentration, as expected for a dynamic quenching process according to the Stern-Volmer equation:

$$\tau^0 / \tau = 1 + K_{SV} [Q] = k_q \tau^0 [Q]$$

where τ^0 and τ are the lifetimes in the absence and in the presence of the quencher Q (i.e. aldehydes), respectively, K_{SV} is the Stern-Volmer constant and k_q is the quenching constant, the experiments yield the following quenching constants. The analysis of the plots reported above yields the following quenching constants:

$$k_q = 3.1 \times 10^8 \text{ M}^{-1}\text{s}^{-1} \text{ for aldehyde } \mathbf{1a}$$

$$k_q = 1.8 \times 10^9 \text{ M}^{-1}\text{s}^{-1} \text{ for aldehyde } \mathbf{1c}$$

Quenching by energy transfer from the lowest excited state of coumarin to populate the lowest triplet excited state of benzaldehyde is ruled out, being endoergonic. Indeed, the S₁ fluorescent excited states of coumarins shows lower energy than the T₁ excited states of the investigated aldehydes.²⁷ The most plausible quenching mechanism is photoinduced electron transfer from the S₁ excited state of coumarin to aldehydes, yielding the corresponding ketyl radicals.

To discuss thermodynamic aspects of the photoinduced electron transfer we need to consider the reduction potentials of aldehydes and of the S₁ excited state of coumarins, which can be evaluated as follows:

$$E(4^+/*4) = E(4^+/4) - E_{00}(4/*4) = 0.79 - 2.66 = -1.87 \text{ V (vs SCE)}$$

$$E(5^+/*5) = E(5^+/10) - E_{00}(5/*5) = 0.83 - 2.72 = -1.89 \text{ V (vs SCE)}$$

Where the energy difference between the ground and the S1 excited state (E_{00}) was estimated from the fluorescence spectrum (wavelength corresponding to the 20% of the maximum emission intensity).

Studies on the reduction potential of aldehydes in different environments highlighted the importance of the amine in the reaction. In fact, the presence of a Lewis acid markedly affects the reduction potentials of these substrates. Considering a reduction potential of -1.96 V vs SCE for aldehyde **1a**, coordination of a lithium atom on the carbonyl compound decreases the potential value to -1.71 V vs SCE. Thanks to these results, we can suppose that the radical cation Et_3N^+ , afforded by the decomposition of oxidized sacrificial agent, can act as Lewis Acid interacting with the carbonyl group of the aldehydes making it more readily reducible (Table 3).²⁸

Entry	Aldehyde	EtOH/H ₂ O	TBAP/THF (0.5 M) ²⁹	LiClO ₄ /THF (0.5 M)
19	1a	-	-1.94 V	-1.71 V
20	1c	-1.34 V ³⁰	-	-

Table 3 Half-wave reduction potentials ($E_{1/2}$ in V vs SCE) of selected aldehydes in different environment.

This explanation was previously reported by Rueping who, in order to confirm the essential role of the ammonium radical in the reaction, demonstrated how the pinacol coupling is completely suppressed by the presence of a base. In our case, the presence of 20 mol% K_2CO_3 and K_3PO_4 on the standard conditions led to a decrease of conversion. The better results obtained can be explained by the higher reduction potential of coumarin dyes in comparison with the Iridium complex used by Rueping (-1.89 V vs. -1.69 V). The high value of the coumarin probably still favours the reaction that was, however, less efficient, confirming the importance of the Brønsted acidic α -ammonium radical (Table 4).

Entry ^[a]	Coumarin	K_2CO_3	K_3PO_4
21	4	0	0
22	5	16	12

Table 4 Pinacol coupling of aldehyde **1a** using compound **4** and **5** in presence of K_2CO_3 and K_3PO_4 . Based on the photochemical investigations we propose the following reaction mechanism: aldehydes are directly reduced by the photocatalyst in the excited state **I** to form the ketyl radical **II**. This

intermediate is then coupled to another ketyl radical yielding the pinacol product. The oxidized photocatalyst **III** is regenerated by the presence of triethylamine (Figure 20).

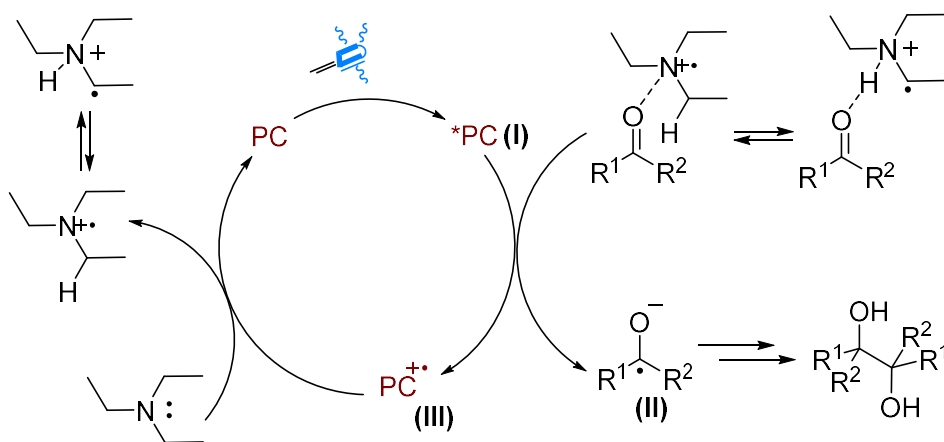


Figure 20 Proposed reaction mechanism for the pinacol coupling reaction.

2.3 Conclusions

In summary, in this chapter I have introduced coumarin dyes as powerful photoreductants in the photoredox catalysis arena. The reaction was effectively promoted and coumarins dyes are able to substitute iridium dyes in this reaction. Quite remarkably, the mechanism of the coupling reaction is completely different from iridium case, as coumarin are able to form the ketyl radical from an oxidative quenching with aldehydes. The sacrificial agent is acting in restoring the organic dye to its ground state. The possibility to apply coumarin in other reaction will be studied further. In addition, as the facile synthesis of coumarins, the possibility of tailoring the redox and photophysical properties of coumarin dyes by introducing different functional groups is useful for extending the application of these dyes to new photocatalytic transformations.

2.4 Experimental procedures

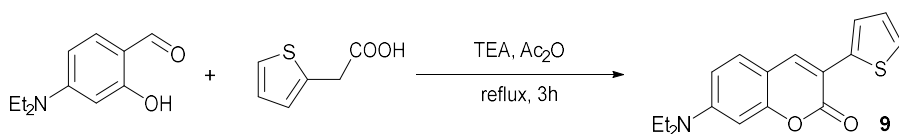
2.4.1 General methods and materials

¹H NMR spectra were recorded on Varian Mercury 400 spectrometer. Chemical shifts are reported in ppm from TMS with the solvent resonance as the internal standard (deuteriochloroform: $\delta = 7.27$ ppm; dimethyl sulfoxide-*d*₆: $\delta = 2.50$ ppm). Data are reported as follows: chemical shift, multiplicity (s = singlet, d = duplet, t = triplet, q = quartet, dd = double duplet, dt = double triplet, bs = broad signal, m = multiplet, quint = quintet), coupling constants (Hz). ¹³C NMR spectra were recorded on Varian MR400 spectrometer. Chemical shifts are reported in ppm from TMS with the solvent as the internal standard (deuteriochloroform: $\delta = 77.0$ ppm; dimethyl sulfoxide-*d*₆: $\delta = 39.5$ ppm). LC-electrospray ionization mass spectra (ESI-MS) were obtained with Agilent Technologies MSD1100 single-quadrupole mass spectrometer. Chromatographic purification was done with 240-400 mesh silica gel. Purification on preparative thin layer chromatography was done on Merck TLC silica gel 60 F₂₅₄.

All reactions were set up under an argon atmosphere in oven-dried glassware using standard Schlenk techniques. Synthesis grade solvents were used as purchased and the reaction mixtures were degassed by four cycles of freeze-pump-thaw.

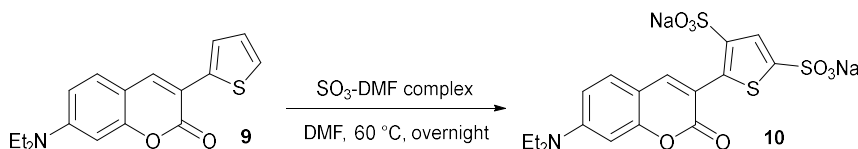
2.4.2 Synthesis of coumarin dyes

Coumarin **3** was prepared according to literature procedure.³¹



Coumarin **4** was prepared using the following procedure. In a one necked round bottom flask (50 mL) equipped with magnetic stirring bar, condenser and glass stoppers, thiophene acetic acid (5.5 mmol, 0.780 mg), 4-(diethylamino)-salicylaldehyde (8.5 mmol, 1.64 g) were dissolved in acetic anhydride (20 mL). Triethylamine (10.5 mmol, 1.46 mL) was added and the mixture was stirred at reflux for three hours. The reaction was cooled down at room temperature, water was added, the organic material was extracted with AcOEt (3 x 50 mL) and the organic layers were dried over Na₂SO₄. Solvent was removed under reduced pressure and the residue was purified by flash column chromatography (SiO₂, cyclohexane to cyclohexane/ethyl acetate, 7/3) to afford **3** as yellow solid (46%, 2.5 mmol, 0.760 g). Spectroscopic properties were according to those reported in literature.

¹H NMR (400 MHz, CDCl₃, 25°C): δ = 7.85 (s, 1H), 7.64 (dd, *J* = 1.1, 3.7 Hz, 1H), 7.33 – 7.27 (m, 2H), 7.07 (dd, *J* = 3.7, 5.1 Hz, 1H), 6.58 (dd, *J* = 2.5, 8.9 Hz, 1H), 6.50 (d, *J* = 2.3 Hz, 1H), 3.40 (q, *J* = 7.1 Hz, 4H), 1.20 (t, *J* = 7.1 Hz, 6H); ¹³C NMR (100 MHz, CDCl₃, 25°C): δ = 160.6, 155.6, 150.6, 137.6, 136.9, 128.9, 127.3, 125.6, 124.8, 114.8, 109.3, 108.8, 97.1, 44.9 (2C), 12.6 (2C).



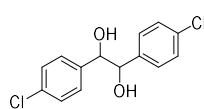
Coumarin **5** was prepared following reported procedure on coumarin **4**. A two necked round bottom flask (100 mL) equipped with stirring bar, glass stopper and vacuum adapter was flame dried under an Argon atmosphere. The flask was charged with **4** (1.2 mmol, 0.360 g) and dissolved in anhydrous N,N-dimethylformamide (30 mL). Sulfur trioxide N,N-dimethylformamide complex (48 mmol, 7.3 g) was added and the reaction mixture was stirred overnight at 60°C under Argon, then cooled to room temperature. Diethyl ether (400 mL) was slowly added under stirring. Two phases were formed: the viscous oil was decanted, and the upper layer was removed. The viscous oil was taken up in aqueous saturated NaHCO₃ (10 mL) and purified by reverse phase chromatography (elution gradient: water to water/acetonitrile 8/2) to give the product as a yellow solid (33%, 0.4 mmol, 0.200 g).

¹H NMR (400 MHz, D₂O, 25°C): δ = 8.10 (s, 1H), 7.69 (s, 1H), 7.31 (d, *J* = 9.0 Hz, 1H), 6.71 (d, *J* = 7.7 Hz, 1H), 6.46 (s, 1H), 3.38 (q, *J* = 6.9 Hz, 5H), 1.14 (t, *J* = 7.0 Hz, 7H); ¹³C NMR (100 MHz, D₂O, 25°C): δ = 162.8, 155.7, 152.0, 146.5, 142.6, 139.5, 139.1, 130.3, 128.4, 110.3, 108.0, 107.6, 96.0, 44.6 (2C), 11.7 (2C).

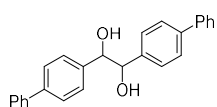
2.4.3 General procedure for photoredox pinacol coupling of aldehyde, ketones and imines.

A dry 10 mL Schlenk tube, equipped with a Rotaflo stopcock, magnetic stirring bar and an argon supply tube, was charged in order and under argon with the photocatalyst **5** (5 mol%, 0.01 mmol, 5.0 mg), substrate (0.2 mmol) and DMF (1.0 mL). The reaction mixture was then subjected to a freeze-pump-thaw procedure (three cycles) and the vessel refilled with argon. Then Et₃N was added (0.8 mmol, 4 equiv., 112 μL). The reaction was irradiated with 16W blue LEDs (approx. 10 cm distance) and stirred for 36 h. After that the reaction mixture was diluted with H₂O (5 mL) extracted with AcOEt (3 x 10 mL). The combined organic layers were washed with brine (10 mL), dried over Na₂SO₄, and the solvent was removed under reduced pressure. Two identical reactions were performed for each substrate and the crudes were reunite before purification. The residue was purified by flash column chromatography (SiO₂) to afford the title compounds in the stated yields.

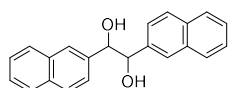
Chapter 2: Photoredox pinacol coupling reactions mediated by coumarins



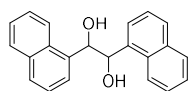
(2a): brown oil; 66% (0.07 mmol, 0.019 g); d.r. = 1.1:1 (*d/l*-**2a**:*meso*-**2a**) was determined by integration of benzylic CH^1H NMR signal. The general procedure was applied using **1a** (0.2 mmol, 0.028 g), **5** (0.01 mmol, 0.005 g) and TEA (0.8 mmol, 112 μL , 4 eq). The title compound was isolated by flash column chromatography (cyclohexane/ethyl acetate, 8/2) as mixture of diastereoisomers in 1.1:1 ratio (*d/l*-**2a**:*meso*-**2a**). ^1H NMR (400 MHz, CDCl_3 , 25°C): $\delta_{d/l,meso} = 7.24$ (*meso*, m, 4H), 7.22–7.17 (*d/l*, m, 4H), 7.11–7.06 (*meso*, m, 4H), 7.03–6.98 (*d/l*, m, 4H), 4.82 (*meso*, s, 2H), 4.60 (*d/l*, s, 2H); ^{13}C NMR (100 MHz, CDCl_3): $\delta_{d/l,meso} = 137.9$ (*meso*, 2C), 137.8 (*d/l*, 2C), 133.8 (4C), 128.4 (*meso*, 4C), 128.3 (*d/l*, 4C), 128.3 (8C), 78.5 (2C), 77.1 (2C); ESI-MS *m/z*: 265.0 [M-OH] $^+$, 305.1 [M+Na] $^+$.



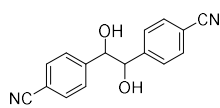
(2b): yellowish solid; 50% (0.05 mmol, 0.018 g); d.r. = 1:1 (*d/l*-**2b**:*meso*-**2b**) was determined by integration of benzylic CH^1H NMR signal. The general procedure was applied using **1b** (0.2 mmol, 0.036 g), **5** (0.01 mmol, 0.005 g) and TEA (0.8 mmol, 112 μL , 4 eq). The title compound was isolated by flash column chromatography (cyclohexane/ethyl acetate, 8/2) as mixture of diastereoisomers in 1:1.7 ratio (*d/l*-**2b**:*meso*-**2b**). ^1H NMR (400 MHz, DMSO-d_6 , 25°C): $\delta_{d/l,meso} = 7.66$ –7.57 (m, 8H), 7.55 (d, $J = 8.2$ Hz, 4H), 7.49 (d, $J = 8.3$ Hz, 6H), 7.46–7.34 (m, 10H), 7.34–7.27 (m, 4H), 7.24 (d, $J = 8.2$ Hz, 4H), 5.40–5.35 (*meso*, m, 2H), 5.29–5.24 (*d/l*, m, 2H), 4.69–4.65 (*meso*, m, 2H), 4.62–4.58 (*d/l*, m, 2H); ^{13}C NMR (100 MHz, DMSO-d_6): $\delta_{d/l,meso} = 142.2$ (4C), 140.3 (4C), 138.8 (4C), 129.3 (*meso*, 2C), 129.2 (*d/l*, 2C), 128.4 (*meso*, 2C), 128.2 (*d/l*, 2C), 127.6 (4C), 126.9 (*meso*, 2C), 126.8 (*d/l*, 2C), 126.1 (*meso*, 2C), 126.0 (*d/l*, 2C), 77.4 (*meso*, 2C), 77.2 (*d/l*, 2C); ESI-MS *m/z*: 349.1 [M-OH] $^+$, 367.3 [M+H] $^+$.



(2c): white solid; 95% (0.095 mmol, 0.029 g); d.r. = 1:2.46 (*d/l*-**2c**:*meso*-**2c**) was determined by integration of benzylic CH^1H NMR signal. The general procedure was applied using **1c** (0.2 mmol, 0.031 g), **5** (0.01 mmol, 0.005 g) and TEA (0.8 mmol, 112 μL , 4 eq). The title compound was isolated by flash column chromatography (cyclohexane/ethyl acetate, 8/2) as mixture of diastereoisomers in 1:2.46 ratio (*d/l*-**2c**:*meso*-**2c**). ^1H NMR (400 MHz, DMSO-d_6 , 25°C): $\delta_{d/l,meso} = 7.89$ –7.77 (m, 8H), 7.77–7.71 (m, 3H), 7.71–7.64 (m, 6H), 7.52–7.44 (m, 3H), 7.44–7.37 (m, 6H), 7.32 (dd, $J = 8.4$, 1.6 Hz, 2H), 5.58–5.53 (*meso*, m, 2H), 5.43–5.40 (*d/l*, m, 2H), 4.93–4.88 (*meso*, m, 2H), 4.85–4.82 (*d/l*, m, 2H); ^{13}C NMR (100 MHz, DMSO-d_6): $\delta_{d/l,meso} = 141.1$ (*meso*, 2C), 140.1 (*d/l*, 2C), 132.5 (*meso*, 2C), 132.4 (*d/l*, 2C), 132.2 (*meso*, 2C), 132.1 (*d/l*, 2C), 127.6 (*meso*, 2C), 127.6 (*d/l*, 2C), 127.4 (*meso*, 2C), 127.3 (*d/l*, 2C), 126.6 (*meso*, 2C), 126.5 (*d/l*, 2C), 126.0 (*meso*, 2C), 125.8 (*d/l*, 2C), 125.7 (*meso*, 2C), 125.7 (*d/l*, 2C), 125.6 (*meso*, 4C), 125.3 (*d/l*, 4C), 77.4 (*meso*, 2C), 77.1 (*d/l*, 2C); ESI-MS *m/z*: 297.1 [M-OH] $^+$, 337.1 [M+Na] $^+$.



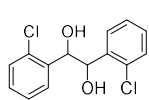
(2d): yellow solid; 60% (0.06 mmol, 0.019 g); d.r. = 1:1 (*d/l*-**2d**:*meso*-**2d**) was determined by integration of benzylic CH^1H NMR signal. The general procedure was applied using **2d** (0.2 mmol, 27 μL), **5** (0.01 mmol, 0.005 g) and TEA (0.8 mmol, 112 μL , 4 eq). The title compound was isolated by flash column chromatography (cyclohexane/ethyl acetate, 3/1) as mixture of diastereoisomers in 1:2.6 ratio (*d/l*-**2d**:*meso*-**2d**). ^1H NMR (400 MHz, DMSO-d_6 , 25°C): $\delta_{d/l,meso} = 8.13$ (*d/l*, d, $J = 8.2$ Hz, 2H), 8.04 (*meso*, d, $J = 8.4$ Hz, 2H), 7.89 (*d/l*, d, $J = 8.0$ Hz, 2H), 7.79–7.74 (m, 4H), 7.64–7.59 (m, 4H), 7.48–7.26 (m, 14H), 5.67 (*meso*, s, 2H), 5.63 (*d/l*, s, 2H); 5.57 (*meso*, s, 2H), 5.42 (*d/l*, s, 2H); ^{13}C NMR (100 MHz, CDCl_3 , 25°C): $\delta_{d/l,meso} = 136.0$ (*meso*, 2C), 135.8 (*d/l*, 2C), 133.6 (*meso*, 2C), 133.5 (*d/l*, 2C), 131.4 (*d/l*, 2C), 130.8 (*meso*, 2C), 128.7 (*d/l*, 2C), 128.6 (*meso*, 2C), 128.5 (4C), 125.9 (*d/l*, 2C), 125.7 (*meso*, 2C), 125.4 (*d/l*, 2C), 125.3 (*meso*, 2C), 125.1 (*d/l*, 2C), 125.0 (*meso*, 2C), 124.9 (*d/l*, 2C), 124.8 (*meso*, 2C), 123.1 (*d/l*, 2C), 123.0 (*meso*, 2C), 74.4 (*meso*, 2C), 74.2 (*d/l*, 2C); ESI-MS *m/z*: 297.1 [M-OH] $^+$, 337.1 [M+Na] $^+$.



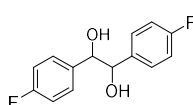
(7e): yellowish sticky solid; 31% (0.03 mmol, 0.008 g); d.r. = 1.1:1 (*d/l*-**7e**:*meso*-**7e**) was determined by integration of benzylic CH^1H NMR signal. The general procedure was applied using **6e** (0.2 mmol, 0.026 g), **10** (0.01 mmol, 0.005 g) and TEA (0.8 mmol, 112 μL , 4 eq). The title compound was isolated by flash column chromatography (cyclohexane/ethyl acetate, 8/2) as mixture of diastereoisomers in 1.5:1 ratio (*d/l*-**7e**:*meso*-**7e**). ^1H NMR (400 MHz, DMSO-d_6 , 25°C): $\delta_{d/l,meso} = 7.75$ –7.70 (*d/l*, m, 4H), 7.70–7.64 (*meso*, m, 4H), 7.44–7.39 (*d/l*, m, 4H), 7.35–7.31 (*meso*, m, 4H), 5.74–5.69 (*meso*, m, 2H), 5.69–5.71 (*d/l*, m, 2H), 4.81 (*meso*, d, $J = 3.6$, 2H), 4.67 (*d/l*, d, $J = 3.3$, 2H).

Chapter 2: Photoredox pinacol coupling reactions mediated by coumarins

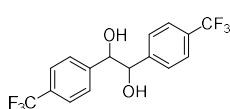
^{13}C NMR (100 MHz, DMSO- d_6 , 25°C): $\delta_{d/l,meso} = 157.9$ (*d/l*, 2C), 157.2 (*meso*, 2C), 140.8 (*d/l*, 4C), 140.7 (*meso*, 4C), 137.7 (*d/l*, 4C), 137.4 (*meso*, 4C), 128.5(2C), 119.1 (*d/l*, 2C), 118.9 (*meso*, 2C), 85.6 (*d/l*, 2C), 85.4 (*meso*, 2C); ESI-MS m/z : 247.0 [M-OH] $^+$, 265.1 [M+H] $^+$.



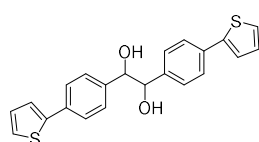
(**7f**): brown oil; 46% (0.046 mmol, 0.013 g); d.r. = 1.2:1 (*d/l*-**7f**:*meso*-**7f**) was determined by integration of benzylic CH 1 H NMR signal. The general procedure was applied using **6f** (0.2 mmol, 22.5 μL), **10** (0.01 mmol, 0.005 g) and TEA (0.8 mmol, 112 μL , 4 eq). The title compound was isolated by flash column chromatography (cyclohexane/ethyl acetate, 7/3) as mixture of diastereoisomers in 1.1:1 ratio (*d/l*-**7f**:*meso*-**7f**). ^1H NMR (400 MHz, CDCl_3 , 25°C): $\delta_{d/l,meso} = 7.67$ (*d/l*, d, $J = 1.6\text{ Hz}$, 2H), 7.65 (*meso*, d, $J = 1.7\text{ Hz}$, 2H), 7.29–7.24 (m, 6H), 7.22–7.14 (m, 6H), 5.59 (*d/l*, s, 2H), 5.35 (*meso*, s, 2H). ^{13}C NMR (100 MHz, CDCl_3 , 25°C): $\delta_{d/l,meso} = 137.2$ (2C), 136.4 (2C), 133.3 (2C), 132.6 (2C), 129.5 (2C), 129.2 (2C), 129.1 (2C), 128.9 (2C), 128.8 (*d/l*, 2C), 128.7 (*meso*, 2C), 126.8 (*d/l*, 2C), 126.4 (*meso*, 2C), 73.0 (*meso*, 2C), 72.2 (*d/l*, 2C); ESI-MS m/z : 265.0 [M-OH] $^+$, 305.1 [M+Na] $^+$.



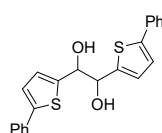
(**7g**): yellowish sticky solid; 45% (0.045 mmol, 0.012 g); d.r. = 1:1 (*d/l*-**7g**:*meso*-**7g**) was determined by integration of benzylic CH 1 H NMR signal. The general procedure was applied using **6g** (0.2 mmol, 21 μL), **10** (0.01 mmol, 0.005 g) and TEA (0.8 mmol, 112 μL , 4 eq). The title compound was isolated by flash column chromatography (cyclohexane/ethyl acetate, 9/1) as mixture of diastereoisomers in 2:1 ratio (*d/l*-**7g**:*meso*-**7g**). ^1H NMR (400 MHz, CDCl_3 , 25°C): $\delta_{d/l,meso} = 7.17$ –7.12 (m, 4H), 7.07–7.01 (m, 4H), 6.99–6.87 (m, 8H), 4.81 (*meso*, s, 2H), 4.61 (*d/l*, s, 2H), 2.90 (*d/l*, bs, 2H), 2.30 (*meso*, s, 2H); ^{13}C NMR (100 MHz, CDCl_3 , 25°C): $\delta_{d/l,meso} = 162.5$ (*meso*, d, $J = 246.4\text{ Hz}$, 2C), 162.4 (*d/l*, d, $J = 246.4\text{ Hz}$, 2C), 135.3 (*d/l*, d, $J = 3.14\text{ Hz}$, 2C), 135.2 (*meso*, d, $J = 3.12\text{ Hz}$, 2C), 128.7 (*meso*, d, $J = 8.04\text{ Hz}$, 4C), 128.6 (*d/l*, d, $J = 8.11\text{ Hz}$, 4C), 115.1 (*d/l*, d, $J = 21.40\text{ Hz}$, 4C), 115.0 (*meso*, d, $J = 21.43\text{ Hz}$, 4C), 78.7 (2C); ^{19}F NMR (377 MHz, CDCl_3): $\delta_{d/l,meso} = -112.84$ (*d/l*, td, $J = 8.6, 4.5\text{ Hz}$, 2F), -112.92 (*meso*, td, $J = 8.5, 4.3\text{ Hz}$, 2F); ESI-MS m/z : 233.0 [M-OH] $^+$, 273.0 [M+Na] $^+$.



(**7h**): pale yellow sticky solid; 61% (0.06 mmol, 0.021 g); d.r. = 1.2:1 (*d/l*-**7h**:*meso*-**7h**) was determined by integration of benzylic CH 1 H NMR signal. The general procedure was applied using **6h** (0.2 mmol, 28 μL), **10** (0.01 mmol, 0.005 g) and TEA (0.8 mmol, 112 μL , 4 eq). The title compound was isolated by flash column chromatography (cyclohexane/ethyl acetate, 6/4) as mixture of diastereoisomers in 1.3:1 ratio (*d/l*-**7h**:*meso*-**7h**). ^1H NMR (400 MHz, CDCl_3 , 25°C): $\delta_{d/l,meso} = 7.54$ –7.48 (m, 8H), 7.27–7.21 (m, 8H), 4.94 (*meso*, s, 2H), 4.73 (*d/l*, s, 2H); ^{13}C NMR (100 MHz, CDCl_3 , 25°C): $\delta_{d/l,meso} = 143.3$ (*meso*, q, $J = 1\text{ Hz}$, 2C), 143.1 (*d/l*, q, $J = 1\text{ Hz}$, 2C), 130.4 (*meso*, q, $J = 32\text{ Hz}$, 4C), 130.3 (*d/l*, q, $J = 32\text{ Hz}$, 4C), 127.3 (*meso*, 2C), 127.2 (*d/l*, 2C), 125.2 (*meso*, q, $J = 4\text{ Hz}$, 2C), 125.0 (*d/l*, q, $J = 3\text{ Hz}$, 2C), 124.0 (*meso*, q, $J = 270\text{ Hz}$, 2C), 123.9 (*d/l*, q, $J = 270\text{ Hz}$, 2C), 78.3 (*meso*, 2C) 77.1 (*d/l*, 2C); ^{19}F NMR (377 MHz, CDCl_3): $\delta_{d/l,meso} = -61.4$ (6F), -61.4 (6F); ESI-MS m/z : 333.0 [M-OH] $^+$, 351.1 [M+H] $^+$.



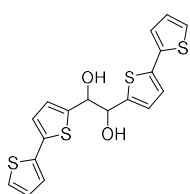
(**7i**): brownish solid; 61% (0.06 mmol, 0.023 g); d.r. = 1:1.5 (*d/l*-**7i**:*meso*-**7i**) was determined by integration of benzylic CH 1 H NMR signal. The general procedure was applied using **6i** (0.2 mmol, 0.037 g), **10** (0.01 mmol, 0.005 g) and TEA (0.8 mmol, 112 μL , 4 eq). The title compound was isolated by flash column chromatography (cyclohexane/ethyl acetate, 8/2) as mixture of diastereoisomers in 1:1.5 ratio (*d/l*-**7i**:*meso*-**7i**). ^1H NMR (400 MHz, DMSO- d_6 , 25°C): $\delta_{d/l,meso} = 7.58$ –7.42 (m, 16H), 7.29 (d, $J = 8.3\text{ Hz}$, 4H), 7.19–7.07 (m, 8H), 5.48–5.43 (*meso*, m, 2H), 5.36–5.32 (*d/l*, m, 2H), 4.66–4.62 (*meso*, m, 2H), 4.62–4.59 (*d/l*, m, 2H); ^{13}C NMR (100 MHz, DMSO- d_6): $\delta_{d/l,meso} = 143.9$ (*meso*, 2C), 143.8 (*d/l*, 2C), 143.1 (*meso*, 2C), 142.2 (*d/l*, 2C), 132.6 (4C), 128.84 (4C), 128.5 (*meso*, 4C), 128.3 (*d/l*, 4C), 125.6 (4C), 124.8 (*meso*, 4C), 124.7 (*d/l*, 4C), 123.7 (*meso*, 2C), 123.7 (*d/l*, 2C), 77.5 (*meso*, 2C), 77.1 (*d/l*, 2C); ESI-MS m/z : 361.1 [M-OH] $^+$, 401.3 [M+Na] $^+$.



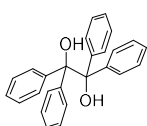
(**7j**): brownish solid; 50% (0.05 mmol, 0.019 g); d.r. = 1:1.3 (*d/l*-**7j**:*meso*-**7j**) was determined by integration of benzylic CH 1 H NMR signal. The general procedure was applied using **6j** (0.2 mmol, 0.037 g), **10** (0.01 mmol, 0.005 g) and TEA (0.8 mmol, 112 μL , 4 eq). The title compound was isolated by flash column chromatography (dichloromethane/ethyl acetate, 97/3) as mixture of diastereoisomers in 1:1.3 ratio (*d/l*-**7j**:*meso*-**7j**). ^1H NMR (400

Chapter 2: Photoredox pinacol coupling reactions mediated by coumarins

MHz, DMSO- d_6 , 25°C): $\delta_{d/l,meso} = 7.62\text{--}7.55$ (m, 10H), 7.42–7.34 (m, 8H), 7.31 (*d/l*, d, $J = 3.6$, 2H), 7.29–7.22 (m, 4H), 6.97 (*d/l*, d, $J = 3.7$, 2H), 6.82 (*meso*, d, $J = 3.7$, 2H), 6.01–5.98 (*meso*, m, 2H), 5.98–5.96 (*d/l*, m, 2H), 4.93–4.89 (*meso*, m, 2H), 4.89–4.84 (*d/l*, m, 2H); ^{13}C NMR (100 MHz, DMSO- d_6): 146.4 (4C), 145.4 (4C), 141.8 (4C), 134.1 (4C), 134.0 (4C), 129.0 (4C), 127.2 (4C), 125.8 (*meso*, 2C), 125.7 (*d/l*, 2C), 124.9 (4C), 122.6 (4C), 73.5 (*meso*, 2C), 73.2 (*d/l*, 2C); ESI-MS m/z : 361.0 [M-OH] $^+$.



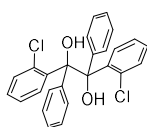
(**7k**): brownish solid; 50% (0.05 mmol, 0.019 g); d.r. = 1:3.7 (*d/l*-**7k**:*meso*-**7k**) was determined by integration of benzylic CH^1H NMR signal. The general procedure was applied using **6k** (0.2 mmol, 0.039 g), **10** (0.01 mmol, 0.005 g) and TEA (0.8 mmol, 112 μL , 4 eq). The title compound was isolated by flash column chromatography (dichloromethane/ethyl acetate, 6/1) as mixture of diastereoisomers in 1:3.7 ratio (*d/l*-**7k**:*meso*-**7k**). ^1H NMR (400 MHz, DMSO- d_6 , 25°C): $\delta_{d/l,meso} = 7.45\text{--}7.43$ (*d/l*, m, 2H), 7.43 (*meso*, dd, $J = 5.1$ Hz, $J = 1.1$ Hz, 2H), 7.22 (*d/l*, dd, $J = 3.6$ Hz, $J = 1.2$ Hz, 2H), 7.19 (*meso*, dd, $J = 3.6$ Hz, $J = 1.2$ Hz, 2H), 7.10 (*d/l*, d, $J = 3.6$ Hz, 2H), 7.07–7.02 (m, 6H), 6.91 (*d/l*, d, $J = 3.7$ Hz, 2H), 6.77 (*meso*, d, $J = 3.7$ Hz, 2H), 6.06 (m, 4H), 4.89 (*meso*, d, $J = 4.2$ Hz, 2H), 4.83 (*d/l*, d, $J = 4.8$ Hz, 2H); ^{13}C NMR (100 MHz, DMSO- d_6): 146.4 (*d/l*, 2C), 145.4 (*meso*, 2C), 137.5 (*meso*, 2C), 137.4 (*d/l*, 2C), 135.7 (*meso*, 2C), 135.6 (*d/l*, 2C), 128.6 (*meso*, 2C), 128.6 (*d/l*, 2C), 126.0 (*d/l*, 2C), 125.9 (*meso*, 2C), 125.3 (*meso*, 2C), 125.3 (*d/l*, 2C), 123.8 (*meso*, 2C), 123.8 (*d/l*, 2C), 123.3 (*meso*, 2C), 123.3 (*d/l*, 2C), 73.7 (*meso*, 2C), 73.5 (*d/l*, 2C); ESI-MS m/z : 373.0 [M-OH] $^+$.



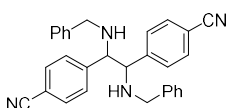
(**12a**): white solid; 58% (0.06 mmol, 0.021 g). The general procedure was applied using **11a** (0.2 mmol, 0.036 g), **10** (0.01 mmol, 0.005 g) and TEA (0.8 mmol, 112 μL , 4 eq). The title compound was isolated by flash column chromatography (cyclohexane/ethyl acetate, 99/1). ^1H NMR (400 MHz, CDCl_3 , 25°C): $\delta = 7.32\text{--}7.25$ (m, 8H), 7.20–7.11 (m, 12H), 3.00 (s, 2H); ^{13}C NMR (100 MHz, CDCl_3): $\delta = 144.1$ (4C), 128.5 (8C), 127.2 (8C), 126.9 (4C), 83.0 (2C); ESI-MS m/z : 349.3 [M-OH] $^+$.



(**12b**): yellowish solid; 55% (0.05 mmol, 0.024 g). The general procedure was applied using **12b** (0.2 mmol, 0.044 g), **10** (0.01 mmol, 0.005 g) and TEA (0.8 mmol, 112 μL , 4 eq). The title compound was isolated by flash column chromatography (cyclohexane/ethyl acetate, 8/2). ^1H NMR (400 MHz, CDCl_3 , 25°C): $\delta = 7.24\text{--}7.20$ (m, 8H), 6.89–6.83 (m, 8H), 2.83 (s, 2H); ^{13}C NMR (100 MHz, CDCl_3): $\delta = 161.7$ (d, $J = 247.4$ Hz, 4C), 139.6 (d, $J = 3.2$ Hz, 4C), 130.2 (d, $J = 8.0$ Hz, 8C), 114.2 (d, $J = 21.1$ Hz, 8C), 82.5 (2C); ^{19}F NMR (377 MHz, CDCl_3 , 25°C) $\delta = -113.8$ (4F); ESI-MS m/z : 421.1 [M-OH] $^+$.

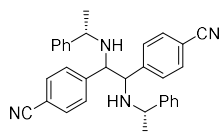


(**12c**): yellowish oil; 37% (0.04 mmol, 0.016 g); The two diastereoisomer present very similar NMR signal avoiding the determination of the d.r.. The general procedure was applied using **12c** (0.2 mmol, 0.043 g), **10** (0.01 mmol, 0.005 g) and TEA (0.8 mmol, 112 μL , 4 eq). The title compound was isolated by flash column chromatography (n-hexane/diethyl ether, 95/5) as mixture of diastereoisomers. ^1H NMR (400 MHz, CDCl_3 , 25°C): $\delta_{d/l,meso} = 7.61$ (d, $J = 1.6$ Hz, 2H), 7.59 (d, $J = 1.6$ Hz, 2H), 7.40–7.36 (m, 4H), 7.34–7.19 (m, 10 H), 6.22 (s, 2H); ^{13}C NMR (100 MHz, CDCl_3): $\delta_{d/l,meso} = 142.2$ (2C), 140.9 (2C), 132.5 (2C), 129.5 (2C), 128.7 (2C), 128.4 (4C), 128.0 (2C), 127.7 (2C), 127.1 (2C), 126.9 (4C), 72.7 (2C); ESI-MS m/z : 417.3 [M-OH] $^+$.

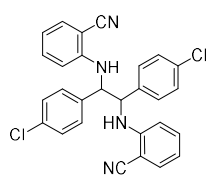


(**14a**): yellowish oil; 50% (0.05 mmol, 0.022 g); d.r. = 1:1.4 (*d/l*-**14a**:*meso*-**14a**) was determined by integration of benzylic CH^1H NMR signals at $\delta = 3.43$, 3.32. The general procedure was applied using **13a** (0.2 mmol, 0.044 g), **10** (0.01 mmol, 0.005 g) and TEA (0.8 mmol, 112 μL , 4 eq). The title compound was isolated by flash column chromatography (cyclohexane/diethyl ether, 7/3) as mixture of diastereoisomers in 1:1.1 ratio (*d/l*-**11a**:*meso*-**11a**). ^1H NMR (400 MHz, CDCl_3 , 25°C): $\delta_{d/l,meso} = 7.57\text{--}7.51$ (m, 4H), 7.47–7.42 (m, 4H), 7.30–7.25 (m, 6H), 7.24–7.19 (m, 8H), 7.18–7.13 (m, 4H), 7.12–7.06 (m, 4H), 7.04–6.99 (m, 6H), 3.84 (*meso*, s, 2H), 3.69 (*d/l*, s, 2H), 3.61 (*d/l*, d, $J = 13.2$ Hz, 2H), 3.56 (*meso*, d, $J = 13.6$ Hz, 2H), 3.43 (*d/l*, d, $J = 13.3$ Hz, 2H), 3.32 (*meso*, d, $J = 13.6$ Hz, 2H); ^{13}C NMR (100 MHz, CDCl_3): $\delta_{d/l,meso} = 146.3$ (*meso*, 2C), 145.5 (*d/l*, 2C), 139.5 (*meso*, 2C), 139.3 (*d/l*, 2C), 132.0 (8C), 129.1 (4C), 128.6 (4C), 128.5 (4C), 128.4 (4C), 128.0 (4C), 127.9 (4C), 127.0 (4C), 118.6 (*meso*, 2C), 118.5 (*d/l*, 2C), 111.6 (*meso*, 2C), 111.3 (*d/l*, 2C), 67.8 (*meso*, 2C), 66.3 (*d/l*, 2C), 51.3 (*meso*, 2C), 51.1 (*d/l*, 2C); ESI-MS m/z : 336.2 [M-BnNH] $^+$.

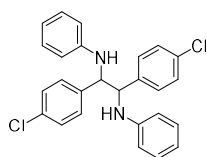
Chapter 2: Photoredox pinacol coupling reactions mediated by coumarins



(14b): yellowish oil; 50% (0.05 mmol, 0.024 g); d.r. = 2.15:3.5:2:1 (*syn-14b:anti-14b:syn-14b*) was determined by integration of benzylic CH^1H NMR signals at $\delta = 5.04, 4.09, 4.27$. The general procedure was applied using **13b** (0.2 mmol, 0.047 g), **10** (0.01 mmol, 0.005 g) and TEA (0.8 mmol, 112 μL , 4 eq). The title compound was isolated by flash column chromatography (cyclohexane/diethyl ether, 6/4) as mixture of diastereoisomers in 2.15:3.5:2:1 ratio (*syn-14b:anti-14b:syn-14b*). ^1H NMR (400 MHz, CDCl_3 , 25°C): $\delta_{\text{syn,anti}} = 7.67\text{--}7.59$ (m, 4H), 7.58–7.49 (m, 4H), 7.49–7.37 (m, 12H), 7.37–7.26 (m, 18H), 7.24–7.17 (m, 2H), 7.05–6.88 (m, 8H), 6.86–6.74 (m, 6H), 5.04 (*syn*, s, 2H), 4.27 (*syn*, s, 2H), 4.09 (*anti*, d, 1H), 3.97 (d, $J = 4.01$ Hz, 1H), 3.92 (*syn*, q, $J = 6.6$ Hz, 2H), 3.75 (*syn*, q, $J = 6.7$ Hz, 2H), 3.62 (*anti*, q, $J = 6.5$ Hz, 1H), 3.36 (*anti*, q, $J = 6.3$ Hz, 1H), 1.72 (d, $J = 6.8$ Hz, 3H), 1.56 (d, $J = 6.5$ Hz, 6H), 1.45 (d, $J = 6.8$ Hz, 9H); ^{13}C NMR (100 MHz, CDCl_3): $\delta_{\text{syn,anti}} = 146.8$ (2C), 146.8 (2C), 146.7 (2C), 145.6 (2C), 145.3 (2C), 144.6, 144.5, 132.0 (4C), 131.9 (4C), 131.7 (2C), 131.6 (2C), 129.1 (4C), 128.7 (4C), 128.5 (2C), 128.5 (2C), 128.5 (4C), 128.4 (4C), 128.4 (2C), 128.3 (2C), 127.3 (2C), 127.0 (4C), 126.5 (4C), 126.4 (4C), 126.3 (4C), 118.7 (4C), 118.6 (2C), 111.2 (2C), 111.2 (2C), 111.0, 110.8, 66.8 (2C), 65.4 (2C), 65.1, 62.5, 56.0 (2C), 55.0 (2C), 54.9 (2C), 24.1 (2C), 23.2 (2C), 22.4 (2C); ESI-MS m/z : 350.2 $[\text{M-PhCH}(\text{Me})\text{NH}]^+$.



(14c): brownish solid; 54% (0.05 mmol, 0.026 g); d.r. = 1:1.1 (*d/l-14c:meso-14c*) was determined by integration of benzylic CH^1H NMR signal. The general procedure was applied using **13c** (0.2 mmol, 0.048 g), **10** (0.01 mmol, 0.005 g) and TEA (0.8 mmol, 112 μL , 4 eq). The title compound was isolated by flash column chromatography (n-hexane/diethyl ether, 9/1) as mixture of diastereoisomers in 1:1.1 ratio (*d/l-14c:meso-14c*). ^1H NMR (400 MHz, CDCl_3 , 25°C): $\delta_{d/l,meso} = 7.40\text{--}7.38$ (m, 4H), 7.30–7.18 (m, 12H), 7.04–6.97 (m, 8H), 6.71–6.68 (m, 4H), 6.36–6.34 (m, 4H), 5.26 (*meso*, m, 4H), 4.94 (*d/l* m, 4H); ^{13}C NMR (100 MHz, CDCl_3): $\delta_{d/l,meso} = 148.4$ (4C), 148.0 (4C), 134.8 (4C), 134.5 (4C), 134.2 (4C), 132.8 (4C), 129.2 (8C), 128.5 (8C), 118.2 (4C), 112.4 (4C), 97.4 (4C), 61.3 (4C); ESI-MS m/z : 483.1 $[\text{M+H}]^+$.



(14d): yellowish oil; 40% (0.04 mmol, 0.018 g); d.r. = 1:1 (*d/l-14d:meso-14d*) was determined by integration of benzylic CH^1H NMR signal. The general procedure was applied using **13d** (0.2 mmol, 0.045 g), **10** (0.01 mmol, 0.005 g) and TEA (0.8 mmol, 112 μL , 4 eq). The title compound was isolated by flash column chromatography (n-hexane/diethyl ether, 9/1) as mixture of diastereoisomers in 1:1.3 ratio (*d/l-14d:meso-14d*). ^1H NMR (400 MHz, CDCl_3 , 25°C): $\delta_{d/l,meso} = 7.26\text{--}7.14$ (m, 8H), 7.1 –6.98 (m, 12H), 6.89 (d, $J = 8.3$ Hz, 4H), 6.73–6.66 (m, 4H), 6.49 (d, $J = 8.0$ Hz, 8H), 4.92 (*meso*, s, 2H), 4.53 (*d/l*, s, 2H), 4.47 (*meso*, s, 2H), 4.45 (*d/l*, s, 2H); ^{13}C NMR (100 MHz, CDCl_3 , 25°C): $\delta_{d/l,meso} = 146.5$ (2C), 145.9 (2C), 138.2 (2C), 136.5 (2C), 133.6 (2C), 133.4 (2C), 129.3 (4C), 129.5 (4C), 128.8 (4C), 128.7 (4C), 128.7 (4C), 128.6 (4C), 118.6 (2C), 118.3 (2C), 114.1 (4C), 113.8 (4C), 63.5 (2C), 61.4 (2C); ESI-MS m/z : 447.2 $[\text{M+H}]^+$.

2.4.4 Photophysical studies

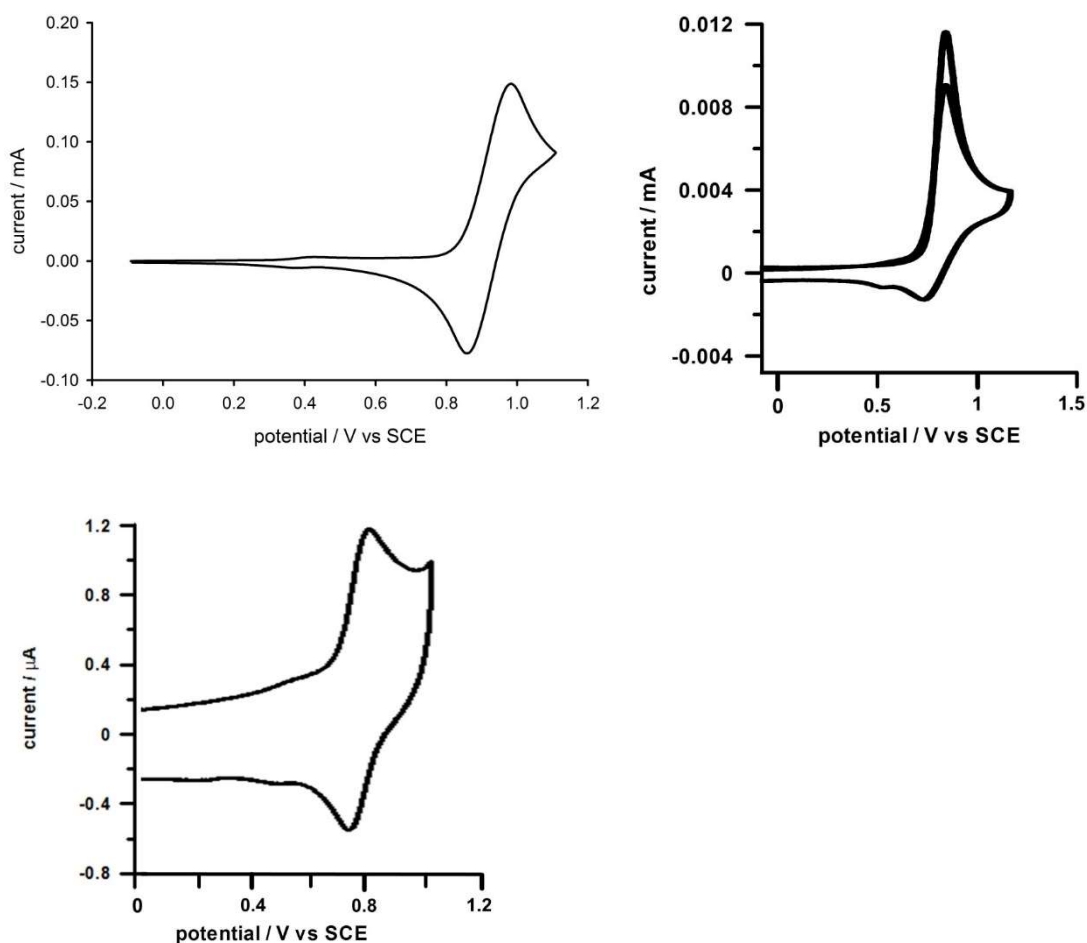


Figure 21 A) Cyclic Voltammetry of an argon-purged solution of **3** (1mM) in CH₃CN in the presence of 0.1M tetraethylammonium hexafluorophosphate (TEAPF₆). Scan rate=0.1Vs⁻¹; working electrode: glassy carbon B) Cyclic Voltammetry of an argon-purged solution of **4** (1mM) in CH₃CN in the presence of 0.1M tetraethylammonium hexafluorophosphate (TEAPF₆). Scan rate=0.2Vs⁻¹; working electrode: glassy carbon; two scans. C) Cyclic Voltammetry of an argon-purged solution of **5** (1.4mM) in CH₃CN in the presence of 0.1M tetraethylammonium.

References

- ¹ a) K. C. Nicolaou, Z. Yang, J. J. Liu, H. Ueno, P. G. Nantermet, R. K. Guy, C. F. Claiborne, J. Renaud, E. A. Couladouros, K. Paulvannan and E. J. Sorensen, *J. Am. Chem. Soc.*, 1995, **117**, 634; b) M. Nazare and H. Waldmann, *Angew. Chem. Int. Ed.*, 2000, **39**, 1125; *Angew. Chem.*, 2000, **112**, 1171; c) S. M. Kim, I. S. Byun and Y. H. Kim, *Angew. Chem. Int. Ed.*, 2000, **39**, 728; *Angew. Chem.*, 2000, **112**, 744.
- ² a) K. S. Kim, J. I. Park and P. Ding, *Tetrahedron Lett.*, 1998, **39**, 6471; b) S. Superchi, M. Contursi and C. Rosini, *Tetrahedron*, 1998, **54**, 11247; c) J. A. Tunge, D. A. Gately and J. R. Norton, *J. Am. Chem. Soc.*, 1999, **121**, 4520; d) C. A. Ray, T. W. Wallace and R. A. Ward, *Tetrahedron Lett.*, 2000, **41**, 3501; e) M. B. Andrus, B. B. V. S. Sekhar, E. L. Meredith and N. K. Dalley, *Org. Lett.*, 2000, **2**, 3035.
- ³ A. Gansäuer and H. Bluhm, *Chemical Reviews*, 2000, **100**, 2771.
- ⁴ E. Fava, A. Millet, M. Nakajima, S. Loescher and M. Rueping, *Angew. Chem. Int. Ed.*, 2016, **55**, 6776.

- ⁵ a) T. Shibata, A. Kabumoto, T. Shiragami, O. Ishitani, C. Pac and S. Yanagida, *J. Phy.Chem.* 1990, **94**,2068; b) O. Ishitani, C. Pac and H. Sakurai, *J. Org. Chem.* 1983, **48**, 2941.
- ⁶ M. -H. Larraufie, R. Pellet, L. Fensterbank, J. -P. Goddard, E. Lacôte, M.Malacria and C. Ollivier, *Angew. Chem. Int. Ed.*, 2011, **50**, 4463.
- ⁷ a) E. L. Tyson, E. P. Farney and T. P. Yoon, *Org. Lett.*, 2012, **14**, 1110; b) J. Du and T. P. Yoon, *J. Am. Chem. Soc.*, 2009, **131**,14604; c) T. P. Yoon, *ACSCatal.*, 2013, **3**, 895; d) M. A. Ischay, M. E. Anzovino, J. Du and T. P. Yoon, *J. Am. Chem. Soc.*, 2008, **130**, 12886; e) Z. Lu, M. Shen and T. P. Yoon, *J. Am. Chem. Soc.*, 2011, **133**,1162.
- ⁸ R. M. Nakajima, E. Fava, S. Loescher, Z. Jiang and M. Rueping, *Angew. Chem. Int. Ed.*, 2015, **54**, 8828.
- ⁹ H.G. Roth, N.A. Romero and D.A. Nicewicz, *Synlett*, 2016, **27**, 714.
- ¹⁰ S. Okamoto, K. Kojiyama, H. Tsujioka and A. Sudo, *Chem. Commun.*, 2016, **52**, 11339.
- ¹¹ N. Noto, T. Koike and M. Akita, *Chem. Sci.*, 2017, **8**, 6375.
- ¹² a) E. Hasegawa, T. Seida, N. Chiba, T. Takahashi and H. Ikeda, *J. Org.Chem.*, 2005, **70**, 9632; b) E. Hasegawa, S. Takizawa, T. Seida, A. Yamaguchi, N. Yamaguchi, N. Chiba, T. Takahashi, H. Ikeda and K. Akiyama, *Tetrahedron*, 2006, **62**, 6581; c) A.G. Griesbeck and M. Reckenthäler, *Beilstein J. Org.Chem.*, 2014, **10**, 1143.
- ¹³ E. Fava, A. Millet, M. Nakajima, S. Loescher and M. Rueping, *Angew. Chem., Int. Ed.*, 2016, **55**, 6776.
- ¹⁴ H. Li, L. Cai, J. Li, Y. Hu, P. Zhou and J. Zhang, *Dyes Pigm.*, 2011,**91**, 309.
- ¹⁵ B. B. Raju and T. S. Varadarajan, *Laser Chem.*, 1995, **16**, 109.
- ¹⁶ M. Fujiwara, N. Ishida, M. Satsuki and S. Suga, *J. Photopolym. Sci. Technol.*, 2002, **15**, 237.
- ¹⁷ K. Hara, Z.-S.Wang, T. Sato, A. Furube, R. Katoh, H. Sugihara, Y. Dan-oh, C. Kasada, A. Shinpo and S. Suga, *J. Phys. Chem. B*, 2005, **109**,15476.
- ¹⁸ Abhay S. Zambare, Firoz A. Kalam Khan, Sureshchandra P. Zambare, Shantanu D. Shinde and Jaiprakash N. Sangshetti, *Current Organic Chemistry*, 2016, **20**, 798.
- ¹⁹ R. H. Vekariya and H. D. Patel, 2014, **44**, 2756.
- ²⁰ W. H. Perkin, *Journal of the Chemical Society*, 1868, **21**, 53.
- ²¹ F. Jafarpour, S. Zarei, M. Barzegar Amiri Olia, N. Jalalimanesh and S. Rahiminejadan, *J. Org. Chem.*, 2013, **78**, 2957.
- ²² D. A. Corbin, C.-H. Lim and G. M. Miyake, *Aldrichimica Acta*, 2019, **42**, 7.
- ²³ J. A. Murphy, *The Journal of Organic Chemistry*, 2014, **79**, 3731.
- ²⁴ a) I. Ghosh, T. Ghosh, J. I. Bardagi and B. König, *Science*, 2014, **346**, 725; b) S. O. Poelma, G. L. Burnett, E. H. Disceky, K. M. Mattson, N. J. Treat, Y. Luo, Z. M. Hudson, S. L. Shankel, P. G. Clark, J. W. Kramer, C. J. Hawker and J. R. de Alaniz, *J. Org. Chem.*, 2016, **81**, 7155.
- ²⁵ S. Okamoto, K. Kojiyama, H. Tsujioka and A. Sudo, *Chem. Commun.*, 2016, **52**, 11339.
- ²⁶ J. Chin, F. Mancin, N. Thavarajah, D. Lee, A. Lough and D. S. Chung, *J. Am. Chem. Soc.*, 2003, **125**, 15276.
- ²⁷ a) H. Gorner and H. J. Kuhn, *J. Phys. Chem.*, 1986, **90**, 5946; b) M. J. van der Burgt, J. Jansen, A. H. Huizer and C. A. G. O. Varma, *J. Mol. Struct.*, 1996, **385**, 175.
- ²⁸ E. M. Arnett and C. A. Palmer, *J. Am. Chem. Soc.*, 1990, **112**, 1354.
- ²⁹ E. M. Arnett and C. A. Palmer, *J. Am. Chem. Soc.*, 1990, **112**, 1354.
- ³⁰ A. J. G. Barwise, A. A. Gorman, R. L. Leyland, P. G. Smith and M. A. J. Rodgers, *J. Am. Chem. Soc.*, 1968, **100**, 1814.
- ³¹ F. Jafarpour, S. Zarei, M. Barzegar Amiri Olia, N. Jalalimanesh and S. Rahiminejadan, *J. Org. Chem.*, 2013, **78**, 2957.

Photoredox alkylradicals generation mediated by coumarin dyes

3.1 Introduction

3.1.1 Alkylradicals generation by photoredox catalysis

Radical intermediates are reaction intermediates that are transiently generated in situ bear an unpaired electron. Classical methods for the generation of alkyl radicals rely on hazardous radical initiators like 2,2'-azobis(isobutyronitrile) (AIBN) and triethylborane, toxic reagents such as tributyltin hydride and in many cases, high-temperature or high-energy UV irradiation are required.¹

Therefore, the use of radical intermediates in chemical synthesis has remained both underexplored and underappreciated.¹

Nowadays, photoredox catalysis represents an innovative mild route for the generation of alkyl radicals and subsequent application in chemical synthesis (Figure 1).²

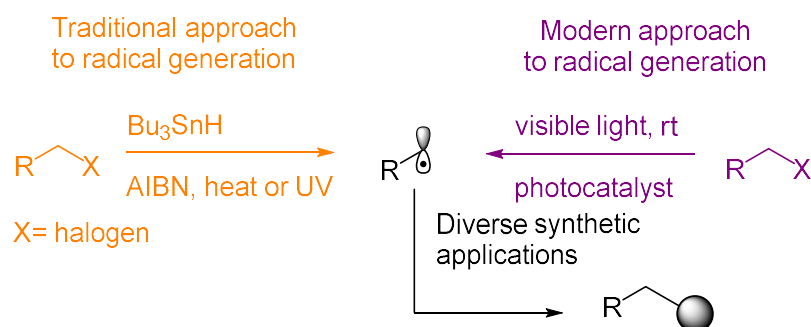


Figure 1 Classical and modern approach to radical intermediates

A typical example in which the photocatalytic generation of alkyl radicals was demonstrated are atom transfer radical addition (ATRA) reactions.³ ATRA reactions are effective methodologies for the direct functionalization of olefins through the generation of alkyl radicals from alkyl halide substrates.⁴ Classical ATRA reactions rely on the use of initiators that are often toxic and hazardous. Alternatively, harsh conditions which limits functional group tolerance are required. Photoredox catalysis can be an effective methodology for ATRA reaction, and in few years, innovative and selective procedures were developed.⁵ Stephenson and co-workers successfully developed the photoredox ATRA reaction of haloalkanes with olefins employing [Ir{dF(CF₃)ppy}₂(dtbbpy)]PF₆ and [Ru(bpy)₃]Cl₂ as the photocatalysts. This methodology is characterized by the mild reaction conditions, excellent yields, high atom efficiencies and a broad substrate scope (Figure 2).⁶

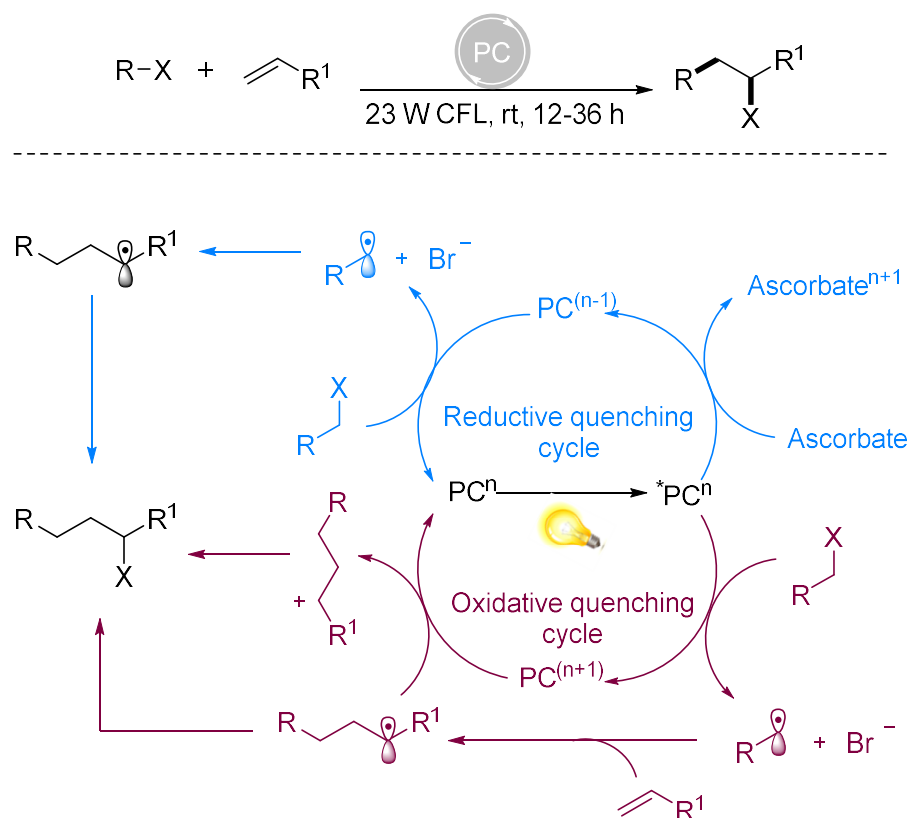


Figure 2: Photocatalyzed ATRA reaction mediated by $[\text{Ir}\{\text{dF}(\text{CF}_3)\text{ppy}\}_2(\text{dtbbpy})]\text{PF}_6$ and $[\text{Ru}(\text{bpy})_3]\text{Cl}_2$

The photocatalyst plays the role of initiator by generating free radicals $\text{R}\cdot$ from haloalkanes. The oxidative quenching cycle (in purple) requires long reaction times. In the case of α -bromo carbonyls, the presence of Lewis acids makes the C-X bond more prone to the reduction.⁷ In alternative, a reductive quenching pathway (in blue) relies on the use of sodium ascorbate as sacrificial electron donor, in combination with MeOH as co-solvent to improve the solubility. The presence of the ascorbate gives access to the strong reductant $(\text{PC})^{n-1}$. The final reduction of the C-X bond allows the formation of the radical intermediate $\text{R}\cdot$.

Furthermore, a relevant example was recently highlighted by Melchiorre *et al.* using *p*-anisaldehyde as photocatalyst.⁸ Under CFL irradiation, the singlet state *p*-anisaldehyde undergoes inter system crossing (ISC) to give the triplet state. The 3p -anisaldehyde is capable to engage an energy transfer with the haloalkene generating the radical which participates to the ATRA chain mechanism.

Kokotos and co-workers contributed to extend the employment of the photoredox ATRA reaction to the bromoacetonitrile as substrate.⁹

Another effective system, based on an organic photocatalyst was described by my research group, that reported an ATRA reactions using BODIPY dyes¹⁰. The easily accessed iodo-bodipy dye **1**, prepared in few reaction conditions starting from commercially available pyrrole, in the presence of

sodium ascorbate, was successfully employed in the ATRA reaction between alkyl bromo derivatives and alkenes (Figure 2).

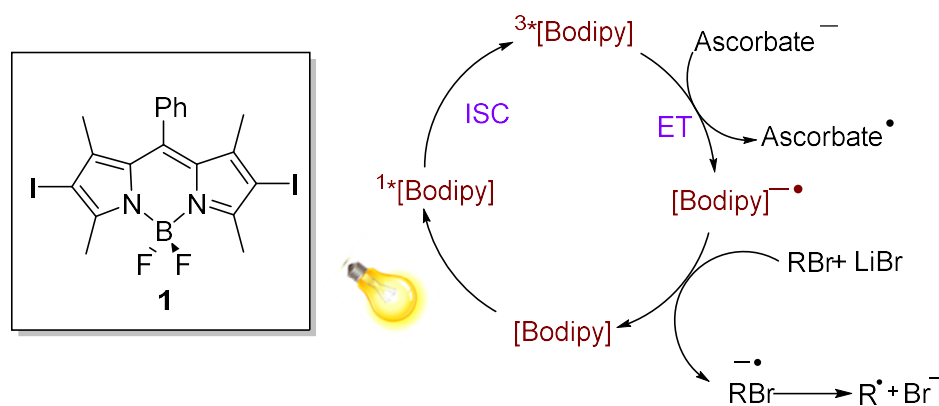
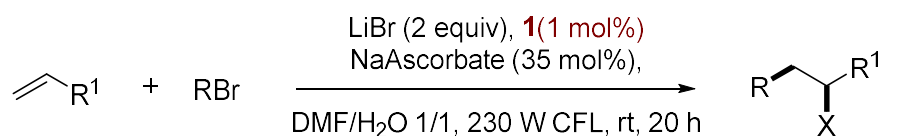


Figure 2: ATRA reaction photocatalyzed by the bodipy dye **1**.

Irradiation of [Bodipy] by a household bulb generates the singlet excited state $^1\text{[Bodipy]}$ which undergoes inter system crossing (ISC) to reach a triplet state $^3\text{[Bodipy]}$. After reduction of the $^3\text{[Bodipy]}$ species to the radical anion $[\text{Bodipy}]^{\bullet-}$ by sodium ascorbate, $[\text{Bodipy}]^{\bullet-}$ has a sufficiently strong reduction potential (-1 to -1.54 V vs. SCE)¹¹ to effectively convert the alkyl halides (-0.5 to -1.5 V vs. SCE)¹² to electrophilic free radicals $\text{R}\cdot$. Addition of $\text{R}\cdot$ to alkenes follows the ATRA mechanism proposed by Stephenson and co-workers (Figure 2).

3.1.2 Generation of alkyl radicals for other applications

Photoredox catalysis for the generation of alkyl radicals was also used in a variety of other C-C bond forming reactions.

A relevant example is the direct enantioselective α -alkylation of aldehydes with alkyl bromides using $[\text{Ru}(\text{bpy})_3]^{2+}$ as reported by McMillan and co-workers (Figure 3).¹³

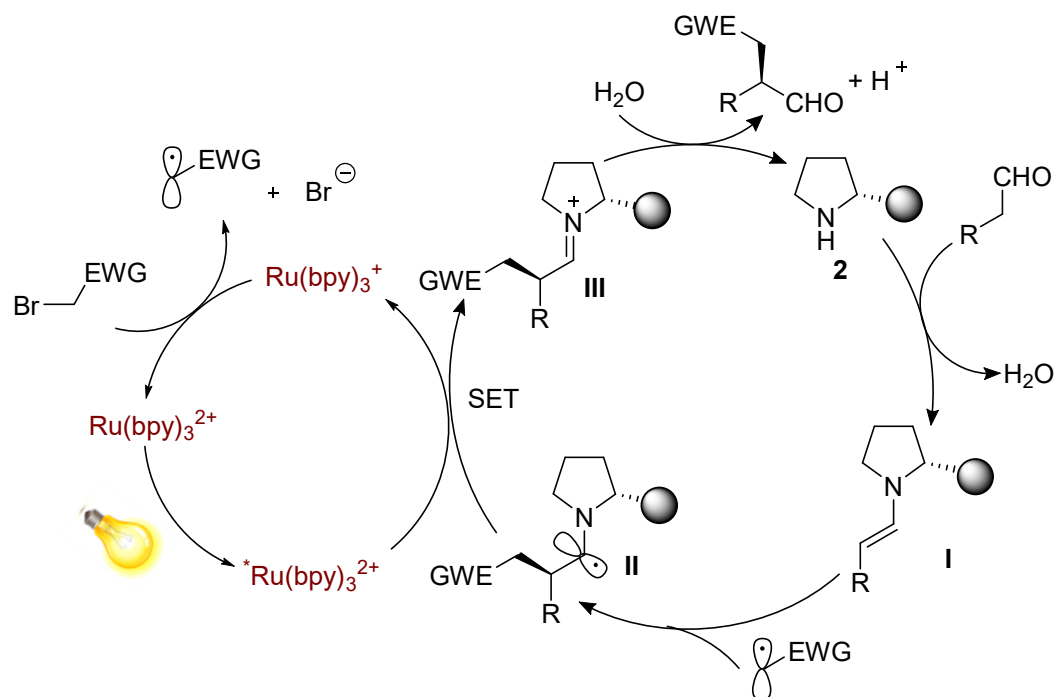
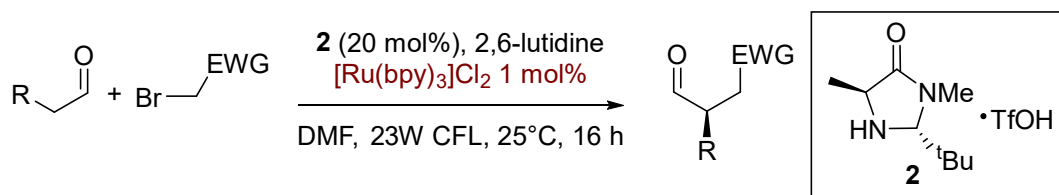


Figure 3 Enantioselective α -alkylation of aldehydes photocatalyzed by $[\text{Ru}(\text{bpy})_3]\text{Cl}_2$

After a photodriven initiation step in which a single electron transfer (SET) involving the photosensitizer $^*[\text{Ru}(\text{bpy})_3]^{2+}$ in the excited state and the α -amino radicals **II** generates the iminium ion **III** and the reduced $[\text{Ru}(\text{bpy})_3]^+$. Alkyl radical $\text{R}\cdot$ was formed by the interaction of $[\text{Ru}(\text{bpy})_3]^+$ species which acts as reductant of the alkyl bromide substrate.

Further examples of photoredox catalysed formation of radical intermediates are the reductive protonation of α -haloketones in the presence of $[\text{Ru}(\text{bpy})_3]^{2+}$ and Hantzsch ester reported by Stephenson *et al.*¹⁴ and the selective oxo-trifluoromethylation of alkenes photocatalyzed by $[\text{fac-Ir}(\text{ppy})_3]$ using Umemoto's reagent as a source for the reactive CF_3 radical, demonstrated by Akita and co-workers.¹⁵

3.1.3 Use of coumarin dyes as photocatalysts of several organic reactions

As the power of coumarin dyes as photo reductant was previously demonstrated, the employment of coumarin dyes as the alternative of inorganic photocatalysts was further extended to a variety of different photoredox reactions. In particular, the photocatalytic generation of electrophilic alkyl radical from halogenated compounds was investigated (-0.5 to -1.5 V vs. SCE).

In this chapter, the employment of coumarin dyes as photocatalyst for the generation of alkyl radicals and their subsequent employment in ATRA reaction will be described. Furthermore, their use in the photoredox α -alkylation of aldehydes, reductive protonation of bromoketones and oxy-trifluoromethylation of alkenes was also attempted. Although BODIPY dyes were able to promote the ATRA reaction, the conditions were quite sensitive to adventitious oxygen, and just open the reaction flask under argon was sufficient to stop irreversibly the reactions. In addition, it was also mandatory the use of ascorbate, because other sacrificial agents like amines were able to decompose the BODIPY dye. Furthermore, the use of ascorbate was possible in a carefully optimized reaction mixture, and as the solubility of the alkene in the media was also a critical point to obtain decent yields. The incredible sensitivity to oxygen of BODIPY in ATRA reactions and the difficulties related to the reaction scope prompted my research to develop more affordable, simple, and robust conditions with another organic dye.

3.2 Results and discussion

3.2.1 Coumarin dyes for the photoredox catalysis of ATRA reactions

The ATRA reaction of ethyl-bromomalonate as the alkyl radical source with hexenol as the olefin was investigated as model reaction. Initial studies were performed in a DMF/H₂O mixture under Blue LEDs irradiation, over 36 hours at room temperature.

First, the visible light absorbing coumarin dyes **3** and **4** (readily synthesized as reported in section 2.2.1) as well as the commercially available ones **5** and **6** were screened (Figure 4).

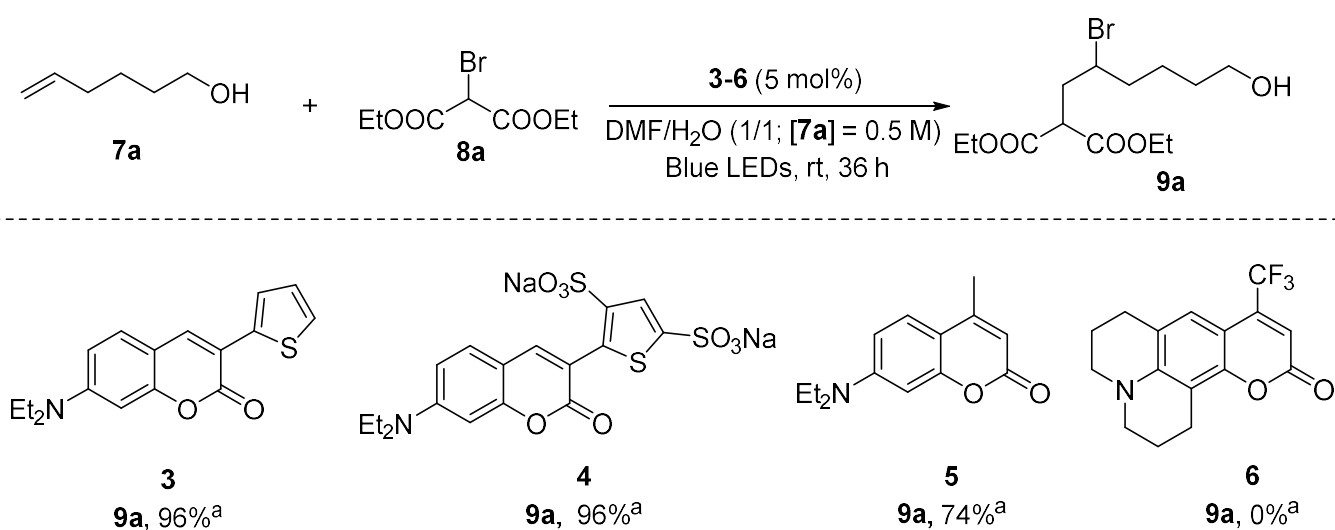


Figure 4 Screening of coumarin dyes **3-6** as photocatalysts in the ATRA reaction. ^a Determined by ¹H-NMR analysis.

To our delight, coumarins **3** and **4** proved to be excellent photocatalysts as well as coumarin **5** which provided a conversion of 74%. As discussed in section 2.2.1, Coumarin **6** confirmed to be inactive as photocatalyst also in this reaction. Presumably, the total inactivity of coumarin **6** can be explained by a twisted intramolecular charge-transfer (TICT) relaxation of the dye in the excited state, as previously discussed in section 1.1.6 that can not favour the interaction with the incoming quencher.

3.2.2 Reaction optimization

Reaction conditions were optimised by screening several solvents, additives, sacrificial agents and photocatalyst loading. The attempts were conducted using coumarins **3** and **4** as photocatalysts, under Blue LEDs irradiations at room temperature over 36 hours (Table 1).

Entry ^[a]	Coumarin	Solvent	Additive	Reducing agent	Conversion (%) ^[b]
1	3	DMF	-	-	33
2	4	DMF	-	-	3
3	4	DMF/H ₂ O (1/1)	-	-	96
4	3	DMF/H ₂ O (1/1)	-	-	96
5	3	CH ₃ CN/H ₂ O (1/1)	-	-	93
6	3	EtOH/H ₂ O (1/1)	-	-	86
7	3	DMSO/H ₂ O (1/1)	-	-	98
8	3	DMF	-	Et ₃ N (4 equiv.)	0
9	4	DMF	-	Et ₃ N (20 mol%)	33
10	3	DMF/H ₂ O (1/1)	LiBr (2 equiv.)	-	96
11	4	DMF/H ₂ O (1/1)	LiBr (2 equiv.)	-	96
12	3 (1 mmol%)	EtOH/H ₂ O (1/1)	-	-	94
13	3 (2.5 mmol%)	EtOH/H₂O (1/1)	-	-	96

Table 1 Screening of parameters (solvents, presence of reducing agents and additives, photocatalyst loading) in the ATRA reaction of olefin **7a** with the alkyl bromide **8a**.^aReaction conditions: **7a** (0.1 mmol), **3-4** (5 mmol%), [**7a**]=0.2M, Blue LEDs, room temperature, 36h; ^b Determined by ¹H-NMR analysis;

Screening of solvents (Entry 1-7) showed the influence of water on the reaction efficiency. In fact, the absence of water as solvent led to poorer conversions (Entry 1-2) in comparison with the mixture of H₂O and other polar solvents (Entry 3-7). The presence of TEA (Entry 8-9) as a sacrificial reducing agent, proved unsuccessful and clearly, it demonstrates that reducing agents do not play any role in the reaction mechanism. Similarly, addition of lithium bromide (Entry 10-11), which increased the

yield in other works,³ was unhelpful in our case. Catalyst loading (Entries 12 and 13) as low as 1 mol% demonstrates the catalyst efficiency.

Entries 3,4,7and13 show excellent results providing yields of over 95%. Preferred reaction conditions are shown in entry 13, employing EtOH/H₂O as the solvent mixture of choice and 2.5 mol% catalyst loading of coumarin 3.

3.2.3 Substrates scope

Substrate scope of several alkyl halides was next investigated. The above mentioned preferred reaction conditions were used on 0.2mmol substrate scale, employing hexenol as olefin (Figure 5).

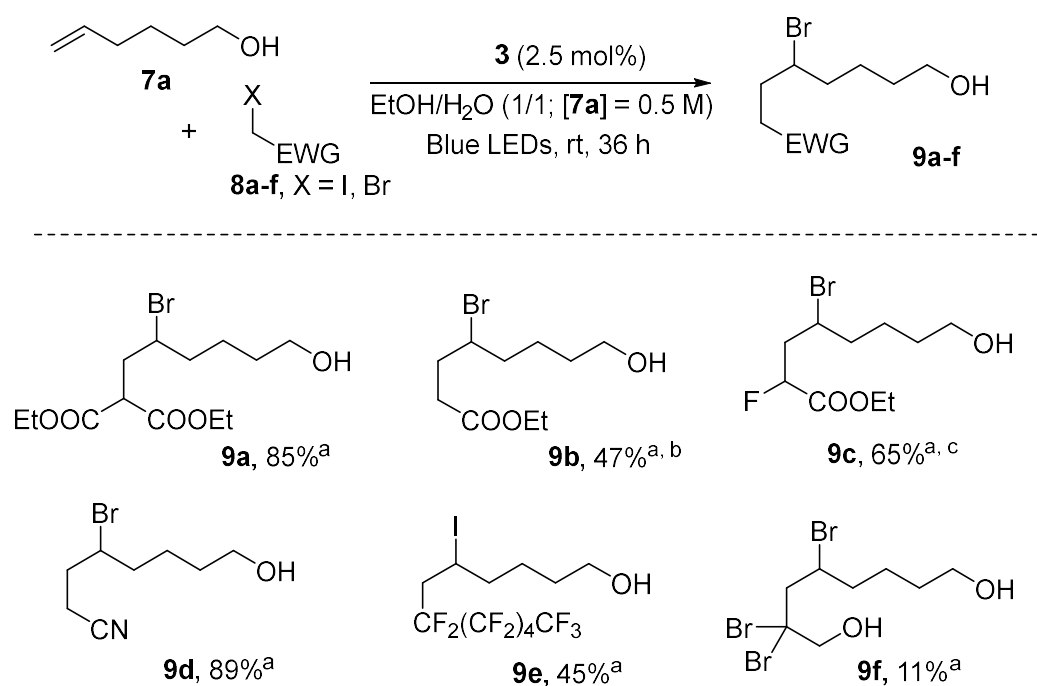


Figure 5 Screening of several alkyl halogenates in the photoredox catalyzed ATRA reaction mediated by coumarin 3. ^a Yield after chromatographic purification. ^b Reaction conditions: 7a (0.2 mmol), 8b (0.6 mmol), 4 (5 mmol%), DMF/H₂O 1/1 [7a]=0.5M, Blue LEDs, room temperature, 36h; ^c Reaction conditions: 7a (0.2 mmol), 8c (0.6 mmol), 4 (5 mmol%), DMF/H₂O 1/1 [7a]=0.5M, Blue LEDs, room temperature, 36h.

Screening of alkyl bromides provided the ATRA products in yields from moderate to excellent. Compound 9a was successfully isolated in an 85% yield. Interestingly, the possibility to use ethylbromoacetate 8b, a substrate quite challenging for other photocatalysts, is noteworthy. The presence of electron withdrawing groups such as fluoride (8c) and nitrile (8d) is well tolerated. The corresponding products were obtained in 65% and 89% respectively. In the case of products 9b and

9c, a marked improvement of the yield was observed through the modification of the experimental conditions. The use of iodo alkyl substrate (**8e**) also proved successful, even though the product was isolated in a moderate 45% yield. The low yield for product **9f** could be explained by subsequent ring closure of the primary alcohol to form the tetrahydrofuran derivative as detected by $^1\text{H-NMR}$ analysis.

Next, screening of several olefins was carried out using the preferred reaction conditions reported in entry 13 (Table 1) and ethyl-bromo malonate as the alkyl halide (Figure 6).

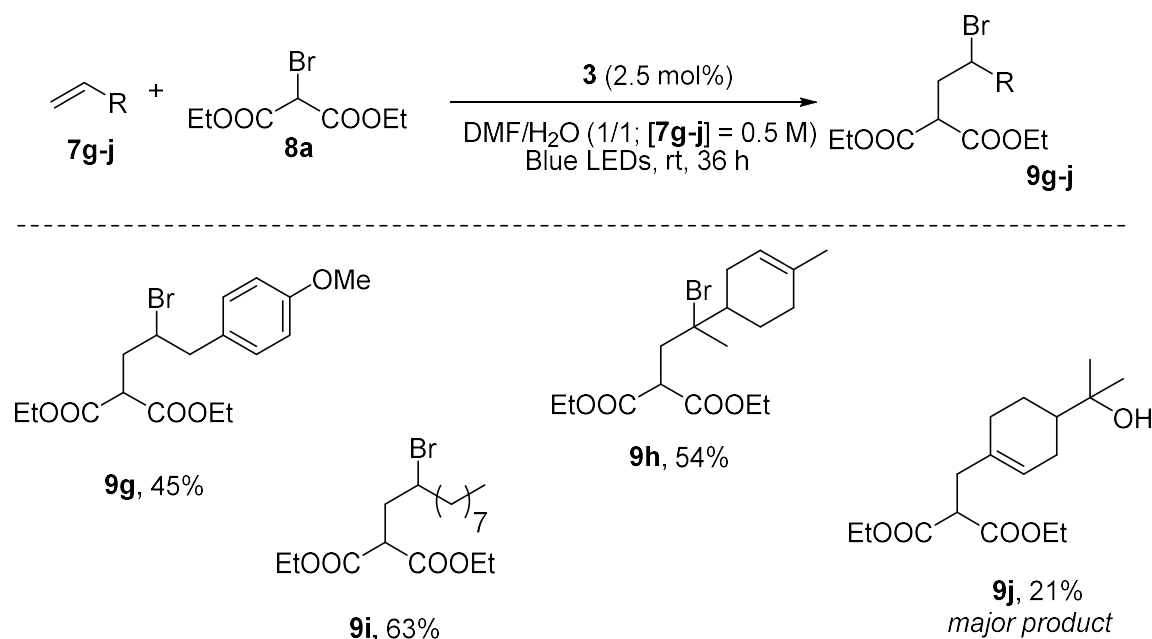


Figure 6 Screening of several alkyl halogenates in the photoredox catalyzed ATRA reaction mediated by coumarin **3**, yields after chromatographic purification.

The employed olefins resulted reactive but the final products were isolated in moderate yields. Worst performances in terms of yield, compared with other photocatalysts,^{16, 17} was observed. The use of 4-allyl anisole provided the product **9g** in 45% of yield. The employment of aliphatic olefins including the cyclohexene derivative **7h** and octene **7i** gave yields of 54% and 63% respectively.

Product **9j**, obtained using β-pinene as olefin, is derived from the opening of the pinene bridge and it further highlighted the radical nature of the process as already reported in other works (Figure 7).

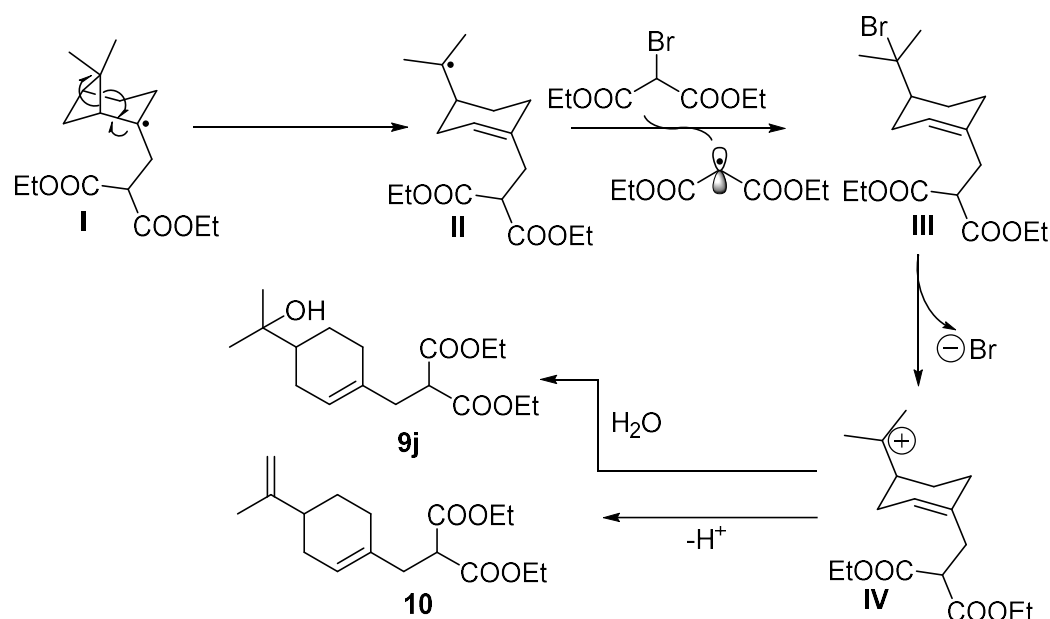


Figure 7 Formation of side product **10** from ATRA reaction using pinene as olefin.

Pinene radical **I** formed after the addition of the free radical on the olefin undergoes rearrangement with a consequent bridge opening **II**. Addition of radical bromine to give the bromine species **III** and the subsequent elimination of the ion bromide generated the carbocation **IV**. The final product **9j** was obtained as major product after addition of water. Traces of compound **10** derived by elimination were observed.

Finally, the ATRA reaction of bromoacetonitrile with 4-allylanisole was attempted. In this case, the conditions reported in entry 3 were used (Figure 8).



Figure 8 Photocatalyzed ATRA reaction between bromoacetonitrile and 4-allylanisole.

The employment of DMF/H₂O as solvent mixture were used to increase the solubility of the substrates and the photocatalyst. Albeit the product **11** was isolated in a moderate yield, it successfully demonstrated the versatility of the developed methodology and allows the use of highly diverse substrates.

A reaction mechanism to explain the role of the photocatalyst and how it is regenerated during the ATRA reaction was hypothesized.

3.2.4 Proposed Mechanism

The proposed mechanism initiated by the reduction by single electron transfer of the alkyl bromide by [Coumarin]* in the excited state to generate the radical carbocation [Coumarin]^{•+} and the radical anion **I**. After elimination of bromide, the radical **II** reacts with the olefins generating the radical **III**. The final alkyl bromide **V** is obtained through two plausible pathways. In a radical-polar crossover mechanism (Pathway A, in pink) the [Coumarin]^{•+} species is reduced by the radical **III** to regenerate the photocatalyst [Coumarin] and to form the carbocation **IV** which gives the final product **V** after addition of bromide ion (Figure 9).

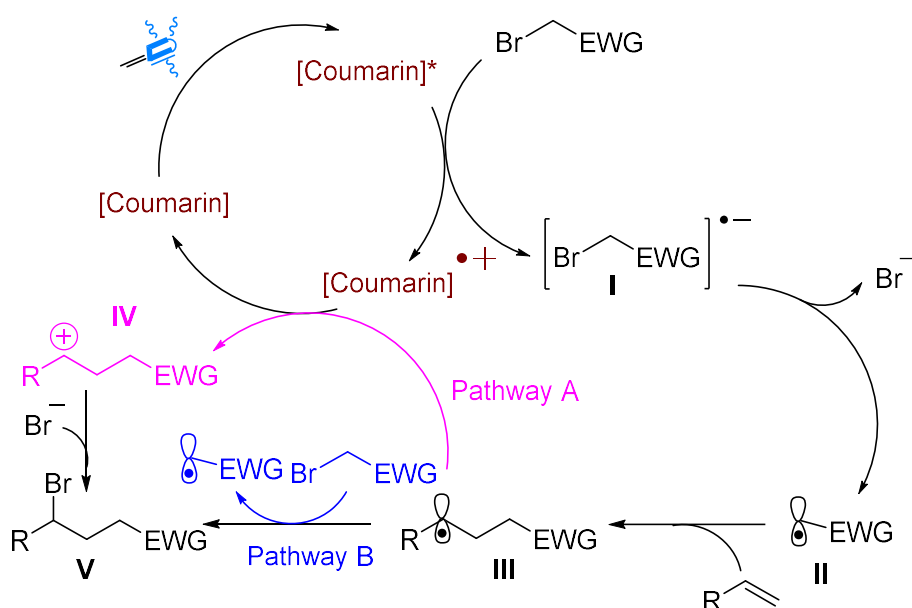


Figure 9 Proposed mechanism for the photocatalyzed ATRA reaction

In the radical chain propagation (Pathway B, in blue), the photocatalyst [Coumarin]* acts as radical initiator. The final product **V** was generated by the reduction of the radical species **III** by the alkyl bromide.

In view of the obtained results in ATRA reactions, the photocatalytical generation of alkyl radical mediated by coumarin dyes in other chemical transformations was attempted.

3.2.5 α -alkylation of cinnamaldehyde by photoredox catalysis

As previously reported, the first example for the photoredox α -alkylation of aldehydes was disclosed by MacMillan and co-workers. This broadly applicable reaction proceeds with high yields (up to 80% in most cases) and enantiomeric excesses (up to 97%). The excellent enantioselectivity is obtained thanks to the chiral organic imidazolidinone catalyst **2**, a derivative which was deeply employed in

several asymmetric organocatalytic transformation including Diels-Alder cycloaddition, Friedel-Crafts alkylation and intramolecular Michael addition as some well-known examples.¹⁸

As a further example on the use of alkyl radicals generated by coumarin mediated photocatalysis, the α -alkylation of hydrocinnamaldehyde with alkyl bromides **12a** and **12b** was investigated. The reaction was performed in the presence of photocatalyst **4**, the chiral catalyst **2**, 2,6-lutidine as base, under Blue LEDs irradiation and over 18 hours (Figure 10).

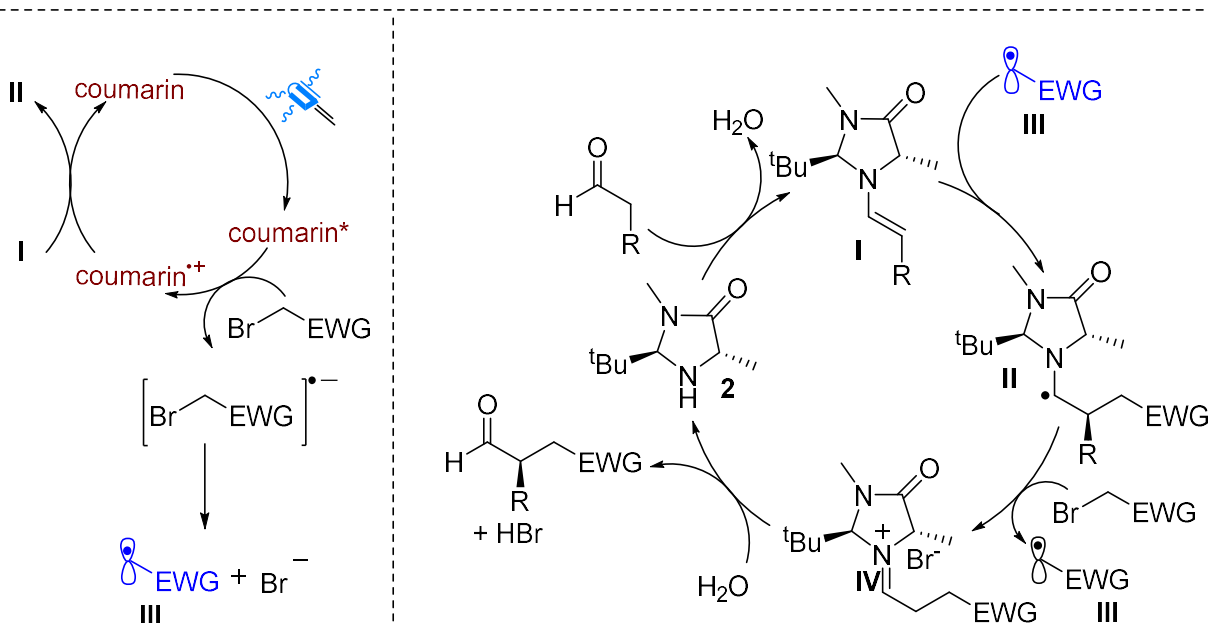
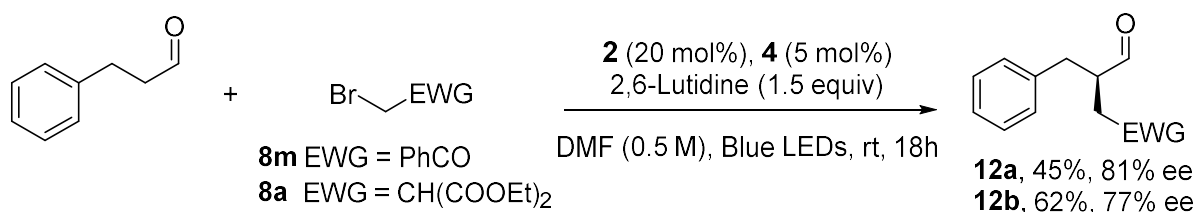


Figure 10 α -alkylation of cinnamaldehyde mediated by coumarin **4**, yields after chromatographic purification.

The α -alkylated aldehydes **12a** and **12b** were successfully obtained in moderate yields and with enantiomeric excesses of 81% and 77% respectively. Disappointingly, compound **12a** was obtained in lower level of yield and enantioselectivity compared with MacMillan's result (yield 92%, ee 90%). However, it is to point out the completely different mechanism in this stereoselective alkylation of aldehyde. In fact in MacMillan conditions, the reaction is carried out by using $[\text{Ru}(\text{bpy})_3]^{2+}$ as the photocatalyst. It is also worth adding that there are example of stereoselective alkylation carried out in the presence of Eosin Y as an organic dye photocatalyst.¹⁹ In the conditions reported by MacMillan the reaction is initiated by a sacrificial oxidation of enamine formed in situ, that is irreversible consumed (as a small amount of the chiral imidazolidinone catalyst) producing the formal

[Ru(I)(bpy)₃] complex. This species is starting a radical chain reaction by reducing the halide and producing the alkyl radical. In our reaction, we have proposed that the organic photocatalyst acts as initiator of a similar the chain mechanism.²⁰ The [coumarin]* in the excited state is able to reduce the alkylating agent giving the formation of the radical species **III** and the radical carbocation [coumarin]^{•+} as previously discussed. Presumably, the single electron transfer between the enamine **I** and the [coumarin]^{•+} species regenerates the [coumarin] in the photocatalytic cycle, yielding the radical amine **II**. The reduction of the radical species **II** by the alkylbromide afforded the iminium ion **IV** which, after hydrolysis, furnished the alkylated aldehyde **12**.

The photocatalyst **4** was employed in the photoredox reductive dehalogenation of bromoacetophenone.

3.2.6 Photoredox reductive dehalogenations mediated by coumarin dyes

An example of photoredox reductive dehalogenations was reported by Stephenson and co-workers as previously discussed. This method relied on the use of the photocatalyst [Ru(bpy)₃]²⁺ to generate the alkyl radical species and the subsequent protonation by Hantzsch ester as hydrogen source.²¹

Hantzsch ester **14** is a 1,4-dihydropyridine derivatives which has found a widespread application in the reduction of various unsaturated compounds.²² The coumarin **4** as photocatalyst of the photoredox reductive dehalogenation of bromoacetophenone in the presence of Hantzsch ester was employed. The reaction was performed under Blue LEDs irradiation, at room temperature and over 36 hours (Figure 11).

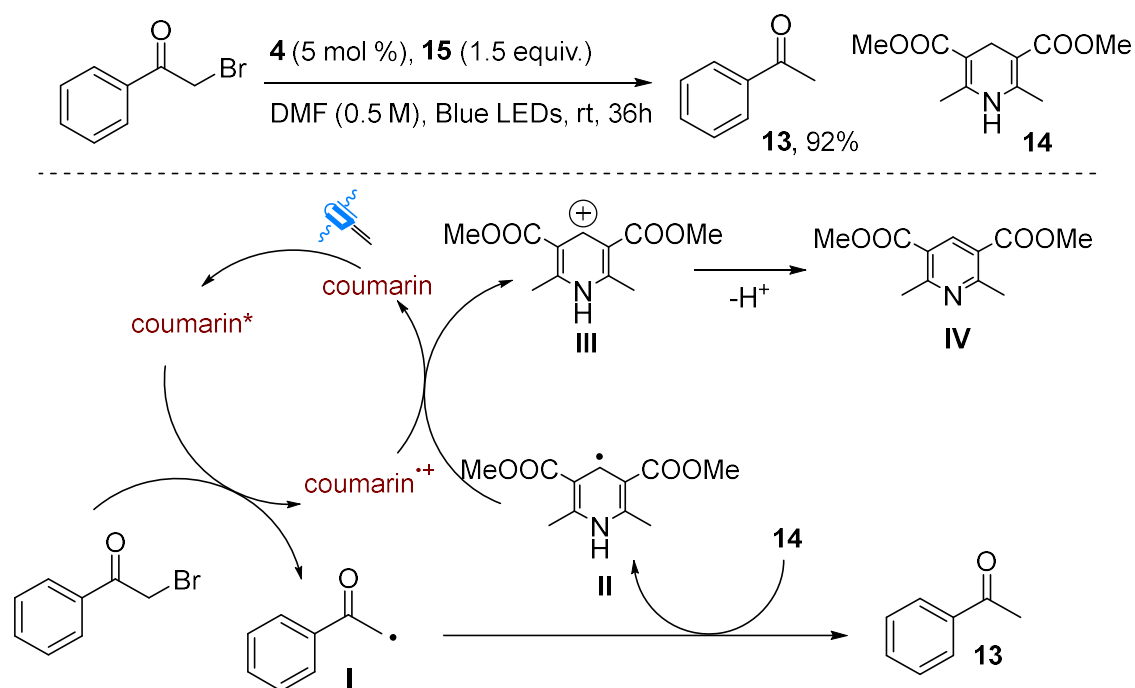


Figure 11 Photoredox reductive dehalogenations mediated by coumarin **4**, yields after chromatographic purification.

Gratifyingly, acetophenone **13** was successfully isolated in an excellent yield of 92%, a data comparable with the results obtained by Stephenson and co-workers. We proposed a mechanism wherein the single electron transfer from the [coumarin]* in the excited state to bromoacetophenone ($E = -1.46$ V vs SCE) forming the alkyl radical **I** and the radical carbocation [coumarin] $^{\bullet+}$. The acetophenone **13** and the dihydropyridine radical species **II** were obtained through Hydrogen Atom Transfer (HAT) between the Hantzsch ester **14** and the alkyl radical **I**. The reduction of [coumarin] $^{\bullet+}$ by the radical species **II** restores the photocatalytic cycle of the coumarin. The formed carbocation **III** undergoes aromatization to give the pyridine derivative **IV**.

As a last example, pleased by the results obtained in the photoredox generation of alkyl radical from the alkyl halogenates, a photocatalyst in oxytrifluoromethylation of alkenes mediated by coumarin **4** was investigated.

3.2.7 Photocatalytical oxy-trifluoromethylation mediated by coumarin dyes

The generation of trifluoromethyl radical $\cdot\text{CF}_3$ by photoredox catalysis was exploited in the oxy-,²³ hydro-²⁴ and amino- trifluoromethylation²⁵ of alkene using [fac-Ir(ppy)₃], [Ru(bpy)₃]Cl₂ and [Ru(bpy)₃](PF₆)₂ respectively as photocatalysts. In these cases, commercially available Umemoto's reagents **15** (Figure 12) as the trifluoromethylating agents were preferred over the more common CF₃I and CF₃SO₂Cl sources for stability reasons. Umemoto's reagent is a dibenzothiophene salt containing a trifluoromethyl group, this $\cdot\text{CF}_3$ source was applied to the trifluoromethylation of various nucleophiles including β -ketoesters at the α -position and indoles at the position 2.

The coumarin **4** was employed as photocatalyst in oxytrifluoromethylation of stilbene in the presence of Umemoto's reagent as $\cdot\text{CF}_3$ source and oxygen nucleophiles such as water or methanol. The attempts were carried out under Blue LEDs irradiation, at room temperature and over 18 hours (Figure 12). The Umemoto's reagent was chosen because of its low reduction potential (-0.74 V vs SCE) as reported by Akita and co-workers.

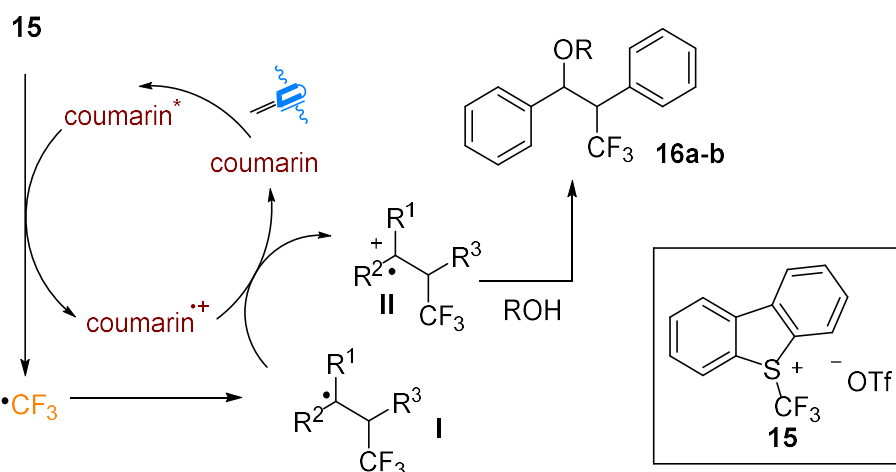
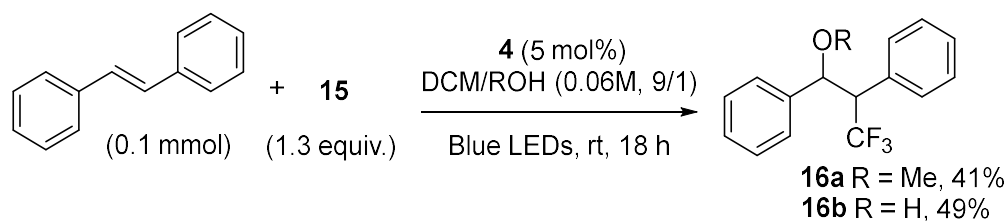


Figure 12 Photoredox oxy-trifluoromethylation of alkenes mediated by coumarin **4**, yields after chromatographic purification.

The dihydro-stilbene derivatives **17a-b** were obtained in similar moderate yields according to oxygenated solvent employed (H₂O or MeOH). The [coumarin]* in the excited state has enough potential to generate the radical $\cdot\text{CF}_3$ and the radical carbocation [coumarin]^{•+} from the Umemoto's reagent **15** by single electron transfer. The addition of trifluoromethyl radical $\cdot\text{CF}_3$ to the alkene gives the alkyl radical **I** which is oxidized by [coumarin]^{•+} giving the alkyl carbocation **II** and the regeneration of the photocatalyst [coumarin]. Nucleophilic attack of O species (water or methanol) on the radical carbocation **II** provides the oxytrifluoromethylated compounds **18a-b**.

3.3 Conclusions

In this chapter, the use of coumarin dyes as photocatalyst was extended to various organic reactions. Coumarins **3** and **4** were employed in photoredox ATRA reactions without the need for sacrificial Et₃N, or other reducing agents. The reaction showed a broad scope and a good tolerance to various electron withdrawing groups. In particular, the good yield obtained using ethylbromoacetate is noteworthy. Coumarin **4** was also applied as photocatalyst in enantioselective α -alkylations of the tetrahydro-cinnamaldehyde proceeding with a good level of enantioselectivity and in the reductive dehalogenation of bromoacetophenone providing an excellent yield. Furthermore, the photoredox generation of trifluoromethyl radical for the oxytrifluoromethylation of stilbene was successfully

carried out employed coumarins **4** as photocatalyst. The possibility to further improve the efficiency of coumarin dyes as photocatalyst by introducing different functional groups will be presented.

3.4 Experimental procedures

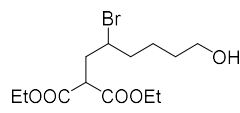
3.4.1 General methods and materials

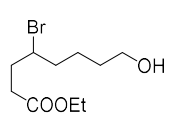
¹H NMR spectra were recorded on Varian Mercury 400 spectrometer. Chemical shifts are reported in ppm from TMS with the solvent resonance as the internal standard (deuteriochloroform: $\delta = 7.27$ ppm; dimethyl sulfoxide-d₆: $\delta = 2.50$ ppm). Data are reported as follows: chemical shift, multiplicity (s = singlet, d = duplet, t = triplet, q = quartet, dd = double duplet, dt = double triplet, bs = broad signal, m = multiplet, quint = quintet), coupling constants (Hz). ¹³C NMR spectra were recorded on Varian MR400 spectrometer. Chemical shifts are reported in ppm from TMS with the solvent as the internal standard (deuteriochloroform: $\delta = 77.0$ ppm; dimethyl sulfoxide-d₆: $\delta = 39.5$ ppm). LC-electrospray ionization mass spectra (ESI-MS) were obtained with Agilent Technologies MSD1100 single-quadrupole mass spectrometer. Chromatographic purification was done with 240-400 mesh silica gel. Purification on preparative thin layer chromatography was done on Merck TLC silica gel 60 F₂₅₄.

All reactions were set up under an argon atmosphere in oven-dried glassware using standard Schlenk techniques. Synthesis grade solvents were used as purchased and the reaction mixtures were degassed by four cycles of freeze-pump-thaw.

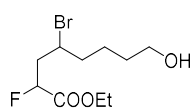
3.4.2 General procedure for photoredox ATRA reaction

A dry 10 mL Schlenk tube, equipped with a Rotaflo Stopcock, magnetic stirring bar and an argon supply tube, was charged in order and under argon with the photocatalyst **3** (2.5 mol%, 0.005 mmol, 1.5 mg), EtOH (500 μ L), H₂O (500 μ L), alkyl halide (0.2 mmol, 1 equiv., or different if specified), olefin (0.4 mmol, 2 equiv., or different if specified). The reaction mixture was degassed via freeze pump thaw (x4), and the vessel refilled with argon. The reaction mixture was positioned approximately 10 cm from the light source (16 W blue LEDs). After vigorous stirring for 36 h, the mixture was transferred in a separator funnel and extracted with AcOEt (3 x 5 mL). The combined organic layers were washed with brine (10 mL), dried over Na₂SO₄ and concentrated under reduced pressure to give the crude products. The residue was purified by flash column chromatography (SiO₂) to afford the title compounds in the stated yields.

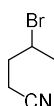
 (**9a**): colorless oil; 85% (0.17 mmol, 0.058 g). The general procedure was applied using **16a** (0.2 mmol, 34 μ L), **15** (0.4 mmol, 48 μ L, 2 equiv.) and **5** (0.005 mmol, 0.0015 g). The title compound was isolated by flash column chromatography (cyclohexane/ethyl acetate, 7/3). ¹H NMR (400 MHz, CDCl₃, 25°C): $\delta = 4.29$ –4.09 (m, 4H), 4.03–3.93 (m, 1H), 3.75 (dd, $J = 10.2, 4.2$ Hz, 1H), 3.63 (t, $J = 6.0$ Hz, 2H), 2.44 (ddd, $J = 14.7, 10.2, 3.1$ Hz, 1H), 2.23 (ddd, $J = 14.8, 10.6, 4.2$ Hz, 1H), 1.92–1.79 (m, 2H), 1.71–1.41 (m, 4H), 1.32–1.19 (m, 6H); ¹³C NMR (100 MHz, CDCl₃, 25°C): $\delta = 168.9, 168.8, 62.5, 61.7, 61.6, 54.6, 50.5, 39.1, 37.8, 31.9, 23.7, 14.01, 13.98$; HRMS (ESI): calculated for C₁₃H₂₃BrNaO₅⁺ [M+Na]⁺ 361.0621, found 361.0624.

 (**9b**): colorless oil; 47% (0.09 mmol, 0.025 g). The general procedure was applied using **8b** (0.6 mmol, 67 μ L, 3 eq.), **7a** (0.2 mmol, 24 μ L), **3** (0.005 mmol, 0.0015 g) and DMF/H₂O (1/1) mixture as reaction solvent. The title compound was isolated by flash column chromatography (cyclohexane/ethyl acetate, 8/2). ¹H NMR (400 MHz, CDCl₃, 25°C): $\delta = 4.12$ (q, $J = 7.1$ Hz, 2H), 4.08–4.00 (m), 3.64 (t, $J = 6.1$ Hz, 2H), 2.62–2.44 (m, 2H), 2.23–2.12 (m), 2.10–1.97 (m), 1.90–1.79 (m, 2H), 1.66–1.46 (m, 4H), 1.24 (t, $J = 8$ Hz, 3H); ¹³C NMR (100 MHz, CDCl₃, 25°C): $\delta = 172.8, 62.6, 60.5, 56.8, 38.9, 33.9, 32.3, 31.9, 23.8, 14.2$; HRMS (ESI): calculated for C₁₀H₁₉BrNaO₃⁺ [M+Na]⁺ 289.0410, found 289.0416.

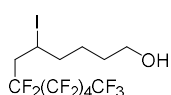
Chapter 3: Photoredox alkylradicals generation mediated by coumarin dyes



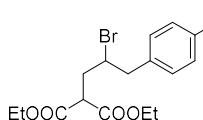
(9c): colorless oil; 65% (0.13 mmol, 0.037 g). The general procedure was applied using **8c** (0.6 mmol, 72 μ L, 3 eq.), **7a** (0.2 mmol, 24 μ L), **3** (0.005 mmol, 0.0015 g) and DMF/H₂O (1/1) mixture as reaction solvent. The title compound was isolated by flash column chromatography (cyclohexane/ethyl acetate, 85/15) and obtained as mixture of diastereoisomers A and B. ¹H NMR (400 MHz, CDCl₃, 25°C): δ = 5.32–4.99 (m), 4.31–4.21 (m, 2H), 4.20–4.12 (m), 3.64 (t, J = 5.8 Hz, 2H), 2.52–2.19 (m, 2H), 1.96–1.79 (m, 2H), 1.70–1.44 (m, 4H), 1.35–1.27 (m, 3H); ¹³C NMR (100 MHz, CDCl₃, 25°C): δ = 169.4 (d, J = 22.8 Hz, A), 169.1 (d, J = 23.4 Hz, B), 87.3 (d, J = 184.7 Hz, A), 86.7 (d, J = 185.2 Hz, B), 62.5 (s, A+B), 61.9 (s, B), 61.8 (s, B), 51.6 (d, J = 1.9, A), 50.6 (d, J = 4.0, B), 41.7 (d, J = 20.6, A), 41.3 (d, J = 21.1, B), 39.0 (s, A+B), 38.0 (s, A+B), 31.8 (s, A), 31.8 (s, B), 23.8 (s, B), 23.7 (s, A), 14.1 (s, B), 14.1 (s, A); ¹⁹F NMR (377 MHz, CDCl₃, 25°C): δ = -190.5 – -190.8 (m), -194.7 – -195.0 (m); HRMS (ESI): calculated for C₁₀H₁₈BrFNaO₃⁺ [M+Na]⁺ 307.0316, found 307.0313.



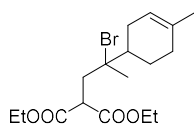
(9d): colorless oil; 89% (0.18 mmol, 0.039 g). The general procedure was applied using **8d** (0.6 mmol, 67 μ L, 3 eq.), **7a** (0.2 mmol, 42 μ L), and **3** (0.005 mmol, 0.0015 g) and DMF/H₂O (1/1) mixture as reaction solvent. The title compound was isolated by flash column chromatography (cyclohexane/ethyl acetate, 8/2). ¹H NMR (400 MHz, CDCl₃, 25°C): δ = 4.05 (m, 1H), 3.64 (m, 2H), 2.59 (m, 2H), 2.16 (m, 1H), 2.06 (m, 1H), 1.87 (m, 2H), 1.59 (m, 4H); ¹³C NMR (100 MHz, CDCl₃, 25°C): δ = 118.7, 62.4, 54.67, 38.6, 34.5, 31.8, 23.8, 16.0; HRMS (ESI): calculated for C₈H₁₅BrNO⁺ [M+H]⁺ 220.0332, found 220.0323



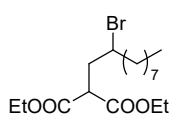
(9e): colorless oil; 35% (0.09 mmol, 0.049 g). The general procedure was applied using **8e** (0.4 mmol, 86 μ L, 2 equiv.), **7a** (0.2 mmol, 24 μ L), **3** (0.005 mmol, 0.0015 g) and DMF/H₂O (1/1) mixture as reaction solvent. The title compound was isolated by flash column chromatography (cyclohexane/ethyl acetate, 85/15). Spectroscopic properties were according to those reported in literature.²⁶ ¹H NMR (400 MHz, CDCl₃, 25°C): δ = 4.39–4.32 (m, 1H), 3.69 (t, J = 5.9 Hz, 2H), 2.98–2.74 (m, 2H), 1.87–1.83 (m, 2H), 1.69–1.50 (m, 4H); ¹³C NMR (100 MHz, CDCl₃, 25°C): δ = 62.5, 41.7 (t, J = 20.9 Hz), 40.0 (d, J = 2.1 Hz), 31.5, 29.7, 26.0, 20.4. ¹⁹F NMR (377 MHz, CDCl₃, 25°C): δ = -79.59 (t, J = 10.0 Hz, 3F), -109.21– -114.58 (m, 2F), -120.56 (s, 2F), -121.63 (s, 2F), -122.40 (s, 2F), -124.56– -125.16 (m, 2F); Elemental Analysis: Found C, 26.3; H, 2.1%; Calc. for C₁₂H₁₂F₁₃IO; C, 26.4; H, 2.2%.



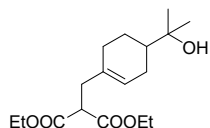
(9g): colorless oil; 45% (0.09 mmol, 0.035 g). The general procedure was applied using **8a** (0.2 mmol, 34 μ L), **7g** (0.4 mmol, 61 μ L, 2 equiv.) and **3** (0.005 mmol, 0.0015 g). The title compound was isolated by flash column chromatography (cyclohexane/ethyl acetate, 95/5). ¹H NMR (400 MHz, CDCl₃, 25°C) δ = 7.14 – 7.07 (m, 2H), 6.87 – 6.79 (m, 2H), 4.27 – 4.06 (m, 5H), 3.81 – 3.73 (m, 4H), 3.13 (dd, J = 6.9, 4.3 Hz, 2H), 2.48 (ddd, J = 14.8, 10.5, 2.9 Hz, 1H), 2.20 (ddd, J = 14.9, 11.0, 4.0 Hz, 1H), 1.28 – 1.19 (m, 6H); ¹³C NMR (100 MHz, CDCl₃, 25°C) δ = 168.9, 168.6, 158.5, 130.2 (2C), 129.8, 113.8 (2C), 61.7, 61.55, 55.18, 54.61, 50.61, 44.93, 37.03, 13.99 (2C).



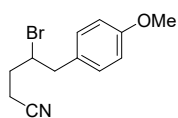
(9h): colorless oil; 54% (0.10 mmol, 0.047 g). The general procedure was applied using **8a** (0.2 mmol, 34 μ L), **7h** (0.4 mmol, 76 μ L, 2 equiv.) and **3** (0.005 mmol, 0.0015 g). The title compound was isolated by flash column chromatography (cyclohexane/ethyl acetate, 8/2). ¹H NMR and ¹³C NMR were conformed to the literature.²⁷



(9i): colorless oil; 63% (0.12 mmol, 0.047 g). The general procedure was applied using **8a** (0.2 mmol, 34 μ L), **7i** (0.4 mmol, 64 μ L, 2 equiv.) and **3** (0.005 mmol, 0.0015 g). The title compound was isolated by flash column chromatography (cyclohexane/ethyl acetate, 95/5). ¹H NMR (400 MHz, CDCl₃, 25°C) δ = 4.26 – 4.12 (m, 4H), 4.01 – 3.93 (m, 1H), 3.76 (dd, J = 10.2, 4.2 Hz, 1H), 2.48 – 2.39 (m, 1H), 2.22 (ddd, J = 14.9, 10.6, 4.2 Hz, 1H), 1.87 – 1.78 (m, 2H), 1.56 – 1.36 (m, 2H), 1.30 – 1.18 (m, 16H), 0.85 (t, J = 6.8 Hz, 3H); ¹³C NMR (100 MHz, CDCl₃, 25°C) δ = 168.97, 168.77, 61.63, 61.55, 55.01, 50.58, 39.41, 37.85, 31.78, 29.33, 29.14, 28.90, 27.37, 22.60, 14.04, 14.02, 13.98.



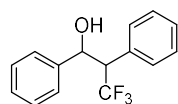
(9j): yellowish oil; 21% (0.04 mmol, 0.016 g). The general procedure was applied using **8a** (0.2 mmol, 34 μ L), **7j** (0.4 mmol, 63 μ L, 2 equiv.) and **3** (0.005 mmol, 0.0015 g). The title compound was isolated by flash column chromatography (cyclohexane/ethyl acetate, 95/5). ^1H NMR and ^{13}C NMR were conformed to the literature.



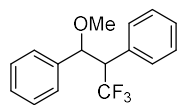
(11): yellowish oil; 41% (0.09 mmol, 0.22 g). The general procedure was applied using **8d** (0.6 mmol, 42 μ L), **7g** (0.2 mmol, 31 μ L, 2 equiv.) and **4** (0.005 mmol, 0.003 g). The title compound was isolated by flash column chromatography (cyclohexane/ethyl acetate, 95/5). ^1H NMR and ^{13}C NMR were conformed to the literature.²⁸

3.4.2 General procedure for trifluoromethylation reaction

In a Schlenk tube with rotaflo stopcock under argon atmosphere at r.t., coumarin **4** (0.05 mmol, 1.5 mg) was dissolved in 2.0 mL of a mixture of DCM and ROH (9/1, water or methanol). Stilbene **18** (0.1 mmol, 0.018 g), Umemoto reagents **15** (0.14 mmol, 0.052g) were then added. The reaction mixture was carefully degassed via freeze-pump thaw (three times), and the vessel refilled with argon. The Schlenk tube was stirred and irradiated with 16 W blue LEDs positioned approximately at 10 cm distance from the reaction vessel. After 18 h of irradiation, 10% aq. Na_2SO_3 (5 mL) was added and the mixture was extracted with DCM (4 x 5 mL). The collected organic layers were dried over Na_2SO_4 , filtered and concentrated under reduced pressure. Products **16a-b** were purified by column flash chromatography on SiO_2 .



(16a): colorless oil; 49% (0.05 mmol, 0.012 g); d.r. = 4.45:1 (syn-20a:anti-20a) was determined by integration of benzylic CHOH ^1H NMR signal. The title compound was isolated by flash column chromatography (cyclohexane/ethyl acetate, 9/1) as mixture of diastereoisomers in 7:1 ratio (syn-**16a**:anti-**16a**). ^1H NMR (400 MHz, CDCl_3 , 25 $^\circ\text{C}$): $\delta_{\text{syn,anti}}$ = 7.35–7.25 (m, 2H), 7.21–7.11 (m, 11H), 7.10–6.98 (m, 7H), 5.38–5.33 (*anti*, m, 1H), 5.21 (*syn*, dd, J = 9.2, 2.9 Hz, 1H), 3.67 (*syn*, p, J = 9.2 Hz, 1H), 3.56 (*anti*, ddd, J = 19.3, 9.7, 5.4 Hz, 1H), 2.27 (*syn*, d, J = 3.3 Hz, 1H), 1.98 (*anti*, d, J = 3.9 Hz, 1H); ^{13}C NMR (100 MHz, CDCl_3): $\delta_{\text{syn,anti}}$ = 140.7, 132.7, 130.2, 129.3 (2C), 128.5, 128.4 (2C), 128.3, 128.2 (2C), 128.1 (2C), 128.0 (2C), 127.9, 126.8 (2C), 126.3, 125.1, 74.7 (*syn*), 72.3 (*anti*), 57.4 (quin, J = 25.0, 2C); ^{19}F NMR (377 MHz, CDCl_3 , 25 $^\circ\text{C}$): $\delta_{\text{syn,anti}}$ = -62.02 (d, J = 9.2 Hz, 3F, *syn*), -63.77 (d, J = 9.2 Hz, 3F, *anti*); HRMS (ESI): calculated for $\text{C}_{15}\text{H}_{14}\text{F}_3\text{O}^+$ $[\text{M}+\text{H}]^+$ 267.0991, found 267.0993.



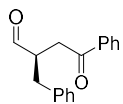
(16b): pale yellow oil; 41% (0.04 mmol, 0.011 g); d.r. = 3.9:1 (syn-**16b**:anti-**16b**) was determined by integration of benzylic CHOH ^1H NMR signal. The title compound was isolated by flash column chromatography (cyclohexane/ethyl acetate, 95/5) as mixture of diastereoisomers in 5.8:1 ratio (syn-**16b**:anti-**16b**). ^1H NMR (400 MHz, CDCl_3 , 25 $^\circ\text{C}$): $\delta_{\text{syn,anti}}$ = 7.20–7.09 (m, 6H *syn* + 6H *anti*), 7.02–6.96 (m, 4H *syn* + 4H *anti*), 4.78 (d, J = 4.9 Hz, 1H *anti*), 4.59 (d, J = 9.3 Hz, 1H *syn*), 3.63 (m, 1H *syn*), 3.45 (m, 1H *anti*), 3.23 (s, 3H *syn*), 3.19 (s, 3H *anti*); ^{13}C NMR (100 MHz, CDCl_3): $\delta_{\text{syn,anti}}$ = 138.7 (*anti*), 138.1 (*syn*), 132.9, 130.5, 129.3 (2C), 128.3 (2C), 128.2 (2C), 128.1, 128.0, 127.8, 127.6 (2C), 127.05, 124.9, 83.5, 81.3, 57.4–56.8 (m), 56.6; ^{19}F NMR (377 MHz, CDCl_3 , 25 $^\circ\text{C}$): $\delta_{\text{syn,anti}}$ = -62.07 (3F, *syn*), -64.28 (3F, *anti*); HRMS (ESI): calculated for $\text{C}_{16}\text{H}_{16}\text{F}_3\text{O}^+$ $[\text{M}+\text{H}]^+$ 281.1148, found 281.1149.

3.5.3 General procedure for enantioselective α -alkylation of aldehydes

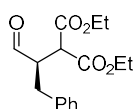
In a Schlenk tube with rotaflo stopcock under argon atmosphere at r.t., coumarin **4** (0.01 mmol, 0.005 mg) and the Macmillan catalyst **2** (0.04 mmol, 0.013 g) were dissolved in 1.0 mL DMF. Tetrahydrocinnamaldehyde (0.6 mmol, 3 equiv., 79 μ L), bromo derivatives **8a** and **8m** (0.2 mmol, 1 equiv.) and 2,6-lutidine (0.3 mmol, 35 μ L) were then added.

The reaction mixture was carefully degassed via freeze-pump thaw (three times), and the vessel refilled with argon. The Schlenk tube was stirred and irradiated with 16 W blue LEDs positioned approximately at 10 cm distance from the reaction vessel. After 18 h of

irradiation, aq. HCl 1M (5 mL) was added and the mixture was extracted with AcOEt (4 x 5 mL). The collected organic layers were dried over Na₂SO₄, filtered and concentrated under reduced pressure. Products **12a-b** were purified by column flash chromatography on SiO₂.



(**12a**): the title compound was isolated by flash column chromatography (SiO₂, cyclohexane/EtOAc, 9/1) as colorless oil (28 mg, 0.11 mmol, 56% yield, 83% ee). Ee was determined by chiral HPLC analysis using Daicel Chiralpak®IC column, hexane/*i*-PrOH 90:10, flow rate 1.00 mL/min, 30°C, λ = 210 nm: τ_{major} = 18.4 min., τ_{minor} = 15.3 min.; ¹H NMR (400 MHz, CDCl₃, 25°C): δ = 9.89 (s, 1H), 7.94–7.80 (m, 2H), 7.58–7.51 (m, 1H), 7.47–7.39 (m, 2H), 7.32–7.25 (m, 2H), 7.21 (ddd, *J* = 12.3, 6.7, 4.1 Hz, 3H), 3.52–3.30 (m, 2H), 3.26–3.08 (m, 1H), 3.05–2.93 (m, 1H), 2.87–2.76 (m, 1H). ¹³C NMR (100 MHz, CDCl₃, 25°C): δ = 203.0, 197.8, 138.1, 136.4, 133.3, 129.0 (2C), 128.7 (2C), 128.6 (2C), 128.0 (2C), 126.7, 48.3, 37.2, 34.7.



(**12b**): the title compound was isolated by flash column chromatography (SiO₂, cyclohexane/EtOAc, 95/5) as colorless oil (36 mg, 0.12 mmol, 62% yield, 89% ee). Ee was determined by chiral HPLC analysis using Daicel Chiralpak®IC column: hexane/*i*-PrOH 90:10, flow rate 1.00 mL/min, 30°C, λ = 210 nm: τ_{major} = 17.8 min., τ_{minor} = 14.1 min. ¹H NMR (400 MHz, CDCl₃, 25°C): δ = 9.76 (d, *J* = 0.5 Hz, 1H), 7.32–7.26 (m, 2H), 7.24–7.15 (m, 3H), 4.33–4.06 (m, 4H), 3.66 (d, *J* = 7.0 Hz, 1H), 3.47–3.28 (m, 1H), 3.10 (dd, *J* = 14.3, 7.5 Hz, 1H), 2.81 (dd, *J* = 14.3, 7.3 Hz, 1H), 1.25 (t, *J* = 7.1 Hz, 6H); ¹³C NMR (100 MHz, CDCl₃, 25°C): δ = 201.1, 168.1, 167.9, 137.4, 129.1 (2C), 128.8 (2C), 126.9, 61.9 (2C), 51.8, 51.5, 33.2, 14.0 (2C).

3.4.4 Procedure for reductive protonation of α-bromoketones.

A Schlenk tube with rotaflo stopcock under argon atmosphere at r.t. was charged with coumarin **4** (0.01 mmol, 0.005 mg), 2-bromoacetophenone **25** (0.2 mmol, 0.040 g), Hantzsch ester **14** (0.3 mmol, 1.5 equiv., 0.068 g) and DMF (1 mL). The reaction mixture was carefully degassed via freeze-pump thaw (three times), and the vessel refilled with argon. The Schlenk tube was stirred and irradiated with 16 W blue LEDs positioned approximately at 10 cm distance from the reaction vessel. After 36 h of irradiation, reaction mixture was injected in GC to confirm the complete conversion of the 2-bromoacetophenone to acetophenone.

References

- ¹ A. Studer and D. P. Curran, *Angew. Chem. Int. Ed.*, 2015, **55**, 58.
- ² R. C. McAtee, E. J. McClain and C. R. J. Stephenson, *Trends in Chemistry*, 2019, **1**, 111.
- ³ J. M. Muñoz-Molina, T. R. Belderrain and P. J. Pérez, *European Journal of Inorganic Chemistry*, 2011, **21**, 3155.
- ⁴ T. Pintauer and K. Matyjaszewski, *Chem. Soc. Rev.*, 2008, **37**, 1087.
- ⁵ E. Voutyritsa, I. Triandafillidi, N. V. Tzouras, N. F. Nikitas, E. K. Pefkianakis, G. C. Vougioukalakis and C. G. Kokotos, *Molecules*, 2019, **24**, 1644.
- ⁶ J. D. Nguyen, J. W. Tucker, M. D. Konieczynska and C. R. J. Stephenson, *J. Am. Chem. Soc.*, 2011, **133**, 4160.
- ⁷ J. D. Nguyen, J. W. Tucker, M. D. Konieczynska and C. R. J. Stephenson, *J. Am. Chem. Soc.*, 2011, **133**, 4160.
- ⁸ E. Arceo, E. Montroni and P. Melchiorre, *Angew. Chem. Int. Ed.*, 2014, **53**, 12064.
- ⁹ a) E. Voutyritsa, I. Triandafillidi, and C. G. Kokotos, *ChemCatChem*, 2018, **10**, 2466–2470. b) E. Voutyritsa, I. Triandafillidi, N. V. Tzouras, N. F. Nikitas, E. K. Pefkianakis, G. C. Vougioukalakis and C. G. Kokotos, *Molecules*, 2019, **24**, 1644.
- ¹⁰ G. Magagnano, A. Gualandi, M. Marchini, L. Mengozzi, P. Ceroni and P. G. Cozzi, *Chem. Commun.*, 2017, **53**, 1591.
- ¹¹ L. Huang, W. Yang and J. Zhao, *J. Org. Chem.*, 2014, **79**, 10240.
- ¹² C. -J. Wallentin, J. D. Nguyen, P. Finkbeiner and C. R. J. Stephenson, *J. Am. Chem. Soc.*, 2012, **134**, 8875.
- ¹³ D. A. Nicewicz and D. W. C. MacMillan, *Science*, 2008, **322**, 77.

- ¹⁴ (a) J. D. Nguyen, J. W. Tucker, M. D. Konieczynska and C. R. J. Stephenson, *J. Am. Chem. Soc.*, 2011, **133**, 4160; (b) C. -J. Wallentin, J. D. Nguyen, P. Finkbeiner and C. R. J. Stephenson, *J. Am. Chem. Soc.*, 2012, **134**, 8875.
- ¹⁵ Y. Yasu, T. Koike and M. Akita, *Angew. Chem., Int. Ed.*, 2012, **51**, 9567.
- ¹⁶ (a) J. D. Nguyen, J. W. Tucker, M. D. Konieczynska and C. R. J. Stephenson, *J. Am. Chem. Soc.*, 2011, **133**, 4160; (b) C. -J. Wallentin, J. D. Nguyen, P. Finkbeiner and C. R. J. Stephenson, *J. Am. Chem. Soc.*, 2012, **134**, 8875.
- ¹⁷ E. Arceo, E. Montroni and P. Melchiorre, *Angew. Chem. Int. Ed.*, 2015, **52**, 12064.
- ¹⁸ Mahrwald, R., Chiral Imidazolidinone (MacMillan's) Catalyst. *Comprehensive Enantioselective Organocatalysis*, 2013, 69.
- ¹⁹ M. Neumann, S. Fuldner, B. König and K. Zeitler, *Angew. Chem. Int. Ed.*, 2010, **50**, 951.
- ²⁰ For important studies about radical chain in photoredox processes: M. A. Cismesia and T. P. Yoon, *Chemical Science*, 2015, **6**, 5426.
- ²¹ J. M. R. Narayanam, J. W. Tucker and C. R. J. Stephenson, *J. Am. Chem. Soc.*, 2009, **131**, 8756.
- ²² a) G. Gelbard, J. Lin and N. Roques, *J. Org. Chem.*, 1992, **57**, 1789; b) Q. Liu, J. Li and X. X. Shen, *Tetrahedron Lett.*, 2009, **50**, 1026; c) T. Itoh, K. Nagata and M. Miyazaki, *Tetrahedron*, 2004, **60**, 6649; d) H. J. Xu, Y. C. Liu and Y. Fu, *Chin. J. Chem.*, 2008, **26**, 599; e) Z. Zhang, J. Gao and J. J. Xia, *Org. Biomol. Chem.*, 2005, **3**, 1617.
- ²³ Y. Yasu, T. Koike and M. Akita, *Angew. Chem. Int. Ed.*, 2012, **51**, 9567.
- ²⁴ S. Mizuta, S. Verhoog, K. M. Engle, T. Khotavivattana, M. O'Duill, K. Wheelhouse, G. R. M. Medebielle and V. Gouverneur, *J. Am. Chem. Soc.*, 2013, **135**, 2505.
- ²⁵ G. Dagousset, A. Carboni, E. Magnier and G. Masson, *Org. Lett.*, 2014, **16**, 4340.
- ²⁶ a) G. Foulard, T. Brigaud and C. Portella, *Tetrahedron*, 1996, **52**, 6187; b) E. Arceo, E. Montroni and P. Melchiorre, *Angew. Chem. Int. Ed.*, 2014, **53**, 12064; c) G. Magagnano, A. Gualandi, M. Marchini, L. Mengozzi, P. Ceroni and P. G. Cozzi, *Chem. Commun.*, 2017, **53**, 1591; d) C.-J. Wallentin, J. D. Nguyen, P. Finkbeiner and C. R. J. Stephenson, *J. Am. Chem. Soc.*, 2012, **134**, 8875.
- ²⁷ G. Magagnano, A. Gualandi, M. Marchini, L. Mengozzi, P. Ceroni and P. G. Cozzi, *Chem. Commun.*, 2017, **53**, 1591.
- ²⁸ E. Arceo, E. Montroni and P. Melchiorre, *Angew. Chem. Int. Ed.*, 2014, **53**, 12064

Development of new efficient coumarins for photoredox catalysis

4.1 Introduction

4.1.1 Development of new efficient coumarin core photocatalysts

The use of 3-thienyl coumarin derivatives proved powerful organic photoreductants in several photoredox transformations largely discussed in chapters 2 and 3. In view of the described results, the development of more efficient photocatalysts with enhanced photophysical and electrochemical properties thereby increasing catalyst efficacy would be most desirable. Important features such as redox potential, photo-stability, quantum yield and excited states lifetime may be addressed in order to improve catalyst efficiency.

The computational and empirical approaches represent two of the most widespread methods for the design of new suitable photocatalysts. Computational investigations/methods have emerged as a power full tool in catalyst design. Numerous examples of computational design of catalysts, catalytic cycles as well as catalysis methods have been development over the recent years.¹ Computational studies can be also applied to photoredox catalysts, in order to improve photophysical properties.²

A relevant example is the design of a set of diaryldihydrophenazine and phenoxazine derivatives for atom transfer radical polymerization (ATRP) of methyl methacrylate through the time dependent density functional theory (TD-DFT) reported by Miyake and co-workers³ (Figure 1).

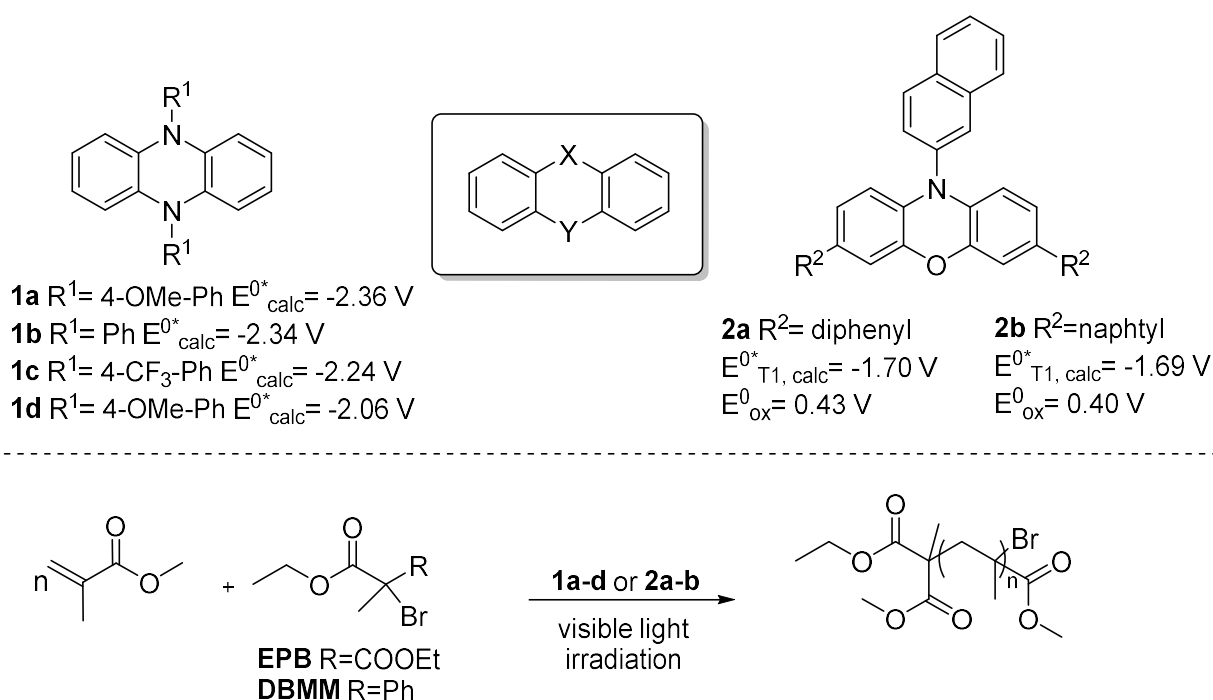


Figure 1 Atom transfer polymerization of methyl methacrylate mediated by compounds **1a-d** and **2a-b**.

The computational calculations allowed to identify suitable diaryldihydrophenazine **1a-d** and phenoxazine derivatives **2a** and **2b** with impressively high reduction potentials and capable to reduce the initiators α -ethylbromoacetate (EBP) as well as 2-bromo-2-methylmalonate (DBMM).⁴ These catalysts showed high initiator efficiencies through activation by visible light to synthesize polymers with tuneable molecular weights and low dispersity's.

More recently, Kwon and co-worker also generated a library of donor-acceptor PCs and used a computer-aided strategy to elucidate the PC property-performance relationship in ATRP in order to obtain an efficient polymerization of styrene.⁵

Computational studies on the design of novel coumarin dyes in photocatalytic applications may allow a deeper understanding of the structural and electrochemical properties of this class of compounds and lead to valuable improvements of the catalyst performance.

In particular, the prediction of specific parameters important in photoredox catalysis, including ground state oxidation potentials as well as and excited state reduction potentials may provide important insights into the development of new 7-amino coumarin derivatives as powerful photocatalyst (Figure 2).

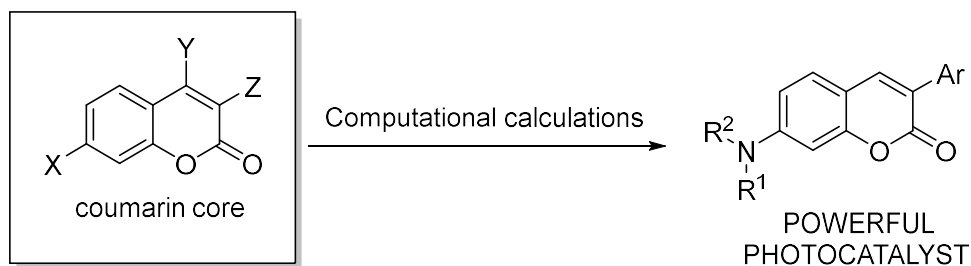


Figure 2 Development of new coumarin through computational calculations.

As an alternative, the more empirical approach in which design is mostly derived from a set of proven principals to direct improvement along the most promising pathway may also lead to new interesting coumarin photoredox catalysts.

Thiophene type structure including oligothiophene,⁶ fused di-thiophene and modified thiophene⁷ as well as diarylamine derivatives such as di- and triphenyl amines⁸ and carbazole⁹ are widespread motifs largely exploited in the development of several dyes for different applications.

Thiophene-type structure showed many attractive characteristics such as unique electrical and electrooptical properties, relatively good environmental stability, and structural versatility. These structures have found application over optoelectronic devices such as electron transport materials and emitters for organic light emitting diodes (OLEDs),¹⁰ dye sensitized solar cells (DSSC),¹¹ organic

field effect transistors (OFETs),¹² nonlinear optics (NLO),¹³ organic solid state lasers (OSLs)¹⁴ (Figure 3).

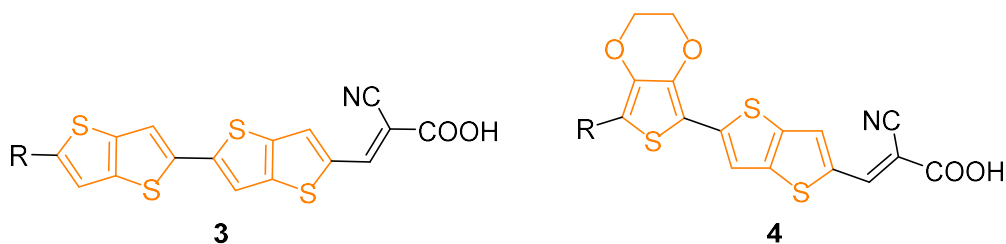


Figure 3 Typical thiophene type motifs used in optoelectronics.

Di- and triarylamine derivatives have been widely used as a building block in the construction of organic sensitizers suitable for use in dye-sensitized solar cells. Thanks to their aromatic biphenyl structures, arylamine derivatives show an electron donor ability and a highly efficient electroluminescence coupled with a high hole mobility and good processability (Figure 4).

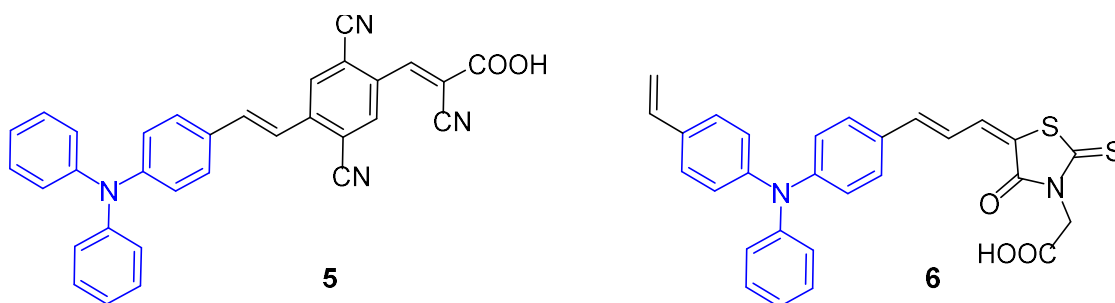


Figure 4 Typical triarylamine derivatives used in optoelectronics.

Furthermore, according to a general strategy developed by Grimm and co-workers,¹⁵ dyes with enhanced photophysical properties were obtained by the replacement of the open-chain alkyl amines such as dimethyl- and diethyl- amine with the azetidines and azetidines in the 7 position of the coumarin dye core (Figure 5).

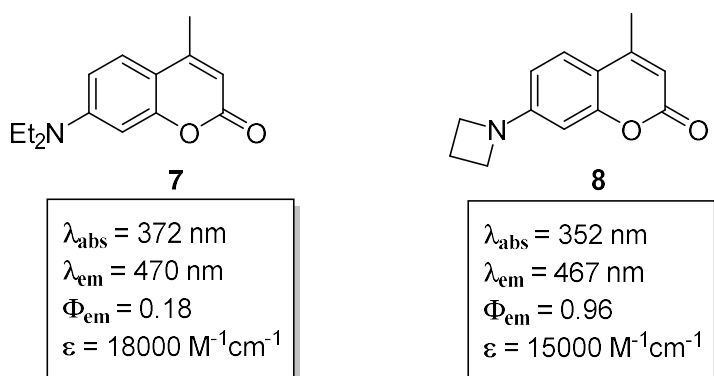


Figure 5 Comparison between coumarins 7 and 8.

As example, the insertion of azetidine in C-7 of the 4-methyl-coumarin **8** showed a marked improvement in quantum yield with respect to the 7-diethylamino analogues **7** while maintaining λ_{abs} and λ_{em} values almost unaltered. Exploiting palladium coupling catalysis, the introduction of triarylamine and thiophene-type motifs on the C-3 aromatic substituent could be carried out. A Buchwald-Hartwig coupling between azetidine and the suitable bromo derivative could be attempted for the synthesis of a 7-azetidine-3-thienyl- coumarin (Figure 6).

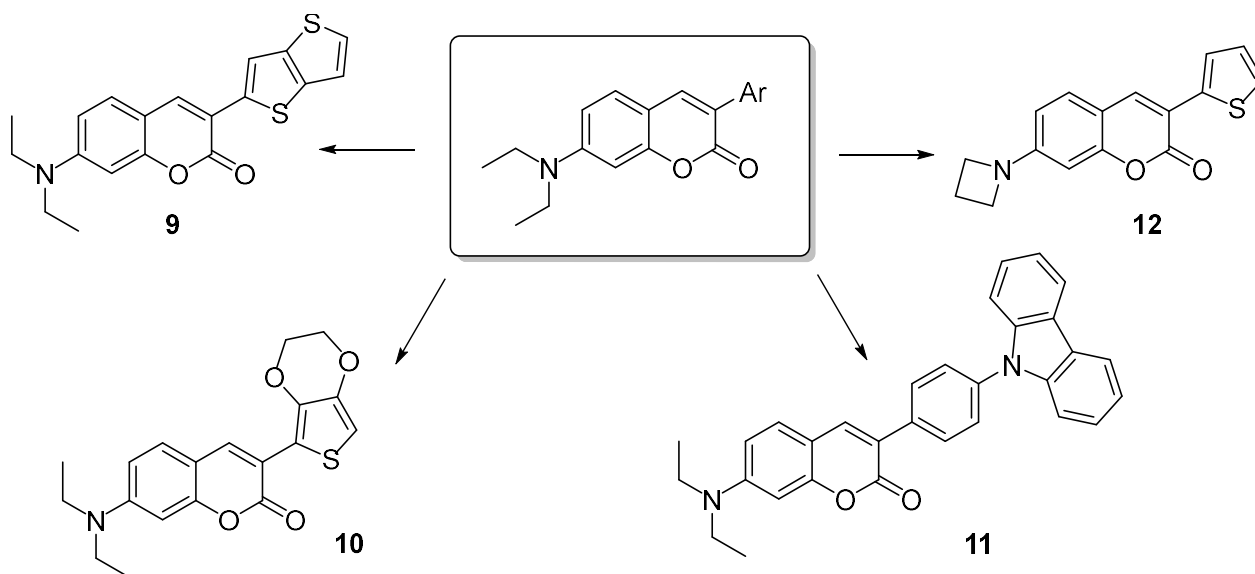


Figure 6 Development of new coumarin through an empirical approach.

In this chapter, the synthesis of more efficient coumarin dyes, derived by a computational and an empirical design, and their employment as photocatalysts in the photoredox pinacol coupling reactions will be discussed.

4.2 Results and discussion

4.2.1 Development of new dye by computational calculations

In collaboration with Prof. Garavelli from University of Bologna, an evaluation of the photoredox potential of coumarin dyes through DFT calculations was performed with the B3LYP functional using a basis set 6-31G*. The photophysical process were studied using DFT calculations and was performed with the CAM-B3LYP and PBE0 functional using a basis set 6-31G*. The study concerned the analysis of twenty-six 7-alkyl amino-coumarin derivatives including phenyl or thienyl substituted coumarins in C3 or C4 as well as the common coumarin 1, 35, 102 and 153 (a more detailed list is reported in section 4.4.1).

Specific parameters including E_{00} , ground state oxidation potential $E(A/A^{\cdot-})$ and reduction potential $E(A^+/A^{\cdot*})$ in the excited state were contemplated. In this way, compound with desirable characteristic (high reduction potential in excited state, and high oxidation potential of the ground state) could be evaluated in silica before an effective synthesis. Based on the results obtained by the in silica screening, new promising compounds were selected, synthesized, and used as photocatalysts in a model reaction in order to test their efficiency, and the affordability of the calculations. I have selected as model reaction, among all the reactions promoted by coumarins the photoredox pinacol coupling described in the chapter 2.

Through this approach, the molecular structures **12**, **13** and **14** showed interesting electrochemical properties showing similar results than coumarin **15**, **16** and **17** successfully employed as photocatalysts of pinacol coupling reactions (Section 2.2.1) (Figure 7).

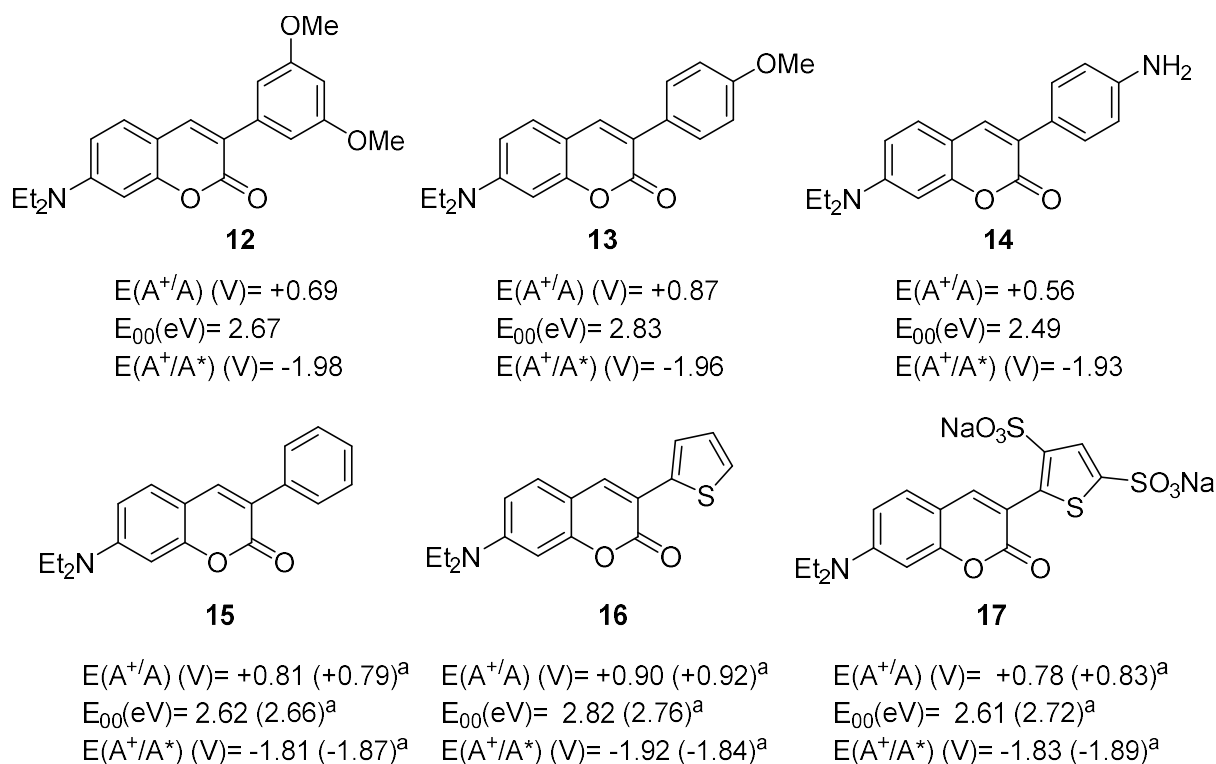


Figure 7 Electrochemical and photophysical properties of coumarins **12-17**. ^a In parenthesis are indicated the experimental values reported in section 2.2.2 .

The comparison between the theoretical and experimental data of coumarins **15**, **16** and **17** exhibits the extreme accuracy of the computational calculations. The molecular structures **12**, **13** and **14** are characterized by the presence of electron donating groups such as methoxy (**12** and **13**) and amino (**14**) on the phenyl in C-3 of the coumarin core. Interestingly, the calculated reduction potentials at the excited state ($E(A^+/A^{\cdot*})$) of these compounds (about -1.95 V vs SCE) is slightly higher than coumarin

dyes **15**, **16** and **17** (about -1.87 V vs SCE). In particular, the comparison between coumarins **12**, **13** and **14**, and coumarin **15** highlights the influence of electron rich substituents in the C-3 position on the reduction potentials.

In view of the performed computational studies, the candidates to synthesize and test in photoredox pinacol coupling reactions were selected (Figure 8).

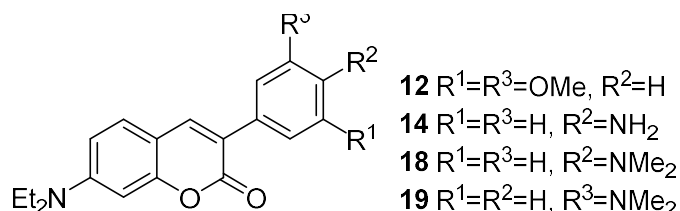


Figure 8 Molecular structures of coumarins **12**, **14**, **18** and **19**.

Compounds **12** and **14** indicated promising electrochemical properties by the computational calculations. Compound **12** was preferred to coumarin **13** despite the similar theoretical values. In addition, the enhanced electron donating effect of alkyl amino substituents on the phenyl in the coumarins **18** and **19** was investigated. Next, the selected candidates **12**, **14**, **18** and **19** were prepared.

4.2.2 Synthesis of coumarins **12**, **14**, **18** and **19**

The synthesis of the selected candidates was performed through two synthetic approaches. In the case of coumarin derivatives **12**, **18** and **19**, a Suzuki coupling of 3-bromo-coumarin derivative **20** with the specific boronic acids **21** was required. In the case of compound **14** the synthesis was carried out in three steps including a nitration of benzeneacetonitrile, the Knoevenagel condensation of compound **23** with (4-diethylamino) salicylaldehyde and a subsequent reduction of the nitro group (Figure 9).

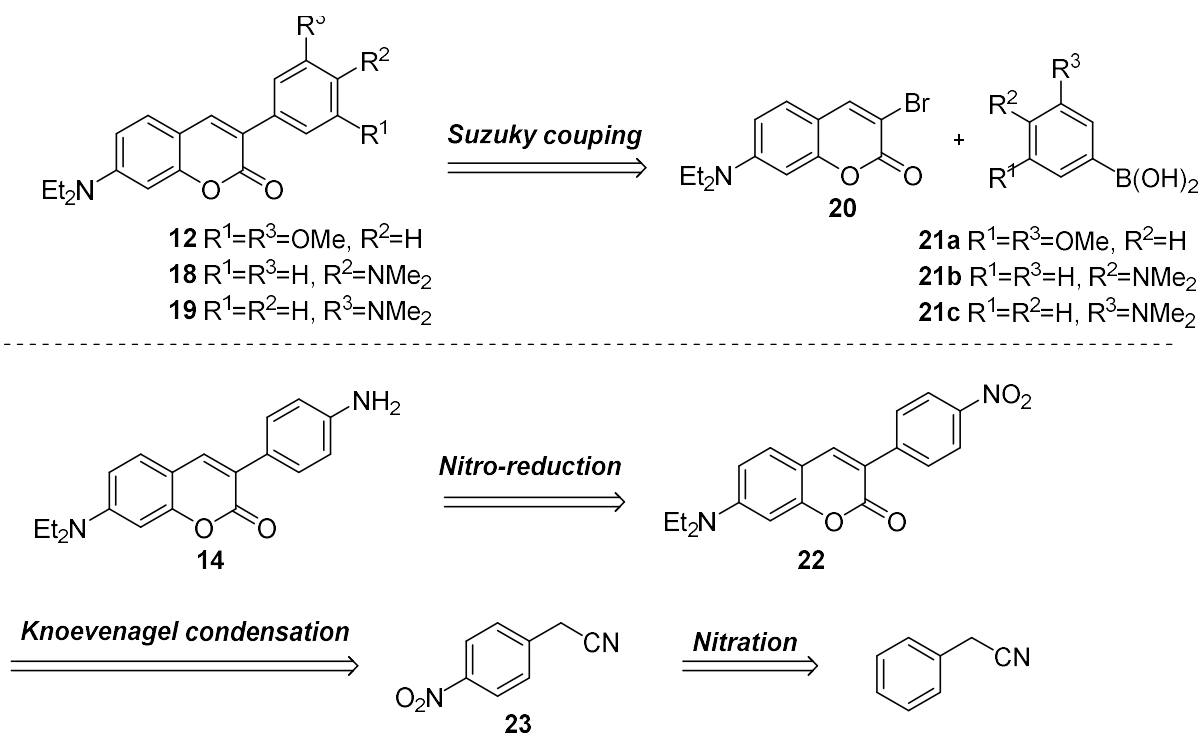


Figure 9 Synthetical approach for coumarin **12**, **14**, **18** and **19**.

The readily available compound **20**, used for the synthesis of coumarins **12**, **18** and **19** was obtained in two steps (Figure 10).

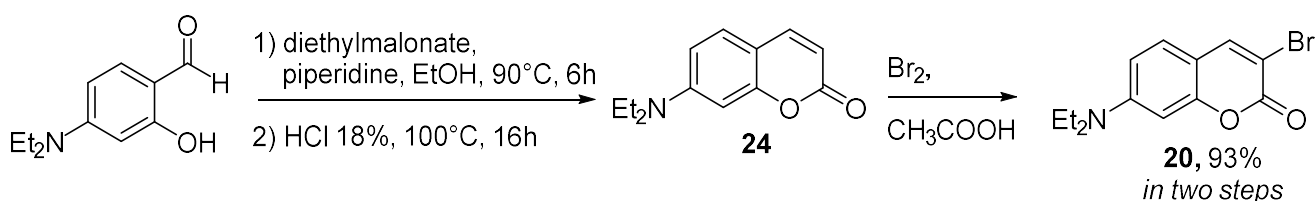


Figure 10 Synthesis of the 3-bromo-coumarin derivative **20**.

Compound **20** was straightforward prepared in a nearly quantitative yield through a Knoevenagel condensation of (4-diethylamino) salicylaldehyde with diethyl malonate and a subsequent treatment with Br_2 .

Boronic acids **21a** and **21b** were not commercially available, they were synthesized in good yields using a classic protocol reported in literature¹⁶ (Figure 11).

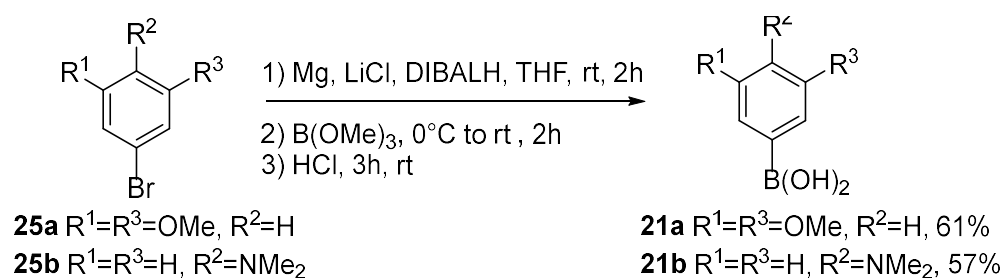


Figure 11 Synthesis of boronic acids **21a** and **21b**.

The formation of the Grignard reagent of the bromobenzene derivatives **25a** and **25b** and a subsequent treatment with trimethoxyborane followed by hydrolysis in acidic water successfully provided the boronic acids **21a** and **21b** in a 61% and 57% of yield, respectively.

The prepared boronic acids **21a** and **21b** and commercially available β -[3-(dimethylamino)phenyl]-boronic acid **21c** were employed in the Suzuki coupling with 3-bromo-coumarin derivative **20** (Figure 12).

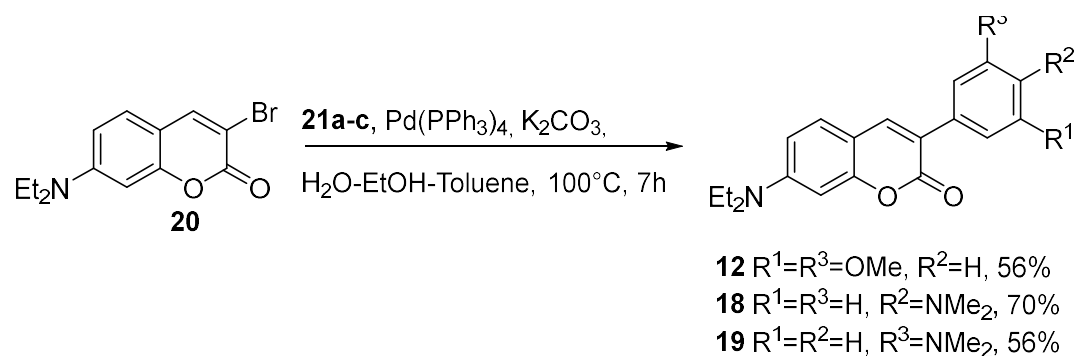
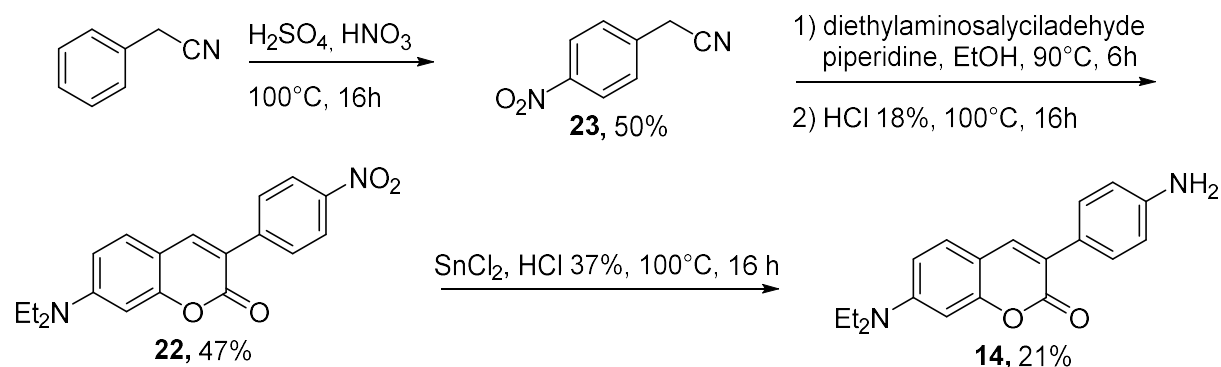


Figure 12 Synthesis of coumarins **12**, **18** and **19**.

The reactions were performed in the presence of palladium tetrakis as catalyst at reflux. Despite the tedious purification processes, the coumarins **12**, **18** and **19** were isolate in yields of 56%, 70% and 56% respectively.

An alternative strategy was adopted for the synthesis of the coumarin **14** due to the presence of aniline amine-substituent which can generate a side-product derived from a Buchwal-Hartwing coupling with bromo derivative **20** (Figure 13).

**Figure 13** Synthesis of coumarin **14**.

The nitrobenzene derivative **23** was prepared, in a 50% yield, by the treatment of benzeneacetonitrile with H_2SO_4 - HNO_3 mixture. The Knoevenagel-type condensation between the compound **23** and (4-diethylamino) salicylaldehyde in the presence of piperidine gave the coumarin **22** in a yield of 47%. Subsequent reduction of the nitro group through treatment with SnCl_2 in acidic environment provided the coumarin **14** in a 21% yield. Even though coumarin **14** was successfully synthesized, the synthesis was not optimized and yields from moderate to poor for every single step were obtained.

Photophysical properties including absorption and emission maxima, molar extinction coefficient, quantum yield and lifetime of the synthesized coumarins were considered. Cyclic voltammetry studies performed on these coumarins furnished data about ground state and excited states potentials (Table 1).

ENTRY	ABSORPTION		EMISSION			ELECTROCHEMISTRY		
	λ (NM)	ϵ ($\text{M}^{-1} \text{CM}^{-1}$)	λ (NM)	Φ_{EM}	τ (NS)	E_{00} (EV)	$E(\text{A}^+/\text{A})$ (V)	$E(\text{A}^+/\text{A}^*)$ (V)
12	402	3.35	475	0.86	2.9	2.78	+0.92	-1.84
14	406	3.23	513	0.80	3.5	2.67	+0.70	-1.97
18	415	2.88	524	0.52	3.7	2.60	+0.62	-1.98
19	398	3.07	480	0.03	2.6	2.78	+0.70	-2.07

Table 1 Photophysical and electrochemical properties of coumarins **12**, **14**, **18** and **19** in DMF solution at 298 K.

The compounds exhibit an absorption and emission maxima in the blue and in the green region, respectively. Coumarins **12** and **14** showed high quantum yields of 0.86 and 0.80, respectively. The

coumarin **19** showed a sharp decrease in fluorescence (0.03). Notably, lifetime of 3.5 and 3.7 ns for coumarins **14** and **18**, respectively were found. The electrochemical data substantially confirmed the values obtained by the theoretical studies on coumarin **12** and **14** as reported in figure 6. The analysed compounds showed high reduction potentials of the excited states ($E(A^+/A^*) \leq -1.84$ V vs SCE) but coumarin **12** ($E(A^+/A) = +0.92$ V vs SCE) exhibits considerable different oxidation potentials with respect to the other coumarins **14**, **18** and **19** ($E(A^+/A) \leq +0.70$ V vs SCE).

With the coumarins **12**, **14**, **18** and **19** in hand, their employment in the photoredox pinacol coupling reaction was investigated.

4.2.3 Use of the coumarins **12**, **14**, **18** and **19** in photoredox pinacol coupling reactions

Photoredox pinacol coupling of *p*-chlorobenzaldehyde using the optimized conditions reported in section 2.2.2 and coumarins **12**, **14**, **18** and **19** was carried out (Figure 14).

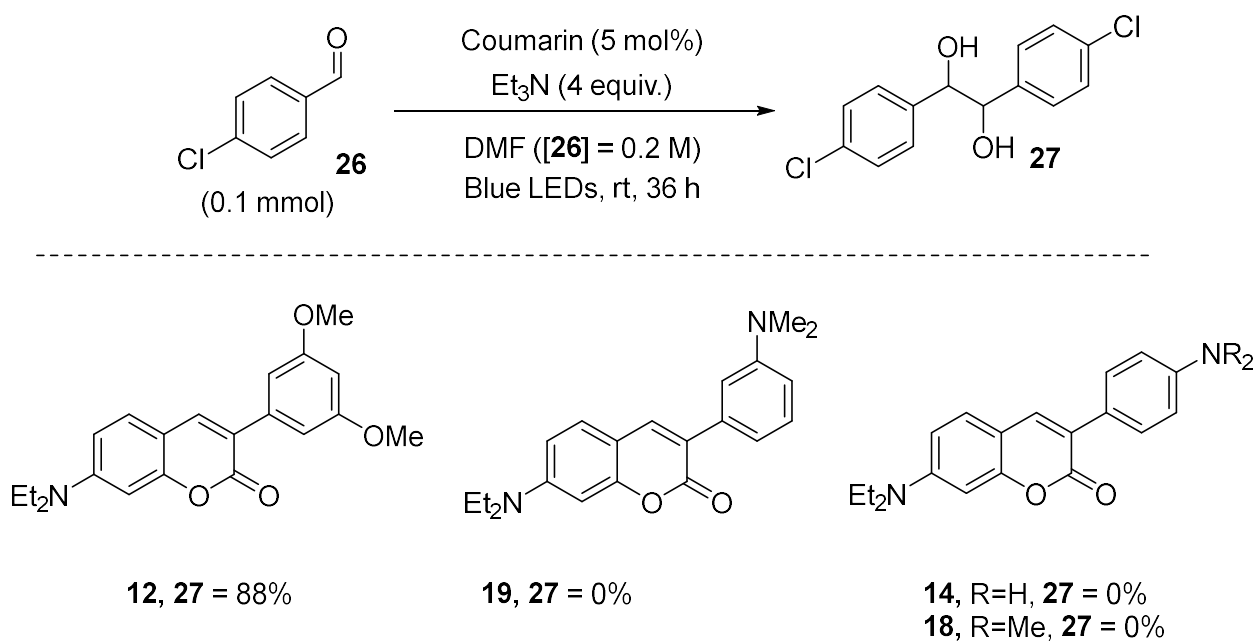


Figure 14 Photoredox pinacol coupling reaction of 4-chlorobenzaldehyde mediated by coumarins **12**, **14**, **18** and **19**. The conversions were determined by $^1\text{H-NMR}$ analysis.

Coumarin **12** provided the product **27** in 88% of conversion, a value comparable to the photocatalysts **15**, **16** and **17** (Section 2.2.1). Unfortunately, all the amino- substituted coumarins **14**, **18** and **19** proved completely inactive as photocatalysts. These different performances could be explained by the dissimilar oxidation potentials of the photocatalyst **12** ($E(A^+/A) = +0.92$ V vs SCE) with respect

to the other candidates ($E(A^+/A) \leq +0.70$ V vs SCE) as depicted in photoredox catalytic cycle (Figure 15).

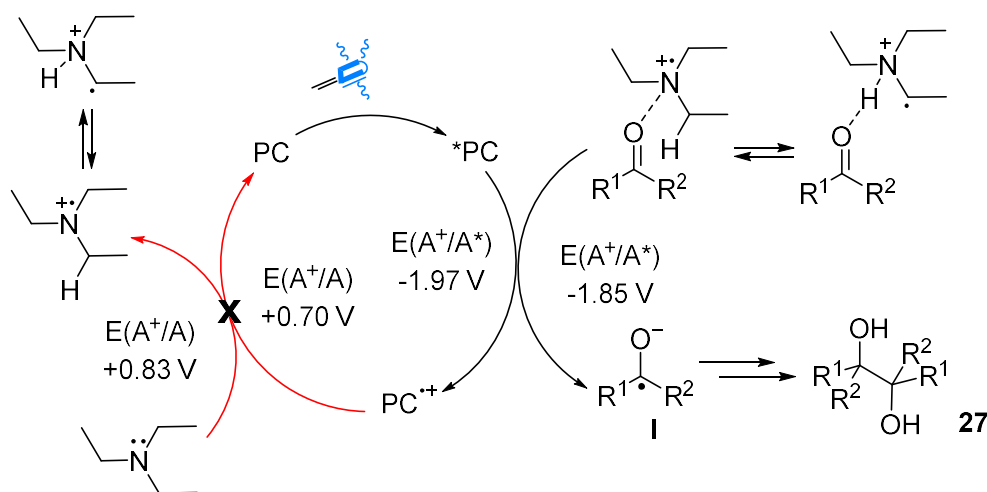


Figure 15 Catalytic cycle of photoredox pinacol coupling mediated by the coumarin dye **14**, **18** and **19**. $E_{1/2}$ in V vs. SCE.

Single electron transfer from the species $[PC]^*$ in the excited state to the chlorobenzaldehyde generates the radical cation $[PC]^{\bullet+}$ and the radical carbonyl anion **I** which undergoes dimerization providing the diol **27**. The radical cation $[PC]^{\bullet+}$ is reduced by triethylamine which acts as a reducing agent giving back the photocatalyst $[PC]$ (in red).

In the case of coumarins **14**, **18** and **19** the low oxidation potential $E(A^+/A) = \leq +0.70$ V does not favour the reduction of the $[PC]^{\bullet+}$ species by trimethylamine ($E(A^+/A) = +0.83$ V vs SCE), making not possible the regeneration of the catalytic cycle.

Therefore, a more suitable reducing agent than A was employed.

The commercially available 1,3-dimethyl-2-phenyl-2,3-dihydro-1H-benzo[d]imidazole (BIH) is a benzoimidazole derivative with a phenyl substituent in position 2 widely used as reductant of α -haloketones,¹⁷ in the opening of cyclopropyl ketones¹⁸ and in the photocatalytic reduction of CO_2 .^{19,20} According to the literature, BIH shows an oxidation potential (A^+/A) of +0.33V vs SCE in CH_3CN .^{21,22}

The oxidation of BIH by the reductant generates the radical benzoimidazole derivative $BIH^{\bullet+}$ which is supposed to act as a Lewis acid to activate the aldehyde, as discussed in section 2.1.2 (Figure 16).

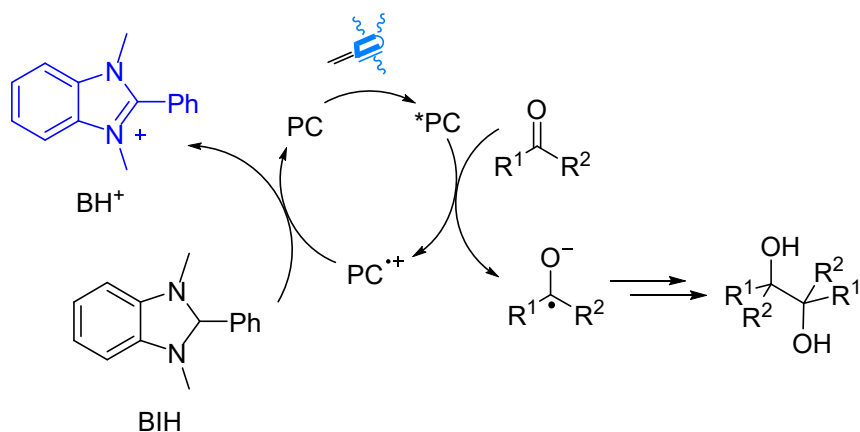


Figure 16 Photoredox catalytic cycle using BIH.

Pinacol coupling of 4-chlorobenzaldehyde mediated by coumarins **14**, **18** and **19** as photocatalysts in the presence of BIH as reducing agent was attempted (Figure 17).

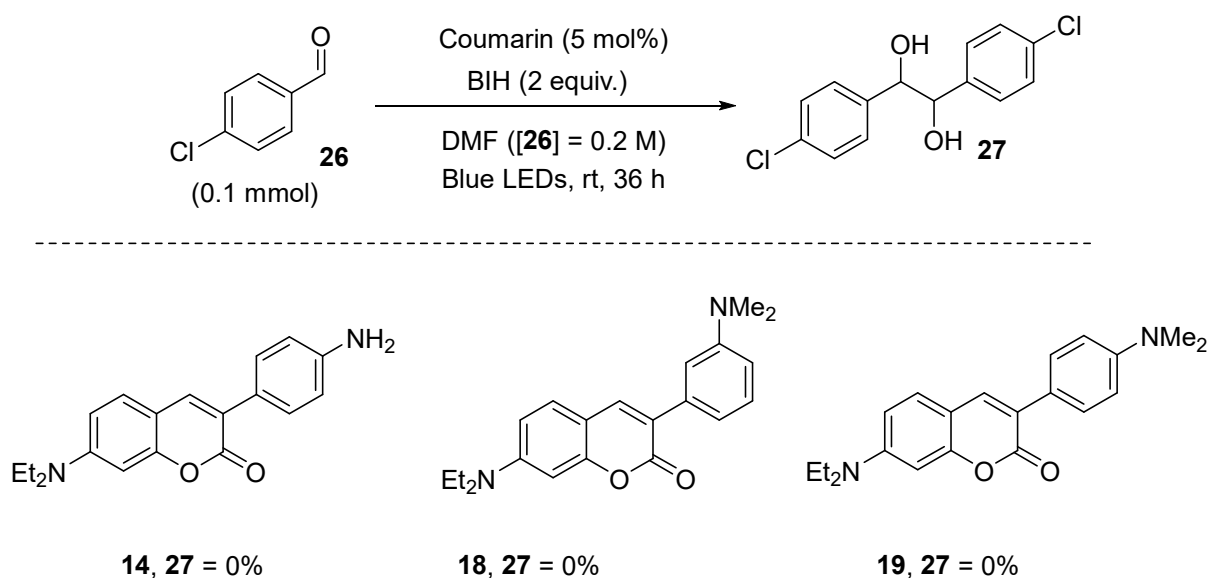


Figure 17 Photoredox pinacol coupling reaction of 4-chlorobenzaldehyde mediated by coumarins **14**, **18** and **19**. The conversions were determined by $^1\text{H-NMR}$ analysis.

The performed experiments provided a zero conversion in all the cases. Presumably, the unsuccessful results are attributed to the benzoimidazolium derivative BH^+ , which, in contrast to triethylamine, is not a suitable Lewis acid due to the delocalization of the positive charge on the aromatic ring.

The addition of oxalic acid, as Brønsted acid, to improve the efficiency of the photoredox coupling reaction, was reported by Rueping *et al.*²³

On the basis of these observations, the addition of oxalic acid in the reaction mixture was evaluated. The attempts were repeated adding a stoichiometric amount of oxalic acid in the reaction mixture. Also, these reaction conditions were tested on the photocatalyst **17** (Figure 18).

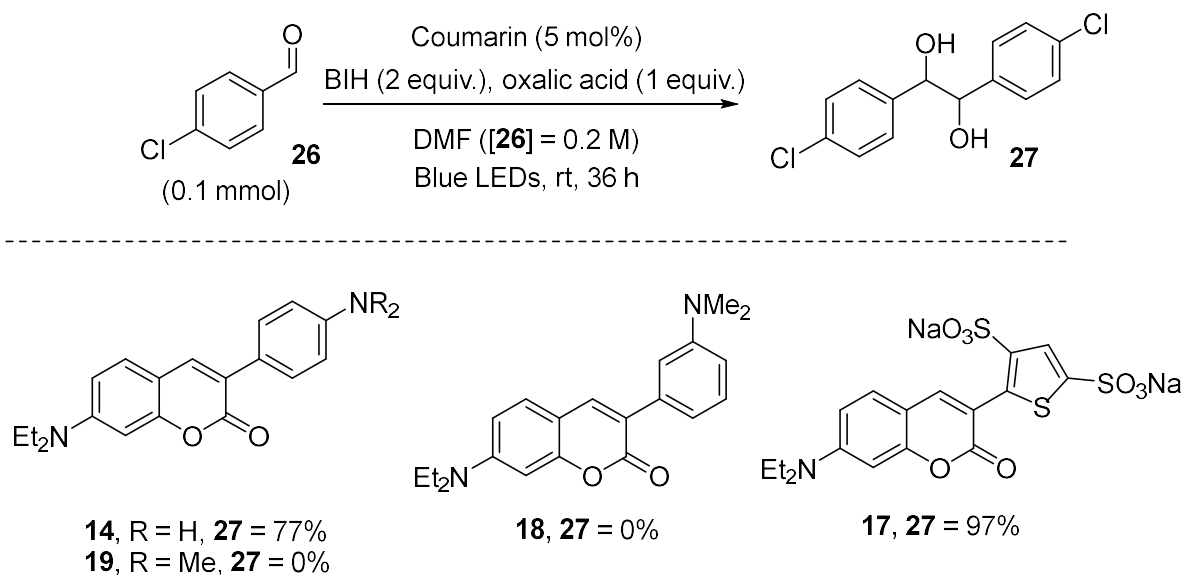


Figure 18 Photoredox pinacol coupling reaction of 4-chlorobenzaldehyde mediated by coumarins **14**, **17**, **18** and **19**. The conversions were determined by $^1\text{H-NMR}$ analysis.

Gratifyingly, coumarin **14** proved active as photocatalyst of pinacol coupling yielding a conversion of 77% demonstrating the importance of a Lewis acid in the activation of the carbonyl group. The inactivity of the photocatalysts **18** and **19** could be attributed to a photo-oxidative degradation caused by the deprotonation of the $-\text{NMe}_2$ group to give the corresponding carbocation. This type of degradation was reported in literature²⁴ but it was not specifically studied in our case.

To our delight, the use of the coumarin **17** as photocatalyst provided an excellent conversion of 97% showing the importance of BIH as reducing agent in the presence of oxalic acid (Table 2).

Entry ^[a]	Coumarin	Reducing agent	Brønsted Acid	Conversion (%) ^[b]
1	17	BIH	Oxalic acid	97
2	17	TEA	-	89
3	17	TEA	Oxalic acid	49

Table 2 Use of coumarin **17** as photocatalyst in different reaction conditions. ^aReaction conditions: **26** (0.1 mmol), sacrificial agent (4 equivalents) (Entry 2-3) (2 equivalents) (Entry 1), **17** (5 mmol%), DMF [**26**] = 0.2M, Blue LEDs, room temperature, 36h ^b The conversions were determined by $^1\text{H-NMR}$ analysis.

As previously reported, the sacrificial agent TEA with (Entry 3, Table 2) or without (Entry 2, Table 2) oxalic acid gave worst results in comparison to the combination BIH and oxalic acid, which provided an almost total conversion to the final compound **27**.

4.2.4 Enantioselective version of photoredox pinacol couplings using chiral acids

Thanks to the excellent results obtained in the presence of BIH and oxalic acid as Brønsted acid, the investigation of an enantioselective version of the photoredox pinacol coupling reaction using chiral Brønsted acids in place of oxalic acid was attempted.

The employment of chiral Lewis acids²⁵ as well as chiral Brønsted acids²⁶ to promote enantioselectivity in photoredox catalysis was reported in literature. Activation of the substrates was obtained by phosphoric acids, as described by Terada *at al.*,²⁷ and by thiourea derivatives exploiting the acidic N-H bond.²⁸

Firstly, the capacity of several Brønsted acids such as the phosphoric acid **28**, the Schreiner's thiourea²⁹ **29** and the sulfonimide **30** to activate the 4-chlorobenzaldehyde was evaluated (Figure 19).

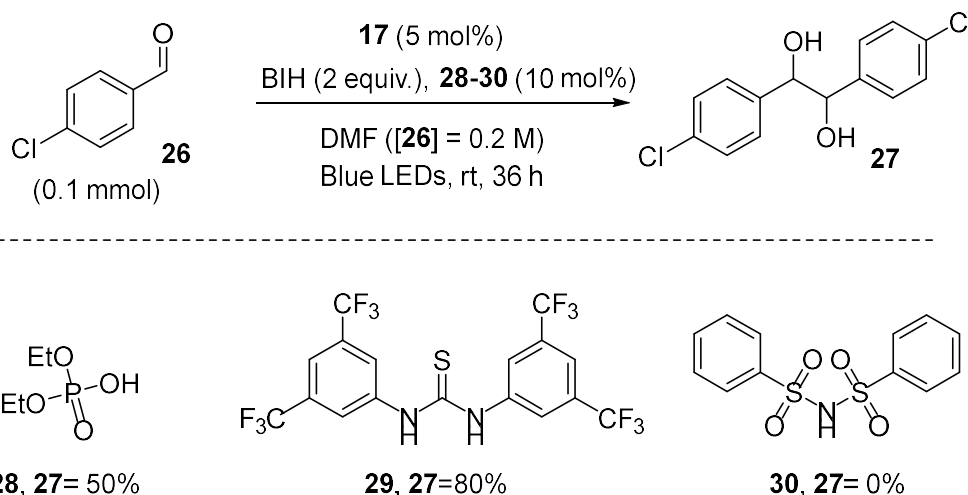


Figure 19 Photoredox pinacol coupling using acids **28**, **29** and **30**. The conversions were determined by ¹H-NMR analysis.

The phosphoric acid **28** and the thiourea **29** furnished conversions of 50% and 80%, respectively and their chiral versions were subsequently evaluated. In contrary, sulfonimide **30** led to a zero conversion and it was not further examined.

The ability of chiral BINOL derivatives **31** and **32** and the chiral thiourea **33** to induce enantioselectivity was investigated (Figure 20).

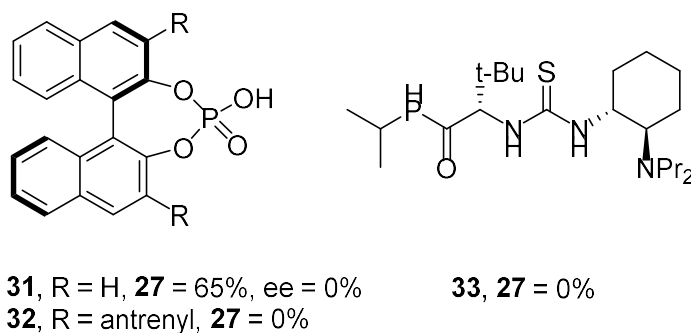
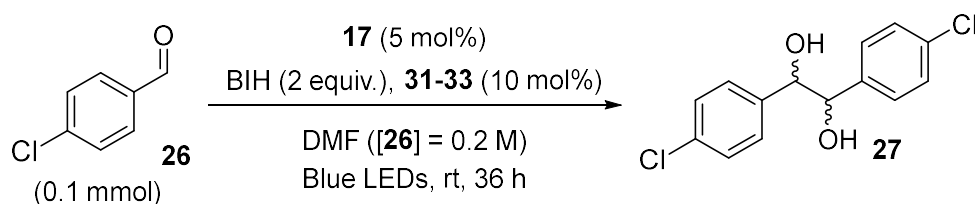


Figure 20 Photoredox pinacol coupling using acids **31**, **32** and **33**. The conversions were determined by $^1\text{H-NMR}$ analysis.

(R)-(-)-1,1'-binaphthyl-2,2'-diyl hydrogen phosphate **31** furnished a conversion of 65% as a diastereomeric mixture syn:anti 1:1 proving unsuccessful to promote stereoselectivity in the reaction. In the (R)-(-)-1,1'-binaphthyl-2,2'-diyl hydrogen phosphate derivative **32**, due to steric hindrance. The use of the chiral thio-urea derivative **33** furnished a zero conversion as well. The attempts to promote enantioselectivity in the photoredox pinacol coupling through chiral acids proved unsuccessful. Further investigations could imply a larger screening of chiral Brønsted and Lewis acids.

4.2.5 Development of new photocatalysts by rational design

New promising coumarins were rationally designed through the indications obtained by the previous experiments and by literature.

The coumarins **9**, **10** and **11**, bearing electron donating groups on aromatic rings in C-3 were developed. In alternative, the modification of the alkyl amine substituent with the insertion of an azetidine in C-7 on the 3-thienyl coumarin (**12**) was attempted (Figure 21).

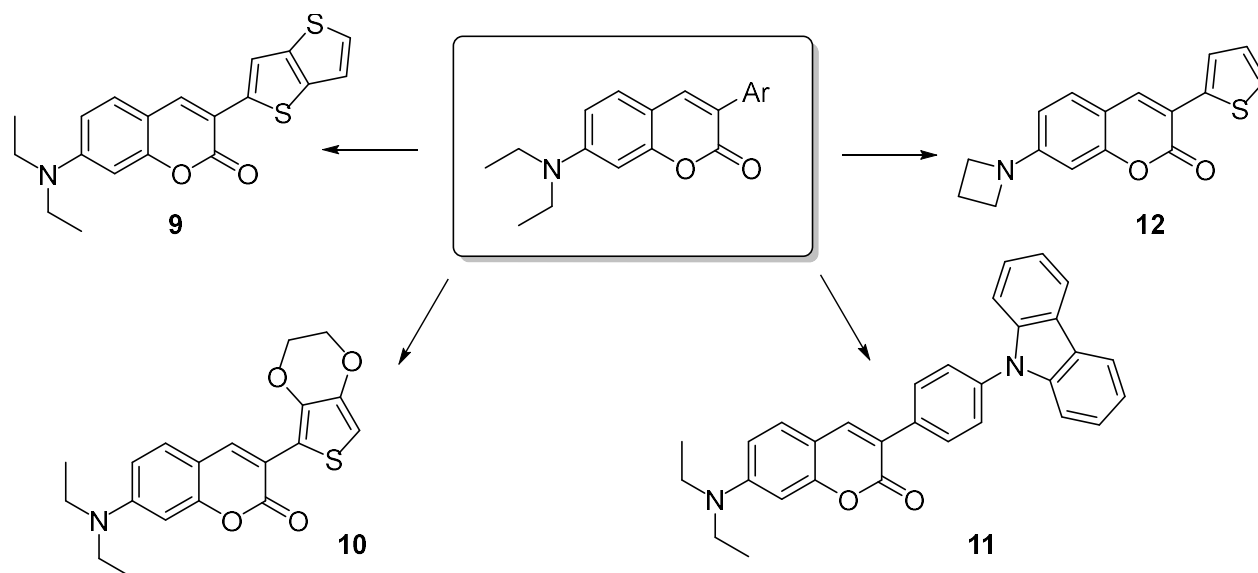


Figure 21 Molecular structure of coumarins **9-12**.

The coumarin **9** shows a thieno[3,2-*b*]thien substituent in C3, similar structures were employed in green electroluminescent devices.³⁰ In the compound **10**, an electron donating 3-4 ethylenedioxy chain was introduced on the thienyl. Carbazole derivatives are considered a very efficient electron donor finding largely application in the development of electroluminescent devices.^{31, 32, 33} The 3-phenyl coumarin derivative **11** is characterized by the presence of N-phenylcarbazolyl substituent. The absence of an α -proton on the amino substituents avoids the photocatalysed decomposition of the photocatalyst, as discussed earlier for the NMe₂ derivatives. The 3- thienyl coumarin **12** may be obtained by the opportunely modification of the C-7 substituent using an azetidine ring.

4.2.6 Synthesis of compound 9-12

Coumarin **9** was synthesized in a single step starting from the 3-bromo-coumarin derivative **20**, previously obtained, through a methodology reported in literature (Figure 22).³⁴

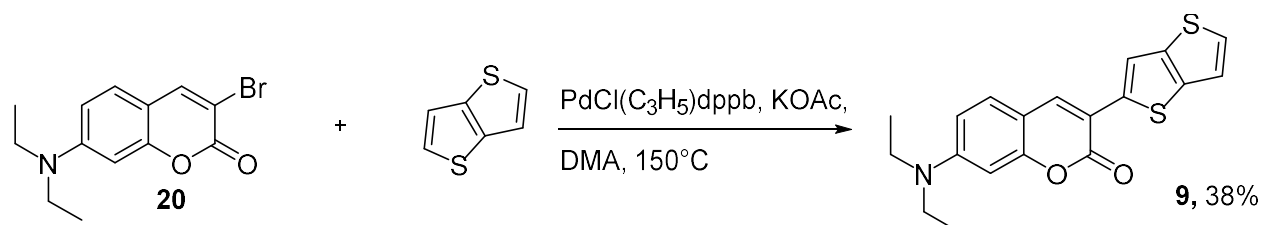


Figure 22 Synthesis of coumarin **9**.

The direct site-selective Pd-catalysed C-H activation of thieno[3,2-*b*]thiophene with the 3-bromo coumarin derivative **20**, required harsh reaction conditions. The required palladium complex

$\text{PdCl}(\text{C}_3\text{H}_5)_2\text{dppb}$ was instantly formed by mixing diallyldipalladium dichloride and 1,1'-(1,4-butanediyl)bis[1,1-diphenyl-phosphine] in DCM. The coumarin **9** was afforded in moderate yield.

Compounds **10** and **11** were obtained through a Suzuki cross coupling between 3-bromo coumarin derivative **20** and the corresponding boronic acids.

In the case of coumarin **11** the carboimidazolyl boronic acid **35** was not commercially available and it was readily synthesized in two steps (Figure 23).

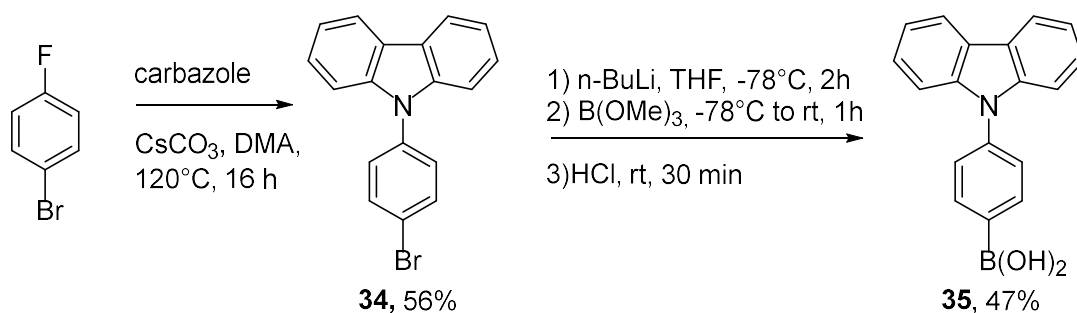


Figure 23 Synthesis of boronic acid **34**.

At first, the carbazole derivative **34** was obtained in a 56% yield through a nucleophilic substitution of 4-bromo-fluorobenzene with carbazole. Despite the presence of a bromine atom, the reaction shows high regioselectivity as reported in literature.^{35,36} A bromine-lithium exchange on the carbazole derivative **34** followed by treatment with trimethoxyborate and hydrolysis in acidic water gave the boronic acid **35** in a 47% yield. The subsequent Suzuki coupling between boronic acids and 3-bromo coumarin derivative **20** gave the coumarins **10** and **11** (Figure 24).

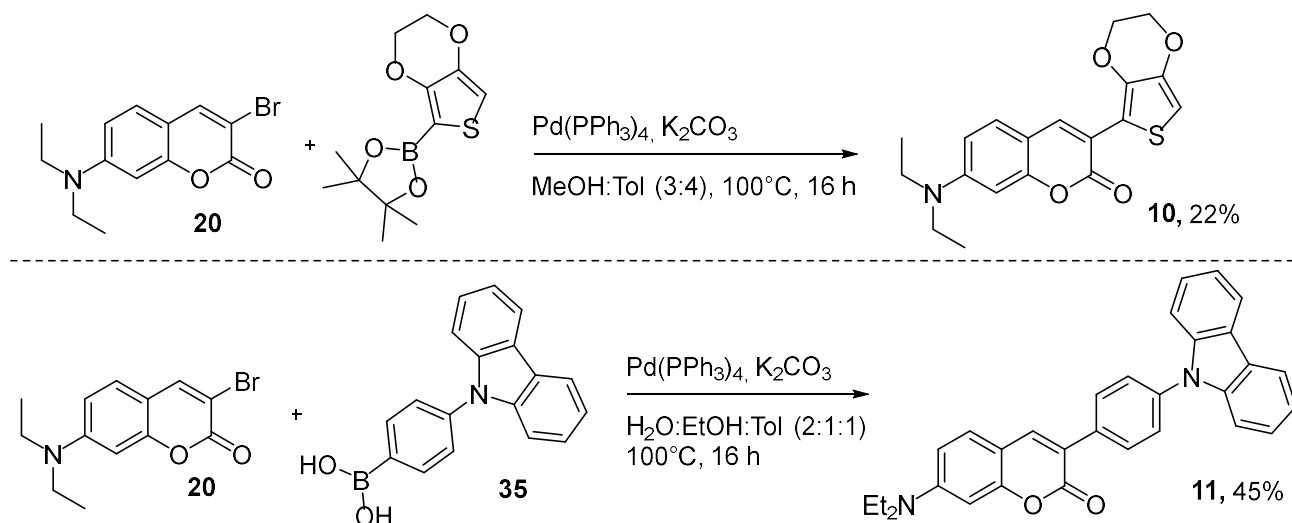


Figure 24 Synthesis of coumarins **10** and **11**.

The reactions were performed using palladium tetrakis as catalyst and the previously synthesized boronic acid **35** and the commercially available 2,3-Dihydrothieno[3,4-b][1,4]dioxine-5-boronic Acid Pinacol Ester. Unfortunately, the coumarins **11** and **12** were obtained in poor yields of 22% and 45%, respectively.

The synthesis 7-azetidin-3-thylenil coumarin derivative **12** was investigated adopting two synthetical approaches (Figure 25).

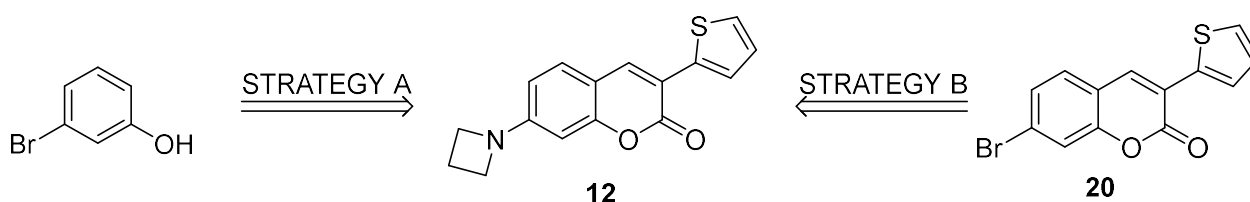


Figure 25 Synthetical approach for the synthesis of coumarin **12**.

Firstly, the strategy A, which included three synthetical steps, was attempted (Figure 26).

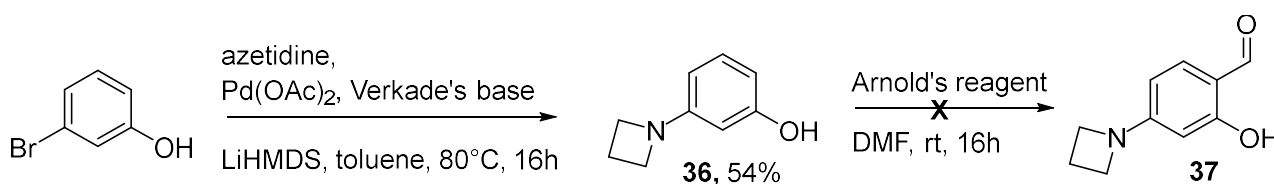


Figure 26 Attempted synthesis of coumarin **12**.

The Buchwald-Hartwig coupling was carried out using Pd(OAc)₂ as palladium source in the presence of the Verkade's base and LiHMDS as reported by Grimm and co-worker.³⁷ The aminophenol **36** was isolated in moderate yield (54%). Formylation of compound **36** was performed through the treatment with the Arnold's reagent as formylating agent. Unfortunately, the reaction provided the aldehyde **37** in trace amounts and the unreacted aminophenol **36**. The final step of this synthetical approach was not carried out. The accomplishment of the Buchwald-Hartwig coupling between the azetidine and the commercially available 3-Bromo salicylaldehyde was next attempted (Figure 27).

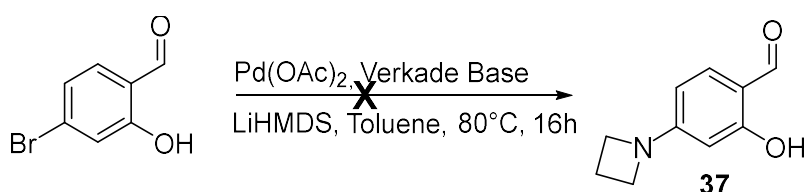


Figure 27 Synthesis of aldehyde **37**.

The reaction was performed using the reaction conditions previously reported. Although the total consumption of the 4-bromosalicylaldehyde was observed, the presence of the aminophenol **37** was not detected. The nature of the obtained crude material was not further investigated.

In view of the problems occurred in the formylation step, the strategy B for the synthesis of coumarin **12** was adopted (Figure 24) through a method successfully employed by Liu *et al.* in the synthesis of 7-azetidino 4-methyl coumarin³⁸ (Figure 28).

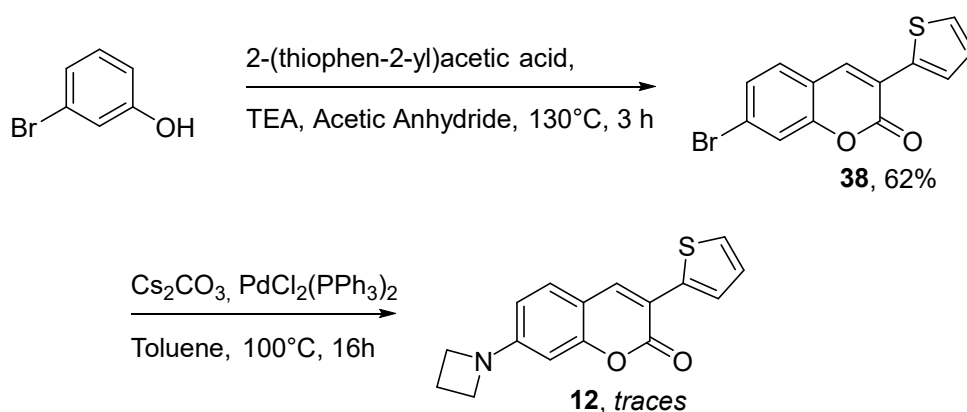


Figure 28 Alternative synthetical approach for the synthesis of the coumarin **12**.

The straightforward synthesis of 7-bromo-3-thienyl-coumarin **38** was carried out through a condensation between 3-bromophenol and 2-(thiophen-2-yl) acetic acid and with (4-diethylamino) salicylaldehyde in the presence of triethylamine and acetic anhydride as solvent. Buchwald-Hartwig coupling between coumarin **38** and the azetidine provided the formation of the 7-azetidino 3-thienyl coumarin **12** in trace amounts. The unsuccess of the reaction was not further investigated but it could be due to the presence of the thienyl group in C-3 to the absence of a Me substituent in position 4, as in the case reported by Liu. After several tedious purifications the coumarin **12** was isolated in a very poor yield and resulted impure by ¹H-NMR analysis. Unfortunately, the photophysical properties of the coumarin **12** and its use as photocatalyst in pinacol coupling reactions could not be investigated. The photophysical and electrochemical aspects of the synthesized compounds **9**, **10** and **11** were evaluated providing data about absorption (λ_{max}), emission (λ_{em}), molar extinction coefficient (ϵ), lifetime. The ground state and excited state potentials were obtained by cyclic voltammetry studies (Table 3).

ENTRY	ABSORPTION		EMISSION			ELECTROCHEMISTRY		
	λ (NM)	ϵ (M ⁻¹ CM ⁻¹)	λ (NM)	Φ_{EM}	τ (NS)	E ₀₀ (EV)	E(A ⁺ /A) (V)	E(A ⁺ /A*) (V)
9	426	2.90	487	0.65	3.2	2.70	+0.72	-1.98
10	408	3.63	483	0.80	2.5	2.74	+0.93	-1.81
11	442	4.25	515	0.61	3.1	2.59	+0.81	-1.78

Table 3: Photophysical and electrochemical properties (E_{1/2} in V vs. SCE) of coumarins **9**, **10** and **11** in DMF solution at 298 K.

The analysed compounds exhibit an absorption in the blue region and an emission at around 500 nm with good quantum yields. Interestingly, the excited state reduction potential (E(A⁺/A*)) and the oxidation potential (E(A⁺/A)) values are comparable with the high-performing coumarins **15**, **16** and **17** used in photoredox catalysis.

In view of these promising properties, the photoredox pinacol coupling reaction of chlorobenzaldehyde mediated by the coumarins **9**, **10** and **11** were performed through the standard reaction conditions **A** (TEA, DMF, under Blue LEDs irradiation, room temperature, 36 hours) as well as the previously discussed optimized conditions **B** (BIH, DMF, oxalic acid, Blue LEDs irradiation, room temperature, 36 hours) (Figure 29).

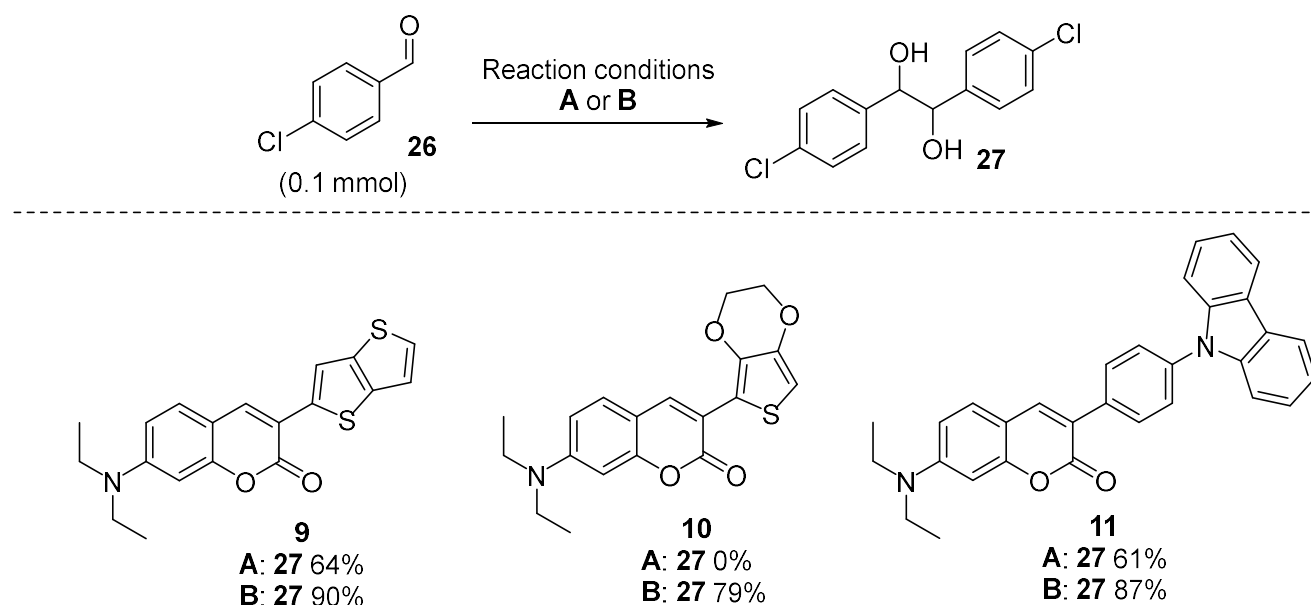


Figure 29 Photoredox pinacol coupling reaction using the coumarins **9**, **10** and **11** as photocatalysts. Reaction conditions for **A**: **26** (0.1 mmol), trimethylamine (4 equivalents), **9-11** (5 mmol%), DMF

[**26**]=0.2M, Blue LEDs, room temperature, 36 h. Reaction conditions for **B**: **26** (0.1 mmol), BIH (2 equivalents), **9-11** (5 mmol%), DMF [**26**]=0.2M, Blue LEDs, room temperature, 36 h. The conversions were determined by ¹H-NMR analysis.

Coumarin **11** furnished an excellent conversion of 87% using the reaction conditions **B** and a good conversion with **A**. These data demonstrate that the photocatalyst was not subjected to a photo-oxidative degradation like the coumarins **18** and **19** as previously discussed.

Using the reaction conditions **B**, the 3-thienyl coumarin derivatives **10** and **11** afforded a conversion of 79% and 90%, respectively. Interestingly, the photocatalyst **10** was completely inactive using the conditions **A**.

In all the studied cases, the reaction conditions **B** furnished a marked improvement to the use of triethylamine as reducing agent (**A**).

4.3 Conclusions

In summary, several coumarin dyes, through either a computation as well as a rational approach were successfully designed, synthesized and applied as photocatalysts in the photoredox pinacol coupling of 4-chlorobenzaldehyde giving conversions from excellent too good in most cases. Furthermore, the reaction conditions of photoredox pinacol coupling were opportunely modified by the use of more suitable reducing agents such as BIH than TEA, in combination with a Brønsted acid (oxalic acid). To our pleasure, an almost total conversion to the diol product was obtained using these reaction conditions in the presence of coumarin **6** as photocatalyst. Unfortunately, attempts to promote the enantioselectivity in the reaction using chiral Brønsted acids was proved unsuccessful.

4.4 Experimental procedures

4.4.1 Computational calculatons

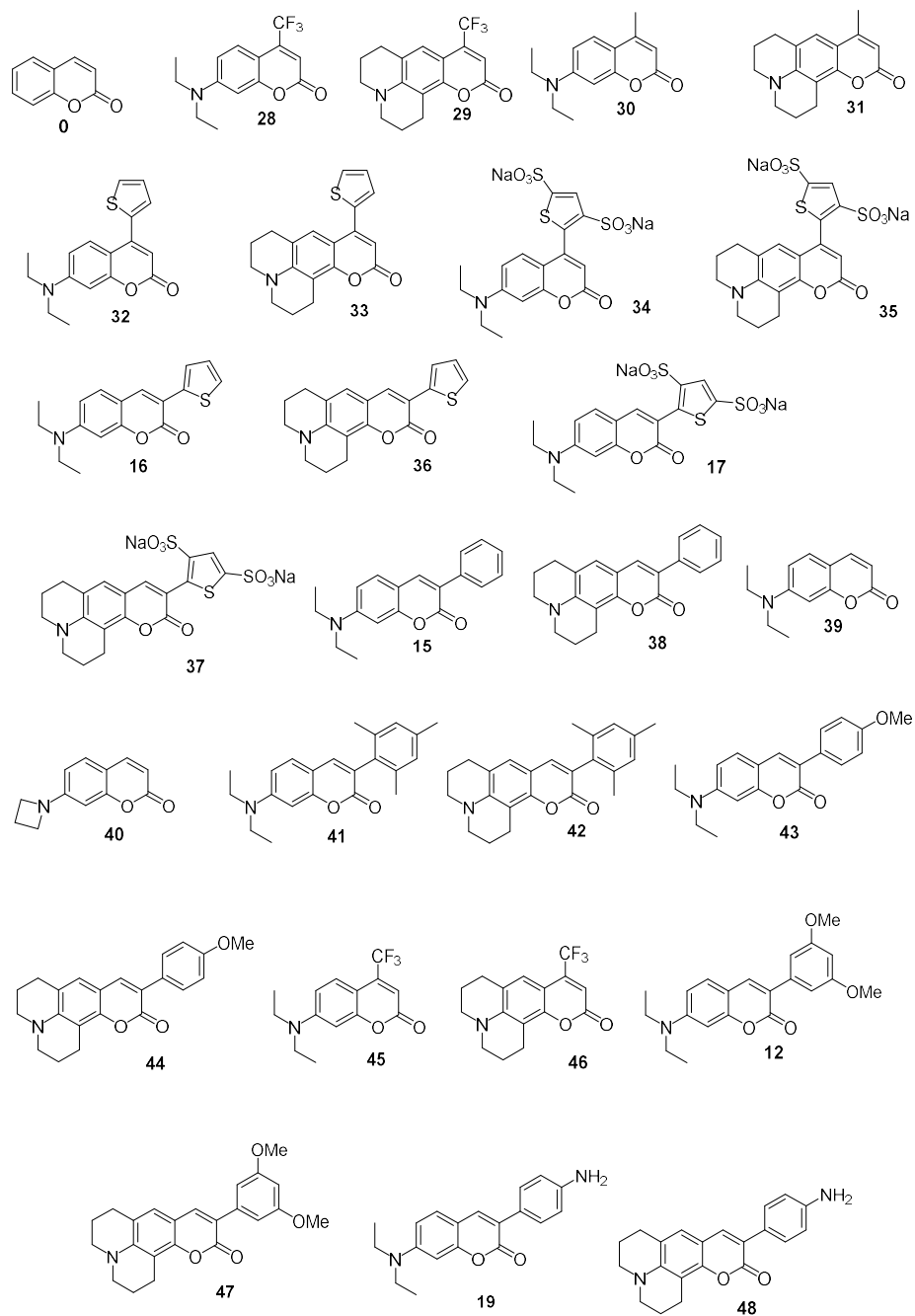


Figure 30 List of the coumarins analyzed in the computational calculations

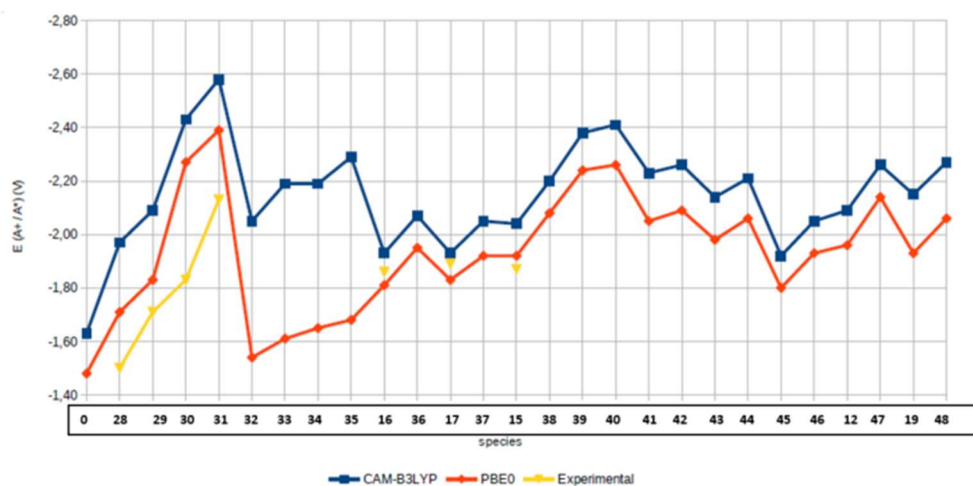


Figure 31 Predicted values for the photoredox potentials of the coumarins using CAM-B3LYP and PBE0

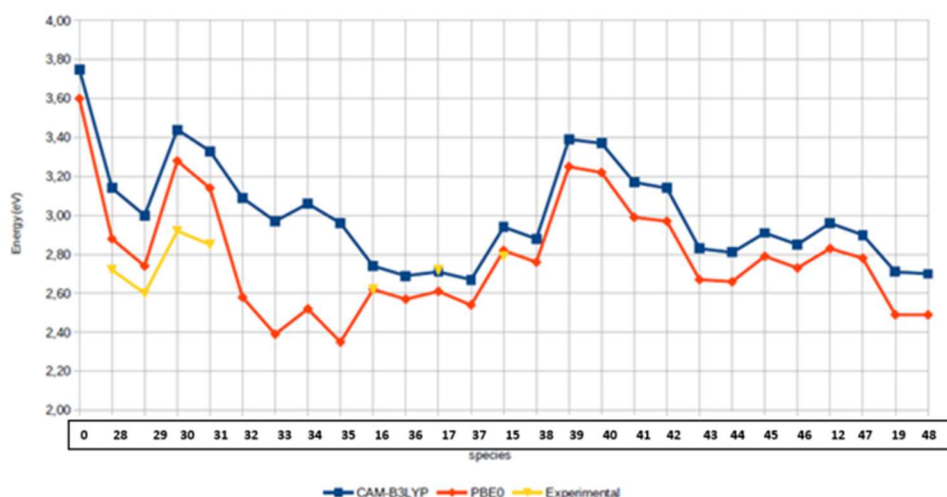


Figure 32 Predicted values for $E_{0,0}$ of the coumarins using CAM-B3LYP and PBE0

4.4.2 General methods and materials

$^1\text{H-NMR}$ spectra were recorded on Varian Mercury 400 spectrometer. Chemical shifts are reported in ppm from TMS with the solvent resonance as the internal standard (CDCl_3 : $\delta = 7.27$ ppm). Data are reported as follows: chemical shift, multiplicity (s = singlet, d = duplet, t = triplet, q = quartet, dd = double duplet, dt = double triplet, bs = broad signal, m = multiplet), coupling constants (Hz). $^{13}\text{C-NMR}$ spectra were recorded on Varian MR400 spectrometer. Chemical shifts are reported in ppm from TMS with the solvent as the internal standard (CDCl_3 : $\delta = 77.0$ ppm). GC-MS spectra were taken by EI ionization at 70 eV on a Hewlett-Packard 5971 with GC injection. LC-electrospray ionization mass spectra (ESI-MS) were obtained with Agilent Technologies MSD1100 single-quadrupole mass spectrometer. Chromatographic purification was done with 240-400 mesh silica gel. All reactions were set up under an argon atmosphere in oven-dried glassware using standard Schlenk techniques.

Anhydrous solvents were supplied by Aldrich in Sureseal® bottles and were used without further purification. All the reagents were purchased from Aldrich and used without further purification unless specified. Triethylamine and DIPEA were stirred one day over KOH and distilled before their use. Coumarin 17 was prepared using the procedure reported in section 2.4.2.

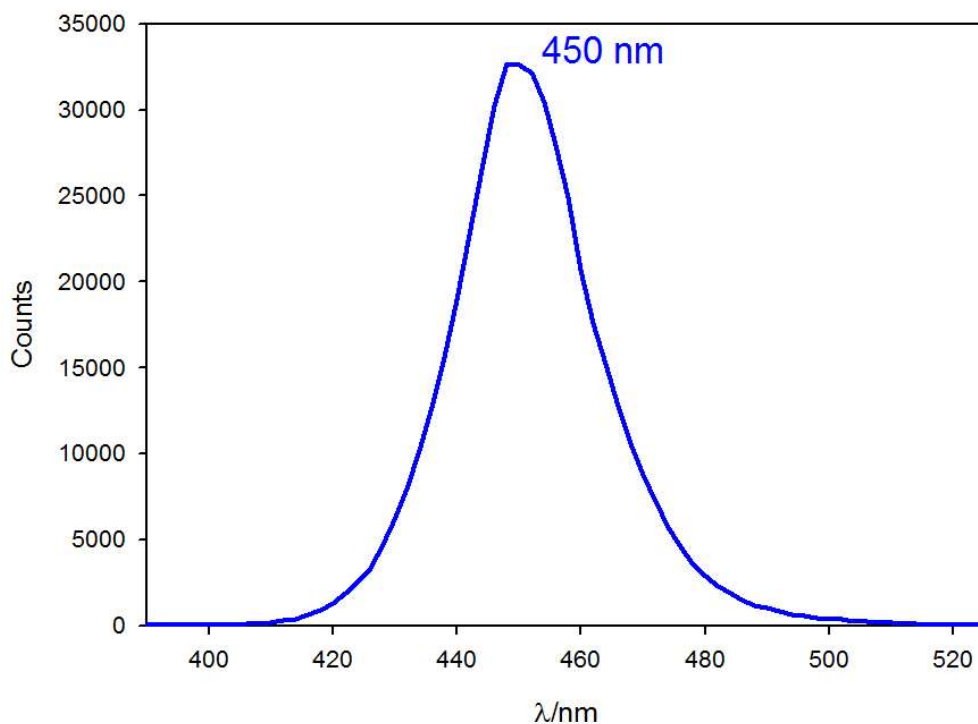
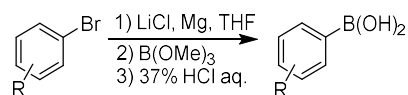
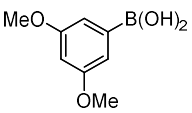


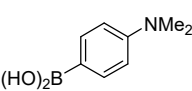
Figure 33 Emission profile of the 16W Blue LED strip used to irradiate the solutions.

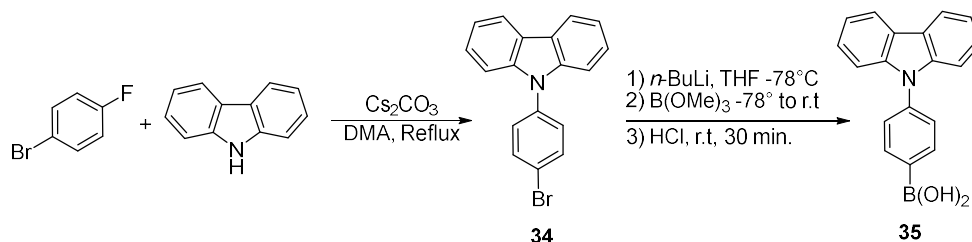
4.4.3 Synthesis and characterization of substrates

Synthesis of boronic acid




 3,5-dimethoxy-phenylboronic acid **21a** was prepared according to reported procedure³⁹: to anhydrous LiCl under inert atmosphere, THF (2 mL), magnesium turnings (4.5 mmol, 100 mg) and DIBALH (1M in THF, 0.02 mmol) were added. A solution of 3,5-dimethoxybromobenzene (1.75 mmol, 380 mg) in THF (4 mL) was added dropwise to the mixture, and the reaction was stirred for 1 hours. The solution was cooled at 0°C, B(OMe)₃ (3.5 mmol, 364 mg, 0.391 mL) was added and the solution was stirred for 1 hour. 37% HCl aq. was slowly added until pH = 4 and the solution was stirred for 30 minutes. The mixture was extracted with AcOEt (3 x 10 mL), the organic phases were dried over Na₂SO₄, and the solvent was removed under reduced pressure to obtain 3,5-dimethoxy-phenylboronic acid as white solid (61% 1.1 mmol, 0.195 g). Spectroscopic properties correspond to the literature.⁴⁰

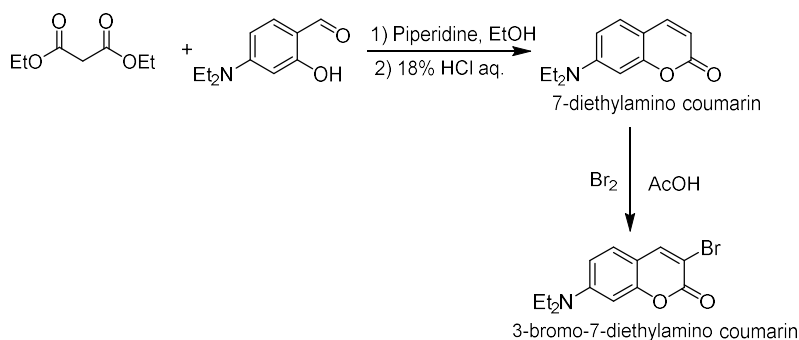

 4-(dimethylamino)-phenylboronic acid **21b** was prepared using the same procedure reported for 3,5-dimethoxy-phenylboronic acid on 4-bromo-*N,N*-dimethylaniline to obtain 4-(dimethylamino)benzene boronic acid Spectroscopic properties correspond to the literature.⁴¹



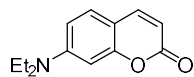
N-(4-bromophenyl)carbazole **34** was prepared according to reported procedure:⁴² A mixture of 4-bromo-fluorobenzene (3.6 mmol, 393 μl), carbazole (0.6 mmol, 300 mg), anhydrous DMA (10 mL) and Cs_2CO_3 (10.5 mmol, 3.6 g) was refluxed until under inert atmosphere disappear of the carbazole (about 20 hours by TLC analysis). The reaction mixture was cooled at room temperature, water (25 mL) and diethyl ether (20 mL) were added. The two phases were separated, and water phase was extracted with diethyl ether (2 x 20 mL). The organic phases were dried over Na_2SO_4 , and the solvent was removed under reduced pressure to obtain sticky solid. Pure compound was obtained after chromatographic purification (SiO_2 , cyclohexane:ethyl acetate 95:5) to give **34** (56%, 1.02 mmol, 0.324 g) as brownish solid; Spectroscopic properties correspond to the literature.^[42]

4-(carbazol-9-yl)phenylboronic acid **35** was prepared according to reported procedure:⁴³ To a stirred solution of **34** (0.93 mmol, 300 mg) in anhydrous THF (10 ml) at -78°C a solution of $n\text{-BuLi}$ (2.5 M in hexanes, 1.4 mmol, 0.56 mL). The reaction was stirred at -78°C for 1.5 hours and $\text{B}(\text{OMe})_3$ (1.86 mmol, 208 μl) was slowly added. The mixture was warmed at room temperature and stirred for 2 hours. HCl (37% aq., 7 mL) was slowly added and the mixture was stirred for 30 minutes. AcOEt (10 mL) was added, the two phases were separated, and water phase was extracted with AcOEt (2 x 10 mL). The organic phases were dried over Na_2SO_4 , and the solvent was removed under reduced pressure to obtain white solid. The solid was washed with small portion of diethyl ether to obtain pure **35** (47%, 0.44 mmol, 0.125 g) as white solid; Spectroscopic properties correspond to the literature.⁴⁴

Synthesis of 3-bromo-7-diethylaminocoumarin **20**

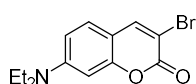


7-diethylaminocoumarin and 3-bromo-7-diethylaminocoumarin were prepared according to literature procedure.⁴⁵



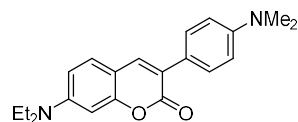
In a two necks round bottom flask under inert atmosphere were added 4-diethylamino salicylaldehyde (10 mmol, 2.2 g), absolute ethanol (20 mL), diethylmalonate (20 mmol, 3.2 g, 3.1 mL) and piperidine (1 mmol, 0.085 g, 99 μL). The solution was refluxed for 7 hours until disappearance of aldehyde, cooled at room temperature and the solvent was removed under reduced pressure. The residue was dissolved in DCM (20 mL), washed with 2 M HCl aq. (2 x 10 mL) and brine (2 x 10 mL). The organic phase was evaporated, the residue was suspended in 18% HCl aq. and refluxed for 2 hours. The solution was cooled at room temperature and 4M NaOH aq. was added until neutral pH. DCM (20 mL) was added and the two phases separated. The organic phase was washed with brine (2x 5 mL), dried over Na_2SO_4 , and the solvent was removed under reduced pressure to obtain 7-diethylaminocoumarin as red solid (93%, 9.3 mmol, 2.02 g); $^1\text{H-NMR}$ (400 MHz, CDCl_3) δ 7.50 (d, $J = 9.3$ Hz, 1H), 7.23 (d, $J = 8.5$ Hz, 1H), 6.53 (dd, $J = 8.8, 2.4$ Hz, 1H), 6.45 (d, $J = 2.2$ Hz, 1H), 6.00 (d, $J = 9.3$ Hz, 1H), 3.38 (q, $J = 7.1$ Hz, 4H), 1.18 (t, $J = 7.1$ Hz, 6H). Spectroscopic properties correspond to the literature.⁴⁷

Chapter 4: Development of new efficient coumarins for photoredox catalysis

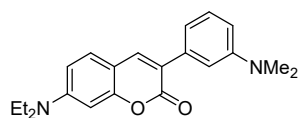


To a solution of 7-diethylaminocoumarin (4.6 mmol, 0.998 g) in glacial acetic acid (10 mL) a solution of bromine (4.6 mmol, 0.735 g, 0.236 mL) in glacial acetic acid (5 mL) was added dropwise under stirring. After 30 minutes the solid was filtered and washed with water (3 x 10 mL) and dried under vacuum to give 3-bromo-7-diethylaminocoumarin in quantitative yield as orange solid; Spectroscopic properties correspond to the literature.⁴⁷

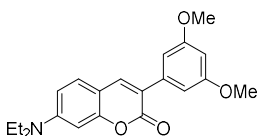
Synthesis of **11**, **12**, **18** and **19** by Suzuki-Miyaura coupling



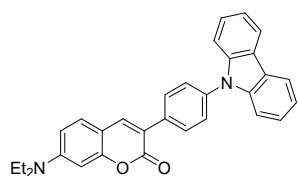
To a degassed mixture of water:ethanol:toluene (10:5:5 mL) under inert atmosphere 3-bromo-7-diethylaminocoumarin (0.17 mmol, 0.050 g), Pd(PPh₃)₄ (0.008 mmol, 9.2 mg), 4-(dimethylamino)benzene boronic acid (0.34 mmol, 0.056 g) e K₂CO₃ (0.51 mmol, 0.070 g) were added. The mixture was refluxed for 7 hours, cooled at room temperature and the solvents were evaporated under reduced pressure. The residue was diluted with DCM (40 mL) and filtered through Celite®. The solvent was evaporated under reduced pressure and the residue was purified by flash chromatography (SiO₂, cyclohexane:ethyl acetate 95:5) to give **19** (70%, 0.12 mmol, 0.040 g) as yellow solid; ¹H-NMR (400 MHz, CDCl₃) δ: 7.63 (m, 3H), 7.30 (d, *J* = 8.8 Hz, 1H), 6.78 (d, *J* = 8.8 Hz, 2H), 6.59 (dd, *J* = 8.7, 2.2 Hz, 1H), 6.54 (d, *J* = 2.0 Hz, 1H), 3.43 (q, *J* = 7.1 Hz, 4H), 2.99 (s, 6H), 1.22 (t, *J* = 7.1 Hz, 6H); ¹³C-NMR (400 MHz, CDCl₃) δ: 162.0, 155.6, 150.1, 149.8, 137.9, 128.9 (2C), 128.4, 123.7, 121.2, 112.2 (2C), 109.5, 108.7, 97.2, 44.8 (2C), 40.5 (2C), 12.5 (2C); ESI-MS *m/z*: 337.2 [M+H]⁺.



(**18**): The general procedure reported for **19** was applied; yield 44% (0.07 mmol, 0.025 g); yellow solid; ¹H-NMR (400 MHz, CDCl₃) δ: 7.67 (s, 1H), 7.28 (t, *J* = 8.2 Hz, 2H), 7.05 (s, 1H), 6.99 (d, *J* = 7.6 Hz, 1H), 6.72 (dd, *J* = 8.3, 2.1 Hz, 1H), 6.57 (dd, *J* = 8.8, 2.4 Hz, 1H), 6.51 (d, *J* = 2.2 Hz, 1H), 3.41 (q, *J* = 7.1 Hz, 4H), 2.97 (s, 6H), 1.20 (t, *J* = 7.1 Hz, 6H); ¹³C-NMR (400 MHz, CDCl₃) δ: 161.6, 156.1, 150.6, 150.3, 140.3, 136.5, 128.9, 128.8, 121.8, 116.8, 112.8, 112.3, 109.1, 108.8, 97.1, 77.3, 77.0, 76.7, 44.8, 40.7, 12.4; ESI-MS *m/z*: 337.2 [M + H]⁺; 673.4 [1M + H]⁺.



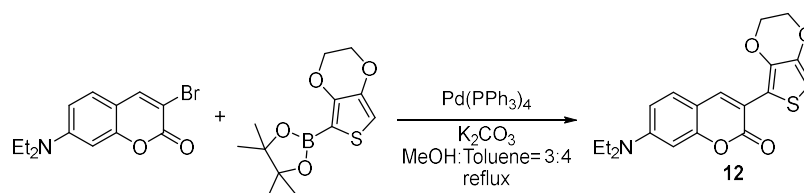
(**12**): The general procedure reported for **19** was applied; yield 56% (0.09 mmol, 0.033 g); red solid; ¹H-NMR (400 MHz, CDCl₃) δ: 7.68 (s, 1H), 7.29 (d, *J* = 8.8 Hz, 1H), 6.84 (d, *J* = 2.2 Hz, 2H), 6.58 (dd, *J* = 8.8, 2.4 Hz, 1H), 6.51 (d, *J* = 2.2 Hz, 1H), 6.44 (t, *J* = 2.2 Hz, 1H), 3.81 (s, 6H), 3.41 (q, *J* = 7.1 Hz, 4H), 1.20 (t, *J* = 7.1 Hz, 6H); ¹³C-NMR (400 MHz, CDCl₃) δ: 161.4, 160.5 (2C), 156.2, 150.5, 140.7, 137.7, 129.0 (2C), 120.6, 108.9, 106.4 (2C), 100.1, 97.0, 55.4 (2C), 44.8 (2C), 12.4 (2C); ESI-MS *m/z*: 353.2 [M + H]⁺



(**11**): The general procedure reported for **19** was applied; yield 45% (70%, 0.08 mmol, 0.035 g); yellow solid; ¹H NMR (400 MHz, CDCl₃) δ: 8.14 (d, *J* = 7.7 Hz, 2H), 7.94 (d, *J* = 8.3 Hz, 2H), 7.81 (s, 1H), 7.60 (d, *J* = 8.3 Hz, 2H), 7.47 (d, *J* = 8.3 Hz, 2H), 7.41 (t, *J* = 7.6 Hz, 2H), 7.35 (d, *J* = 8.7 Hz, 1H), 7.28 (t, *J* = 7.4 Hz, 2H), 6.62 (dd, *J* = 8.9, 2.1 Hz, 1H), 6.57 (s, 1H), 3.44 (q, *J* = 7.2 Hz, 4H), 1.23 (t, *J* = 7.0 Hz, 6H); ¹³C-NMR (400 MHz, CDCl₃) δ: 161.7, 156.3, 150.7, 140.8, 140.8, 134.9, 129.6 (2C), 129.1, 126.8 (2C), 125.9 (2C), 123.4, 120.3 (2C), 119.9 (2C), 119.8, 109.9 (2C), 109.1, 109.1, 97.1, 44.9, 12.5.; ESI-MS *m/z*: 459.2 [M + H]⁺.

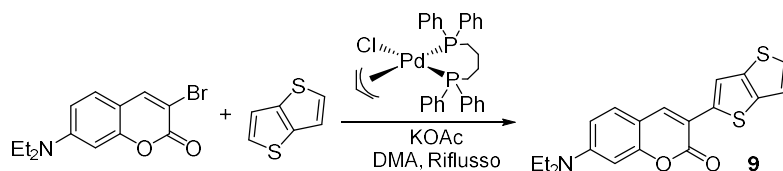
Chapter 4: Development of new efficient coumarins for photoredox catalysis

Synthesis of 12



To a solution of 3-bromo-7-diethylaminocoumarin (0.34 mmol, 0.100 g) in degassed methanol:toluene (3:4, 10 mL) mixture, Pd(PPh₃)₄ (0.017 mmol, 19.6 mg), boronic acid (0.75 mmol, 0.201 g) e K₂CO₃ (1.5 mmol, 0.207 g) were added. The mixture was refluxed for 8 hours, cooled at room temperature and the solvent removed under reduced pressure. Water (5 mL) and DCM (20 mL) were added to the residue. The two phases were separated, and water phase was extracted with DCM (2 x 10 mL). The organic phases were dried over Na₂SO₄, and the solvent was removed under reduced pressure to obtain orange solid. Pure compound was obtained after chromatographic purification (SiO₂, cyclohexane:ethyl acetate 75:25) to give **10** (22%, 0.07 mmol, 0.026 g) as yellow solid; ¹H-NMR (400 MHz, CDCl₃) δ: 8.42 (s, 1H), 7.30 (d, *J* = 8.8 Hz, 1H), 6.59 (dd, *J* = 8.9, 2.4 Hz, 1H), 6.51 (d, *J* = 2.1 Hz, 1H), 6.39 (s, 1H), 4.39 – 4.31 (m, 2H), 4.28 – 4.19 (m, 2H), 3.41 (q, *J* = 6.9 Hz, 4H), 1.20 (t, *J* = 7.1 Hz, 6H); ESI-MS *m/z*: 358.2 [M + H]⁺.

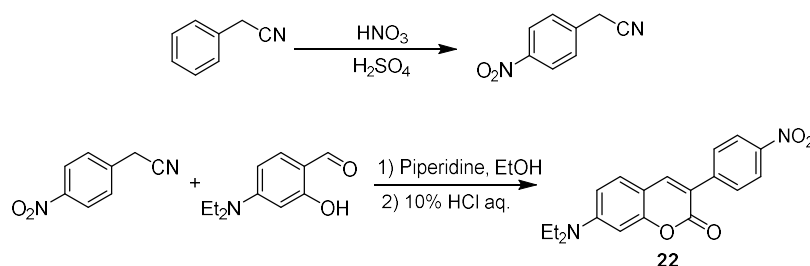
Synthesis of 9



Compound **9** was prepared according to reported procedure.^[46]

Thieno[3,2-*b*]thiophene (0.5 mmol, 70 mg), KOAc (0.5 mmol, 49 mg), 3-bromo-7-diethylaminocoumarin (0.25 mmol, 74 mg), and palladium complex (0.0025 mmol, 1.5 mg) were dissolved in degassed DMA (6 mL). The mixture was refluxed for 8 hours, cooled at room temperature. Water (5 mL) and AcOEt (20 mL) were added to the mixture. The two phases were separated, and water phase was extracted with AcOEt (2 x 10 mL). The organic phases were dried over Na₂SO₄, and the solvent was removed under reduced pressure to obtain orange solid. Pure compound was obtained after chromatographic purification (SiO₂, cyclohexane:ethyl acetate 85:15) to give **9** (38%, 0.09 mmol, 0.034 g) as yellow solid; ¹H-NMR (400 MHz, CDCl₃) δ: 7.96 (s, 1H), 7.84 (s, 1H), 7.37 – 7.29 (m, 2H), 7.22 (d, *J* = 5.2 Hz, 1H), 6.60 (d, *J* = 8.9 Hz, 1H), 6.52 (s, 1H), 3.42 (q, *J* = 7.0 Hz, 4H), 1.21 (t, *J* = 7.2 Hz, 6H); ESI-MS *m/z*: 356.0 [M + H]⁺.

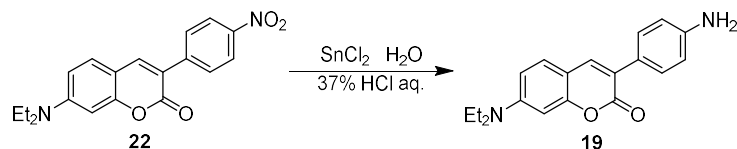
Synthesis of 22



22 was prepared according to reported procedure:^[47] 4-diethylamino-salicyl aldehyde (1.2 mmol, 0.232 g) was dissolved in absolute ethanol (7 mL) under inert atmosphere. 2-(4-nitrophenyl)acetonitrile^[48] (1.2 mmol, 0.200 g) was added to the solution followed by 5 drops of piperidine. The reaction mixture was stirred overnight, and the solvent was evaporated under reduce pressure to obtain a red solid. The solid was added to 10% HCl aq. (10 mL) and the suspension was refluxed for 6 hours. The mixture was cooled at room temperature, the result orange solid was filtered off and washed with water. The solid was purified by flash chromatography (SiO₂, cyclohexane:ethyl acetate 8:2) to obtain **22** as orange solid (43%, 0.516 mmol, 0.174 g); ¹H-NMR (400 MHz, CDCl₃) δ: 8.26 (d, *J* =

8.7 Hz, 2H), 7.92 (d, $J = 8.7$ Hz, 2H), 7.83 (s, 1H), 7.36 (d, $J = 8.9$ Hz, 1H), 6.64 (dd, $J = 8.8, 2.3$ Hz, 1H), 6.54 (d, $J = 2.1$ Hz, 1H), 3.46 (q, $J = 7.1$ Hz, 4H), 1.25 (t, $J = 7.1$ Hz, 6H); ^{13}C -NMR (400 MHz, CDCl_3) δ : 160.9, 156.7, 151.4, 146.7, 142.5, 142.1, 129.6, 128.6 (2C), 123.5 (2C), 117.7, 109.4, 108.7, 97.0, 45.0, 12.4; ESI-MS m/z : 339.2 $[\text{M}+\text{H}]^+$.

Synthesis of **19**



19 was prepared according to reported procedure.⁴⁹ In a two necks round bottom flask under air tin(II) chloride hydrate (0.9 mmol, 0.195 g) was dissolved in HCl (37% aq., 1.5 mL). Compound **22** (0.12 mmol, 0.044 g) was slowly added to the solution, the mixture was refluxed for 4 hours and cooled at room temperature. NaOH 1 M was slowly added to the mixture until neutral pH and the mixture was extracted with AcOEt (3 x 15 mL). The organic phases were washed with brine (2 x 5 mL), dried over Na_2SO_4 , and the solvent was removed under reduced pressure to give a brown solid. The crude was further purified by flash column chromatography (SiO_2 , cyclohexane:ethyl acetate 8:2) to obtain **19** as red solid, 21% yield (0.03 mmol, 0.008 g); ^1H -NMR (400 MHz, CDCl_3) δ : 7.58 (s, 1H), 7.50 (d, $J = 8.2$ Hz, 2H), 7.26 (d, $J = 8.9$ Hz, 1H), 6.73 (d, $J = 8.1$ Hz, 2H), 6.56 (d, $J = 8.9$ Hz, 1H), 6.50 (s, 1H), 3.39 (q, $J = 6.9$ Hz, 4H), 1.19 (t, $J = 7.0$ Hz, 6H); ^{13}C -NMR (400 MHz, CDCl_3) δ : 161.9, 155.8, 150.0, 146.2, 138.5, 129.2 (2C), 128.5, 125.9, 121.1, 114.8 (2C), 109.3, 108.8, 97.2, 44.8 (2C), 12.5 (2C).

4.4.4 General procedure for photoredox pinacol coupling of aldehydes.

A dry 10 mL Schlenk tube, equipped with a Rotaflo stopcock, magnetic stirring bar and an argon supply tube, was charged in order and under argon with the photocatalyst (5 mol%, 0.01 mmol), aldehyde **26** (0.2 mmol) and DMF (1.0 mL). The reaction mixture was then subjected to a freeze-pump-thaw procedure (three cycles) and the vessel refilled with argon. Then the Et_3N was added (0.8 mmol, 4 equiv., 112 μL). The reaction was irradiated with 16W blue LEDs (approx. 10 cm distance) and stirred for 36 h. After that the reaction mixture was diluted with H_2O (5 mL) extracted with AcOEt (3 x 10 mL). The combined organic layers were washed with brine (10 mL), dried over Na_2SO_4 , and the solvent was removed under reduced pressure. Two identical reaction were performed for each substrate and the crudes were reunite before purification. The residue was purified by flash column chromatography (SiO_2) to afford the title compounds in the stated yields. Diastereoisomeric ratio was determined by integration of benzylic CH ^1H NMR signal; ^1H NMR (400 MHz, CDCl_3 , 25°C): $\delta_{d/l,meso} = 7.24$ (*meso*, m, 4H), 7.22–7.17 (*d/l*, m, 4H), 7.11–7.06 (*meso*, m, 4H), 7.03–6.98 (*d/l*, m, 4H), 4.82 (*meso*, s, 2H), 4.60 (*d/l*, s, 2H); ^{13}C NMR (100 MHz, CDCl_3): $\delta_{d/l,meso} = 137.9$ (*meso*, 2C), 137.8 (*d/l*, 2C), 133.8 (4C), 128.4 (*meso*, 4C), 128.3 (*d/l*, 4C), 128.3 (8C), 78.5 (2C), 77.1 (2C); ESI-MS m/z : 265.0 $[\text{M}-\text{OH}]^+$, 305.1 $[\text{M}+\text{Na}]^+$.

References

- 1 a) K. N. Houk and P. H.-Y. Cheong, *Nature*, 2008, **455**, 309; b) S. Hammes-Schiffer, *Accounts of Chemical Research*, 2017, **50**, 561.1
- 2 D. M. Arias-Rotondo and J. K. McCusker, *Chemical Society Reviews*, 2016, **45**, 5803.
- 3 a) B. G. McCarthy, R. M. Paerson, C. H. Lim, S. M. Sartor, N. H. Damraur and G. M. Miyake, *J. Am. Chem. Soc.*, 2018, **140**, 5088; b) J. C. Theriot, C.-H. Lim, H. Yang, M. D. Ryan, C. B. Musgrave and G. M. Miyake, *Science*, 2016, **352**, 1082 (2016); c) R. M. Pearson, C. H. Lim, B. G. McCarthy, C. B. Musgrave and G. M. Miyake, *J. Am. Chem. Soc.*, 2016, **138**, 11399. D) C. H. Lim, M. D. Ryan, B. G. McCarthy, J. C. Theriot, S. M. Sartor, N. H. Damraurer, C. B. Musgrave and G. M. Miyake, *J. Am. Chem. Soc.*, 2017, **139**, 348.
- 4 D. A. Corbin, C. -H. Lim and G. M. Miyake, *Aldrichimica Acta*, 2019, **52**, 7.
- 5 V. K. Singh, C. Yu, S. Badgular, Y. Kim, Y. Kwon, D. Kim, J. Lee, T. Akhter, G. Thangavel, L. S. Park, J. Lee, P. C. Nandajan, R. Wannemacher, B. Milian-Medina, L. L  r, K. S. Kim, J. Gierschner and M. S. Kwon, *Nature Catalysis*, 2018, **1**, 794.

- ⁶ I. Perepichka, D. Perepichka, H. Meng, and F. Wudl, *Advanced Materials*, 2005, **17**, 2281.
- ⁷ G. Zhang, H. Bala, Y. Cheng, D. Shi, X. Lv, Q. Yu and P. Wang, *Chem. Commun.*, 2009, 2198.
- ⁸ N. Zhijun and T. He, *Chem. Commun.*, 2009, 5483.
- ⁹ J. Hongji, S. Jian and J. Zhang, *Current Organic Chemistry*, 2012, **16**, 2014.
- ¹⁰ M. S. Alsalthi, J. Alam, L. A. Dass, M. Raja, *Int. J. Mol. Sci.*, 2011, **12**, 2036.
- ¹¹ L. Yijiang, N. Xiang, X. Feng, P. Shen, W. Zhou, C. Weng, B. Zhaoa and S. Tan, *Chem. Commun.*, 2009, 2499.
- ¹² M. Faisal, A. Saeed, Q. Abbas, M. Kazi, N. Abbas, A. Thebo, D. Khan and P. Channar, *J. Mater. Sci.: Mat. Electron*, 2018, 1.
- ¹³ S. Karna, Y. Zhang, M. Samoc, P. Prasad, B. Reinhardt and A. Dillard, *J. Chem. Phys.*, 1993, **99**, 9984.
- ¹⁴ M. Zavelani-Rossi, G. Lanzani, M. Anni, G. Gigli, R. Cingolani, G. Barbarella and L. Favaretto, *Synthetic Metals*, 2003, **139**, 901.
- ¹⁵ J. B. Grimm, B.P. English, J. Chen, J.P. Slaughter, Z. Zhang, A. Revyakin, R. Patel, J. J. Macklin, D. Normanno, R. H. Sigler, T. L. Lionnet, L.D. Lavis, *Nature Methods*, 2015, **13**, 244-250.
- ¹⁶ T. Leermann, F. R. Leroux and F. Colobert, *Org Lett.*, 2011, **13**, 4479.
- ¹⁷ C. Tanner, *J. Org. Chem.*, 1989, **54**, 3842.
- ¹⁸ C. Tanner and P. Luelo, *J. Am. Chem. Soc.*, 1992, **114**, 713.
- ¹⁹ Y. Tamaki, K. Koike, T. Morimoto and O. Ishitani, *J. Catal.*, 2013, **304**, 22.
- ²⁰ D. Hong, Y. Tsukakoshi, H. Kotani, T. Ishizuka and T. Kojima, *J. Am. Chem. Soc.*, 2017, **139**, 6538.
- ²¹ Y. Yamazaki, H. Takeda and O. Ishitani, *J. Photochem. Photobiol. C*, 2015, **25**, 106.
- ²² H. G. Roth and D. A. Nicewicz, *Synlett*, 2016, **27**, 714.
- ²³ M. Nakajima, E. Fava, S. Loescher, Z. Jiang and M. Rueping, *Angew. Chem., Int. Ed.*, 2015, **54**, 8828.
- ²⁴ A. N. Butkevich, M. L. Bossi, G. Lukinavicius and S. W. Hell, *J. Am. Chem. Soc.*, 2019, **141**, 981.
- ²⁵ Z. D. Miller, B. J. Lee and T. P. Yoon, *Angew. Chem Int. Ed.*, 2017, **56**, 11891.
- ²⁶ L. J. Rono, G. Y. Hatice, D. Y. Wang, M. F. Armstrong and R. R. Knowles, *J. Am. Chem. Soc.*, 2013, 135, 17735.
- ²⁷ M. Terada, *Synthesis*, 2010, **12**, 1929.
- ²⁸ P. M. Pihko, *Angew. Chem. Int. Ed.*, 2004, **43**, 2062.
- ²⁹ P. R. Schreiner and A. Wittkop, *Org. Lett.*, 2002, **4**, 2217.
- ³⁰ P. Kotchapradist, N. Prachumrak, T. Sunonnam, R. Tarsang, S. Namuangruk and T. Sudyoasuk, *Dyes Pigm.*, 2015, **112**, 227.
- ³¹ H. -L. Chen, H. -C. Lin, C. -D. Wu and T. -H. Wang, U.S. Pat. Appl. Publ., 2006, US 20060063034 A1 20060323.
- ³² T. Z. Yu, Z. Y. Zhu, Y. J. Bao, Y. L. Zhao, X. X. Liu and H. Zhang, *Dyes Pigm.*, 2017, **147**, 260.
- ³³ H. Jiang, J. Sun and J. Zhang, *Current Organic Chemistry*, 2012, **16**, 2014.
- ³⁴ T. M. Ha Vuong, D. Villemin, H. -H. Nguyen, T. T. Le, T. T. Dang, H. Nguyen, *Chemistry - An Asian Journal*, 2017, **12**, 2819.
- ³⁵ G. Bartoli and P. E. Todesco, *Acc. Chem. Res.*, 1977, **10**, 125.
- ³⁶ N. A. Senger, B. Bo, Q. Cheng, J. R. Keeffe, S. Gronert and W. Wu, *J. Org. Chem.*, 2012, **77**, 9535.
- ³⁷ J. B. Grimm, B. P. English, J. Chen, J. P. Slaughter, Z. Zhang, A. Revyakin, R. Patel, J. J. Macklin, D. Normanno, R. H. Sigler, T. L. Lionnet and L. D. Lavis, L.D., *Nature Methods*, 2015, **13**, 244-250.
- ³⁸ X. Liu, Q. Qiao, W. Tian, W. Liu, J. Chen, M. J. Lang and Z. Xu, *J. Am. Chem. Soc.*, 2016, **138**, 6960.
- ³⁹ T. Leermann, F. R. Leroux and F. Colobert, *Org. Lett.*, 2011, **13**, 4479.
- ⁴⁰ S. M. Elbert, P. Wagner, T. Kanagasundaram, F. Rominger and M. Mastalerz, *Chem.: Eur. J.* **2017**, **23**, 935-945.
- ⁴¹ S. M. Elbert, P. Wagner, T. Kanagasundaram, F. Rominger and M. Mastalerz, *Chem.: Eur. J.* **2017**, **23**, 935-945.

- ⁴² L. Wang, E. Ji, N. Liu and B. Dai, *Synthesis*, 2016, **48**, 737.
- ⁴³ L. Guo, K. F. Li, M. S. Wong and K. W. Cheah, *Chem. Commun.* 2013, **49**, 3597.
- ⁴⁴ S. Fan, J. You, Y. Miao, H. Wang, Q. Bai, X. Liu, X. Li and S. Wang, *Dyes Pigm.*, 2016, **129**, 34.
- ⁴⁵ H. Sun, H. Guo, W. Wu, X. Liu, J. Zhao, *Dalton Transactions*, 2011, **40**, 7834.
- ⁴⁶ T. M. Ha Vuong, D. Villemin, H.-H. Nguyen, T. T. Le, T. T. Dang and H. Nguyen, *Chemistry – An Asian Journal*, 2017, **12**, 2819.
- ⁴⁷ B. Zhang, C. Ge, J. Yao, Y. Liu, H. Xie and J. Fang, *J. Am. Chem. Soc.*, 2015, **137**, 757.
- ⁴⁸ G. R. Robertson, *Org. Synth.* **1922**, 2, 57.
- ⁴⁹ L. Wang, E. Ji, N. Liu, B. Dai, *Synthesis* 2016, **48**, 737.

Allylation of aldehydes by dual photoredox and nickel catalysis

5.1 Introduction

5.1.1 Nozaki-Hiyama-Kishi reaction

The allylation of carbonyl compounds is a crucial transformation in organic synthesis for the preparation of homoallylic alcohols.¹ Organometallic allylating compounds² are important reagents for synthesis and they are easily accessible by Barbier methodologies.³ However, in many organometallic procedures a stoichiometric amount of another metal, used as stoichiometric sacrificial reductant, is crucial. For example, in the catalytic version of the Nozaki–Hiyama–Kishi reaction, a chemoselective and well established allylation methodology based on chromium,⁴ the use of an excess of manganese as the terminal reductant is mandatory, the reaction is heterogeneous, and the final work-up of the reaction results in the production of waste (Mn, Mn salts, etc.) (Figure 1). In addition, it is important to add a “scavenger”, a reagent able to liberate the chromium alkoxide intermediate and allowed its successive reduction. Without scavengers the redox cycle is not continued, and the reduction of the Cr(III) alkoxy intermediate is becoming difficult, as the donor properties of the OR bond. Instead, by the use of Me₃SiCl, the chromium alkoxy intermediate is silylated, and a more easily reducible Cr(III)Cl fragment is formed.

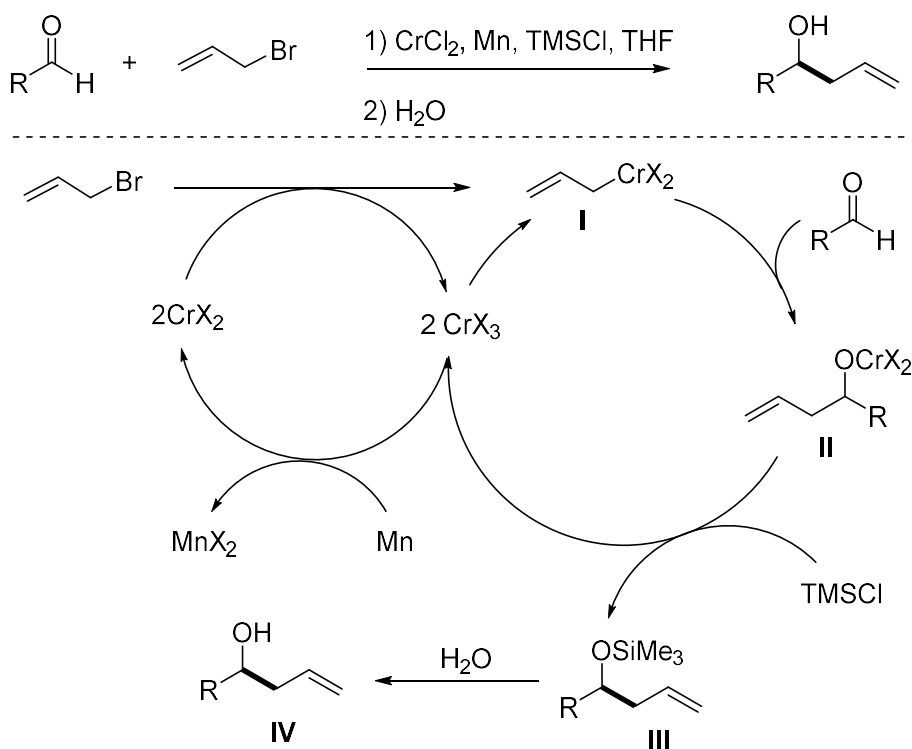


Figure 1 Nozaki-Hiyama-Kishi reaction.

The chromium catalyst CrCl_2 reacts with allyl bromide giving the organochromium **I** species and one equivalent of CrX_3 . Alkoxide **II** is then formed by addition of **I** to the aldehyde. A ligand exchange between **II** and TMSCl provides the silyl ether **III** and liberates the CrX_3 which is again reduced to Cr(II) by the presence of Mn. The silyl ether **III** is stable in the reaction conditions and is liberated after the work-up to give the homoallylic alcohol **IV**. Stereoselective variant of the Nozaki-Hiyama Kishi reaction was reported, based on the mentioned catalytic cycle in the presence of suitable chiral ligands.⁵ The Nozaki-Hiyama Kishi reaction, for the wide tolerability of functional groups and for its versatility, was applied to the total synthesis of natural products.⁶ Furthermore, stereoselective addition of vinyl halides (by the use of nickel complexes) and alkyl halides (by the use of cobalt complexes) was described by Kishi.⁷ Among all the nucleophilic organometallic species, η^3 -nickel allyl complexes were introduced in literature many years ago by Corey and Semmelack,⁸ as nucleophilic reagents. Although a chemoselectivity was observed, the low reactivity and the use of highly toxic nickel complexes (such as Ni(CO)_4) or reactive and instable nickel complexes (such as Ni(COD)_2) hampered the study and the employment of the organometallic reagent. In addition, the Ni(II) allyl species was generated by the use of stoichiometric amount of the Ni(0) complexes (either Ni(CO)_4 or Ni(COD)_2) by oxidative addition. More recently, Durandaretti and Périchon⁹ described an allylation and Reformatsky reactions catalysed by Ni(II) bipyridine complexes in the presence of a stoichiometric amount of manganese or zinc metal as terminal reductants.¹⁰ These reactions are promoted by the *in situ* formation of η^3 -nickel allyl or enolate complexes which are capable to react with electrophilic species. Major drawbacks of these methodologies are still the employment of stoichiometric amount of metal as reductant. The metal (Zn or Mn) is oxidized to the M(II) state, that is normally discharged at the end of the reaction. These reactions, are generating waste and the metal can be not re-used as a reduction to the active M(0) state will be necessary. However, the possible use of metallaphotoredox catalysis can solve the problem of reducing the waste, by replacing the stoichiometric metal reductant with an organic species, if combined with the action of photoredox catalysis.

5.1.2 Metallaphotoredox catalysis

Metallaphotoredox catalysis, i.e. metal catalysis merged with photoredox catalysis, is a new and rapidly growing research subject.¹¹ The key seminal papers, published by Sanford,¹² Molander,¹³ Doyle and MacMillan,¹⁴ were followed by many other publications, dealing with new concepts, and with the applications of different metals (Figure 2).

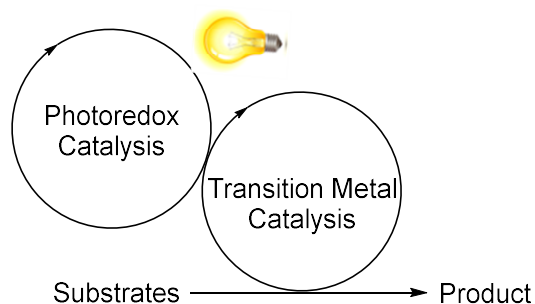


Figure 2 Generic representation for metallaphotoredox catalysis.

The driving force of this dual photoredox and metal catalysis is the single electron transfer which occurs from the photocatalyst to the metal catalyst under visible light irradiation. The catalytic generation of active organometallic intermediates takes place, triggering the organic substrates toward a diverse array of valuable transformations. This novel strategy has allowed the accomplishment of difficult reactions in organic synthesis under mild reaction conditions.

In particular, nickel metallaphotoredox catalysis represents a new tool for cross-coupling reactions¹⁵ and the formation of carbon-heteroatom bonds.¹⁶ In fact, nickel catalysts proved to activate traditionally inert substrates through the promotion of facile oxidative additions with alkyl electrophiles and the high tolerance to several alkyl coupling partners.

An elegant example is the decarboxylative coupling between alkyl or aryl halides and carboxylic acids to forge new Csp^3 - Csp^2 bonds, reported by McMillan and co-workers (Figure 3).¹⁷

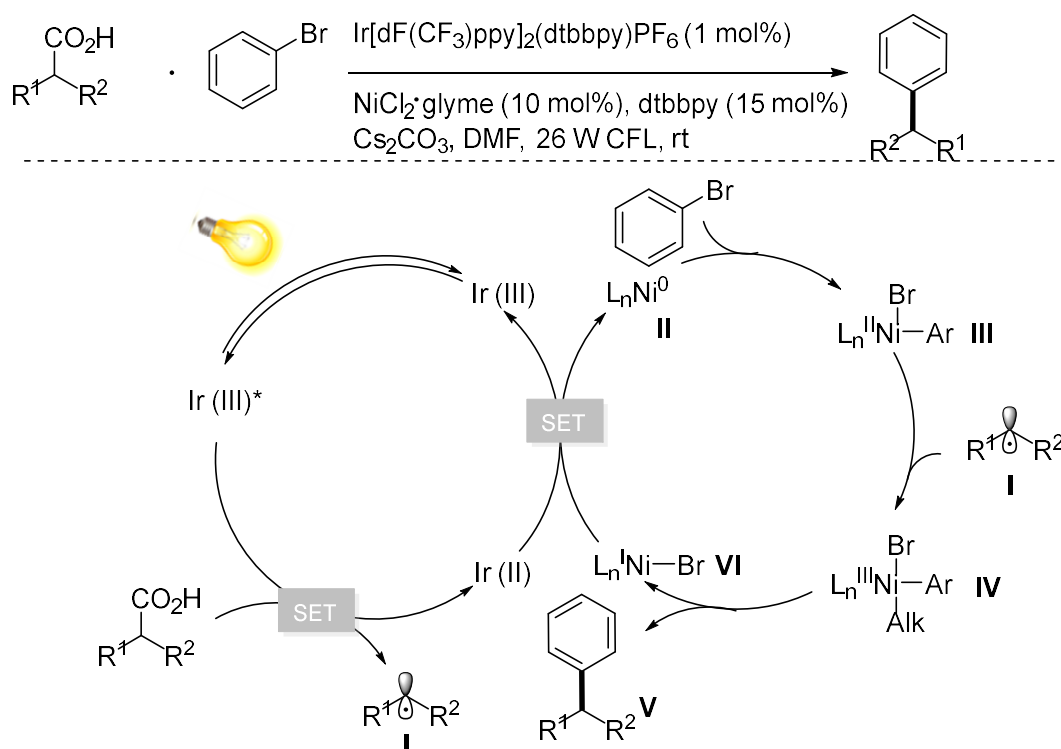


Figure 3 Decarboxylative coupling between alkyl or aryl halides and carboxylic acids.

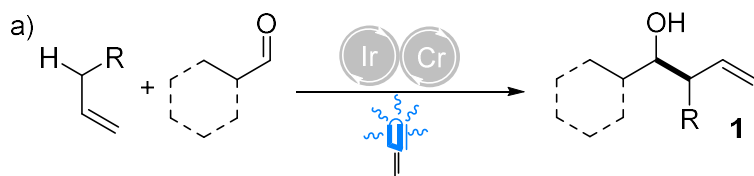
The oxidative decarboxylation of the carboxylic acid is mediated by the excited state Ir(III)*, radical **I** and the Ir(II) species are then formed by a single electron transfer (SET). In parallel, Ni complex **II** undergoes oxidative addition with the aryl bromine generating the Ni(II) complex **III** which traps the acid-derived radical **I**. The reductive elimination of Ni(III) complex **IV** provided the cross-coupled product **V** and the Ni(I) complex **VI**. Finally, the two catalytic cycles are restored by a SET process from Ir(II) and Ni(I) complex **VI**.

This general strategy has been employed to efficiently form new C-C bonds under mild reaction conditions using several unconventional cross coupling partners. Carboxylic acids (including aminoacids and ketoacids) alcohols,¹⁸ potassium alkyltrifluoroborates,¹⁹ alkylsilicates²⁰ and 4-alkyl-1,4-dihydropyridines²¹ are some well-known examples.

5.1.3 Metallaphotoredox catalysis for the allylation of aldehyde

Although interesting allylation reactions of carbonyl compounds have been described through photoredox methodologies,²² these methods lack generality and are limited in scope.

Quite recently, a remarkable example of the diastereoselective allylation of aldehydes through a combination of photoredox and chromium(II) catalysis with not functionalized allyl (hetero-) arenes was reported by Glorius and co-workers²³ (Figure 4).



R = electron-rich aryl, heteroaryl, amino d.r. >19:1 to 11:1; up to 95% yield

Figure 4 Photoredox allylation of aldehydes reported by Glorius.

The reaction relies on the ability of $[\text{Ir}(\text{dF}(\text{CF}_3)\text{ppy})_2(\text{bpy})][\text{PF}_6]$ to engage in a SET with the Cr(II) catalyst under visible light irradiation. The reactions gave the allylic alcohols **1** in excellent yields and diastereoselectivity with primary and secondary aliphatic aldehydes while tertiary aliphatic aldehydes were unreactive. The presence of several functional groups including trifluoromethyl, ethers and halides in case of substituted aromatic aldehydes were well tolerated.

Further, a highly enantioselective version of the metallaphotoredox allylation of aldehydes was disclosed by Kanai and co-workers (Figure 5).²⁴

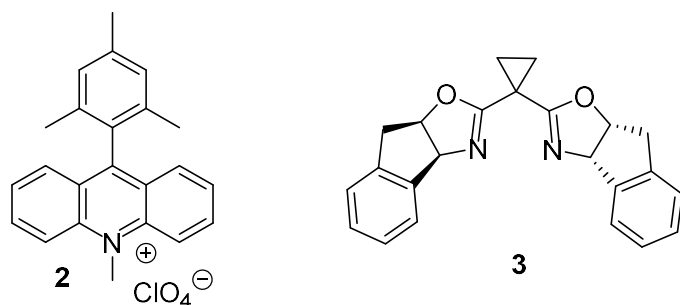


Figure 5 Photoredox allylation of aldehydes reported by Kanai.

The reaction was performed in the presence of an electron donor acridium salt **2** as photocatalyst, $\text{Mg}(\text{ClO}_4)_2$ as an additive and a complex formed between CrCl_2 and the chiral indane-BOX derivative **3**. The reaction provided excellent results in the presence of substituted benzaldehydes (up to 20/1 dr, 99% ee) and aliphatic aldehydes. Cyclic and linear alkenes were tolerated and gave the corresponding allylic alcohol with excellent enantioselectivities (up to 88%).

A mechanistic hypothesis for the photoredox allylations of aldehydes, reported by both Glorius and Kanai, was proposed (Figure 6).

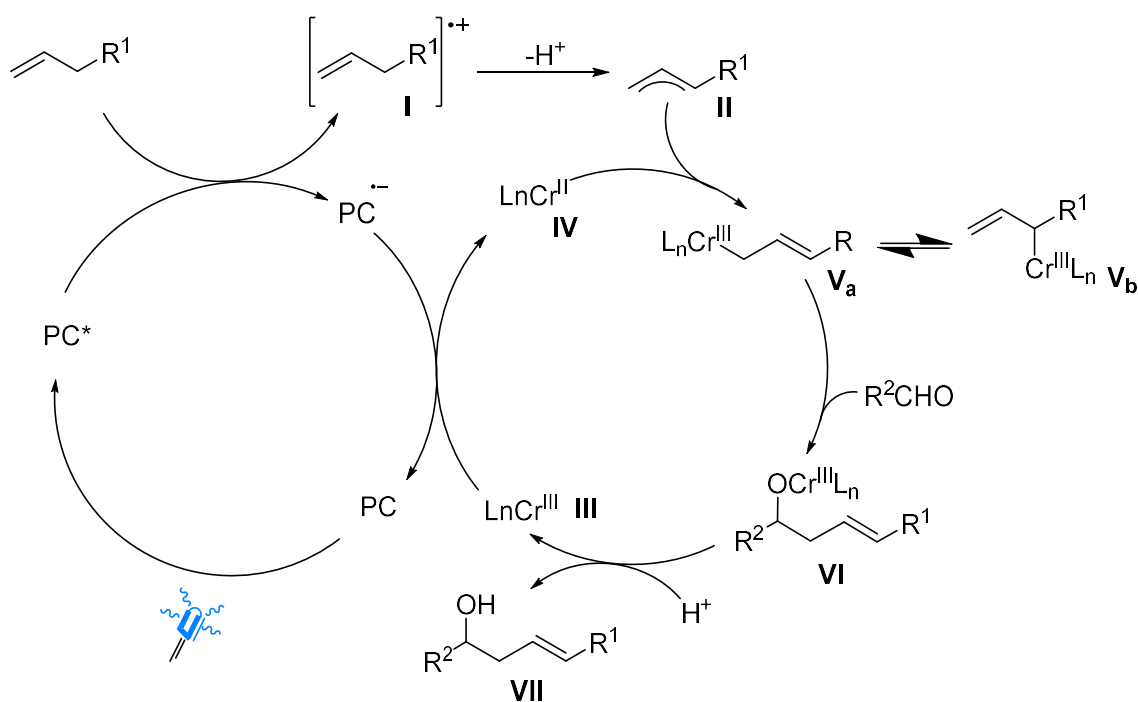


Figure 6 Proposed catalytic cycle for the photoredox allylation of aldehydes.

In both cases, the photocatalyst acts as an oxidant in its excited state [PC]*, forming the reduced photocatalyst PC^{•-} and the allylic radical **I** which undergoes a deprotonation to give the allyl radical **II**. Single electron transfer from PC^{•-} species and the chromium (III) **III** gives the low-valent L_nCr^{II} **IV** and the regeneration of the photocatalyst [PC]. Radical capture of allyl radical **II** by L_nCr^{II} **IV** forms the L_nCr^{III} allyl radical V_{a-b} which react with the aldehyde to give the alkoxide **VI**. The subsequent acidic hydrolysis furnished the allylic alcohol **VII**.

5.1.4 Allylation of aldehydes by dual photoredox nickel catalysis .

As we have stated in the introduction, the Ni(II) mediated allylation of aldehyde was described by the use of metal reductant such as Mn. In view of the discussion presented above, the group hypothesized the possibility to use photoredox catalysis for replacing the stoichiometric reductant for nickel. In our work hypotheses Ni(0), obtained by a photoredox cycle is able to interact with an alkene precursor giving the allylating reagent in situ. On the basis of such hypotheses, we started to investigate the development of a novel dual photoredox nickel catalysed allylation of aldehydes. In fact, the use of nickel metallaphotoredox catalysis avoids stoichiometric amounts of metals as reducing agent, that was previously reported by Durandetti and Périchon, and represents an alternative to the employment of expensive and reactive chromium(II) complexes as reported by Glorius and Kanai. In this chapter, the employment of a combination of Ni(II) complex and [Ir(ppy)₂(dtbbpy)](PF₆) or [Ru(bpy)₃]²⁺, in the presence of inexpensive reagents, for the allylation of aldehydes will be discussed.

5.2 Results and Discussions

5.2.1 Initial investigations

Initial studies were performed, using 2-naphthaldehyde as the substrate, common [NiCl₂(glyme)] as the Ni(II) source and commercially available 4,4'-di-tert-butyl-2,2'-dipyridyl (dtbbpy) as the ligand. The photocatalyst [Ir(ppy)₂(dtbbpy)](PF₆) was chosen for its high reduction ability (E_{1/2}^{red} = -1.69 V vs Fc) . Reactions were performed in degassed DMF under Blue LEDs irradiation and over 16 hours (Figure 7).

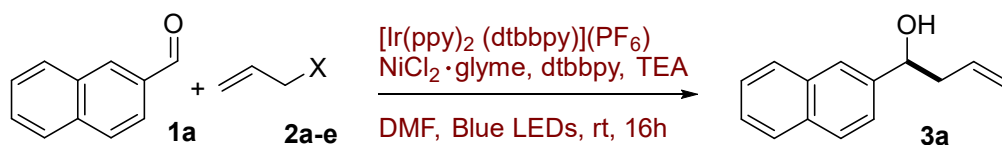


Figure 7 Allylation of 2-naphthaldehyde by a dual nickel-photoredox catalysis.

Various common allylating agents including allyl halogenates (Entries 1-3), alcohol (Entry 4) and acetate (Entry 5) were tested (Table 1).

Entry ^[a]	X	Conversion ^[b]
1	Cl	0
2	Br	0
3	I	0
4	OH	0
5	OAc	36

Table 1 Screening of the most common allylating agents for the allylation of 2-naphthaldehyde. The conversions were determined by ¹H-NMR analysis.

Allyl halogenates **2a**, **2b** and **2c** (Entries 1-3) resulted unreactive as well as allyl alcohol **2d** (Entry 4). To our delight, allyl acetate **2e** (Entry 4) provided the corresponding homoallylic alcohol product **3a** in a 36% of conversion and was therefore used as the allylating reagent of choice in the optimization of the protocol.

5.2.2 Reaction optimization

The reaction optimization implied the screening of several parameters including ligands, Ni(II) source, photocatalyst, reducing agents, solvents and reaction times. 2-naphthaldehyde was used as the model substrate.

Several ligands were screened including pyridine (Entry 1-2), bipyridine (Entry 3-4) and phenantroline derivatives (Entry 5-8) and ethylenebis(diphenylphosphine) (dppe) (Entry 10) (Table 2).

Entry ^[a]	Ligand	Conversion ^[b]
1	pyridine ^[c]	0
2	terpyridine	17
3	dtbbpy	36
4	4,4'-dimethoxy-2,2'-bipyridine	35
5	<i>o</i> -phenantroline	46
6	4,7-diphenyl-1,10-phenanthroline	37
7	5,6-dimethyl-1,10-phenanthroline	36
8	neocuproine	20
9	dppe	22
10	No ligand	21

Table 2 Screening of ligands for Ni(II). The conversions were determined by ¹H-NMR analysis.

Pyridine (Entry 1) and terpyridine (Entry 2) gave, a 0% and 17% of conversion respectively, presumably they prevent the formation of the allylnickel complex in the catalytic cycle (see further below for a more detailed explanation in section 5.2.4).

The bipyridine- (Entry 3-4) as well as the phenantroline derivatives (Entry 5-8) provided moderate conversions. In particular, *o*-phenantroline (Entry 5) afforded the homoallylic alcohol product **3a** in a 46% of conversion. The employment of a diphosphine-type ligand such as dppe (Entry 9) did not lead to a relevant improvement with respect to the absence of ligand (Entry 10).

Further screening of solvents, Ni(II) source, photocatalysts and reducing agents was performed using *o*-phenantroline as the ligand. The highlights of this optimization are reported here below (Table 3) (for more detailed information see section 5.4.2).

Entry ^[a]	Solvent	Ni(II) Source	Reducing agent	Photocatalyst source	Time Reaction (h)	Conversion ^{b]}
1	CH ₃ CN	[NiCl ₂ (glyme)]	TEA	[Ir(ppy) ₂ (dtbbpy)](PF ₆)	16	48
2	DMF/H ₂ O	[NiCl ₂ (glyme)]	TEA	[Ir(ppy) ₂ (dtbbpy)](PF ₆)	16	46
3	CH ₃ CN	[NiBr₂(glyme)]	TEA	[Ir(ppy) ₂ (dtbbpy)](PF ₆)	16	56
4	CH ₃ CN	[NiBr ₂ (glyme)]	DIPEA	[Ir(ppy) ₂ (dtbbpy)](PF ₆)	16	65
5	CH ₃ CN	[NiBr ₂ (glyme)]	DIPEA (4 equivalents)	[Ir(ppy) ₂ (dtbbpy)](PF ₆)	16	60
6	CH ₃ CN	[NiBr ₂ (glyme)]	DIPEA (2 equivalents)	[Ir(ppy) ₂ (dtbbpy)](PF ₆)	16	35
7	CH ₃ CN	[NiBr ₂ (glyme)]	DIPEA	[Ru(bpy)₃]Cl₂	16	68
8	CH ₃ CN	[NiBr ₂ (glyme)]	DIPEA	[Ru(bpy) ₃]Cl ₂	48	94 (75%)

Table 3 Highlights of several reaction parameters. The conversions were determined by ¹H-NMR analysis.

Acetonitrile (Entry 1) provided a 48% of conversion as reaction solvent and its use was preferred to DMF (table 2 entry 5). Interestingly, the reaction is not water sensitive as demonstrating by entry 2. The best performing Ni(II) source was [NiBr₂(glyme)] (Entry 3) in comparison to Ni(II) salts including halide or perchlorate as well as Ni(II) complexes such as Ni(acac)₂ and Ni(COD)₂ (see table 7). The hindered base DIPEA (Entry 4) proved the best reducing agent (see table 8). Different amount of the reducing agent, (Entry 5-6) affected the efficiency of the reaction. The employment of [Ru(bpy)₃]Cl₂ as photocatalyst (Entry 7) gave a conversion of 68% similar to [Ir(dF(CF₃)ppy)₂(bpy)](PF₆) and it was preferred due to the lower cost. Other photocatalysts including {Ir[dF(CF₃)ppy]₂(dtbbpy)}(PF₆) and Cu(dap)₂Cl proved unsuccessful (see table 9). Finally, the best reaction conditions were obtained performing the reaction over 48 hours (Entry 8), the final homoallylic alcohol product **3a** was obtained in a conversion of 94% and it was successfully isolated in a 75% yield.

Furthermore, the addition of protonating agents such as trifluoroethanol and 2,4,6 trimethylpyridinium salt to favour the formation of the homoallylic product **3a** from the homoallylic O-nickel complex (see section 5.2.3 for more details) proved unsuccessful.

The reaction conditions reported in entry 8 were employed in the screening of both aromatic and aliphatic aldehydes as well as ketones.

5.2.3 Substrates scope

Aldehydes substrate scope was investigated on a 0.2 mmol scale. First, a large variety of aromatic aldehydes were screened (Figure 8).

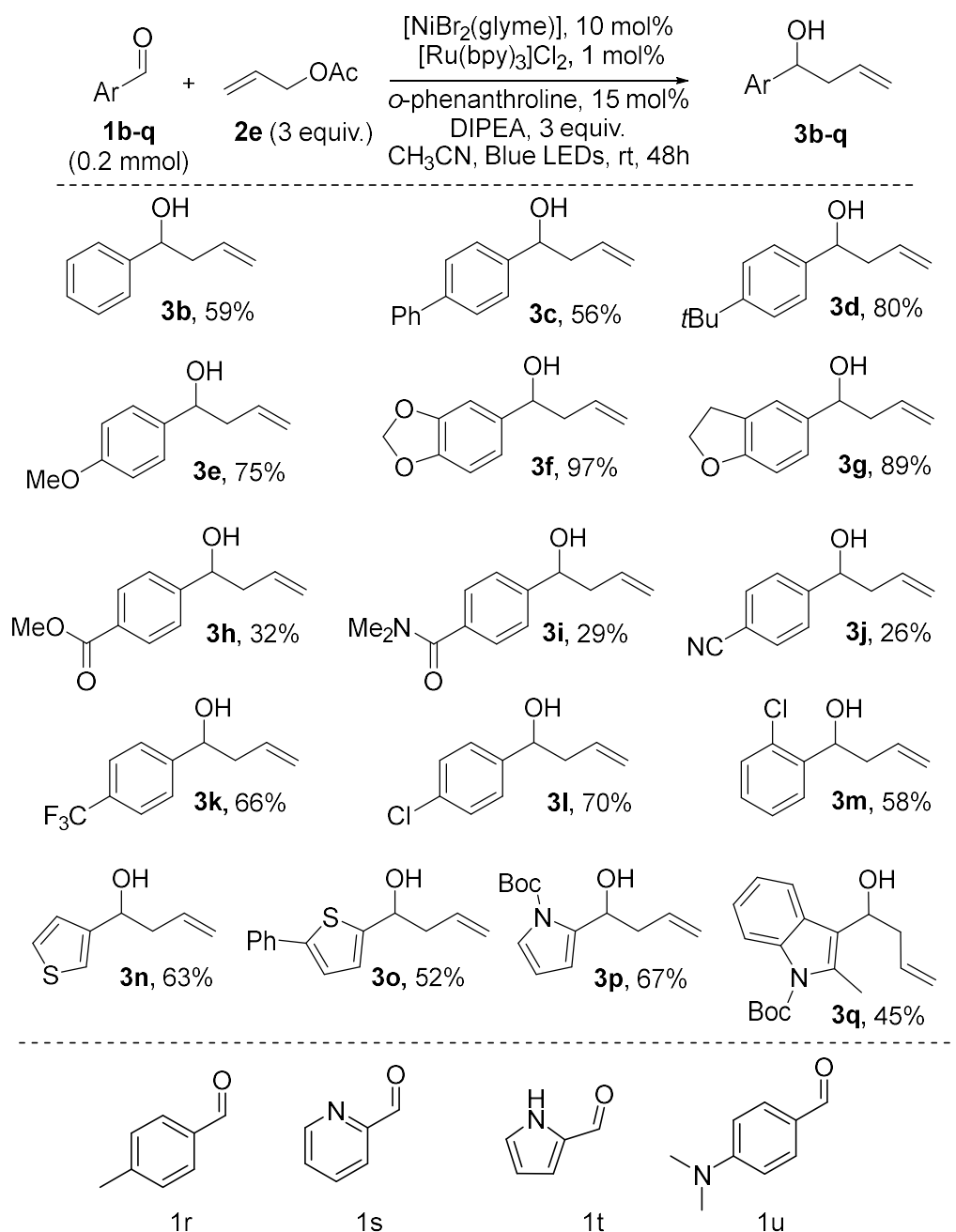


Figure 8 Substrates scope of several aromatic aldehydes. Yields after chromatographic purification.

In general, substituted aromatic and heteroaromatic aldehydes are suitable substrates for the reaction. Functional groups were well tolerated, including ethers, esters, amide, nitriles, trifluoromethyl and halides. Benzaldehyde **1b** provided a yield of 59%. The introduction of weakly donating group such as *t*-butyl (**3d**) gave an 80% of yield. Good to excellent yields were obtained in the presence of electron rich substrates such as the alkoxy derivatives **2e**, **2f** and **2g**. In particular, piperonal **1f** provided the corresponding homoallylic alcohol product **3f** in an isolated yield of 97%. Disappointingly, substrates bearing various electron-withdrawing groups, including esters, amides and nitriles proved more difficult and the corresponding products were isolated only in moderate

yield. Also, 4-trifluoromethyl (**3k**) and 4-chloro (**3l**) benzylic alcohol derivatives were isolated in 66% and 70% of yield, respectively. Several heteroaromatic compounds including thienyl (**1n** and **1o**), pyrrolyl (**1p**) and indolyl (**1q**) derivatives also gave good yields. Unfortunately, the pyridine- (**1s**) and pyrrole (**1t**) derivatives resulted unreactive. Interestingly, pyrrole-2-carboxaldehyde proved reactive only in the presence of *tert*-butyloxycarbonyl (BOC) as protecting group. Alkylamino groups were not tolerated, as in the case of the aldehyde **1u**.

The developed method (entry 8 table 3) was successfully applied to various aromatic aldehydes showing a high tolerance to several functional groups.

In view of these excellent results obtained, the evaluation of linear and unsaturated aliphatic aldehydes was performed (Figure 9).

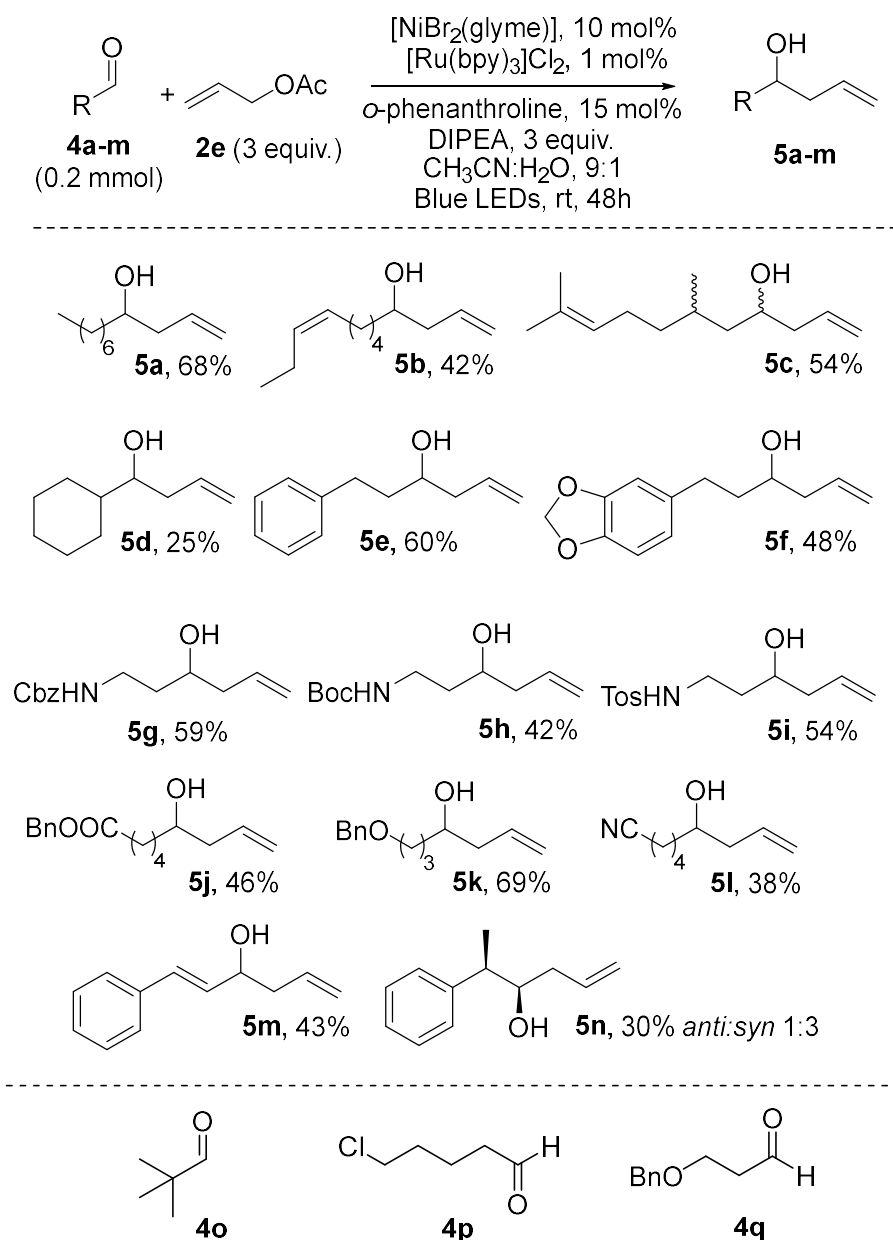


Figure 9 Substrates scope of several aliphatic aldehydes. Yields after chromatographic purification.

The performed attempts required the use of DMF-H₂O 9/1 as solvent mixture due to the formation of by-products derived from aldol condensation. The presence of water avoids the formation of reactive enamines, generated by the secondary amine formed from the oxidative decomposition of DIPEA, which subsequently give self-condensation with aliphatic aldehydes. Alkyl aldehydes (**4a-d**) gave yields from poor to moderate. The most encumbered cyclohexane derivative (**4d**) and pivalaldehyde (**4o**) showed a reduced reactivity giving the corresponding product with a 25% and 0% of yield, respectively. Phenylpropanol derivatives (**5e** and **5f**) were obtained in a 60% and 58% of yield, respectively. The presence of nitrogen protective groups including carbamate (**5g**), BOC (**5g**) and tosylate (**5i**) is well tolerated. Functional groups such as ester (**5j**) and nitrile (**5k**) provided moderate yields while chlorine (**4p**) was unreactive. In the case of benzyloxy substituent, the distance from the carbonyl group is crucial for the reaction efficiency: the butyraldehyde derivative **4l** provided a 69% of yield while the 3(-Benzyloxy)propionaldehyde (**4q**) proved unreactive. The styryl aldehyde **4m** was also successfully tested giving a yield of 43%. Finally, reaction with chiral aldehyde **4n** provided a 30% yield and a quite moderate diastereomeric ratio (*anti:syn* 1:3), in favor of a Felkin-controlled allylation.

5.2.4 Use of different allylating agents

To further demonstrate the applicability of the method, the reaction was also performed in the presence of mono- and di- substituted allyl acetates and propargyl acetate.

Allylation of 2-naphthaldehyde and tetrahydro-cinnamaldehyde with allyl acetates bearing substituents in position 1 and 3 was attempted. Commercially available cinnamyl acetate **2f**, 2-hexenyl acetate **2g**, 1,3-diphenylallyl acetate **2h** were evaluated as allylating source. Furthermore, an intramolecular allylation of the readily synthesized 2-[(1*E*)-3-(acetyloxy)-1-propen-1-yl]-benzaldehyde **2i** was investigated (Figure 10).

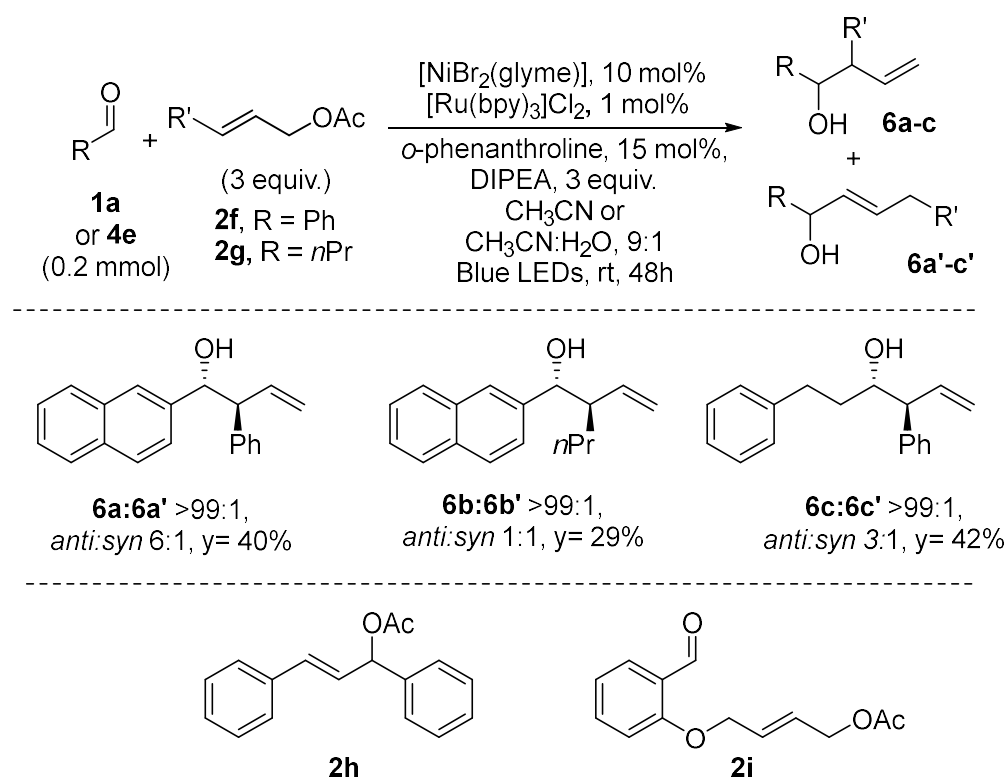


Figure 10 Allylation of aldehydes with substituted allyl acetates in the dual photoredox catalytic reaction. Yields after chromatographic purification.

The use of 3-substituted allyl acetate gave the possibility to obtain the regioisomers **6a-c** and **6a'-c'** as final product. The performed attempts provided the corresponding homoallylic alcohol **6a**, **6b** and **6c**, as racemic mixture, in an excellent regioselectivity (**6:6'** >99:1) but just moderate results in terms of yield and diastereoisomeric ratio. The disubstituted 1,3-diphenylallyl acetate **2h** was unreactive for steric hindrance. Furthermore, the use of 2-[(1E)-3-(acetyloxy)-1-propen-1-yl]-benzaldehyde **2i** with the purpose to promote an intramolecular allylation gave a zero conversion presumably because of the ring tension involved in the cyclization process.

The protocol was also extended to the propargylation of 2-naphthaldehyde using propargyl acetate **2d** (Figure 11).

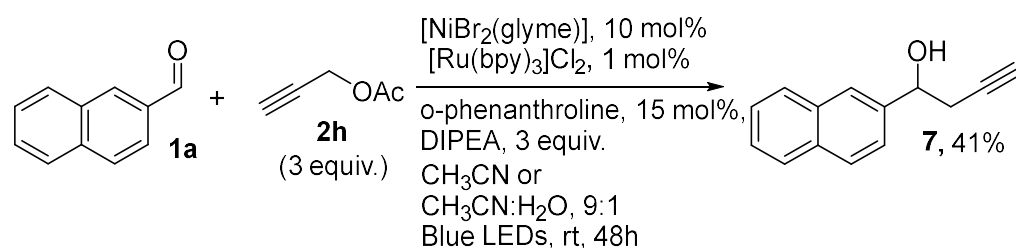


Figure 11 Propargylation of the 2-naphthaldehyde **1a**. Yield after chromatographic purification.

The propargyl alcohol derivative **7** was successfully isolated in 41% of yield and it demonstrated the versatility of the developed protocol. Further investigations were not performed.

Finally, the reactivity of aromatic and aliphatic ketones was investigated.

5.2.5 Photoredox allylation of ketones

Using the optimized conditions, the allylation of ketones was attempted (Figure 12).

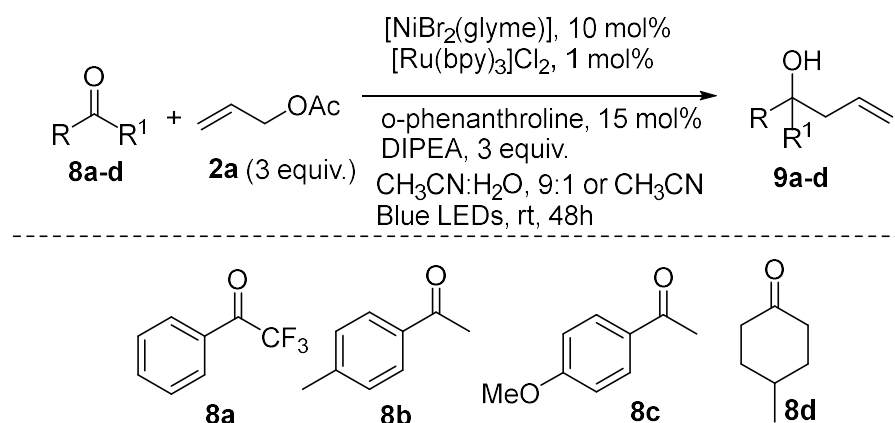


Figure 12 Allylation of ketones.

A low reactivity of ketones, as electrophilic substrates for addition process, was observed. Among the aromatic (**8a-c**) and aliphatic ketones (**8d**) tested, only trifluoroacetophenone **8a** gave the corresponding homoallylic alcohol product in trace amounts probably due to the presence of an electron withdrawing group in α position, which weakly enhances the electrophilicity of the CO group.

The allylation of 2-naphthaldehyde **1a** in the presence of the ketone acetoanisole **8c** in the reaction mixture was performed. Only the homoallylic alcohol product **3a** was detected demonstrating the high tolerance of the reaction to ketones (Figure 13).

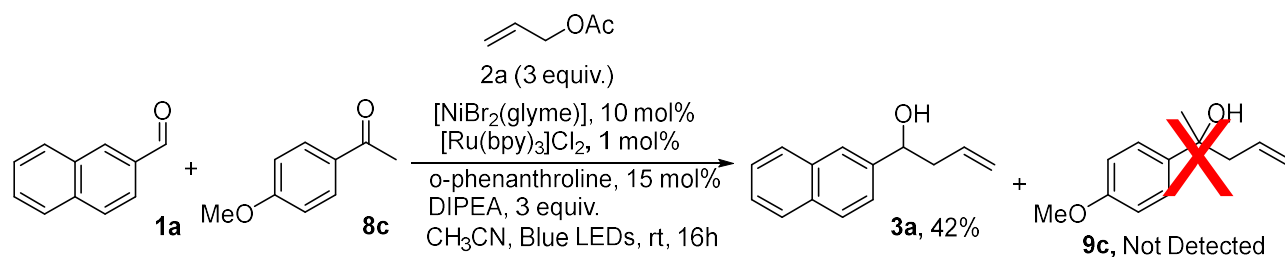


Figure 13 Reaction of aldehyde **1a** in the presence of acetoanisole **8c**. Yield after chromatographic purification.

In the end of the substrate scope, the allylation by dual nickel photoredox catalysis was successfully apply to aromatic and aliphatic aldehydes showing good tolerance to several functional groups. Furthermore, an example of propargylation of the 2-naphtaldehyde, using the developed method, was demonstrated. On the other hand, ketones proved unreactive.

Mechanistic studies about the allylation of aldehydes by dual photoredox and nickel catalysis were carried out.

5.2.6 Mechanistic investigations

In collaboration Prof. P.Ceroni and co-workers from University of Bologna, photochemical studies about the behaviour of the photocatalyst $[\text{Ru}(\text{bpy})_3]\text{Cl}_2$ during the reactions were performed. Absorption spectra of the solvent mixture before (in red) and upon (in blue) 24 hours of Blue LEDs irradiation showed the excellent stability of $[\text{Ru}(\text{bpy})_3]\text{Cl}_2$ during the reaction (Figure 14).

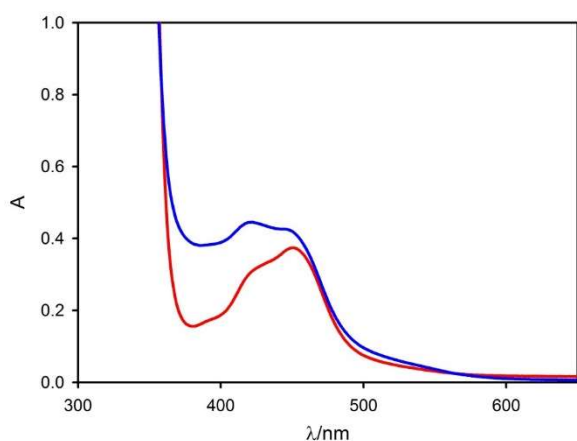


Figure 14 Absorption spectrum of the reaction mixture under standard conditions diluted 1:100 before (red solid line) and upon 24 hours irradiation with blue LEDs (blue solid line).

Experiments to get insights into the mechanism of this reaction were performed by analysis of the quenching of the photocatalyst's luminescence by each of the components of the reaction.

The emission intensity decay of $[\text{Ru}(\text{bpy})_3]\text{Cl}_2$ did change upon the addition of allyl acetate 0.6 M, *o*-phenantroline 0.03 M and tetrahydro-cinnamaldehyde 0.2 M (same concentration used to perform the reaction). Those reagents do not quench the emission of the $[\text{Ru}(\text{bpy})_3]\text{Cl}_2$ (Figure 15).

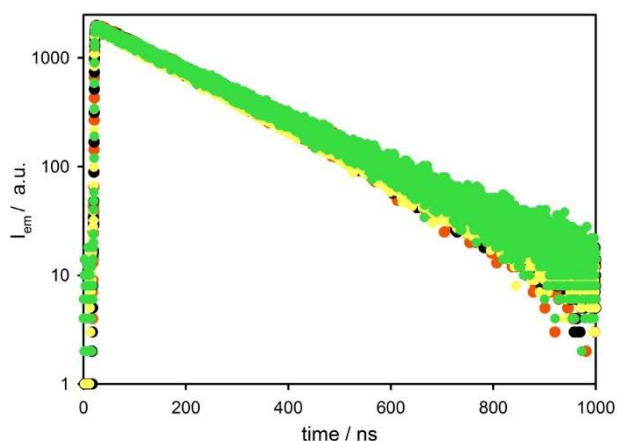


Figure 15 Emission intensity decays of $[\text{Ru}(\text{bpy})_3]\text{Cl}_2$ (4×10^{-5} M) in acetonitrile solution in absence (orange dots) and in presence of allyl acetate 0.6 M (black dots), *o*-phenanthroline 0.03 M (yellow dots) and hydrocinnamaldehyde 0.2 M (green dots), upon excitation at 405 nm.

Instead, DIPEA and $[\text{NiBr}_2(\text{glyme})]$ were able to quench the emission of the metal complex, with different quenching constant.

The analysis of the Stern-Volmer plots (see Figure 19-20 in section 5.4.5) yielded the following quenching constants:

- (1) $k_q = 7.7 \times 10^6 \text{ M}^{-1}\text{s}^{-1}$ for DIPEA
- (2) $k_q = 4.7 \times 10^9 \text{ M}^{-1}\text{s}^{-1}$ for $[\text{NiBr}_2(\text{glyme})]$

Indeed, upon the addition of an excess of the ligand *o*-phenanthroline, the $[\text{NiBr}_2(\text{glyme})]$ was not a quencher anymore for $[\text{Ru}(\text{bpy})_3]\text{Cl}_2$ emission. The concentration of $[\text{NiBr}_2(\text{glyme})]$ was 10 times diluted compare to the concentration used to perform the reaction (Figure 16).

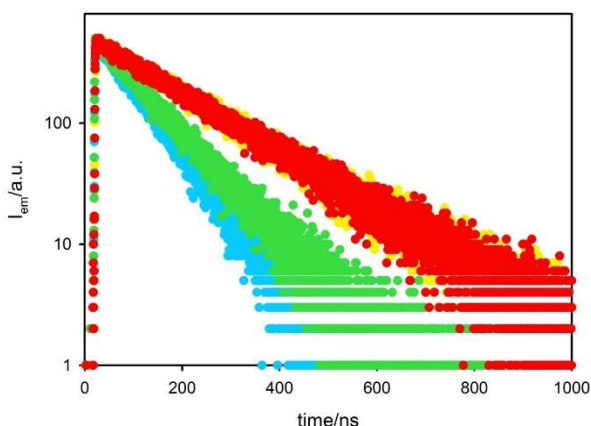


Figure 16 Emission intensity decays of $[\text{Ru}(\text{bpy})_3]\text{Cl}_2$ (4×10^{-5} M) in air-equilibrated acetonitrile solution (yellow dots) and upon addition of (i) $[\text{NiBr}_2(\text{glyme})]$ 0.02 M (light-blue dots), (ii) $[\text{NiBr}_2(\text{glyme})]$ 0.02 M and *o*-phenanthroline 0.03 M (green dots), (iii) $[\text{NiBr}_2(\text{glyme})]$ 0.02 M and *o*-phenanthroline 0.1 M (red dots). Excitation at 405 nm.

The importance of each of components was evaluated by several tests (Table 4).

Entry	Deviation from standard conditions	Conversion (Yields) ^b
1	No DIPEA	0
2	No nickel	0
3	No light	0
4	No degassed solvent	0

Table 4 Variation of some reaction parameters.

As expected, the absence of the reducing agent (Entry 1), Ni(II) source (Entry 2), Blue LEDs irradiation (Entry 3) and the use of no degassed solvent (Entry 4) in the reaction gave a zero conversion. In particular, as demonstrated by entry 4, the reaction was sensitive to traces of oxygen, due to the use of Ir(III) and Ru(II) polypyridine complexes, characterized by long lifetime of the lowest excited state, but degassing the reaction mixture by freeze-pump-thaw cycles was sufficient for a good reaction outcome.

It was worth noting that [NiBr₂(glyme)] is a pre-catalyst and in the presence of the *o*-phenanthroline ligand, different Ni(II) complexes are formed in which bromide and glyme ligands are replaced by one, two or three *o*-phenanthrolines (Figure 17).²⁵

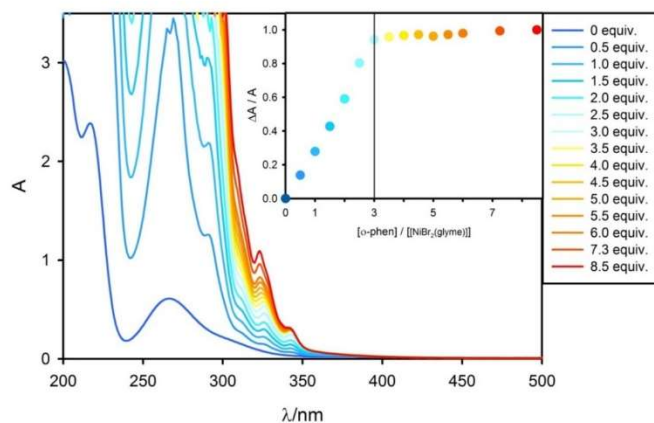


Figure 17 Absorption spectrum (blue solid line) of [NiBr₂(glyme)] 2×10^{-4} M in CH₃CN upon addition of *o*-phenanthroline up to 8.5 equivalents (red solid line). Inset shows normalized absorption changes at 344 nm as function of *o*-phenanthroline equivalents added. The stoichiometry of the system results in 1:3 [NiBr₂(glyme)]: *o*-phenanthroline.

The catalytic nickel-mediated allylation reactions reported in the literature²⁶ suggested the presence of a Ni(II)/Ni(0) cycle. In the cross coupling reaction of aromatic substrates, performed with allylic acetates in the presence of Zn(0) or Mn(0) as stoichiometric reductants, However, a careful

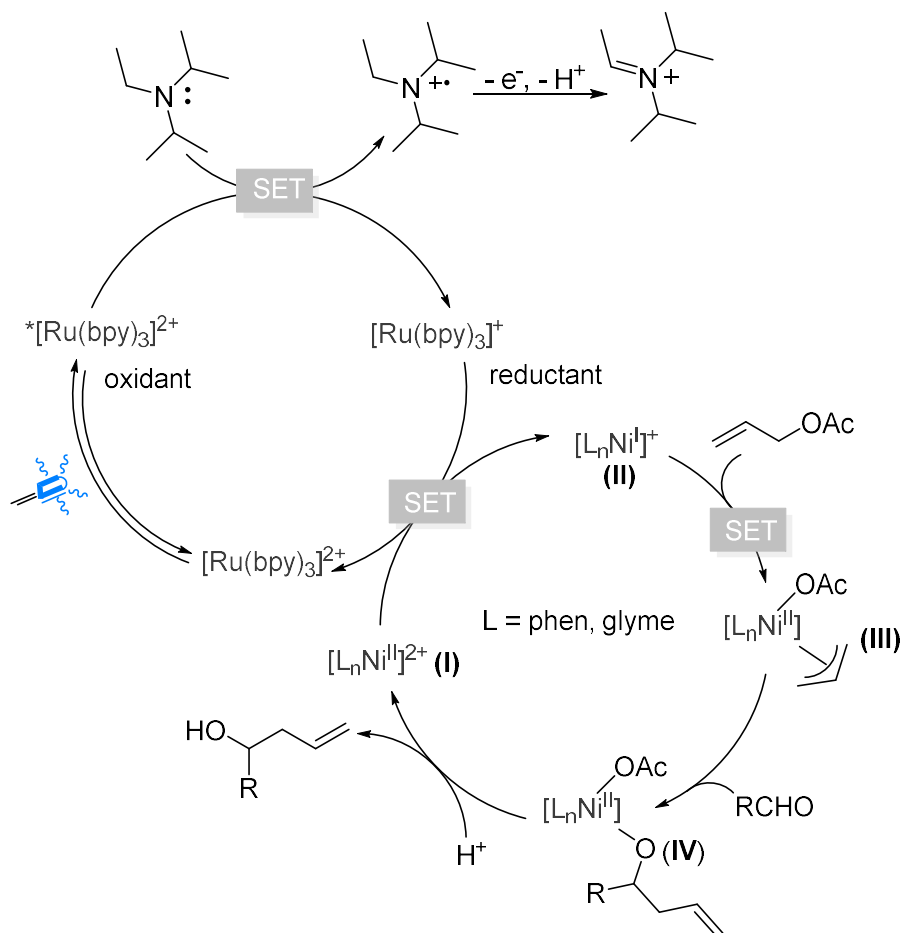


Figure 19 Suggested mechanism for the allylation reaction with the allylacetates.

The dual catalytic cycle is initiated by the well-known reductive quenching of the $[\text{Ru}(\text{bpy})_3]^{2+}$ photocatalyst by DIPEA,²⁹ producing the reduced $[\text{Ru}(\text{bpy})_3]^+$ complex ($E_{1/2} = -1.33 \text{ V vs. SCE}$).³⁰ The photogenerated $[\text{Ru}(\text{bpy})_3]^+$ complex is able to reduce not only $[\text{L}_n\text{Ni}^{\text{II}}]^{2+}$ (I) to $[\text{L}_n\text{Ni}^{\text{I}}]^+$ (II), but also the nickel complex intermediate containing the allyl ligand to generate the catalytically active species $[\text{L}_n\text{Ni}^{\text{II}}(\eta^3\text{-allyl})(\text{OAc})]$ ³¹ (III). The homoallylic alcohol is presumably formed by protonation of the homoallylic η^1 -nickel complex (IV), or by reductive elimination of the formed Ni hydride, due to the presence of protons released by the decomposition of oxidized DIPEA.

5.3 Conclusions

In conclusion, we developed a novel photoredox nickel catalysed allylation of aldehydes, by the *in situ* formation of an η^3 -allylnickel complex, using an inexpensive tertiary amine as a sacrificial reductant, and avoiding the use of metals such as magnesium, zinc, or manganese. The reaction shows a broad substrate scope for both aromatic and aliphatic aldehydes and good functional groups

tolerance. Further studies on the preparation of organometallic reagents by photoredox dual approaches and on the improvement of the enantioselective variant will be investigated.

5.4 Experimental procedures

5.4.1 General methods and materials

¹H-NMR spectra were recorded on Varian Mercury 400 spectrometer. Chemical shifts are reported in ppm from TMS with the solvent resonance as the internal standard (CDCl₃: δ = 7.27 ppm). Data are reported as follows: chemical shift, multiplicity (s = singlet, d = doublet, t = triplet, q = quartet, dd = double doublet, dt = double triplet, bs = broad signal, m = multiplet), coupling constants (Hz). ¹³C-NMR spectra were recorded on Varian MR400 spectrometer. Chemical shifts are reported in ppm from TMS with the solvent as the internal standard (CDCl₃: δ = 77.0 ppm). GC-MS spectra were taken by EI ionization at 70 eV on a Hewlett-Packard 5971 with GC injection. LC-electrospray ionization mass spectra (ESI-MS) were obtained with Agilent Technologies MSD1100 single-quadrupole mass spectrometer. Chromatographic purification was done with 240-400 mesh silica gel. All reactions were set up under an argon atmosphere in oven-dried glassware using standard Schlenk techniques.

Anhydrous solvents were supplied by Aldrich in Sureseal® bottles and were used without further purification. All the reagents were purchased from Aldrich and used without further purification unless specified. Triethylamine and DIPEA were stirred one day over KOH and distilled before their use.

Aldehydes **1p**,^[32] **1q**,^[33] **1o**,^[34] **3f**,^[35] cinnamyl acetate **2b**,^[36] allyl pivalate,^[37] *tert*-butyl allyl carbonate,^[38] 3-hexen-2-yl acetate **2c**^[39] (*E*)-1,3-diphenyl-3-acetoxy-prop-1-ene^[40] and (*Z*)-1,4-bis(acetyloxy)but-2-ene^[41] were prepared according to the procedure reported in literature.

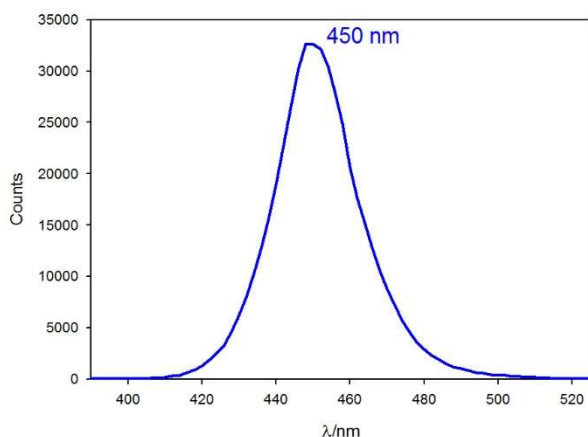
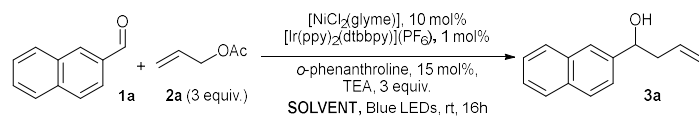


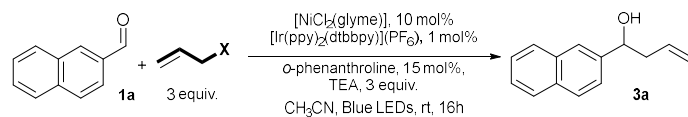
Figure 20 Emission profile of the 16W Blue LED strip used to irradiate the solutions.

5.4.2 Screening of reaction conditions



Entry ^[a]	Solvent	Yield ^[b]
1	DMF	46
2	CH ₃ CN	48
3	DCE	29
4	THF	39
5	DMSO	35
6	DME	27
7	MeOH	14
8	Dioxane	25
9	DMF/H ₂ O 9/1	46

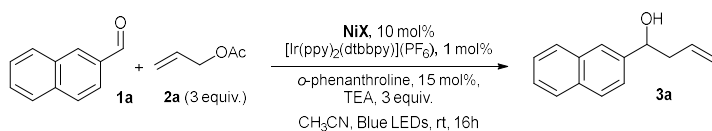
Table 5 Screening of reaction solvent. [a] Reaction conditions reported in the above figure on 0.1 mmol scale. [b] Determined by ¹H-NMR analysis.



Entry ^[a]	X	Yield ^[b]
1	OC(O) <i>t</i> Bu	40
2	OC(O) <i>t</i> Bu	42
3	OH	8
4	OPh	11

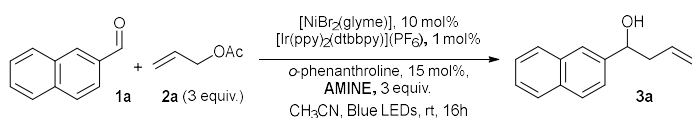
Table 6 Screening of allylating agent. [a] Reaction conditions reported in the above figure on 0.1 mmol scale. [b] Determined by ¹H-NMR analysis.

Chapter 5: Allylation of aldehydes by dual photoredox and nickel catalysis



Entry ^[a]	Nickel source	Yield ^[b]
1	[NiCl ₂ (glyme)]	48
2	Ni(ClO ₄) ₂	32
3	NiBr ₂	36
4	NiI ₂	47
5	Ni(COD) ₂	35
6	[Ni(<i>o</i> -phenanthroline) ₃](BF ₄) ₂ ^[c]	45
7	Ni(acac) ₂	35
8	[NiBr ₂ (glyme)]	56

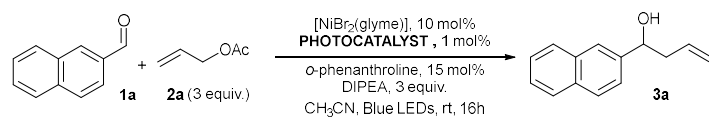
Table 7 Screening of nickel source. [a] Reaction conditions reported in the above figure on 0.1 mmol scale. [b] Determined by ¹H-NMR analysis. [c] No *o*-phenanthroline was added.



Entry ^[a]	Reducing agent	Yield ^[b]
1	-	0
2	TEA	56
3	Ph ₃ N	0
4	DIPEA	65
5	DIPEA ^[c]	60
6	DIPEA ^[d]	35

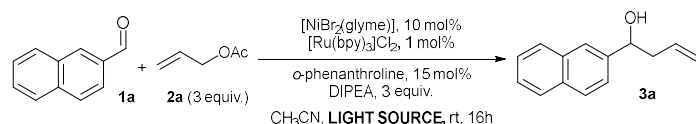
Table 8 Screening of reducing agent. [a] Reaction conditions reported in the above figure on 0.1 mmol scale. [b] Determined by ¹H-NMR analysis. [c] 4 equiv. of DIPEA were used. [d] 2 equiv of DIPEA were used.

Chapter 5: Allylation of aldehydes by dual photoredox and nickel catalysis



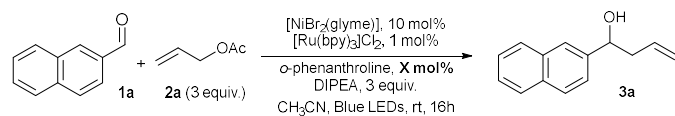
Entry ^[a]	Photocatalyst	Yield ^[b]
1	-	0
2	[Ir(ppy) ₂ (dtbbpy)](PF ₆)	65
3	{Ir[dF(CF ₃)ppy] ₂ (dtbbpy)}(PF ₆)	31
4	Cu(dap) ₂ Cl	0
5	[Ru(bpy) ₃]Cl ₂	68

Table 9 Screening of photocatalyst. [a] Reaction conditions reported in the above figure on 0.1 mmol scale. [b] Determined by ¹H-NMR analysis.



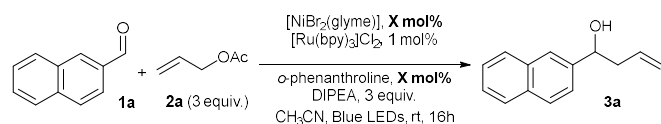
Entry ^[a]	Light source	Yield ^[b]
1	Blue LED 450 nm 16W	68
2	Single red LED 630 nm 2.7W	0

Table 10 Test with different light source. [a] Reaction conditions reported in the above figure on 0.1 mmol scale. [b] Determined by ¹H-NMR analysis.



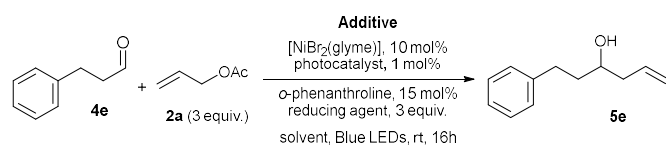
Entry ^[a]	mol% <i>o</i> -phenanthroline	Yield ^[b]
1	15	68
2	30	51
3	60	42

Table 11 Screening of ligand amount. [a] Reaction conditions reported in the above figure on 0.1 mmol scale. [b] Determined by ¹H-NMR analysis.



Entry ^[a]	mol% [NiBr ₂ (glyme)]	mol% <i>o</i> -phenanthroline	Yield ^[b]
1	10	15	68
2	1	1.5	47

Table 12 Screening of nickel/complex amount. [a] Reaction conditions reported in the above figure on 0.1 mmol scale. [b] Determined by ¹H-NMR analysis.

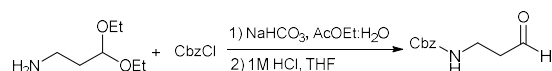


Entry ^[a]	Photocatalyst	Reducing agent	Solvent	Additive	Yield ^[b]
1	[Ru(bpy) ₃]Cl ₂	DIPEA	CH ₃ CN	-	45
2	[Ir(ppy) ₂ (dtbbpy)](PF ₆)	DIPEA	CH ₃ CN	-	56
3	[Ru(bpy) ₃]Cl ₂	DIPEA	CH ₃ CN/H ₂ O 10/1	-	60
4	[Ir(ppy) ₂ (dtbbpy)](PF ₆)	DIPEA	CH ₃ CN/H ₂ O 10/1	-	60
5	[Ru(bpy) ₃]Cl ₂	DIPEA	CH ₃ CN	H ₃ BO ₃ (30 mol%)	43
6	[Ru(bpy) ₃]Cl ₂	TEOA ^[c]	CH ₃ CN	-	25

Table 13 Screening of the conditions for aliphatic aldehydes. [a] Reaction conditions reported in the above figure on 0.2 mmol scale. [b] Determined by ¹H-NMR analysis after chromatographic purification. [c] Triethanol amine.

5.4.3 Synthesis and characterization of substrates

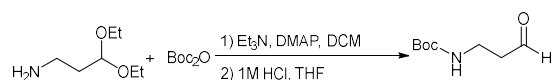
Synthesis of aldehyde 4g



To a solution of 3,3-diethoxy-1-aminopropane (250 μ L, 1.54 mmol) in AcOEt (3 mL) were added NaHCO₃ (650 mg, 7.7 mmol, 5 equiv.), water (3 mL) and benzyl chloroformate (331 μ L, 2.3 mmol, 1.5 equiv.). The resulting mixture was allowed to stir overnight at room temperature and checked by GC-MS and TLC (cHex/AcOEt 6/4) to complete conversion. After that, the layers were separated, and the aqueous phase was extracted with AcOEt (3 x 5 mL), dried over Na₂SO₄ and concentrated. The crude was dissolved in THF (0.5 mL), treated with 1M HCl (250 μ L, 12 mol%) at 0°C and stirred overnight at room temperature. After the reaction mixture was diluted with Et₂O (10 mL) and washed with a saturated solution of NaHCO₃ (5 mL), the combined organic phase was dried over Na₂SO₄ and concentrated to obtain a yellowish oil. The crude was further purified by flash column chromatography (cHex/AcOEt 7/3) to obtain **1q** as yellow solid, 51% yield (0.79 mmol, 164 mg). Spectroscopic data were according to the literature.^[42]

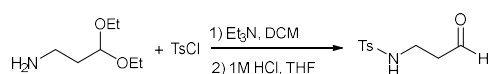
Chapter 5: Alkylation of aldehydes by dual photoredox and nickel catalysis

Synthesis of aldehyde 4h



To a solution of 3,3-diethoxy-1-aminopropane (250 μ L, 1.54 mmol) in DCM (3 mL) were added Et₃N (428 μ L, 3.1 mmol, 2 equiv.), 4-(dimethylamino)pyridine (2 mg, 0.016 mmol, 1.0 mol%) and a solution of di-*tert*-butyl dicarbonate (371 mg, 1.7 mmol, 1.1 equiv.) in DCM (1.5 mL) drop-wise at 0°C. The resulting mixture was allowed to stir overnight at room temperature and checked by GC-MS and TLC (cHex/AcOEt 6/4). After the mixture was quenched with H₂O (10 mL), the layers separated, and the aqueous phase was extracted with Et₂O (3 x 10 mL), the combined organic phase washed with Brine (10 mL), dried over Na₂SO₄ and concentrated. The crude was dissolved in THF (1 mL), treated with 1M HCl (550 μ L, 40 mol%) at 0°C and left stirring at room temperature and it was monitored by TLC (cHex/AcOEt 7/3). A saturated solution of NaHCO₃ was added, extracted with Et₂O (3 x 10 mL), the combined organic phase was dried over Na₂SO₄ and concentrated to obtain a yellowish oil. The crude was further purified by flash column chromatography (cHex/AcOEt 8/2) to obtain **51h** as yellowish oil, 31% yield (0.47 mmol, 82 mg). Spectroscopic data were according to the literature.

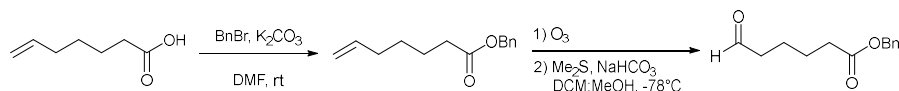
Synthesis of aldehyde 4i



To a solution of 3,3-diethoxy-1-aminopropane (300 μ L, 1.85 mmol) in DCM (8 mL) was added Et₃N (310 μ L, 2.22 mmol, 1.2 equiv.). The solution was cooled to 0°C and *p*-toluenesulfonyl chloride (389 mg, 2.04 mmol, 1.1 equiv.) was carefully added. The resulting mixture was allowed to stir overnight at room temperature and checked by TLC (cHex/AcOEt 6/4). The mixture was quenched with saturated aqueous NH₄Cl solution (10 mL), the layers separated, and the aqueous phase was extracted with DCM (3 x 10 mL), dried over Na₂SO₄, and concentrated to a brownish oil. Sulphonamide (255 mg, 0.85 mmol) was dissolved in THF (2 mL), treated with 1M HCl (850 μ L, 1 equiv.) and left stirring at room temperature for 2.5 hours. After that the reaction mixture was extracted with AcOEt (3 x 10 mL), the combined organic phases were washed with Brine (5 mL), dried over Na₂SO₄ and concentrated to obtain a brownish oil. The crude was further purified by flash column chromatography (cHex/AcOEt 8/2) as brown oil, 51% yield (0.44 mmol, 99 mg). Spectroscopic data were according to the literature.⁴³

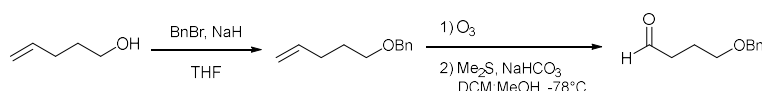
GC-MS of the product: rt 19.09, *m/z* = 227 (M⁺, 0.5), 199 ([M-CO]⁺, 14), 171 ([TsNH₂]⁺, 50), 155 (Ts⁺, 48), 91 (C₇H₇⁺, 100).

Synthesis of aldehyde 4j



To a solution of 6-heptenoic acid (400 μ L, 2.95 mmol) in dry DMF (9 mL), potassium carbonate (1.22 g, 8.8 mmol, 3 equiv.) and benzyl bromide (421 μ L, 3.54 mmol, 1.2 equiv.) were added sequentially. The mixture was left stirring at room temperature overnight and after the consumption of the starting material (monitored by TLC cHex/AcOEt 6/4), water was added (5 mL) and the aqueous phase extracted with AcOEt (1 x 5 mL) and DCM (2 x 10 mL), the combined organic phases were dried over Na₂SO₄ and concentrated to a yellow oil. The residue was dissolved in a mixture of DCM/MeOH 3/1 (15 mL), cooled to -78°C and ozone was bubbled until the mixture turned blue. Oxygen was then bubbled for few minutes, dimethyl sulfide (685 μ L, 9.3 mmol, 3.2 equiv.) and sodium bicarbonate (780 mg, 9.27 mmol, 3 equiv.) were added in sequence. The suspension was warmed to room temperature, left stirring overnight, then filtered on Celite® and the solvents removed under reduced pressure. The crude was purified by flash column chromatography (cHex/AcOEt 9/1) to obtain **51k** as colorless oil, 70% yield (2.1 mmol, 455 mg). Spectroscopic data were according to the literature.^[44]

Synthesis of aldehyde 4k

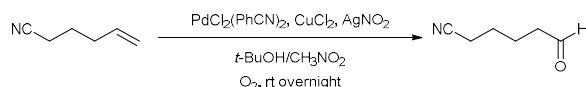


To a suspension of NaH (60% in mineral oil, 426 mg, 10.7 mmol, 1.1 equiv.) in dry THF (10 mL), 4-penten-1-ol (1 mL, 9.7 mmol) was slowly added at 0°C. The mixture was left stirring at room temperature for 2 hours. Benzyl bromide (1.27 mL, 10.6 mmol, 1.1 equiv.) was added at 0°C and the reaction mixture allowed to stir at room temperature overnight. After the consumption of the starting material, the mixture was quenched with H₂O (5 mL) and the aqueous phase extracted with Et₂O (3 x 10 mL). The combined organic phase dried over Na₂SO₄ and concentrated to obtain a yellow oil. The residue was dissolved in a mixture of DCM/MeOH 3/1 (40 mL), cooled down to -78°C and ozone was bubbled until the mixture turned blue. Oxygen was then bubbled for few minutes and dimethyl sulfide (2.3 mL, 31 mmol, 3.2 equiv.) and sodium bicarbonate (2.44 g, 30 mmol, 3 equiv.) added in sequence. The suspension was

Chapter 5: Allylation of aldehydes by dual photoredox and nickel catalysis

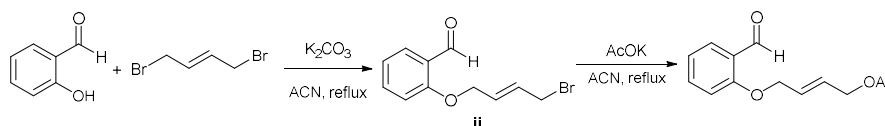
warmed to room temperature, left stirring overnight, then filtered on Celite® and the solvents removed under reduced pressure. The crude was purified by flash column chromatography (cHex/AcOEt 10/1) to obtain **1r** as colorless oil 68% yield (6.6 mmol, 1.2 g). Spectroscopic data were according to the literature.^[45]

Synthesis of aldehyde **4l**



A solution of bis(benzonitrile)palladium(II) chloride (25 mg, 0.06 mmol, 12 mol%), copper(II) chloride (4 mg, 0.03 mmol, 6 mol%) and silver nitrite (5 mg, 0.03 mmol, 6 mol%) in *tert*-butanol (9 mL) and nitromethane (1 mL) mixture was sparged with oxygen gas for few minutes and after that, 5-hexenenitrile (60 μL , 0.5 mmol) was added. The reaction mixture was left stirring overnight at room temperature under oxygen atmosphere. After complete consumption of the alkene, the mixture was diluted with H_2O (5 mL) and extracted with DCM (3 x 10 mL). The dark organic phase was filtered through Celite®, dried over Na_2SO_4 and concentrated to obtain a yellow oil. Purification by flash column chromatography (cHex/AcOEt 9/1) gave a mixture of the aldehyde and the ketone, as colorless oil, 44% yield (0.24 mmol, 35 mg pur. 74%). The purity of the aldehyde was calculated by integrating in the $^1\text{H-NMR}$ spectrum the signals of the CHO proton (9.77 ppm, s, 1H) and the methyl group of the ketone (2.16 ppm, s, 3H).^[46]

Synthesis of aldehyde for intramolecular reaction



To a solution of salicylaldehyde (250 μL , 2.35 mmol) in dry ACN (6 mL), K_2CO_3 (357 mg, 2.58 mmol, 1.1 equiv.) and (*E*)-1,4-dibromo-2-butene (554 mg, 2.58 mmol, 1.1 equiv.) were added. The mixture was stirred under reflux for 4 hours and was cooled to room temperature and filtered on Celite®. The filtrate was then concentrated under reduced pressure and the crude purified by flash column chromatography (cHex/AcOEt 9/1) to give the intermediate **ii** as a yellowish oil (49% yield, 1.16 mmol, 295 mg).^[47] To a suspension of potassium acetate (183 mg, 1.86 mmol, 1.6 equiv.), previously flamed under vacuum with a heating gun in dry ACN (5 mL), intermediate **ii** was added and the mixture was refluxed overnight. After the consumption of **ii** (monitored by TLC, cHex/AcOEt 8/2), the mixture was cooled to room temperature and filtered on Celite®. The filtrate was then concentrated under reduced pressure to give the desired product as yellowish oil in 44% yield (1.04 mmol, 245 mg).

$^1\text{H-NMR}$ (400 MHz, CDCl_3 , 25°C): δ = 10.51 (d, J = 0.7 Hz, 1H), 7.83 (dd, J = 7.7, 1.8 Hz, 1H), 7.52 (ddd, J = 8.4, 7.4, 1.8 Hz, 1H), 7.05 – 7.00 (m, 1H), 6.95 (d, J = 8.4 Hz, 1H), 6.00 – 5.97 (m, 2H), 4.66 – 4.61 (m, 4H), 2.07 (s, 3H); $^{13}\text{C-NMR}$ (100 MHz, CDCl_3 , 25°C): δ = 189.6, 170.6, 160.7, 135.8, 128.6, 128.2, 127.7, 121.0 (2C), 112.7, 68.0, 63.8, 20.8; GC-MS: rt 18.64; m/z = 234 (M^+ , 0.5), 174 ($[\text{M}-\text{AcOH}]^+$, 6), 121 ($\text{C}_7\text{H}_5\text{O}_2^+$, 46), 113 ($[\text{M}-\text{PhCHOO}]^+$, 100).

Synthesis of $[\text{Ni}(\text{phen})_3](\text{BF}_4)_2$ complex

The complex was prepared following the reported procedure^[48] using NaBF_4 instead of NaClO_4 .

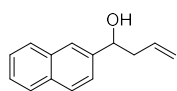
$\text{NiCl}_2 \cdot 6\text{H}_2\text{O}$ (0.2 mmol, 48 mg), *o*-phenanthroline (0.6 mmol, 108 mg) and NaBF_4 (0.4 mmol, 44 mg) were added to distilled water (10 mL). The solution was heated at 80 °C for 2 hours, the pink precipitate was filtered off and washed with distilled water (2 x 3 mL). The title compound was obtained as pink solid in 63% yield (0.13 mmol, 100 mg).

5.4.4 General procedure for photoredox nickel-catalyzed allylation of aldehydes and characterization of the products

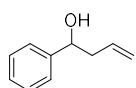
A dry 10 mL Schlenk tube, equipped with a Rotaflo stopcock, magnetic stirring bar and an argon supply tube, was first charged under argon with the ruthenium photocatalyst (1 mol%, 0.002 mmol, 1.0 mg), $[\text{NiBr}_2(\text{glyme})]$ catalyst (10 mol%, 0.02 mmol, 6 mg) and phenanthroline ligand (15 mol%, 0.03 mmol, 6 mg). Dry ACN (1 mL in order to obtain a 0.2 M substrate solution) was then added (the protocol was changed in the case of the aliphatic substrates, where 100 μL of H_2O were added to the solvent ACN) and the reaction mixture was further subjected to a freeze-pump-thaw procedure (three cycles) and the vessel refilled with argon. Then DIPEA (0.6 mmol, 3 equiv., 104 μL), allyl acetate **2a** (0.6 mmol, 3 equiv.) and the substrate **1** (0.2 mmol) were added. The reaction was irradiated with 16W blue LEDs and stirred from 48 h to 64h. After that the reaction mixture was quenched with aqueous HCl 1M (approx. 1 mL) and extracted with AcOEt (4 x 3 mL). The combined organic layers were dried over anhydrous Na_2SO_4 and the

Chapter 5: Allylation of aldehydes by dual photoredox and nickel catalysis

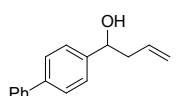
solvent was removed under reduced pressure. The crude was studied by $^1\text{H-NMR}$ spectroscopy and purified by flash column chromatography (SiO_2) to afford the products **3** in the stated yields.



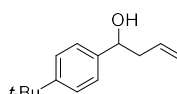
(3a): brown oil, 75% (0.15 mmol, 30 mg). The general procedure was applied using **1a** (0.2 mmol, 32 mg) and **2a** (0.6 mmol, 64 μL , 3 equiv.). The title compound was isolated by flash column chromatography (cyclohexane/ethyl acetate). $^1\text{H-NMR}$ (400 MHz, CDCl_3 , 25°C): δ = 7.85 – 7.78 (m, 4H), 7.51 – 7.42 (m, 3H), 5.88 – 5.77 (m, 1H), 5.21 – 5.12 (m, 2H), 4.89 (dd, J = 7.2, 5.9 Hz, 1H), 2.66 – 2.52 (m, 2H); $^{13}\text{C-NMR}$ (100 MHz, CDCl_3 , 25°C): δ = 141.2, 134.3, 133.2, 132.9, 128.2, 127.9, 127.6, 126.1, 125.8, 124.4, 124.0, 118.5, 73.3, 43.7; MS (ESI): m/z = 181.2 [M-OH] $^+$.



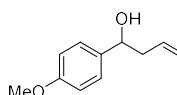
(3b): brown oil, 59% (0.12 mmol, 17 mg). The general procedure was applied using **1b** (0.2 mmol, 20.4 μL) and **2a** (0.6 mmol, 64 μL , 3 equiv.). The title compound was isolated by flash column chromatography (cyclohexane/ethyl acetate). $^1\text{H-NMR}$ (400 MHz, CDCl_3 , 25°C): δ = 7.36 – 7.12 (m, 5H), 5.86 – 5.74 (m, 1H), 5.18 – 5.11 (m, 2H), 4.72 (dd, J = 7.6, 5.4 Hz, 1H), 2.56 – 2.44 (m, 2H), 2.06 (br s, 1H); $^{13}\text{C-NMR}$ (100 MHz, CDCl_3 , 25°C): δ = 143.8, 134.4, 128.4 (2C), 127.5, 125.8 (2C), 118.4, 73.3, 43.8; MS (ESI): m/z = 131.2 [M-OH] $^+$.



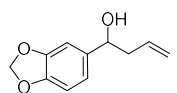
(3c): brown oil, 56% (0.11 mmol, 25 mg). The general procedure was applied using **1c** (0.2 mmol, 36 mg) and **2a** (0.6 mmol, 64 μL , 3 equiv.). The title compound was isolated by flash column chromatography (cyclohexane/ethyl acetate). $^1\text{H-NMR}$ (400 MHz, CDCl_3 , 25°C): δ = 7.60 – 7.56 (m, 4H), 7.45 – 7.41 (m, 4H), 7.36 – 7.30 (m, 1H), 5.89 – 5.79 (m, 1H), 5.22 – 5.15 (m, 2H), 4.78 (t, J = 5.4 Hz, 1H), 2.62 – 2.48 (m, 2H); $^{13}\text{C-NMR}$ (100 MHz, CDCl_3 , 25°C): δ = 142.9, 140.8, 140.5, 134.4, 128.7 (2C), 127.2, 127.1 (2C), 127.0 (2C), 126.2 (2C), 118.5, 73.02, 43.8; MS (ESI): m/z = 207.2 [M-OH] $^+$.



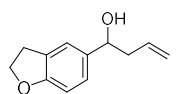
(3d): brown oil, 80% (0.16 mmol, 33 mg). The general procedure was applied using **1d** (0.2 mmol, 33 μL) and **2a** (0.6 mmol, 64 μL , 3 equiv.). The title compound was isolated by flash column chromatography (cyclohexane/ethyl acetate). $^1\text{H-NMR}$ (400 MHz, CDCl_3 , 25°C): δ = 7.37 (d, J = 8.3 Hz, 2H), 7.28 (d, J = 8.4 Hz, 2H), 5.82 (ddt, J = 17.1, 10.1, 7.1 Hz, 1H), 5.20 – 5.10 (m, 2H), 4.70 (t, J = 6.5 Hz, 1H), 2.57 – 2.44 (m, 2H), 1.32 (s, 9H); $^{13}\text{C-NMR}$ (100 MHz, CDCl_3 , 25°C): δ = 150.4, 140.9, 134.7, 125.5 (2C), 125.3 (2C), 118.1, 73.1, 43.6, 34.5, 31.3 (3C); MS (ESI): m/z = 187.2 [M-OH] $^+$.



(3e): brown oil, 73% (0.15 mmol, 26 mg). The general procedure was applied using **1e** (0.2 mmol, 24 μL) and **2a** (0.6 mmol, 64 μL , 3 equiv.). The title compound was isolated by flash column chromatography (cyclohexane/ethyl acetate). $^1\text{H-NMR}$ (400 MHz, CDCl_3 , 25°C): δ = 7.30 – 7.23 (m, 2H), 6.90 – 6.84 (m, 2H), 5.78 (ddt, J = 17.2, 10.2, 7.1 Hz, 1H), 5.17 – 5.08 (m, 2H), 4.67 (t, J = 6.5 Hz, 1H), 3.79 (s, 3H), 2.51 – 2.46 (m, 2H); $^{13}\text{C-NMR}$ (100 MHz, CDCl_3 , 25°C): δ = 159.0, 136.0, 134.6, 127.0 (2C), 118.2, 113.8 (2C), 73.0, 55.2, 43.7.



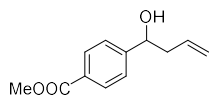
(3f): brown oil, 97% (0.19 mmol, 37 mg). The general procedure was applied using **1f** (0.2 mmol, 38 mg) and **2a** (0.6 mmol, 64 μL , 3 equiv.). The title compound was isolated by flash column chromatography (cyclohexane/ethyl acetate). $^1\text{H-NMR}$ (400 MHz, CDCl_3 , 25°C): δ = 6.85 (d, J = 1.5 Hz, 1H), 6.80 – 6.72 (m, 2H), 5.92 (s, 2H), 5.82 – 5.70 (m, 1H), 5.16 – 5.09 (m, 2H), 4.62 (t, J = 6.5 Hz, 1H), 2.48 – 2.42 (m, 2H); $^{13}\text{C-NMR}$ (100 MHz, CDCl_3 , 25°C): δ = 147.7, 146.8, 138.0, 134.4, 119.2, 118.3, 108.0, 106.4, 100.9, 73.2, 43.8; MS (ESI): m/z = 175.2 [M-OH] $^+$.



(3g): brown oil, 89% (0.18 mmol, 34 mg). The general procedure was applied using **1g** (0.2 mmol, 24 μL) and **2a** (0.6 mmol, 64 μL , 3 equiv.). The title compound was isolated by flash column chromatography (cyclohexane/ethyl acetate). $^1\text{H-NMR}$ (400 MHz, CDCl_3 , 25°C): δ = 7.21 – 7.19 (m, 1H), 7.08 – 7.04 (m, 1H), 6.73 (d, J = 8.2 Hz, 1H), 5.79 (ddt, J = 17.2, 10.2, 7.1 Hz, 1H), 5.17 – 5.09 (m, 2H), 4.64 (t, J = 6.6 Hz, 1H), 4.55 (t, J = 8.7 Hz, 2H),

Chapter 5: Allylation of aldehydes by dual photoredox and nickel catalysis

3.18 (t, $J = 8.7$ Hz, 2H), 2.50 – 2.44 (m, 2H); ^{13}C -NMR (100 MHz, CDCl_3 , 25°C): $\delta = 159.6, 136.1, 134.7, 127.2, 125.8, 122.5, 118.1, 108.9, 73.3, 71.3, 43.8, 29.7$; MS (ESI): $m/z = 173.2$ [M-OH] $^+$.

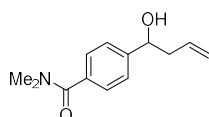


(3h): brown oil, 32% (0.06 mmol, 13 mg). The general procedure was applied using **1h** (0.2 mmol, 33 mg)

and **2a** (0.6 mmol, 64 μL , 3 equiv.). The title compound was isolated by flash column chromatography

(cyclohexane/ethyl acetate). ^1H -NMR (400 MHz, CDCl_3 , 25°C): $\delta = 8.00$ (dt, $J = 8.4, 1.9$ Hz, 1H), 7.44 –

7.40 (m, 2H), 5.83 – 5.71 (m, 1H), 5.19 – 5.15 (m, 1H), 5.15 – 5.12 (m, 1H), 4.80 (ddd, $J = 8.0, 4.8, 3.6$ Hz, 1H), 3.90 (s, 3H), 2.58 – 2.40 (m, 2H); ^{13}C -NMR (100 MHz, CDCl_3 , 25°C): $\delta = 166.8, 148.9, 133.8, 129.7$ (2C), 129.3, 125.7 (2C), 119.0, 72.7, 52.0, 43.8; MS (ESI): $m/z = 189.2$ [M-OH] $^+$.

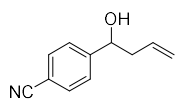


(3i): brown oil, 28% (0.06 mmol, 12 mg). The general procedure was applied using **1i** (0.2 mmol, 35 mg) and

2a (0.6 mmol, 64 μL , 3 equiv.). The title compound was isolated by flash column chromatography

(cyclohexane/ethyl acetate). ^1H -NMR (400 MHz, CDCl_3 , 25°C): $\delta = 7.39$ – 7.34 (m, 4H), 5.77 (dddd, $J =$

17.0, 10.3, 7.6, 6.6 Hz, 1H), 5.17 – 5.11 (m, 2H), 4.74 (dd, $J = 7.7, 5.0$ Hz, 1H), 3.08 (s, 3H), 2.95 (s, 3H), 2.55 – 2.40 (m, 2H); ^{13}C -NMR (100 MHz, CDCl_3 , 25°C): $\delta = 171.4, 145.3, 135.4, 134.0, 127.2$ (2C), 125.7 (2C), 118.7, 72.8, 43.8, 39.6, 39.5; MS (ESI): $m/z = 202.2$ [M-OH] $^+$.

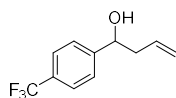


(3j): brown oil, 26% (0.05 mmol, 9 mg). The general procedure was applied using **1j** (0.2 mmol, 39 mg) and **2a**

(0.6 mmol, 64 μL , 3 equiv.). The title compound was isolated by flash column chromatography

(cyclohexane/ethyl acetate). ^1H -NMR (400 MHz, CDCl_3 , 25°C): $\delta = 7.58$ (d, $J = 8.4$ Hz, 2H), 7.43 (d, $J = 8.5$

Hz, 2H), 5.79 – 5.67 (m, 1H), 5.14 – 5.08 (m, 2H), 4.76 (dd, $J = 7.7, 4.9$ Hz, 1H), 2.54 – 2.36 (m, 2H); ^{13}C -NMR (100 MHz, CDCl_3 , 25°C): $\delta = 149.2, 133.3, 132.1$ (2C), 126.4 (2C), 119.2, 118.7, 110.9, 72.3, 43.6; MS (ESI): $m/z = 156.2$ [M-OH] $^+$.

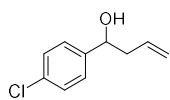


(3k): brown oil, 66% (0.13 mmol, 28 mg). The general procedure was applied using **1k** (0.2 mmol, 27 μL) and

2a (0.6 mmol, 64 μL , 3 equiv.). The title compound was isolated by flash column chromatography

(cyclohexane/ethyl acetate).

^1H -NMR (400 MHz, CDCl_3 , 25°C): $\delta = 7.59$ (d, $J = 8.2$ Hz, 2H), 7.46 (d, $J = 8.1$ Hz, 2H), 5.83 – 5.71 (m, 1H), 5.18 (m, 1H), 5.16 – 5.13 (m, 1H), 4.78 (dd, $J = 7.9, 4.8$ Hz, 1H), 2.57 – 2.40 (m, 2H), 2.19 (br s, 1H); ^{13}C -NMR (100 MHz, CDCl_3 , 25°C): $\delta = 147.7, 133.7, 129.7$ (q, $J = 32.4$ Hz), 126.1 (2C), 125.3 (q, $J = 3.6$ Hz), 124.3 (q, $J = 272.1$ Hz), 119.2 (2C), 72.5, 43.9; ^{19}F -NMR (377 MHz, CDCl_3 , 25°C): $\delta = -61.28$; MS (ESI): $m/z = 199.2$ [M-OH] $^+$.

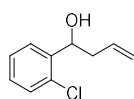


(3l): brown oil, 70% (0.14 mmol, 15 mg). The general procedure was applied using **1l** (0.2 mmol, 28 mg) and **2a**

(0.6 mmol, 64 μL , 3 equiv.). The title compound was isolated by flash column chromatography

(cyclohexane/ethyl acetate). ^1H -NMR (400 MHz, CDCl_3 , 25°C): $\delta = 7.32$ – 7.25 (m, 4H), 5.82 – 5.71 (m, 1H),

5.17 – 5.14 (m, 1H), 5.12 (m, 1H), 4.70 (dd, $J = 7.8, 5.1$ Hz, 1H), 2.53 – 2.39 (m, 2H); ^{13}C -NMR (100 MHz, CDCl_3 , 25°C): $\delta = 142.2, 133.9, 133.1, 128.5$ (2C), 127.2 (2C), 118.8, 72.5, 43.8; MS (ESI): $m/z = 165.1$ [M-OH] $^+$.



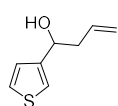
(3m): brown oil, 58% (0.12 mmol, 21 mg). The general procedure was applied using **1m** (0.2 mmol, 22.4 μL) and **2a**

(0.6 mmol, 64 μL , 3 equiv.). The title compound was isolated by flash column chromatography (cyclohexane/ethyl

acetate). ^1H -NMR (400 MHz, CDCl_3 , 25°C): $\delta = 7.55$ (dd, $J = 7.7, 1.3$ Hz, 1H), 7.34 – 7.16 (m, 3H), 5.91 – 5.80 (m,

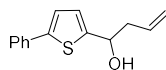
1H), 5.20 – 5.13 (m, 3H), 2.66 – 2.59 (m, 1H), 2.42 – 2.32 (m, 1H); ^{13}C -NMR (100 MHz, CDCl_3 , 25°C): $\delta = 141.1, 134.2, 131.7, 129.4, 128.4, 127.04, 126.99, 118.7, 69.6, 42.0$; MS (ESI): $m/z = 165.1$ [M-OH] $^+$.

Chapter 5: Allylation of aldehydes by dual photoredox and nickel catalysis



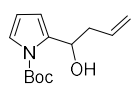
(3n): brown oil, 63% (0.13 mmol, 19 mg). The general procedure was applied using **1n** (0.2 mmol, 39 mg) and **2a** (0.6 mmol, 64 μ L, 3 equiv.). The title compound was isolated by flash column chromatography (cyclohexane/ethyl acetate).

$^1\text{H-NMR}$ (400 MHz, CDCl_3 , 25 $^\circ\text{C}$): δ = 7.29 (dd, J = 5.0, 3.0 Hz, 1H), 7.19 (d, J = 2.9 Hz, 1H), 7.07 (dd, J = 5.0, 1.2 Hz, 1H), 5.86 – 5.73 (m, 1H), 5.22 – 5.10 (m, 2H), 4.83 (dt, J = 8.0, 4.2 Hz, 1H), 2.61 – 2.46 (m, 2H); $^{13}\text{C-NMR}$ (100 MHz, CDCl_3 , 25 $^\circ\text{C}$): δ = 145.3, 134.2, 126.0, 125.6, 120.7, 118.5, 69.5, 43.0; MS (ESI): m/z = 137.2 $[\text{M-OH}]^+$.



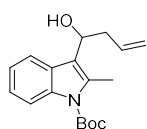
(3o): brown oil, 52% (0.10 mmol, 24 mg). The general procedure was applied using **1o** (0.2 mmol, 38 mg) and **2a** (0.6 mmol, 64 μ L, 3 equiv.). The title compound was isolated by flash column chromatography

(cyclohexane/ethyl acetate). $^1\text{H-NMR}$ (400 MHz, CDCl_3 , 25 $^\circ\text{C}$): δ = 7.57 (d, J = 8.1, 2H), 7.38 – 7.33 (m, 2H), 7.27 (d, J = 7.2 Hz, 1H), 7.15 (d, J = 3.6 Hz, 1H), 6.93 (d, J = 3.6 Hz, 1H), 5.85 (ddt, J = 17.2, 10.2, 7.1 Hz, 1H), 5.25 – 5.15 (m, 2H), 4.96 (t, J = 6.3 Hz, 1H), 2.70 – 2.58 (m, 2H), 2.20 (br s, 1H); $^{13}\text{C-NMR}$ (100 MHz, CDCl_3 , 25 $^\circ\text{C}$): δ = 147.2, 143.5, 134.4, 133.7, 128.8 (2C), 127.4, 125.7 (2C), 124.6, 122.5, 118.9, 69.5, 43.6; MS (ESI): m/z = 213.2 $[\text{M-OH}]^+$.



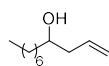
(3p): brown oil, 67% (0.14 mmol, 33 mg). The general procedure was applied using **1p** (0.2 mmol, 39 mg) and **2a** (0.6 mmol, 64 μ L, 3 equiv.). The title compound was isolated by flash column chromatography (cyclohexane/ethyl acetate).

$^1\text{H-NMR}$ (400 MHz, CDCl_3 , 25 $^\circ\text{C}$): δ = 7.14 (dd, J = 3.4, 1.7 Hz, 1H), 6.20 – 6.18 (m, 1H), 6.08 (t, J = 3.4 Hz, 1H), 5.90 (ddt, J = 17.1, 10.2, 6.9 Hz, 1H), 5.17 – 5.04 (m, 2H), 4.93 (t, J = 6.4 Hz, 1H), 3.94 (br s, 1H), 2.68 – 2.62 (m, 2H), 1.59 (s, 9H); $^{13}\text{C-NMR}$ (100 MHz, CDCl_3 , 25 $^\circ\text{C}$): δ = 150.2, 137.5, 135.3, 121.9, 116.9, 111.7, 110.2, 84.5, 66.2, 39.2, 28.0 (3C); MS (ESI): m/z = 220.4 $[\text{M-OH}]^+$.



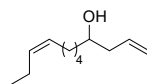
(3q): brown oil, 45% (0.09 mmol, 27 mg). The general procedure was applied using **1q** (0.2 mmol, 24 μ L) and **2a** (0.6 mmol, 64 μ L, 3 equiv.). The title compound was isolated by flash column chromatography (cyclohexane/ethyl acetate).

$^1\text{H-NMR}$ (400 MHz, CDCl_3 , 25 $^\circ\text{C}$): δ = 8.10 – 8.07 (m, 1H), 7.80 – 7.75 (m, 1H), 7.27 – 7.15 (m, 2H), 5.84 – 5.71 (m, 1H), 5.18 – 5.06 (m, 2H), 5.04 (dd, J = 7.9, 6.3 Hz, 1H), 2.86 – 2.57 (m, 2H), 2.55 (s, 3H), 1.67 (s, 9H); $^{13}\text{C-NMR}$ (100 MHz, C_6D_{12} , 25 $^\circ\text{C}$): δ = 150.7, 136.0, 134.6, 133.6, 127.7, 123.4, 122.3, 119.7, 119.6, 117.9, 115.4, 83.8, 67.8, 41.6, 28.2 (3C), 14.1; MS (ESI): m/z = 284.3 $[\text{M-OH}]^+$.



(5a): brown oil, 68% (0.14 mmol, 24 mg). The general procedure was applied using **4a** (0.2 mmol, 31 μ L) freshly distilled at 59 $^\circ\text{C}$ /21 mbar and **2a** (0.6 mmol, 64 μ L, 3 equiv.). The title compound was isolated by flash column chromatography

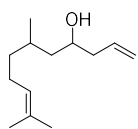
(cyclohexane/ethyl acetate). $^1\text{H-NMR}$ (400 MHz, CDCl_3 , 25 $^\circ\text{C}$): δ = 5.86 – 5.75 (m, 1H), 5.13 – 5.08 (m, 2H), 3.63 (ddt, J = 9.7, 7.8, 4.9 Hz, 1H), 2.36 – 2.24 (m, 2H), 2.16 – 2.08 (m, 2H), 2.03 (br s, 1H), 1.63 – 1.20 (m, 10H), 0.85 (dd, J = 6.8, 5.9 Hz, 3H); $^{13}\text{C-NMR}$ (100 MHz, CDCl_3 , 25 $^\circ\text{C}$): δ = 134.9, 118.0, 70.7, 41.9, 36.8, 31.8, 29.6, 29.3, 25.7, 22.6, 14.1; GC-MS: rt 10.62; m/z = 170 (M^+ , 0.5), 152 ($[\text{M-H}_2\text{O}]^+$, 0.5), 129 ($[\text{M-CH}_2=\text{CHCH}_2]^+$, 18), 111 ($[\text{M-H}_2\text{O-CH}_2=\text{CHCH}_2]^+$, 15), 69 ($[\text{CH}_2=\text{CHCH}_2\text{CH}_2\text{CH}_2]^+$, 100), 55 ($[\text{CH}_2=\text{CHCH}_2\text{CH}_2]^+$, 41).



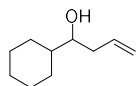
(5b): yellow oil, 42%. (0.08 mmol, 14 mg). The general procedure was applied using **4b** (0.2 mmol, 34 μ L) freshly distilled at 68 $^\circ\text{C}$ /13 mbar and **2a** (0.6 mmol, 64 μ L, 3 equiv.). The title compound was isolated by flash column chromatography (cyclohexane/ethyl acetate).

$^1\text{H-NMR}$ (400 MHz, CDCl_3 , 25 $^\circ\text{C}$): δ = 5.81 (dddd, J = 12.5, 9.6, 7.6, 6.4 Hz, 1H), 5.38 – 5.26 (m, 2H), 5.14 – 5.08 (m, 2H), 3.66 – 3.60 (m, 1H), 2.32 – 2.24 (m, 1H), 2.16 – 2.10 (m, 1H), 1.98 (m, 5H), 1.56 (br s, 1H), 1.49 – 1.29 (m, 7H), 0.94 (t, J = 7.5 Hz, 3H); $^{13}\text{C-NMR}$ (100 MHz, CDCl_3 , 25 $^\circ\text{C}$): δ = 134.8, 131.7, 128.9, 118.0, 70.6, 41.9, 36.7, 29.7, 27.0, 25.2, 20.5, 14.3.

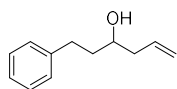
Chapter 5: Allylation of aldehydes by dual photoredox and nickel catalysis



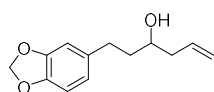
(5e): colorless oil, 54% (0.11 mmol, 21 mg) as a mixture of *syn* and *anti* diastereomers. The general procedure was applied using **4c** (0.2 mmol, 38 μ L) and **2a** (0.6 mmol, 64 μ L, 3 equiv.). The title compound was isolated by flash column chromatography (cyclohexane/ethyl acetate). $^1\text{H-NMR}$ (400 MHz, CDCl_3 , 25 $^\circ\text{C}$) mixture of diastereoisomers: δ = 5.86 – 5.76 (m, 1H), 5.13 – 5.03 (m, 3H), 3.76 – 3.70 (m, 1H), 2.31 – 2.22 (m, 1H), 2.16 – 2.04 (m, 1H), 2.04 – 1.87 (m, 2H), 1.66 (s, 3H), 1.69 – 1.55 (m, 2H), 1.58 (s, 3H), 1.51 – 1.05 (m, 4H), 0.90 (dd, J = 6.4, 6.4 Hz, 3H); $^{13}\text{C-NMR}$ (100 MHz, CDCl_3 , 25 $^\circ\text{C}$) mixture of diastereoisomers: δ = 134.9, 134.8, 131.2, 124.7, 118.1, 118.0, 68.7, 68.3, 44.3, 44.2, 42.8, 42.1, 37.8, 36.7, 29.3, 28.9, 25.7, 25.4, 25.3, 20.2, 19.1, 17.6.



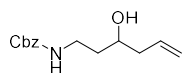
(5d): brown oil, 25% (0.05 mmol, 8 mg). The general procedure was applied using **4d** (0.2 mmol, 24 μ L) freshly distilled at 44 $^\circ\text{C}$ /27 mbar and **2a** (0.6 mmol, 64 μ L, 3 equiv.). The title compound was isolated by flash column chromatography (cyclohexane/ethyl acetate). $^1\text{H-NMR}$ (400 MHz, CDCl_3 , 25 $^\circ\text{C}$): δ = 5.82 (dddd, J = 12.5, 9.2, 8.0, 6.4 Hz, 1H), 5.15 – 5.09 (m, 2H), 3.39-3.35 (m, 1H), 2.35-2.28 (m, 1H), 2.11 (dt, J = 14, 8.4 Hz, 1H), 1.84 (d, J = 12.6 Hz, 1H), 1.77-1.63 (m, 4H), 1.54 (d, J = 16 Hz, 1H), 1.38-0.95 (m, 6H); $^{13}\text{C-NMR}$ (100 MHz, CDCl_3 , 25 $^\circ\text{C}$): δ = 135.4, 117.9, 74.7, 43.0, 38.8, 29.1, 28.1, 26.5, 26.2, 26.1.



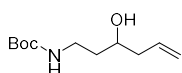
(5e): brown oil, 60% (0.12 mmol, 21 mg). The general procedure was applied using **4e** (0.2 mmol, 26 μ L) previously distilled and **2a** (0.6 mmol, 64 μ L, 3 equiv.). The title compound was isolated by flash column chromatography (cyclohexane/ethyl acetate). $^1\text{H-NMR}$ (400 MHz, CDCl_3 , 25 $^\circ\text{C}$): δ = 7.29 – 7.14 (m, 5H), 5.86 – 5.76 (m, 1H), 5.16 – 5.10 (m, 2H), 3.67 (ddd, J = 12.2, 7.6, 4.7 Hz, 1H), 2.84 – 2.75 (m, 1H), 2.72 – 2.64 (m, 1H), 2.35 – 2.28 (m, J = 12.2, 6.9, 4.3, 1.3 Hz, 1H), 2.24 – 2.12 (m, 1H), 1.81 – 1.75 (m, 2H), 1.61 (br s, 1H); $^{13}\text{C-NMR}$ (100 MHz, CDCl_3 , 25 $^\circ\text{C}$): δ = 142.0, 134.6, 128.4 (2C), 128.4 (2C), 125.8, 118.3, 69.9, 42.0, 38.4, 32.0; GC-MS: rt 12.93; m/z = 176 (M^+ , 1), 158 ($[\text{M-H}_2\text{O}]^+$, 3), 135 ($[\text{M-CH}_2=\text{CHCH}_2]^+$, 20), 117 ($[\text{M-H}_2\text{O-CH}_2=\text{CHCH}_2]^+$, 30), 91 (C_7H_7^+ , 100); MS (ESI): m/z = 314.2 $[\text{M-2 H}_2\text{O-2H}]^+$, 159.0 $[\text{M-H}_2\text{O+H}]^+$.



(5f): brown oil, 48% (0.10 mmol, 21 mg). The general procedure was applied using **4f** (0.2 mmol, 36 mg) previously synthesized and **2a** (0.6 mmol, 64 μ L, 3 equiv.). The title compound was isolated by flash column chromatography (cyclohexane/ethyl acetate). $^1\text{H-NMR}$ (400 MHz, CDCl_3 , 25 $^\circ\text{C}$): δ = 6.72 (s, 1H), 6.69 (d, J = 7.8 Hz, 1H), 6.63 (d, J = 7.9 Hz, 1H), 5.90 (s, 2H), 5.85 – 5.74 (m, 1H), 5.15 – 5.10 (m, 2H), 3.67 – 3.61 (m, 1H), 2.65 (ddt, J = 30.1, 13.9, 7.9 Hz, 2H), 2.33 – 2.26 (m, 1H), 2.15 (dt, J = 7.9, 4.3 Hz, 1H), 1.75 – 1.69 (m, 2H), 1.59 (br s, 1H); $^{13}\text{C-NMR}$ (100 MHz, CDCl_3 , 25 $^\circ\text{C}$): δ = 147.5, 145.6, 135.8, 134.5, 121.1, 118.3, 108.9, 108.1, 100.7, 69.7, 42.1, 38.6, 31.7; MS (ESI): m/z = 219.2 $[\text{M-H}]^+$, 203.2 $[\text{M-OH}]^+$.

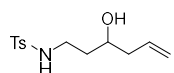


(5g): yellow oil, 59% (0.12 mmol, 29 mg). The general procedure was applied using **4g** (0.2 mmol, 41 mg) previously synthesized and **2a** (0.6 mmol, 64 μ L, 3 equiv.). The title compound was isolated by flash column chromatography (cyclohexane/ethyl acetate). $^1\text{H-NMR}$ (400 MHz, CDCl_3 , 25 $^\circ\text{C}$): δ = 7.36 – 7.27 (m, 5H), 5.79 (dt, J = 16.8, 7.3 Hz, 1H), 5.21 – 5.04 (m, 5H), 3.72 – 3.66 (m, 1H), 3.52 – 3.44 (m, 1H), 3.21 (dt, J = 19.3, 5.3 Hz, 1H), 2.60 (br s, OH), 2.28 – 2.15 (m, 2H), 1.67 (dddd, J = 14.2, 8.7, 5.6, 3.1 Hz, 1H), 1.52 (ddd, J = 14.6, 10.6, 5.4 Hz, 1H); $^{13}\text{C-NMR}$ (100 MHz, CDCl_3 , 25 $^\circ\text{C}$): δ = 157.0, 136.5, 134.5, 128.5 (2C), 128.1 (3C), 118.1, 68.5, 66.7, 41.9, 38.1, 36.6; GC-MS: rt 19.88; m/z = 249 (M^+ , 0.5), 208 ($[\text{M-CH}_2=\text{CHCH}_2]^+$, 3), 108 ($[\text{PhCH}_2\text{OH}]^+$, 20), 91 (C_7H_7^+ , 100); MS (ESI): m/z = 272.0 $[\text{M+Na}]^+$, 250.2 $[\text{M+H}]^+$.

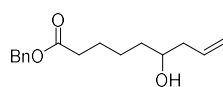


(5h): yellow oil, 42% (0.09 mmol, 20 mg). The general procedure was applied using **4h** (0.22 mmol, 39 mg) previously synthesized and **2a** (0.6 mmol, 64 μ L, 3 equiv.). The title compound was isolated by flash column chromatography (cyclohexane/ethyl acetate). $^1\text{H-NMR}$ (400 MHz, CDCl_3 , 25 $^\circ\text{C}$): δ = 5.86 – 5.75 (m, 1H), 5.12 – 5.07 (m, 2H), 4.87 (br s, 1H), 3.71 – 3.64 (m, 1H), 3.46 – 3.36 (m, 1H), 3.15 – 3.07 (m, 1H), 2.93 (br s, 1H), 2.28 – 2.16 (m, 2H), 1.67 – 1.36 (m, 2H), 1.41 (s, 9H); $^{13}\text{C-NMR}$ (100 MHz, CDCl_3 , 25 $^\circ\text{C}$): δ = 156.9, 134.8, 117.8, 79.4, 68.3, 41.8, 37.4, 37.0, 28.4 (3C).

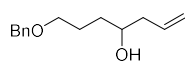
Chapter 5: Allylation of aldehydes by dual photoredox and nickel catalysis



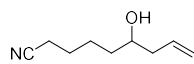
(5i): brown oil, 54% (0.09 mmol, 25 mg). The general procedure was applied using **4i** (pur. 70%, 0.2 mmol, 56 mg) previously synthesized and **2a** (0.6 mmol, 64 μ L, 3 equiv.). The title compound was isolated by flash column chromatography (cyclohexane/ethyl acetate). $^1\text{H-NMR}$ (400 MHz, CDCl_3 , 25 $^\circ\text{C}$): δ = 7.72 (d, J = 8.3 Hz, 2H), 7.32 – 7.25 (m, 2H), 5.71 (dddd, J = 16.9, 10.3, 7.9, 6.5 Hz, 1H), 5.22 (br s, 1H), 5.13 – 5.05 (m, 2H), 3.72 (ddd, J = 12.3, 7.8, 4.4 Hz, 1H), 3.16 (dtd, J = 12.5, 7.5, 4.9 Hz, 1H), 3.00 (ddt, J = 12.2, 7.1, 4.9 Hz, 1H), 2.40 (s, 3H), 2.25 – 2.16 (m, 1H), 2.13 – 2.05 (m, 1H), 2.01 (br s, 1H), 1.66 (dddd, J = 14.4, 7.8, 5.0, 3.0 Hz, 1H), 1.52 (dddd, J = 14.3, 9.3, 7.1, 4.9 Hz, 1H); $^{13}\text{C-NMR}$ (100 MHz, CDCl_3 , 25 $^\circ\text{C}$): δ = 143.3, 136.9, 133.9, 129.6 (2C), 127.1 (2C), 118.8, 69.5, 42.0, 41.0, 35.2, 21.5; MS (ESI): m/z = 270.0 $[\text{M}+\text{H}]^+$, 252.0 $[\text{M}-\text{H}_2\text{O}]^+$.



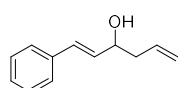
(5j): yellow oil, 46% (0.10 mmol, 25 mg). The general procedure was applied using **4j** (0.2 mmol, 46 mg) previously synthesized and **2a** (0.6 mmol, 64 μ L, 3 equiv.). The title compound was isolated by flash column chromatography (cyclohexane/ethyl acetate). $^1\text{H-NMR}$ (400 MHz, CDCl_3 , 25 $^\circ\text{C}$): δ = 7.37 – 7.28 (m, 5H), 5.79 (dddd, J = 21.1, 9.4, 7.9, 6.5 Hz, 1H), 5.13 – 5.07 (m, 4H), 3.64 – 3.58 (m, 1H), 2.36 (t, J = 7.5 Hz, 2H), 2.26 (dddt, J = 12.1, 6.8, 4.2, 1.3 Hz, 1H), 2.14 – 2.06 (m, 1H), 1.74 – 1.30 (m, 7H); $^{13}\text{C-NMR}$ (100 MHz, CDCl_3 , 25 $^\circ\text{C}$): δ = 173.4, 136.0, 134.7, 128.5 (2C), 128.16 (2C), 128.15, 118.1, 70.3, 66.1, 41.9, 36.3, 34.2, 25.1, 24.8; GC-MS: rt 19.58; m/z = 262 (M^+ , 0.5), 244 ($[\text{M}-\text{H}_2\text{O}]^+$, 0.5), 221 ($[\text{M}-\text{CH}_2=\text{CHCH}_2]^+$, 3), 129 ($[\text{M}-\text{PhCH}_2\text{O}-\text{C}_2\text{H}_5]^+$, 5), 91 (C_7H_7^+ , 100); MS (ESI): m/z = 263.2 $[\text{M}+\text{H}]^+$, 261.2 $[\text{M}-\text{H}]^+$, 245.2 $[\text{M}-\text{H}_2\text{O}+\text{H}]^+$.



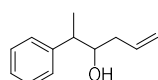
(5k): yellow oil, 69% (0.14 mmol, 30 mg). The general procedure was applied using **4k** (0.2 mmol, 36 mg) previously synthesized and **2a** (0.6 mmol, 64 μ L, 3 equiv.). The title compound was isolated by flash column chromatography (cyclohexane/ethyl acetate). $^1\text{H-NMR}$ (400 MHz, CDCl_3 , 25 $^\circ\text{C}$): δ = 7.35 – 7.25 (m, 5H), 5.87 – 5.76 (m, 1H), 5.13 – 5.08 (m, 2H), 4.50 (s, 2H), 3.68 – 3.62 (m, 1H), 3.50 (t, J = 6.0 Hz, 2H), 2.35 (br s, 1H), 2.30 – 2.11 (m, 2H), 1.81 – 1.59 (m, 3H), 1.48 (ddd, J = 14.3, 11.1, 7.2 Hz, 1H); $^{13}\text{C-NMR}$ (100 MHz, CDCl_3 , 25 $^\circ\text{C}$): δ = 138.2, 135.0, 128.4 (2C), 127.7 (2C), 127.6, 117.7, 73.0, 70.5, 70.4, 42.0, 34.0, 26.2; GC-MS: rt 16.44; m/z = 201 ($[\text{M}-\text{H}_2\text{O}-\text{H}]^+$, 0.5), 179 ($[\text{M}-\text{CH}_2=\text{CHCH}_2]^+$, 0.5), 160 ($[\text{M}-\text{H}_2\text{O}-\text{CH}_2\text{CHCH}_3]^+$, 3), 107 ($\text{C}_8\text{H}_{11}^+$, 10), 91 (C_7H_7^+ , 100), 71 ($\text{C}_5\text{H}_{11}^+$, 19); MS (ESI): m/z = 221.2 $[\text{M}+\text{H}]^+$, 203.2 $[\text{M}-\text{OH}]^+$.



(5l): yellow oil, 38% (0.08 mmol, 13 mg). The general procedure was applied using **4l** (pur. 74%, 0.2 mmol, 33 mg) previously synthesized and **2a** (0.6 mmol, 64 μ L, 3 equiv.). The title compound was isolated by flash column chromatography (cyclohexane/ethyl acetate). $^1\text{H-NMR}$ (400 MHz, CDCl_3 , 25 $^\circ\text{C}$): δ = 5.84 – 5.74 (m, 1H), 5.15 – 5.10 (m, 2H), 3.64 (tt, J = 8.5, 4.3 Hz, 1H), 2.34 (t, J = 7.0 Hz, 2H), 2.32 – 2.25 (m, 1H), 2.16 – 2.09 (m, 1H), 1.75 – 1.40 (m, 7H); $^{13}\text{C-NMR}$ (100 MHz, CDCl_3 , 25 $^\circ\text{C}$): δ = 134.4, 119.6, 118.4, 70.1, 42.0, 35.7, 25.4, 24.8, 17.1.

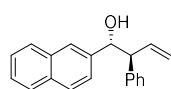


(5m): yellow oil, 43%. (0.09 mmol, 15 mg). The general procedure was applied using **1m** (0.2 mmol, 26 μ L) and **2a** (0.6 mmol, 64 μ L, 3 equiv.). The title compound was isolated by flash column chromatography (cyclohexane/ethyl acetate). $^1\text{H-NMR}$ (400 MHz, CDCl_3 , 25 $^\circ\text{C}$): δ = 7.39 – 7.35 (m, 2H), 7.33 – 7.27 (m, 2H), 7.25 – 7.20 (m, 1H), 6.60 (d, J = 16.0 Hz, 1H), 6.23 (dd, J = 15.9, 6.3 Hz, 1H), 5.90 – 5.79 (m, 1H), 5.21 – 5.13 (m, 2H), 4.39 – 4.31 (m, 1H), 2.48 – 2.32 (m, 2H); $^{13}\text{C-NMR}$ (100 MHz, CDCl_3 , 25 $^\circ\text{C}$): δ = 136.6, 134.0, 131.5, 130.3, 128.5 (2C), 127.6, 126.4 (2C), 118.5, 71.7, 42.0.

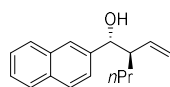


(5n): yellow oil, 30% with *syn:anti* dr of 3:1 (0.06 mmol, 11 mg). The general procedure was applied using **1n** (0.2 mmol, 26 μ L) freshly distilled at 52 $^\circ\text{C}$ /3 mbar and **2a** (0.6 mmol, 64 μ L, 3 equiv.). The title compound was isolated by flash column chromatography (cyclohexane/ethyl acetate). $^1\text{H-NMR}$ (400 MHz, CDCl_3 , 25 $^\circ\text{C}$): δ = 7.38 – 7.18 (m, 5H), 5.93 – 5.83 (m, 1H *anti*), 5.84 – 5.73 (m, 1H), 5.14 – 5.06 (m, 2H), 3.76 – 3.68 (m, 1H), 2.83 – 2.73 (m, 1H), 2.41 – 2.33 (m, 1H *anti*), 2.22 – 2.14 (m, 1H), 2.15 – 2.07 (m, 1H from minor isomer), 2.06 – 1.98 (m, 1H), 1.63 (s, 2H), 1.34 (d, J = 7.0 Hz, 3H), 1.29 (d, J = 7.1 Hz, 1H from minor isomer); $^{13}\text{C-NMR}$ (100 MHz, CDCl_3 , 25 $^\circ\text{C}$): δ = 144.4, 143.2, 135.04, 135.00, 128.48, 128.46 (2C), 128.1, 127.7 (2C), 126.6, 126.4, 118.1, 117.7, 74.99, 74.97, 45.4, 39.5, 38.9, 29.7, 17.7, 16.4; major isomer: δ = 144.4, 135.04, 128.46 (2C), 127.7 (2C), 126.4, 118.1, 74.97, 45.4, 39.5, 16.4.

Chapter 5: Allylation of aldehydes by dual photoredox and nickel catalysis

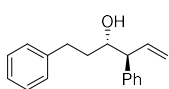


(6a): brown oil, 40% (0.08 mmol, 22 mg) with **6a** as the major isomer (**6a:6a'** > 99:1, d.r. 6:1) The general procedure was applied using **1a** (0.2 mmol, 36 mg) and **2f** (0.6 mmol, 106 mg, 3 equiv.). The title compound was isolated by flash column chromatography (cyclohexane/ethyl acetate). ¹H-NMR (400 MHz, CDCl₃, 25°C) major diastereoisomer: δ = 7.79 – 7.66 (m, 3H), 7.61 (s, 1H), 7.44 – 7.40 (m, 2H), 7.30 – 7.23 (m, 2H), 7.21 – 7.05 (m, 4H), 6.36 – 6.22 (m, 1H), 5.33 – 5.17 (m, 2H), 5.02 (dd, *J* = 7.5, 1.6 Hz, 1H), 3.67 (t, *J* = 8.2 Hz, 1H), 2.46 (bs, 1H); ¹³C-NMR (100 MHz, CDCl₃, 25°C) δ = 140.6, 139.4, 137.7, 133.0, 132.9, 128.4, 128.3, 127.9, 127.5 (2C), 126.6, 125.8, 125.7 (2C), 124.7, 118.5, 77.3, 59.0; MS (ESI): *m/z* = 257.2 [M-OH]⁺.



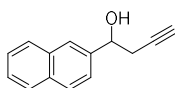
(6b): brown oil, 56% (0.11 mmol, 25 mg) with **6b** as the major isomer (**6b:6b'** > 99:1, d.r. 1:1). The general procedure was applied using **1a** (0.2 mmol, 36 mg) and **2g** (0.6 mmol, 85 mg, 3 equiv.). The title compound was isolated by flash column chromatography (cyclohexane/ethyl acetate). ¹H-NMR (400 MHz, CDCl₃, 25°C)

mixture of diastereoisomer: δ = 7.79 (m, 8H), 7.51 – 7.36 (m, 6H), 5.69 (ddd, *J* = 17.1, 10.2, 9.2 Hz, 1H), 5.55 (ddd, *J* = 17.1, 10.3, 9.1 Hz, 1H), 5.31 – 5.16 (m, 2H), 5.11 – 4.97 (m, 2H), 4.82 – 4.74 (m, 1H), 4.54 (dd, *J* = 8.0, 1.5 Hz, 1H), 2.51 (m, 1H), 2.41 (m, 1H), 1.45 – 1.03 (m, 8H), 0.85 (t, *J* = 7.2 Hz, 3H), 0.75 (t, *J* = 7.1 Hz, 3H); ¹³C-NMR (100 MHz, CDCl₃, 25°C) δ = 140.1, 140.0, 139.3, 138.6, 133.2, 133.1, 133.0, 132.9, 128.0, 127.95, 127.93, 127.7, 127.6, 126.1, 126.0, 125.8, 125.7, 125.5, 124.8, 124.7, 118.8, 117.3, 77.1, 76.8, 52.4, 51.1, 32.6, 31.7, 20.4, 20.3, 14.0, 13.9; ; MS (ESI): *m/z* = 223.3 [M-OH]⁺.



(6c): brownish oil, 42% (0.08 mmol, 21 mg) with **6c** as the major isomer (**6c:6c'** > 99:1, d.r. 3:1). The general procedure was applied using **4e** (0.2 mmol, 26 μL) previously distilled and **2f** (0.6 mmol, 106 mg, 3 equiv.) previously synthesized. The title compound was isolated by flash column chromatography (cyclohexane/ethyl acetate). ¹H-

NMR (400 MHz, CDCl₃, 25°C): δ = 7.35 – 7.04 (m, 10H), 6.25 (ddd, *J* = 17.1, 10.2, 8.9 Hz, 1H from minor isomer), 6.10 (ddd, *J* = 16.7, 10.4, 9.2 Hz, 1H), 6.00 (dd, *J* = 18.5, 8.8 Hz, 1H from minor isomer), 5.24 – 5.17 (m, 2H), 5.14 – 5.08 (m, 1H from minor isomer), 3.88 (t, *J* = 8.8 Hz, 1H from minor isomer), 3.82 – 3.77 (m, 1H), 3.55 (dd, *J* = 12.4, 4.4 Hz, 1H from minor isomer), 3.33 (dd, *J* = 12.4, 4.4 Hz, 1H from minor isomer), 3.29 – 3.23 (m, 1H), 2.86 – 2.78 (m, 1H + 1H from minor isomer), 2.61 (ddd, *J* = 13.8, 9.6, 7.1 Hz, 1H + m, 1H from minor isomer), 1.87 (br s, 1H), 1.73 – 1.58 (m, 2H); ¹³C-NMR (100 MHz, CDCl₃, 25°C) major diastereoisomer: δ = 142.0, 141.3, 138.3, 128.7, 128.4, 128.3, 127.9, 126.7, 118.0, 77.3, 76.7, 73.2, 57.5, 36.0, 32.0; MS (EI): *m/z* = 252 (M⁺, 0.5), 118 ([PhCH₂CH=CH₂]⁺, 100), 91 (C₇H₇⁺, 67).



(7): yellowish oil, 41% (0.08 mmol, 14 mg). The general procedure was applied using **1a** (0.2 mmol, 28 mg) and **2h** (80 wt. % in toluene 0.6 mmol, 67 μL, 3 equiv.). The title compound was isolated by flash column chromatography (cyclohexane/ethyl acetate).

¹H-NMR (400 MHz, CDCl₃, 25°C): δ = 7.94 – 7.71 (m, 4H), 7.54 – 7.40 (m, 3H), 5.04 (t, *J* = 6.3 Hz, 1H), 2.79 – 2.65 (m, 2H), 2.49 (bs, 1H), 2.08 (t, *J* = 2.6 Hz, 1H); ¹³C-NMR (100 MHz, CDCl₃, 25°C): δ = 139.9, 133.3, 133.2, 128.5, 128.2, 127.8, 126.4, 126.2, 124.8, 123.8, 80.7, 72.6, 71.3, 29.6; MS (ESI): *m/z* = 179.1 [M-OH]⁺.

Procedure for the allylation reaction with Ni(COD)₂

A dry 10 mL Schlenk tube, equipped with a Rotaflo stopcock, magnetic stirring bar and an argon supply tube, was first charged in glove box with the Ni(COD)₂ (0.1 mmol, 28 mg) and phenanthroline (0.1 mmol, 20 mg). Dry ACN (1 mL) and allyl acetate **2a** (0.12 mmol, 12 mg, 13 μL) were then added. After 10 min aldehyde **1a** (0.1 mmol, 16 mg) was added and the reaction was stirred for 24h. After that the reaction mixture was quenched with HCl 1M (approx. 1 mL) and extracted with AcOEt (4 x 3 mL). The combined organic layers were dried over anhydrous Na₂SO₄ and the solvent was removed under reduced pressure. The crude was purified by flash column chromatography (SiO₂) to afford the product **3a** in 70% yield (0.07 mmol, 14 mg). The test without ligand and DIPEA was performed using the same procedure reported above and no product was observed.

5.4.5 Mechanistic studies

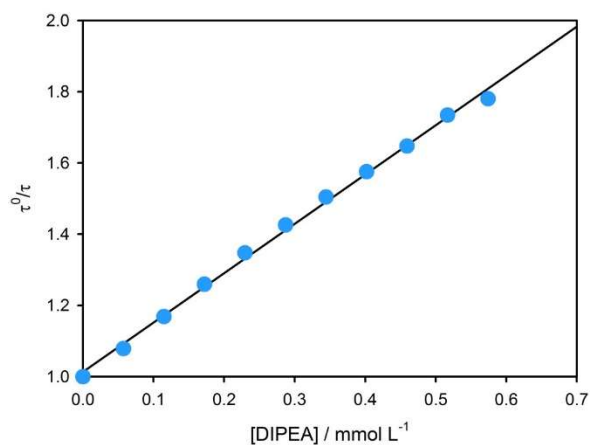


Figure 21. Emission intensity decays of $[\text{Ru}(\text{bpy})_3]\text{Cl}_2$ in acetonitrile solution in the absence (τ^0) and in the presence (τ) of increasing amount of DIPEA (blue dots). The slopes represent the Stern-Volmer constant (K_{SV}), i.e. the product of the quenching constant (k_q) and τ^0 .

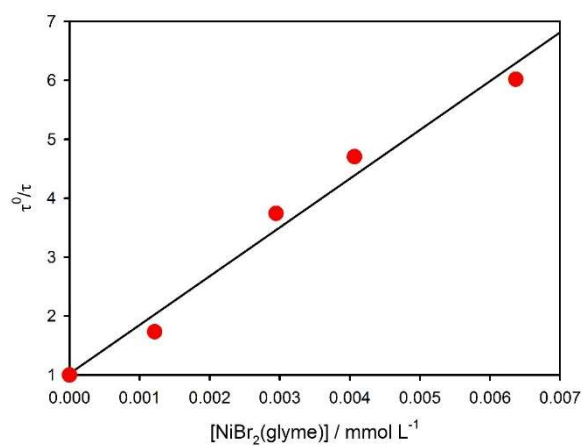


Figure 22. Emission intensity decays of $[\text{Ru}(\text{bpy})_3]\text{Cl}_2$ in acetonitrile solution in the absence (τ^0) and in the presence (τ) of increasing amount of $[\text{NiBr}_2(\text{glyme})]$ (red dots). The slopes represent the Stern-Volmer constant (K_{SV}), i.e. the product of the quenching constant (k_q) and τ^0 .

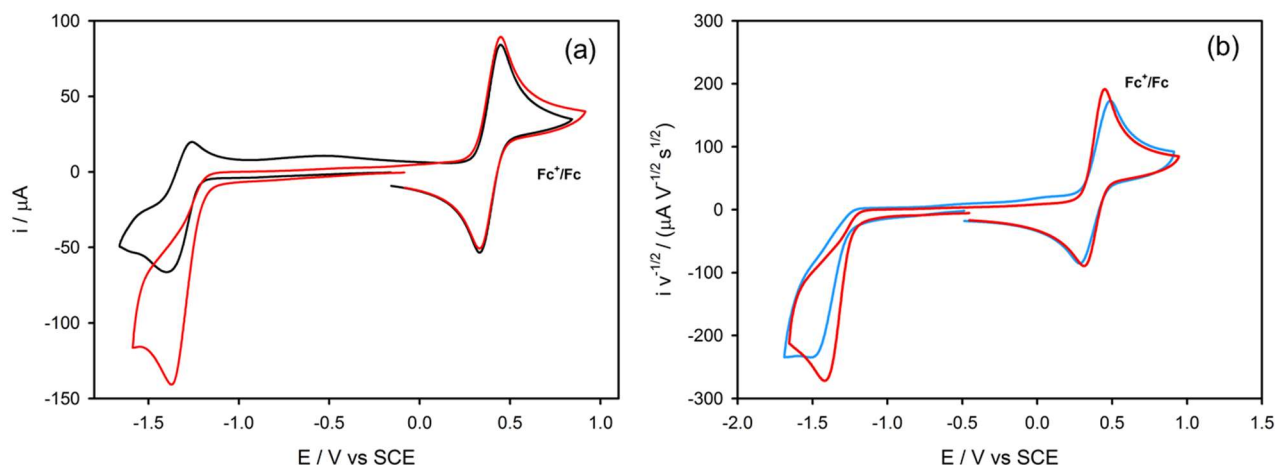


Figure 23 (a). Cyclic voltammetry of an argon-purged solution of $[\text{Ni}(\text{phen})_3](\text{BF}_4)_2$ (3mM) in CH_3CN in the presence of 0.3M tetraethylammonium tetrafluoroborate (TEABF_4) (black solid line) and upon addition of allyl acetate (0.6M) (red solid line). Scan rate = 0.2V/s-1; working electrode: glassy carbon. Ferrocene (Fc) was used as internal standard. Plot (b). Cyclic voltammetry of an argon-purged solution of $[\text{Ni}(\text{phen})_3](\text{BF}_4)_2$ (3mM) in CH_3CN in the presence of 0.3M tetraethylammonium tetrafluoroborate (TEABF_4) upon addition of allyl acetate (0.6M) at 0.2 V/s (red solid line) and 2 V/s (blue solid line). Working electrode: glassy carbon. Ferrocene (Fc) was used as internal standard (plot (b)).

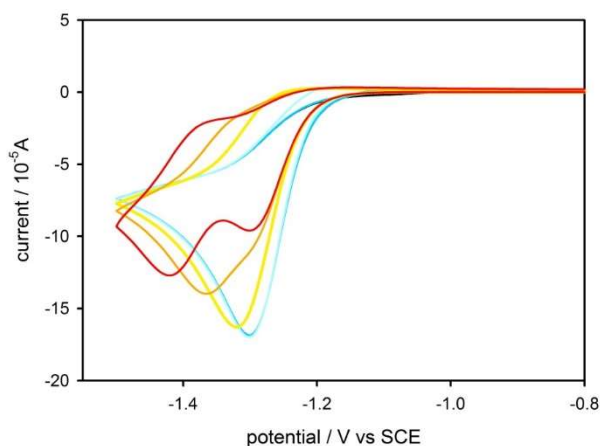


Figure 24 Simulated cyclic voltammograms using DigiSim. Simulation parameters: 25 °C, 0.2V/s, concentration of $[\text{LnNiII}]^{2+}$ 3mM and allyl acetate 0.6M, $E_0[\text{Ni}(\text{II})/\text{Ni}(\text{I})] = -1.30$ V vs SCE, $k_s(4) = 1 \times 10^4$ cm/s, $k(5) = 1 \times 10^4 \text{ M}^{-1}\text{s}^{-1}$, $k_s(6) = 1 \times 10^4$ cm/s and $k(7) > 1 \text{ s}^{-1}$. The variable parameter is the reduction potential $E_0[\text{Ni}(\text{III})/\text{Ni}(\text{II})]$: -1.00 V (black solid line), -1.10 V (blue solid line), -1.20 V (light blue solid line); -1.30 V (yellow solid line), -1.35V (orange solid line) and -1.40 V (red solid line).

References

- ¹ For selected reviews, see: (a) M. Yus, J. C. Gonzalez-Gomez and F. Foubelo, *Chem. Rev.*, 2013, **111**, 5595; (b) P. -S. Wang, M. -L. Shen and L. -Z. Gong, *Synthesis*, 2018, **50**, 956; (c) K. Spielmann, G. Niel, R. M. de Figueiredo and J.-M. Campagne, *Chem. Soc. Rev.*, 2018, **47**, 1159.
- ² R. B. Kargbo and G. R. Cook, *Curr. Org. Chem.*, 2007, **11**, 1287.
- ³ E. J. Corey and L. Kurti, *Enantioselective Chemical Synthesis*, Elsevier, 2010, p. 79
- ⁴ a) Y. Okude, S. Hirano, T. Hiyama and H. Nozaki, *J. Am. Chem. Soc.*, 1977, **99**, 3179; (b) K. Namba, J. Wang, S. Cui and Y. Kishi, *Org. Lett.*, 2005, **7**, 5421; (c) A. Fürstner and N. Shi, *J. Am. Chem. Soc.*, 1996, **118**, 12349; (d) M. Bandini, P. G. Cozzi, P. Melchiorre and A. Umani-Ronchi, *Angew. Chem., Int. Ed.*, 1999, **38**, 3357.

- ⁵ G. C. Hargaden and P. J. Guiry, *Adv. Synth. Catal.*, 2007, **349**, 2407.
- ⁶ A. Gil, F. Albericio and M. Álvarez, *Chemical Reviews*, 2017, **117**, 8420.
- ⁷ a) H. Guo, C.-G. Dong, D.-S. Kim, D. Urabe, J. Wang, J. T. Kim and Y. Kishi, *J. Am. Chem. Soc.*, 2009, **131**, 15387; b) M. Kurosu, M.-H. Lin and Y. Kishi, *J. Am. Chem. Soc.*, 2004, **126**, 12248.
- ⁸ E. J. Corey and M. F. Semmelhack, *J. Am. Chem. Soc.*, 1967, **89**, 2755.
- ⁹ (a) M. Durandetti and J. Périchon, *Synthesis*, 2006, **9**, 1542; (b) M. Durandetti, C. Gosmini and J. Périchon, *Tetrahedron*, 2007, **63**, 1146.
- ¹⁰ Martin has described a nickel-catalyzed carboxylation of allylic alcohols with CO₂, in the presence of a phenanthroline derivative as ligand, and zinc as stoichiometric reductant; see: M. van Gemmeren, M. Borjesson, A. Tortajada, S.-Z. Sun, K. Okura and R. Martín, *Angew. Chem., Int. Ed.*, 2017, **56**, 6558.
- ¹¹ J. Twilton, C. Lee, P. Zhang, M. H. Shaw, R. W. Evans and D. W. C. MacMillan, *Nat. Rev. Chem.*, 2017, **1**, 52.
- ¹² D. Kalyani, K. B. McMurtrey, S. R. Neufeldt and M. Sanford, *J. Am. Chem. Soc.*, 2011, **133**, 18566.
- ¹³ J. C. Tellis, D. N. Primer and G. A. Molander, *Science*, 2014, **345**, 433.
- ¹⁴ Z. Zuo, D. T. Anheman, L. Chu, A. G. Doyle and D. W. C. MacMillan, *Science*, 2014, **345**, 437.
- ¹⁵ G. A. Molander, J. A. Milligan, J. A. Phelan and S. O. Badir, *Angew. Chem., Int. Ed.*, 2019, **58**, 6152.
- ¹⁶ C. Cavedon, P. H. Seeberger and B. Pieber, *Eur. J. Org. Chem.*, 2019, **3**, 1.
- ¹⁷ J. Twilton, C. Le, P. Zhang, M. H. Shaw, R. W. Evans and D. W. C. MacMillan, *Nature Rev. Chem.*, 2017, **1**, 1.
- ¹⁸ J. Twilton, C. Le, P. Zhang, M. H. Shaw, R. W. Evans and D. W. C. MacMillan, *Nature Rev. Chem.*, 2017, **1**, 1.
- ¹⁹ J. C. Tellis, D. N. Primer and G. A. Molander, *Science*, 2014, **345**, 433.
- ²⁰ V. Corcé, L.-M. Chamoreau, E. Derat, J.-P. Goddard, C. Ollivier and L. Fensterbank, *Angew. Chem. Int. Ed.*, 2015, **54**, 11414.
- ²¹ K. Nakajima, S. Nojima and Y. Nishibayashi, *Angew. Chem. Int. Ed.*, 2016, **55**, 14106.
- ²² (a) Y. Nishigaichi, A. Suzuki, T. Saito and A. Tukawa, *Tetrahedron Lett.*, 2005, **46**, 5149; (b) Y. Nishigaichi, T. Orimi and A. Tukawa, *J. Organomet. Chem.*, 2009, **694**, 3837; (c) A. L. Berger, K. Donabauer and B. König, *Chem. Sci.*, 2018, **9**, 7230.
- ²³ J. L. Schwarz, F. Shafers, A. Tlahuext, L. Luckeimerand and F. Glorius, *J. Am. Chem. Soc.*, 2018, **140**, 12705.
- ²⁴ H. Mitsunuma, S. Tanabe, H. Fuse, K. Ohkubo and M. Kanai, *Chem. Sci.*, 2019, **10**, 3459.
- ²⁵ J. A. Broomhead and F. O. Dwyer, *Aust. J. Chem.*, 1962, **16**, 51.
- ²⁶ (a) L. L. Anka-Lufford, M. R. Prinsell and D. J. Weix, *J. Org. Chem.*, 2012, **77**, 9989; (b) D. J. Weix, *Acc. Chem. Res.*, 2015, **48**, 1767.
- ²⁷ a) Y. G. Budnikova, D. G. Yakhvarov, V. I. Morozov, Y. M. Kargin, A. V. Il'yasov, Y. N. Vyakhireva and O. G. Sinyashin, *Russ. J. Gen. Chem.*, 2002, **72**, 184. For electrochemical studies of [Ni(o-phen)₃]²⁺ performed in DMF, see: ref. 16 and (b) W. H. Smith and Y.-M. Kuo, *J. Electroanal. Chem.*, 1985, **188**, 203.
- ²⁸ Quite recently, isolation and characterization of LnNi(I) complexes (L = bipyridine, phenanthroline) and their involvement in cross coupling reactions were reported; see: M. M. Beromi, G. W. Brudvig, N. Hazari, H. M. C. Lant and B. Q. Mercado, *Angew. Chem., Int. Ed.*, 2019, **58**, 6094.
- ²⁹ (a) M. Wrighton and J. Markham, *J. Phys. Chem.*, 1973, **77**, 3042; (b) S. P. Pitre, C. D. McTiernan, H. Ismaili and J. C. Scaiano, *J. Am. Chem. Soc.*, 2013, **135**, 13286. For a photocatalytic cycle in which tertiary amines are working as a stoichiometric reductant, see for example: (c) Z. Duan and A. Lei, *Org. Lett.*, 2016, **18**, 4012.
- ³⁰ N. E. Tokel-Takvoryan, R. E. Hemingway and A. J. Bard, *J. Am. Chem. Soc.*, 1973, **95**, 6582.
- ³¹ At the present time, we can only speculate about the reactive species and its coordination; for the synthesis of phenanthroline allyl nickel complex see: I. Svoboda and M. Pashchanka, *J. Organomet. Chem.*, 2009, **694**, 3912. Further mechanistic studies and calculations are planned.
- ³² T. Masquelin, E. Broger, K. Müller, R. Schmid and D. Obrecht, *Helvetica Chimica Acta*, 1994, **77**, 1395.
- ³³ G. Rassu, C. Curti, V. Zambrano, L. Pinna, N. Brindani, G. Pelosi and F. Zanardi, *Chem.: Eur. J.*, 2016, **22**, 12637.

- ³⁴ V. G. Albano, M. Bandini, M. Melucci, M. Monari, F. Piccinelli, S. Tommasi and A. Umani-Ronchi, *Adv. Synth. Catal.*, 2005, **347**, 1507.
- ³⁵ A. Gualandi, M. Marchini, L. Mengozzi, M. Natali, M. Lucarini, P. Ceroni and P. G. Cozzi, *ACS Catal.*, 2015, **5**, 5927.
- ³⁶ X. Huo, R. He, J. Fu, J. Zhang, G. Yang and W. Zhang, *J. Am. Chem. Soc.*, 2017, **139**, 9819.
- ³⁷ K. J. Schwarz, J. L. Amos, J. C. Klein, D. T. Do and T. N. Snaddon, *J. Am. Chem. Soc.*, 2016, **138**, 5214.
- ³⁸ J. M. Kraus, H. C. Gits and R. B. Silverman, *Tetrahedron Lett.*, 2012, **53**, 1319.
- ³⁹ I. Dubovyk, I. D. G. Watson and A. K. Yudin, *J. Org. Chem.*, 2013, **78**, 1559.
- ⁴⁰ I. D. G. Watson, S. A. Styler and A. K. Yudin, *J. Am. Chem. Soc.*, 2004, **126**, 5086.
- ⁴¹ T. S. Ahmed and R. H. Grubbs, *J. Am. Chem. Soc.*, 2017, **139**, 1532.
- ⁴² a) B.-L. Zhao, Y. Lin, H.-H. Yan and D.-M. Du, *Org. Biomol. Chem.*, 2015, **13**, 11351. b) N. T. Jui, J. A. O. Garber, F. G. Finelli and D. W. C. MacMillan, *J. Am. Chem. Soc.*, 2012, **134**, 11400.
- ⁴³ a) B.-L. Zhao, Y. Lin, H.-H. Yan and D.-M. Du, *Org. Biomol. Chem.*, 2015, **13**, 11351. b) N. T. Jui, J. A. O. Garber, F. G. Finelli and D. W. C. MacMillan, *J. Am. Chem. Soc.*, 2012, **134**, 11400.
- ⁴⁴ a) B. R. Kusuma, L. B. Peterson, H. Zhao, G. Vielhauer, J. Holzbeierlein and B. S. J. Blagg, *J. Med. Chem.*, 2011, **54**, 6234. b) A. L. Aguilar, J. Escribano, P. Wentworth Jr. and T. D. Butters, *ChemMedChem*, 2014, **9**, 2809.
- ⁴⁵ a) T. Koyanagi, G. Leriche, D. Onofrei, G. P. Holland, M. Mayer and J. Yang, *Angew. Chem. Int. Ed.*, 2016, **55**, 1890.
- ⁴⁶ K. E. Kim, J. Li, R. H. Grubbs and B. M. Stoltz, *J. Am. Chem. Soc.*, 2016, **138**, 13179.
- ⁴⁷ M. Zhao, H. Yang, M.-M. Li, J. Chen and L. Zhou, *Org. Lett.*, 2014, **16**, 2904.
- ⁴⁸ W. H. Smith and Y.-M. Kuo, *J. Electroanal. Chem. Interfacial Electrochem.*, 1985, **188**, 189.

Use of coumarins in photoredox polymerization processes

6.1 Introduction

6.1.1 Photocatalysts in Polymerization Reactions

Photopolymerization reactions are already encountered for applications in various industrial sectors including radiation curing,¹ microelectronics,² laser direct imaging (LDI) technology,³ Computer-To-Plate processing, 3D printing through the stereo-lithography approach,⁴ holographic recording and information storage,⁵ manufacture of optical elements,⁶ dentistry,⁷ medicine (e.g. surgical glue),⁸ design of structured materials on the nanoscale size and imaging areas.⁹

The driving force of the photopolymerization is a photoinitiator (PI) or a PhotoInitiating System (PIS) which, under irradiation, generates active species initiating the polymerization processes through a radical or a cationic mechanism and, rarely, anionic ones.

A photopolymerization reaction can be initiated through different pathways. The homolytic bond cleavage (Type I) and hydrogen abstraction (Type II) are most classical systems for the activation of the PI and the subsequent generation of radical species. In the case of cationic mechanism, a photolysis of *onioium* compounds (iodonium, sulfonium, pyridium) is required for triggering the polymerization process (Figure 1).

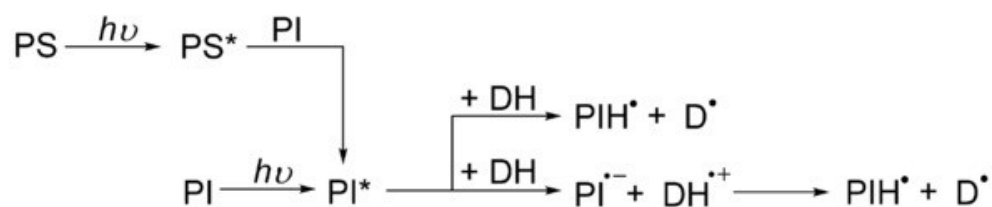


Figure 1 Type II photopolymerization mechanism.

In Type II mechanism, the hydrogen abstraction takes place in the presence of a hydrogen donor (co-initiator). This system is characterized by a rather moderate reactivity due to numerous kinetic limitations, hence additional components are introduced to overcome these restrictions. The development of a multi-component system, composed by hydrogen donor DH, an electron acceptor A (usually an iodium salt) and the PI, is necessary to increase the yield (Figure 2).

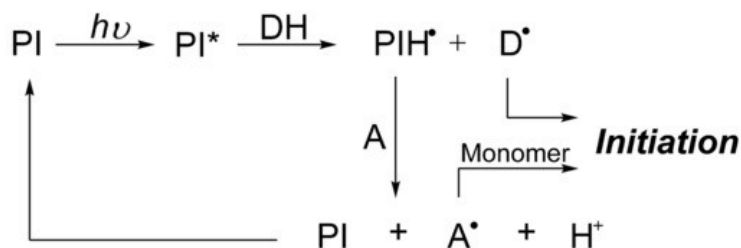


Figure 2 A three-component systems with PI/DH/A.

An ultimate improvement of three-component initiator systems was achieved when the PIs acts as a photocatalyst PC and it is regenerated during the polymerization giving the access to very efficient process.

Accordingly, the photopolymerization using a given PI system depends of the relationships between the photoinitiation efficiency P_{Eff} and the polymerization ability P_{Ab} . The P_{Abs} are visualized by the polymerization rates and the final conversions of the monomer whereas P_{Eff} are reflected by the initiation quantum yield Φ_{I} (number of starting polymer chains per absorbed photon).

In photoredox catalytic polymerization, a long lifetime of the excited state ($^*\text{PC}$), adapted redox potentials and a good reversibility of the oxidation and reduction states are the most important features of a PC. The successful results are undoubtedly related to the precise mixtures of several components which act as $^*\text{PC}$ reductants or oxidants.

Generally, systems such as PC/iodonium salt (Ph_2I^+)/silane and PC/iodonium salt (Ph_2I^+)/NPG, have provided high performance photoredox catalytic polymerization.

In particular, in PC/iodonium salt (Ph_2I^+)/NPG system, an oxidative pathway is hypothesized (Figure 3).

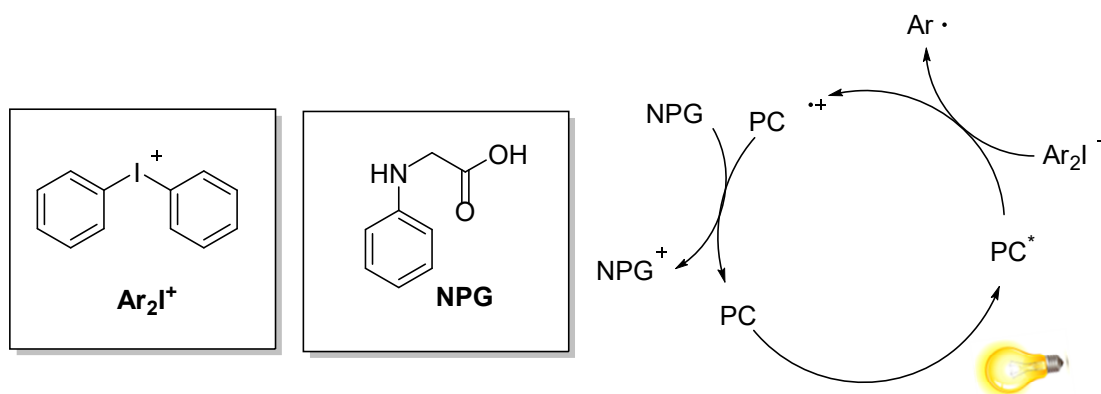


Figure 3 Oxidative pathway for PC/ (Ph_2I^+)/NPG system.

Ph_2I^+ reacts with the PC^* species. The unstable radical $\text{Ph}_2\text{I} \cdot$ breaks into PhI and the polymerization initiator $\text{Ph}\cdot$. The PC is regenerated by the subsequent reduction of $\text{PC}^{\bullet+}$ species by NPG generating the NPG^+ species.

6.1.2 Organophotocatalysts based systems

Despite metal-based photocatalysts MPCs are widely used in photocatalysis, development of metal-free organophotocatalysts OPCs is currently a very important issue in order to restrict the utilization of metal-based PCs which are expensive, rather toxic and must be removed from the synthesized polymer. Organic dyes are exploited in three-component polymerization systems¹⁰ but their short-term storage stability¹¹ and their degradability during the polymerization process¹² limits their utilization in catalytic amounts. The methylene blue MB^+ /amine/iodonium salt combination is a well-known system to generate phenyl radicals for FRP through the reductive quenching of excited state $\text{MB}^{+\bullet}$ with the amine.¹³ An elegant example is reported by Stransbury and co-workers¹⁴ (Figure 4).

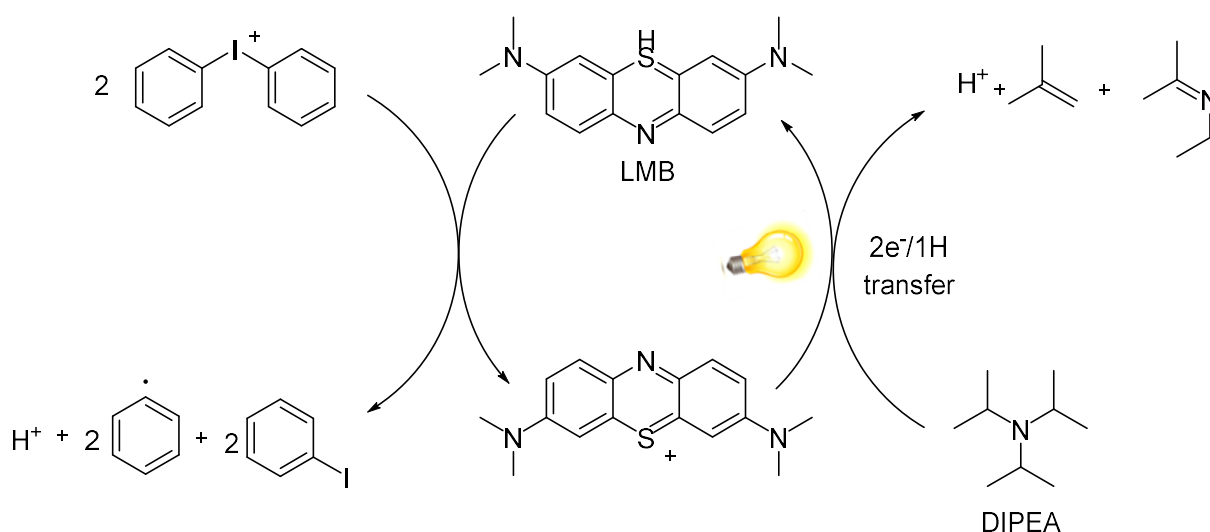


Figure 4 Reaction mechanism for the MB^+ /DIPEA/ Ph_2I^+ .

The free radical polymerization (FRP) of (meth)acrylates initiated by this visible-light MB^+ /DIPEA/ Ph_2I^+ system through an organic photoredox catalytic process. Interestingly, a two electron transfer from DIPEA to $\text{MB}^{+\bullet}$ generates a leuco-methylene blue (LMB) species. In absence of light irradiation, LMB slowly reacted with the iodonium salt to liberate phenyl radicals to initiate the FRP of methyl methacrylate allowing the regeneration of the dye.

Other examples of OPCs are the polyaromatic compounds. Pyrene derivatives, carbazole derivatives, N-, naphthacene, bis[(triisopropyl)silyl]-anthracene, bis[(triisopropyl)silyl]pentacene, truxene derivatives and triazine derivatives have been recently proposed as OPCs for polymer synthesis.¹⁵

Systems which work through an oxidative quenching are less common. A final example is the truxene-acridinedione Tr-AD which is used in combination with an amine, usually phenyl-*N*-*tert*-butylnitron PBN and a phenacyl bromide such as α -bromoacetophenone¹⁶ (Figure 5)

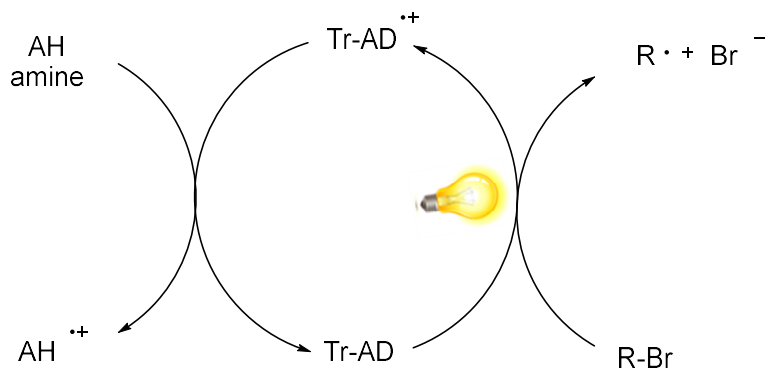


Figure 5 Photocatalytic polymerization system for the TrAD/Phen-Br/AH system.

6.1.3 Use of coumarins as photoinitiators

Coumarin **1** and **2** were successfully employed in photo-redox catalysis as photocatalysts of several organic transformations, as largely discussed in chapter 2 and 3 (Figure 6).

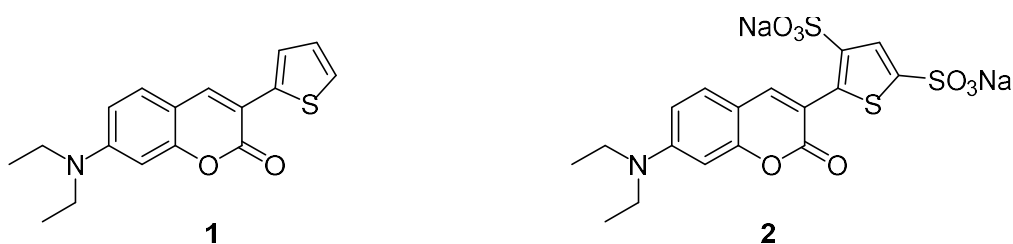


Figure 6 Molecular structure of coumarins **1** and **2**.

In order to extend the use of new synthesized 3-thienyl coumarin derivatives **1** and **2** to different fields of applications, their employment in high performance photoinitiating systems for both the free radical polymerization (FRP) of (meth)acrylates and the cationic polymerization (CP) of epoxides using mild irradiation conditions was investigated. Furthermore, their application in photosensitive 3D printing resins as well as the formation of hydrogels, exploiting the water solubility, of **2** was attempted.

In this chapter, the use of 3-thienyl coumarin derivatives **1** and **2** as versatile photoinitiators for 3D printing, polymerization in water and photocomposite synthesis will be discussed. All the results concerning polymerization in this chapter were carried out in the laboratory of Prof. J. Lalavèe

(Institut de Science des Matériaux de Mulhouse) I would like to thank professor Lalavèè and his co-workers for the work done.

6.2 Results and discussion

6.2.1 Light absorption properties of the investigated compounds

As discussed in section 2.2.2, coumarins **1** and **2** are characterized by very high molar extinction coefficients (ϵ) both in the near UV and the visible ranges (**1**: $\epsilon = 35200 \text{ M}^{-1} \text{ cm}^{-1}$ at $\lambda_{\text{max}} = 421 \text{ nm}$, and **2**: $\epsilon = 28100 \text{ M}^{-1} \text{ cm}^{-1}$ at $\lambda_{\text{max}} = 405 \text{ nm}$). Remarkably, their absorption peaks are intense in the 270–510 nm spectral range, ensuring an excellent overlap with the emission spectra of the near UV or visible LEDs (Figure 7).

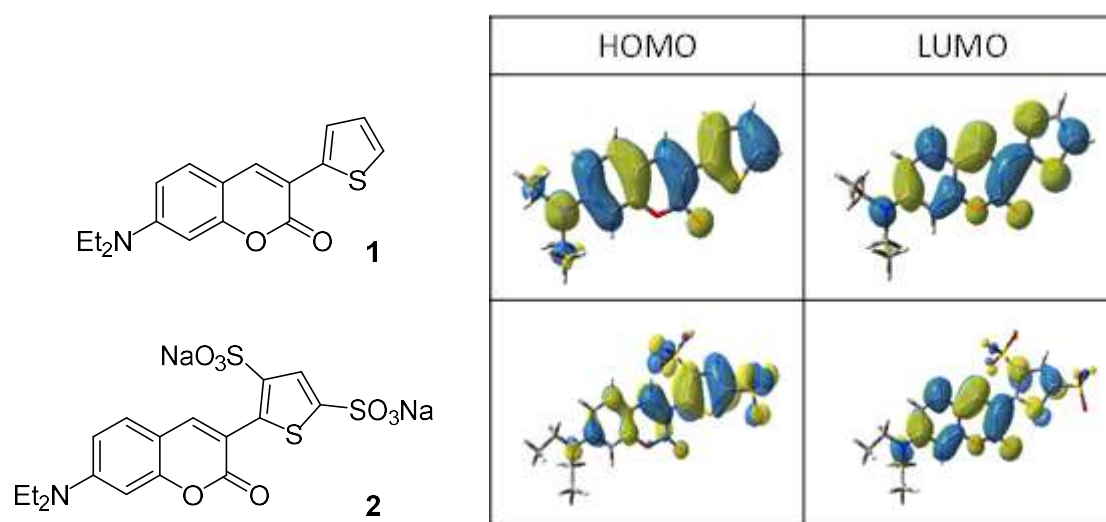


Figure 7 HOMO and LUMO of compounds **1** and **2**.

The frontier orbitals (Highest Occupied Molecular Orbital, HOMO, and Lowest Unoccupied Molecular Orbital, LUMO) for both coumarins **1** and **2** are strongly delocalized all over the π -conjugated system in both compounds clearly showing a $\pi \rightarrow \pi^*$ lowest energy transition. Coumarin **1** exhibits a higher delocalization of both the HOMO and LUMO over all the π scaffolds than respect to coumarin **2** in agreement with a lower HOMO–LUMO gap leading to a bathochromic shift of $\sim 20 \text{ nm}$.

6.2.2 Cationic photopolymerization (CP) of epoxides

A full study on the cationic polymerization (CP) of epoxides (using EPOX as a benchmark monomer) in thin films (25 μm) was performed under air using the new compounds **1** and **2** under irradiation with the 405 nm LEDs as a convenient soft irradiation source. Following the polymerization (conversion) in function of the time gave the curves 1, 2 and 3. (Figure 8).

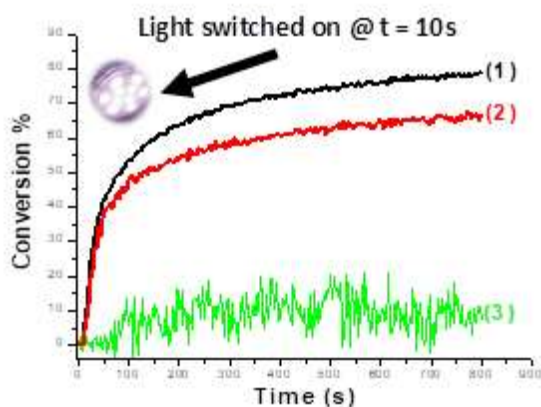


Figure 8 Polymerization profiles (epoxy function conversion vs irradiation time) for EPOX under air (thickness = 25 μm) upon exposure to 405 nm LEDs in the presence of the two-component photoinitiating systems: (1) **1**/Iod (0.2%/1% w/w); (2) **1**/Iod (0.5%/1% w/w); and (3) **2**/Iod (0.2%/1% w/w). The irradiation starts for $t = 10$ s.

The CP in the presence of a two-component photoinitiating system based on the **1**/Iod system is very efficient in terms of R_p (rate of polymerization) and final epoxy function conversion (C). A slightly lower FC in the epoxy function at 0.5% concentrations of **1** w/w (curve 2) than respect to 0.2% (w/w) (curve 1) was observed, giving a 67% and 80% of FC, respectively. This behaviour can be attributed to the inner filter effect because the light penetration decreases for higher coumarin contents even for thin samples. In fact, it is obvious that at higher concentrations, the colour of the obtained thin polymer becomes darker and darker in agreement with this inner filter (Figure 9).

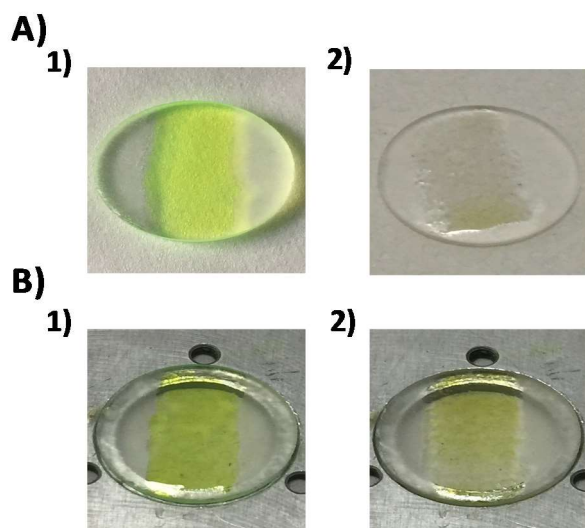


Figure 9 Photos of EPOX thin film (25 μm) upon irradiation with the LED @405 nm for 800s in the presence of the two-component photoinitiating systems: a) (1): A/Iod (0.2%/1% w/w) before polymerization; and (2): A/Iod (0.2%/1% w/w) after polymerization; respectively, under air. b) (1): A/Iod (0.5%/1% w/w) before polymerization; and (2): A/Iod (0.5%/1% w/w) after polymerization; respectively, under air.

Using Iod alone, at the same irradiation conditions, no polymerization occurs showing the huge effect of **1** on the initiating ability. Therefore, **1** can be considered as a very good photoinitiator in combination with an iodonium salt (see the chemical mechanism in section 6.2.7).

In addition, a new peak ascribed to the formation of the polyether network during the photopolymerization reaction arises at $\sim 1080\text{ cm}^{-1}$ (see the FTIR spectra in the $750\text{--}1150\text{ cm}^{-1}$ range in Fig. 3B for 0.2% **1** (w/w), and 3C for 0.5% **1** (w/w), respectively) (Figure 10).

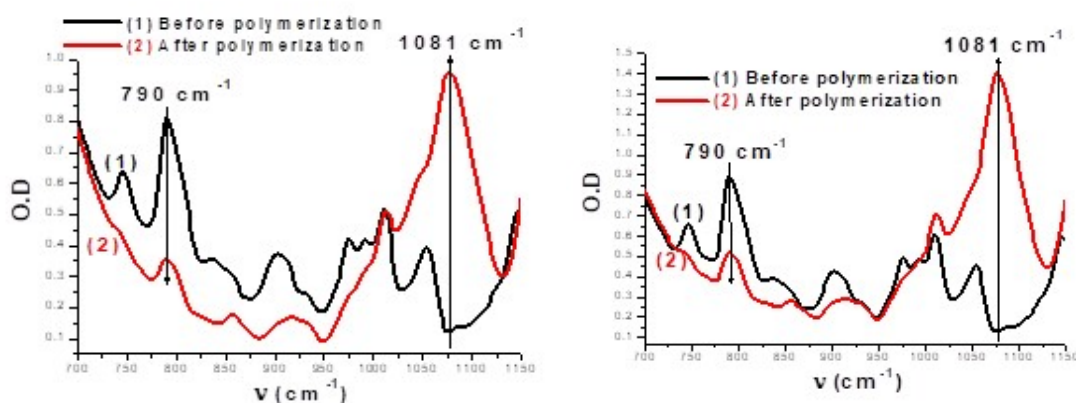


Figure 10 a) IR spectra recorded before and after polymerization for **1**/Iod (0.2%/1% w/w) upon exposure to 405nm LEDs. b) IR spectra recorded before and after polymerization for **1**/Iod (0.5%/1% w/w) upon exposure to 405nm LEDs.

In the same context, the 2/Iod system was tested but no polymerization was observed when using the 405nm LEDs nm under air (curve 3, figure 8). The polyether peak is lower for 2/Iod compared with those for 1/Iod systems (Figure 11).

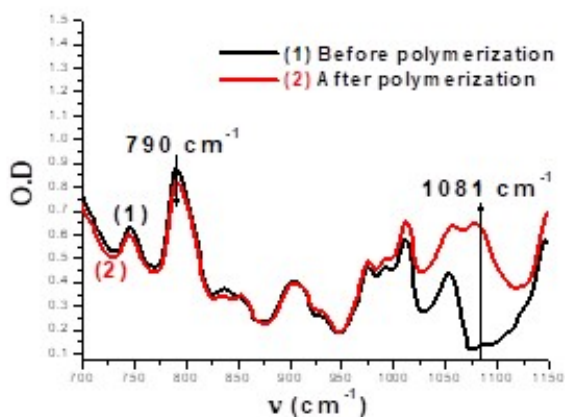


Figure 11 IR spectra recorded before and after polymerization for 2/Iod (0.2%/1% w/w) upon exposure to 405nm LEDs.

The efficiency trend for CP using the 405nm LEDs clearly follows the order $1 \gg 2$. This behaviour can be partly connected to the absorption properties of the coumarin derivatives as 1 is the most efficient PI and has a higher extinction coefficient than 2.

6.2.3 Free radical photopolymerization of acrylates (TMPTA)

The FRP of TMPTA in thin films (25 μm), in laminate and in the presence of the 1/Iod or 1/Iod/NPG couples is quite efficient using the 405nm LEDs (Figure 12).

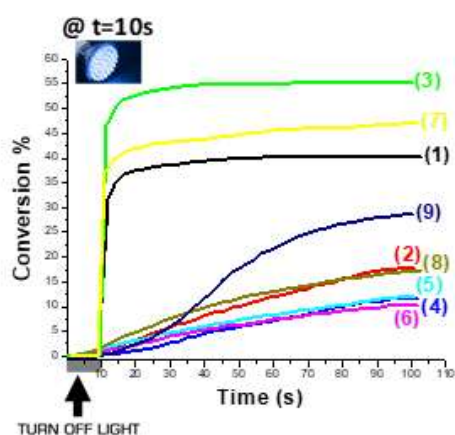


Figure 12 Polymerization profiles of TMPTA (acrylate function conversion vs. irradiation time) in laminate (thickness = 25 μm) upon exposure to 405 nm LEDs in the presence of the two and three-

component photoinitiating systems: (1) **1**/Iod (0.2%/1% w/w); (2) **1**/NPG (0.2%/1% w/w); (3) **1**/Iod/NPG (0.5%/1%/1% w/w); (4) **1**/EDB (0.2%/1% w/w); (5) **2**/Iod (0.2%/1% w/w); (6) **2**/NPG (0.2%/1% w/w); (7) **2**/Iod/NPG (0.2%/1%/1% w/w); (8) **2**/EDB (0.2%/1% w/w) and (9) Iod/NPG (1%/1% w/w); respectively. The irradiation starts for $t = 10$ s.

For **1**, Iod or NPG alone, no or very low polymerization occurs showing the huge role of **1** for the global performance of the system. The **2**/Iod couple is not able to initiate the FRP thin samples of acrylates under exposure to the 405nm LEDs (curve 5). This can be probably ascribed to its low initiating radical yield. This is also in agreement with its low initiating ability for CP (see above). A photoredox catalyst behaviour was observed upon using the coumarin/Iod/NPG (0.2%/1%/1% w/w) three-component PISs under exposure to the 405nm LEDs. The addition of the amine (NPG) leads to an increase of the FC to 56% with **1**/Iod/NPG (0.2%/1%/1% w/w) (curve 3) compared to 40% with **1**/Iod (0.2%/1% w/w) (curve 1). A similar behaviour is also observed with **2**: FC = 47% with **2**/Iod/NPG (0.2%/1%/1% w/w) (curve 7) compared to **2**/Iod (0.2%/1% w/w) (curve 5), for which no polymerization occurs. In comparison, the two-component system Iod/NPG (1%/1% w/w) shows a mild polymerization profile (curve 9), highlighting the crucial role of **1** and **2**.

In the same context, good polymerization profiles for the FRP of TMPTA in thick samples are also obtained when using the 405nm LEDs (Figure 13).

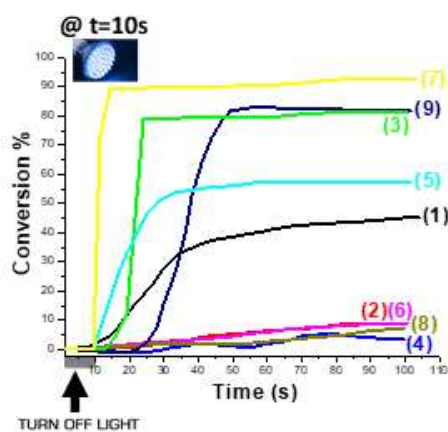


Figure 13 Polymerization profiles of TMPTA (acrylate function conversion vs. irradiation time) under air (thickness = 1.4 mm) upon exposure to 405 nm LEDs in the presence of the two and three-component photoinitiating systems: (1) **1**/Iod (0.2%/1% w/w); (2) **1**/NPG (0.2%/1% w/w); (3) **1**/Iod/NPG (0.5%/1%/1% w/w); (4) **1**/EDB (0.2%/1% w/w); (5) **2**/Iod (0.2%/1% w/w); (6) **2**/NPG (0.2%/1% w/w); (7) **2**/Iod/NPG (0.2%/1%/1% w/w); (8) **2**/EDB (0.2%/1% w/w) and (9) Iod/NPG (1%/1% w/w); respectively. The irradiation starts for $t = 10$ s.

The FRP of 1.4 mm thick samples of acrylates under air is very efficient in terms of R_p (rate of polymerization) and final acrylate function conversion (FC) using two and three-component photoinitiating systems based on coumarin/Iod (0.2%/1% w/w) and coumarin/Iod/NPG combinations (0.2%/1%/1% w/w) upon irradiation with the 405nm LEDs. For comparison, Iod alone was tested and no polymerization was observed using the same irradiation conditions, showing the role of **1** or **2**. The **2**/Iod PIS (curve 5) shows higher final conversion of the acrylate functions than the **1**/Iod system (curve 1). This can be ascribed to the color of the obtained thick polymer (Figure 14).

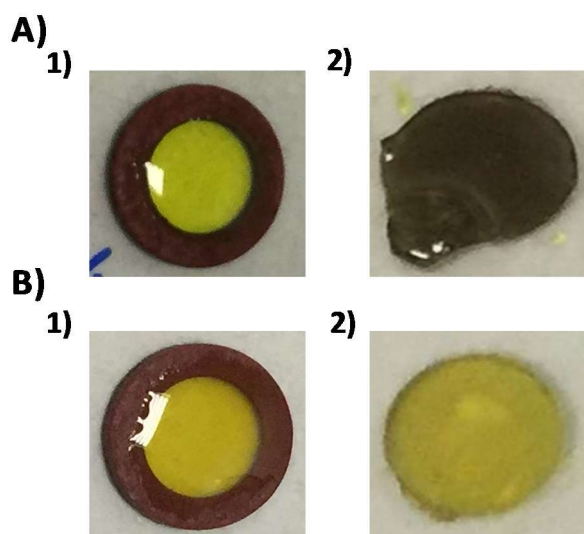


Figure 14 Photos of TMPTA thick film (1.4 mm) upon irradiation with the LED @405 nm for 100 s in the presence of the two-component photoinitiating systems: (A): (1): A/Iod (0.2%/1% w/w) before polymerization; and (2): A/Iod (0.2%/1% w/w) after polymerization; respectively, under air. (B): (1): B/Iod (0.2%/1% w/w) before polymerization; and (2): B/Iod (0.2%/1% w/w) after polymerization; respectively, under air.

In the case of the presence of **1**/Iod as the PIS, the colour changed from fluorescent green (**A1**) to dark olive green (**A2**) leading to a strong inner filter effect during the polymerization. The phenomenon is not observed in the presence of **2**/Iod as the PIS (**B1** and **B2**). Remarkably, a tack free polymer is obtained when using **2** as the PI and exhibits good bleaching properties, while when using **1** as the PI the colour of the obtained polymer remains dark suggesting rather poor bleaching properties during the polymerization. Interestingly, when NPG is introduced in order to regenerate **1** or **2** in a three-component coumarin/Iod/ NPG system, it was possible to obtain again a high performance for FRP in thick samples as demonstrated by the increment of the efficiency to 79% with **1**/Iod/NPG (0.2%/1%/1% w/w) (curve 3, Figure 13) after 24 s of irradiation instead of only 20% with **1**/Iod (curve 1, Fig 13).

Similarly, with **2**, a clear increase of the performance is also noted i.e. a conversion of 87% after 13 s for **2**/Iod/NPG (0.2%/1%/1% w/w) vs. 13% for **2**/Iod (0.2%/1% w/w) (Fig. 4B). In comparison, the two-component system Iod/NPG (1%/1% w/w) shows a good polymerization profile at least with the 405nm LEDs for FRP thick samples (curve 9) but it shows a low rate of polymerization (curve 9) in comparison with those obtained by adding the coumarin derivatives (curve 3 and 7). When using coumarin/amine (such as NPG or EDB) (0.2%/ 1% w/w) systems, no polymerization was observed (curves 2, 4, 6 and 8, Figure 13 and 14). This can be probably ascribed to their low initiating radical yields. This shows that these coumarin derivatives are probably poor photoinitiators in a photoreduction process (electron transfer from NPG or EDB to coumarin) using an amine. Compounds **1** and **2** are more efficient in oxidation processes in combination with Iod.

6.2.4 Free radical photopolymerization of methacrylates (BisGMA/TEGDMA)

In this part, a comparative study of the different coumarin/Iod couples is given for the FRP of a benchmark methacrylate resin (BisGMA/TEGDMA 70%/30% w/w) (Figure 15).

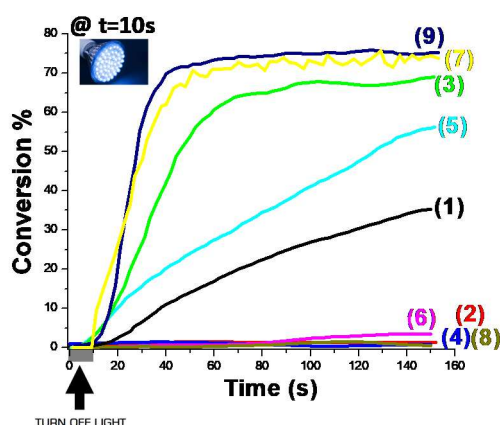


Figure 15 Polymerization profiles (methacrylate function conversion vs. irradiation time) for a BisGMA-TEGDMA blend under air (thickness = 1.4 mm) upon exposure to 405 nm LEDs in the presence of the two and three-component photoinitiating systems: (1) **1**/Iod (0.2%/1% w/w); (2) **1**/NPG (0.2%/1% w/w); (3) **1**/Iod/NPG (0.5%/1%/1% w/w); (4) **1**/EDB (0.2%/1% w/w); (5) **2**/Iod (0.2%/1% w/w); (6) **2**/NPG (0.2%/1% w/w); (7) **2**/Iod/NPG (0.2%/1%/1% w/w); (8) **2**/EDB (0.2%/1% w/w) and (9) Iod/NPG (1%/1% w/w); respectively. The irradiation starts for t = 10 s.

As expected, Iod alone is not able to initiate the polymerization of methacrylates in line with its lack of absorption for $\lambda > 300$ nm, again showing the huge role of these coumarin derivatives for the access to efficient systems. The **2**/Iod two-component PIS shows a noteworthy efficiency: FC ~57% > FC

of **1**/Iod ~36% (curve 5 vs. curve 1, respectively). **2** exhibits superiority over **1**, and this can be probably ascribed to the short oxygen inhibition time for polymerization under air, which is observed for **1** in thick films.

In addition, some photographs of BisGMA/TEGDMA thick films (1.4 mm) upon irradiation with the 405nm LEDs for 150 s in the presence of coumarin/Iod two-component photoinitiating systems under air before and after polymerization were performed (Figure 16).

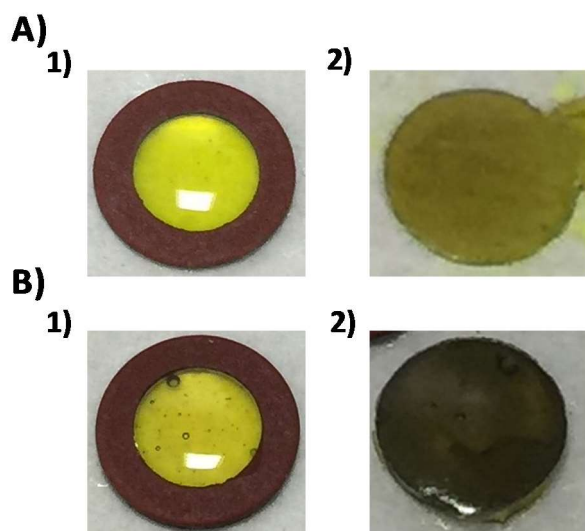


Figure 16 Photos of BisGMA/TEGDMA thick film (1.4 mm) upon irradiation with the LED @405 nm for 150 s in the presence of the two-component photoinitiating systems: a) (1): A/Iod (0.2%/1% w/w) before polymerization; and (2): A/Iod (0.2%/1% w/w) after polymerization; respectively, under air. b) (1): B/Iod (0.2%/1% w/w) before polymerization; and (2): B/Iod (0.2%/1% w/w) after polymerization; respectively, under air.

Remarkably, a tack free polymer is obtained when using **2** as the PI. In both cases, the colour of the obtained polymer remains dark suggesting rather poor bleaching properties during the polymerization. When Iod is replaced by an amine such as NPG or EDB, the coumarin/NPG (or EDB) (0.2%/1% w/w) systems show no efficiency using the 405nm LEDs (curves 2 and 4 for **1** and curves 6 and 8 for **2**, respectively in figure 15). Again, the photo-oxidative process in coumarin/Iod couples shows preponderance over the photo-reductive process in coumarin/ amine (NPG or EDB), for which no polymerization occurs. For the three-component system coumarin/Iod/NPG (0.2%/ 1%/1% w/w), the addition of the amine (NPG) as a hydrogen donor shows rather similar polymerization profiles to those obtained for the two-component system Iod/NPG (1%/1% w/w) (curves 3 for **1** and 7 for **2** vs. curve 9 for Iod/NPG, respectively in figure 15). This trend indicates that the coumarin derivatives are less important for methacrylate polymerization in thick films when using three-component PISs.

6.2.5 3D printing experiments using coumarin/Iod & coumarin/Iod/NPG systems

Some 3D printing experiments upon laser diode irradiation at 405 nm were successfully performed under air using different coumarin/Iod and/or coumarin/Iod/NPG systems in TMPTA, BisGMA/TEGDMA or EPOX/TMPTA (Figure 17).

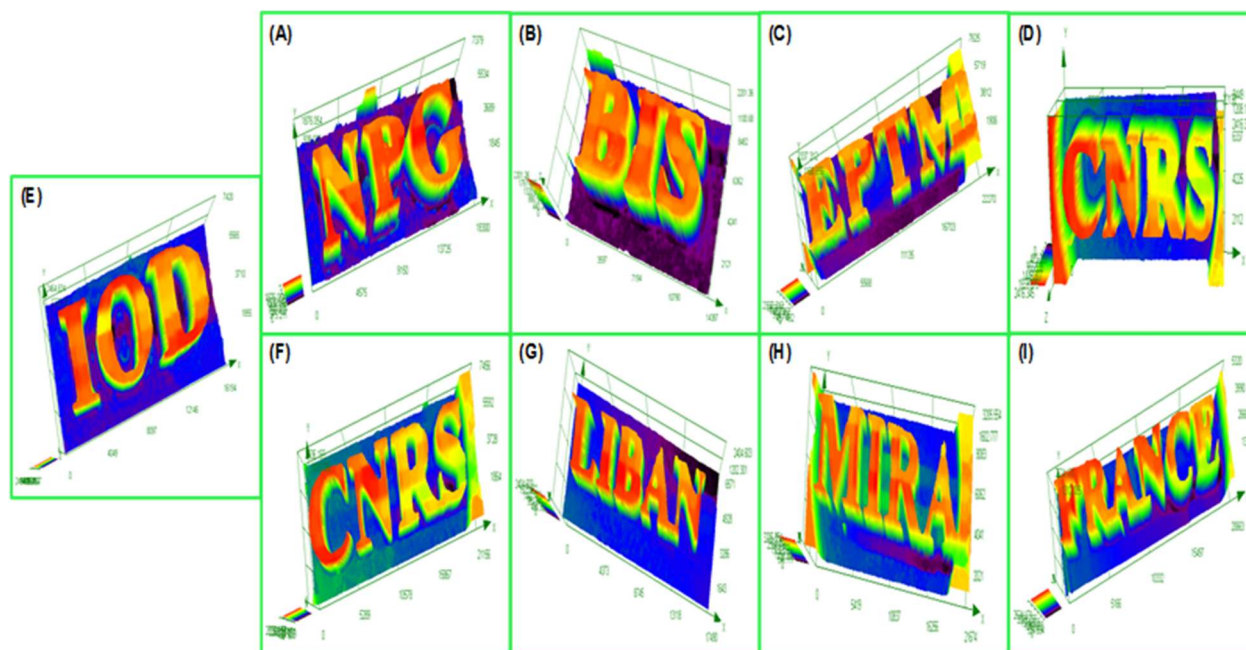


Figure 17. Free radical photopolymerization experiments for 3D printing upon laser diode @405 nm: Characterization of the patterns by numerical optical microscopy; a) ComB/Iod/NPG (0.012%/0.061%/0.061% w/w) in BisGMA/TEGDMA (thickness = 1880 μm); b) 1/Iod/NPG (0.025%/0.125%/0.125% w/w) in BisGMA/TEGDMA (thickness = 2200 μm); c) 1/Iod (0.04%/0.2% w/w) in EPOX/TMPTA (thickness = 2340 μm); d) 1/Iod (0.05%/0.25% w/w) in TMPTA (thickness = 2420 μm); e) 2/Iod (0.015%/0.077% w/w) in BisGMA/TEGDMA (thickness = 2460 μm); f) 1/Iod (0.04%/0.2% w/w) in TMPTA (thickness = 2840 μm); g) 2/Iod/NPG (0.018%/0.091%/0.091% w/w) in TMPTA (thickness = 2400 μm); h) 1/Iod/NPG (0.02%/0.1%/0.1% w/w) in TMPTA (thickness = 3200 μm); and i) 2/Iod (0.05%/0.025% w/w) in TMPTA (thickness = 2620 μm); respectively.

Indeed, the high photosensitivity of these resins (see above) allows an efficient polymerization process in the irradiated area in 3D experiments. Thick polymer samples were obtained with high spatial resolution and a very short writing time (~ 1 min). 3D written patterns are characterized by numerical optical microscopy and excellent spatial resolution (only limited by the size of the laser diode beam: spot of 50 μm).

6.2.6 Photopolymerization in water for hydrogel synthesis using **2**/MDEA

As **2** has shown a good efficiency in radical polymerization and is water soluble, the following section focuses on the use of **2** for the formation of hydrogels which have become very popular due to their unique properties (softness, flexibility and biocompatibility). In this work, the hydrogels were prepared from the photopolymerization of HEA or HEMA in water (50% water/50% HEMA or HEA) upon irradiation with the 405nm LEDs in the presence of **2**/MDEA (0.2%/1% w/w) (Figure 18).



Figure 18 Hydrogels formation using **2**/MDEA system under N₂, upon irradiation with LED @405 nm.

The mixture was first degassed by nitrogen bubbling in order to reduce the oxygen inhibition. Remarkably, **2** is very soluble in water compared to its rather low solubility in organic resins such as TMPTA; interestingly this latter compound is also characterized by very high molar extinction coefficients (ϵ) in water (Fig. S5[†]). This behaviour demonstrates that **2** can be considered as an excellent water soluble photoinitiator for the production of hydrogels. The generated hydrogels were analysed by thermogravimetric analysis (TGA) i.e. the results obtained for **2**/MDEA (0.2%/1% w/w) based hydrogels show a loss of water of 78%.

6.2.7 Near-UV conveyor experiments for access to photocomposites

The current photocomposites were synthesized by impregnation of glass fibers by an organic resin (50% glass fibers/ 50% resin; thickness of the composite ~2 mm) and then irradiation of the sample; BisGMA/TEGDMA (70%/30% w/w) or TMPTA were used as organic resins (Figure 19).



Figure 19 Composite produced upon Near-UV light (LED@395 nm), Belt Speed = 2m/min, using the free radical polymerization (FRP) in the presence of glass fibers/acrylate resin (0.2% **2** + 1% Iod + 1% NPG in TMPTA). Glass fibers: ~ 2mm of thickness for one layer; 50% glass fibers/50% organic resin.

The results show that the coumarin derivatives were able to fully cure the composites; a very fast curing polymerization was observed. In fact, the surface became tack-free after only one pass (for 2 m min⁻¹ belt speed) of irradiation with the LED @395 nm and within one or few passes at the bottom of the sample, using one layer of glass fibers (thickness = 2 mm).

Furthermore, no significant colour changing of the initial composition was observed using coumarin derivatives, but sometimes a brown colour appeared. This behavior demonstrates that the coumarin derivatives exhibit an outstanding reactivity for the production of composite materials with an excellent depth of cure upon near-UV light irradiation.

6.2.8 Chemical mechanisms

Steady state photolysis experiments for the different initiating systems were carried out. The photolysis of **1**/Iod (Figure 20 B) in acetonitrile upon irradiation with a LED @375 nm is very fast compared to that of **1** alone (Figure 20 A).

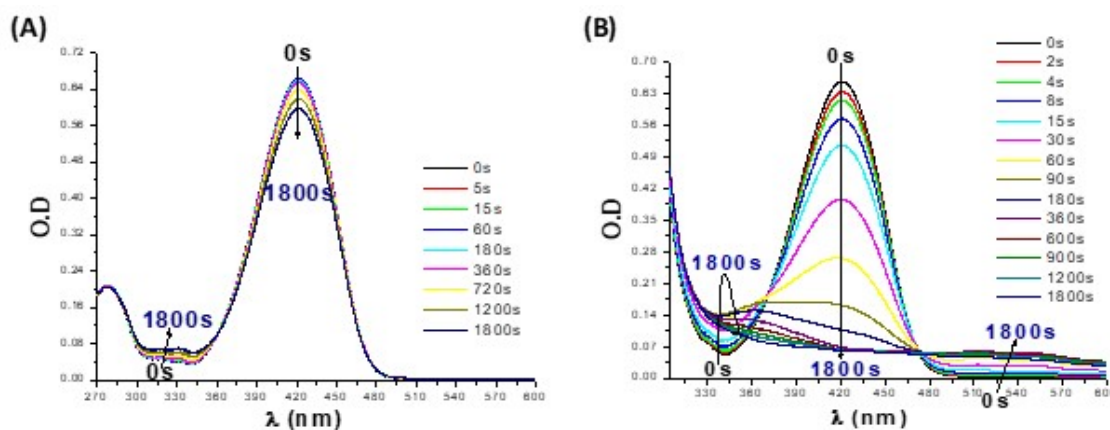


Figure 20 a) Photolysis of **1** in absence of Iod; b) **1**/Iod photolysis.

A new photoproduct (characterized by a significant new absorption for $\lambda > 470$ nm) is formed in any case which, accordingly, is due to the **1**/Iod interaction. Accordingly, it is noteworthy to mention that the photobleaching character is in line with the high reactivity/efficiency of this system in polymerization (Figure 21).

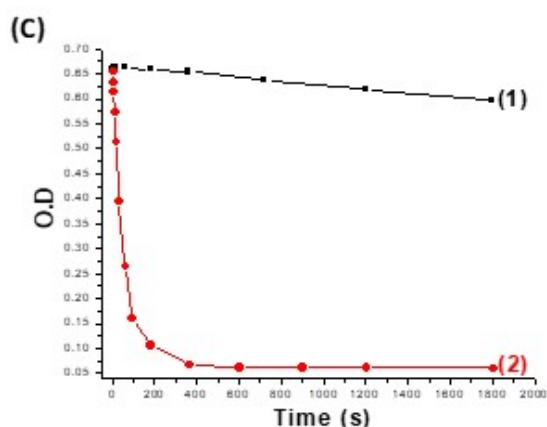


Figure 21 Degradation of **1** without (1) and with (2) Iod vs. irradiation time – upon exposure to the LED @375 nm in ACN.

The degradation of **1** is clear comparing the optical density of the solution with the irradiation time in the presence of Iod (curve 2) and without the addition of Iod (curve 1). The photolysis of **2** in the presence of Iod is also much faster than that for **2** alone also suggesting a strong **2**/Iod interaction. Fluorescence and fluorescence quenching experiments in acetonitrile for the coumarin derivatives are performed (Figure 22)

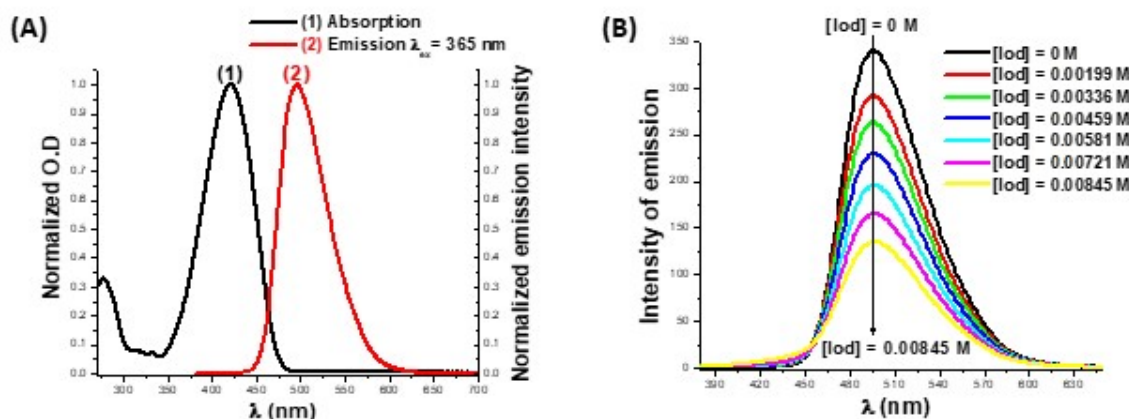


Figure 22: a) Singlet state energy determination in acetonitrile for **1**; b) Fluorescence quenching of **1**/Iod.

The crossing point of the absorption and fluorescence spectra allows the determination of the singlet excited state energy (E_{S1}) of $E_{S1} = 2.68$ V for **1** and 2.72 V for **2** (Figure 23a) in full agreement with the results in table 1.

The free energy changes (ΔG_{et}) for the electron transfer reaction between coumarins as electron donors and Iod as an electron acceptor were calculated from the classical equation (1) (see section 6.4.5) using the oxidation potentials E_{ox} and the excited state energies (E_{S1} or E_{T1}) of coumarins (Table 1).

PI/Iod	E_{ox} (eV)	E_{S1} (eV)	$\Delta G_{et(S1)}$ (Coumarin/Iod) (eV)	E_{T1} (eV)	$\Delta G_{et(T1)}$ (Coumarin/Iod) (eV)
1 /Iod	0.81	2.68	-1.67	1.81	-0.8
2 /Iod	0.8	2.72	-1.72	1.56	-0.56

Table 1 Parameters characterizing the chemical mechanisms associated with **1**/Iod and **2**/Iod in acetonitrile.

Favourable ¹**1** (or ¹**2**)/Iod fluorescence quenching processes were shown to be in full agreement with highly favorable ΔG_{et} (-1.67 eV and -1.72 eV, respectively). A triplet state pathway cannot be ruled out (triplet state energy (ET_1) calculated from molecular orbital calculations (uB3LYP/6-31G* level of theory) in fact the free energy changes ($\Delta G_{et}(T_1)$) for ³coumarin/Iod are also favourable (-0.80 eV for **1** and -0.56 eV for **2**).

A global mechanism for the photoinitiated polymerization was proposed (Figure 23).

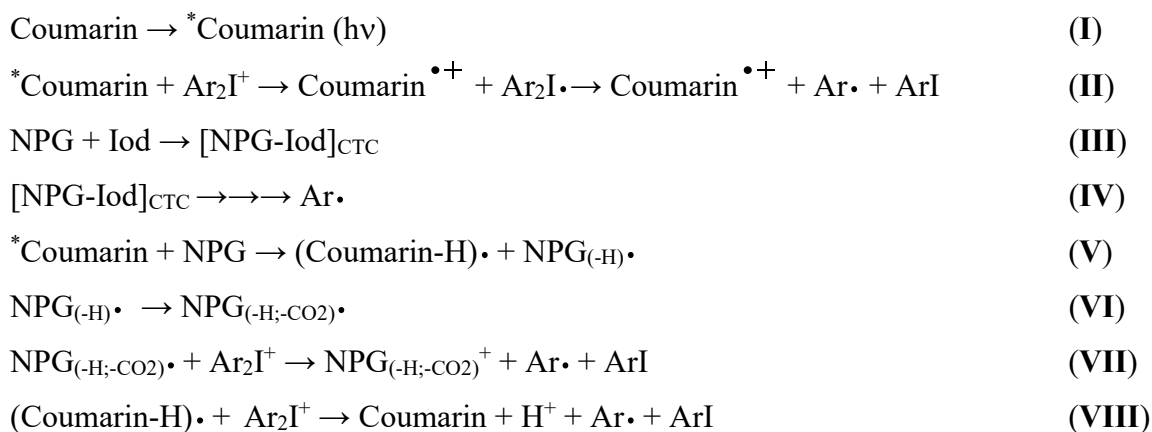


Figure 23 Proposed chemical mechanisms for photoinitiated polymerization by **1** or **2**.

A coumarin/Iod interaction is proposed to occur by irradiation of coumarin (I) through the classical¹⁷ reduction of the iodonium salt (II), confirmed by Electron Spin Resonance (ESR) results.¹⁸ The aryl radicals are excellent initiating species for addition onto a (meth)acrylate double bond ($k_{\text{add}} = 10^8 \text{ M}^{-1} \text{ s}^{-1}$)¹⁹ in full agreement with the good efficiency of the coumarin/Iod couples. Finally, it is proposed that NPG which is an N-aromatic electron donor can form a charge transfer complex (CTC) with an electron poor iodonium salt (III) similar to what was very recently published.²⁰ This [NPG-Iod]CTC structure is quite convenient as it provides enhanced visible light absorption to the photoinitiating system, and the photolysis at 405 nm leads to an efficient release of Ar• radicals (IV) as confirmed by the photopolymerization study (curve 9 in Figure 12 and 13). The coumarin/NPG interaction can correspond to an electron/proton transfer reaction (V). Then, a proposed decarboxylation reaction in NPG (VI) leading to $\text{NPG}_{(-\text{H};-\text{CO}_2)}\cdot$ is responsible for avoiding any back electron transfer reaction. $\text{NPG}_{(-\text{H};-\text{CO}_2)}\cdot$ can be considered as the initiating species for the free radical polymerization in coumarin/ NPG systems even if this process is not very efficient. For the three-component system, VII and VIII presumably occur as in other previously studied dye/amine/iodonium salt systems. Therefore, $\text{NPG}_{(-\text{H};-\text{CO}_2)}\cdot$, Ar• and coumarin^{•+}, and $\text{NPG}_{(-\text{H};-\text{CO}_2)}^+$ can be considered as the initiating species for FRP and for CP, respectively.

6.2.9 Coumarin derivatives as Photoredox Catalysts in Three-Component System

The 1/Iod/NPG three-component PIS works through mainly an oxidative cycle as the coumarin/Iod interaction is much more efficient than the coumarin/amine interaction (Figure 24).

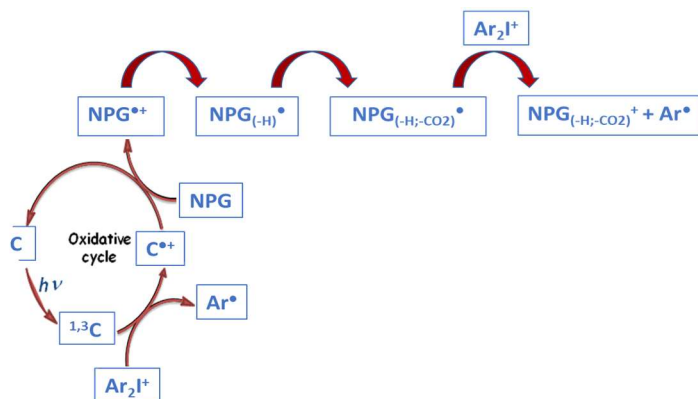


Figure 24 Proposed oxidative cycle for Coum/Iod/NPG systems.

First, the coumarin reacts with the iodonium salt ArI^+ to form its oxidized form $C^{\bullet+}$ that can later react with the NPG to be regenerated through a photoredox catalytic cycle. The concomitant regeneration of coumarins ensures a photoredox catalyst behaviour in line with the observed improved efficiency of the polymerization (coumarin/Iod/NPG better than coumarin/Iod). This behaviour is also observed in steady state photolysis (Figure 25).

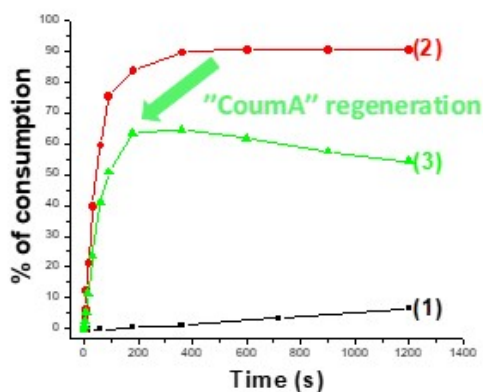


Figure 25 Consumption of 1 (A (1) without Iod salt; (2) with Iod salt; and (3) with Iod salt + NPG, vs. time of irradiation with LED@375 nm.

The consumption of coumarin achieved with three-component PISs of 54% of the coumarin/Iod/NPG system (curve 3) is lower than that achieved when using two-component PISs based on coumarin/Iod combinations (90%, curve 2) showing a partial regeneration of the coumarin.

6.3 Conclusions

In this chapter, coumarin derivatives **1** and **2** are proposed for the development of new high performance photoinitiators/photoredox catalysts for the photoinitiation of both the cationic polymerization of epoxides and the free radical polymerization of (meth) acrylates upon violet and blue LEDs irradiation. Both high final conversions and polymerization rates are achieved. These coumarin derivatives are efficient photoredox catalysts because these compounds combine suitable oxidation potentials at the excited state, highly favourable free energy changes ΔG_{et} and good absorbance under Violet LEDs exposure. The high performance of these coumarin derivatives (**1** and **2**) in initiating systems is also shown for new photosensitive 3D printing resins upon exposure to a laser diode. One of these new photoinitiators (**2**) was also successfully used for the preparation of hydrogels due to its high solubility in water. These new initiating systems were also used for the synthesis of photocomposites. The developments of high-performance photosensitive systems in water will be investigated in future.

6.4 Experimental procedures

6.4.1 Synthesis of **1** and **2**

The procedure for the synthesis of **1** and **2** is reported in section 2.2.2.

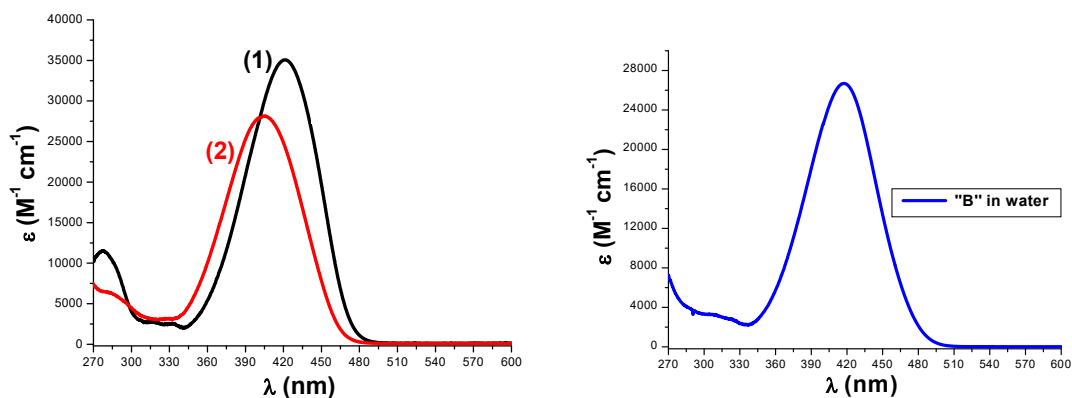


Figure 26 Absorbtion of coumarins **1** and **2** in CH_3CN ; b) Absorption of coumarin **2** in water

6.4.2 Other chemical compounds

All the other chemical compounds were selected with highest purity available and used as received. Di-*tert*-butyl-diphenyl iodonium hexafluorophosphate (Iod or SpeedCure 938) was obtained from Lambson Ltd. *N*-Methyldiethanolamine (MDEA) was obtained from Alfa Aesar. *N*-Phenylglycine (NPG), ethyl-4-(dimethylamino)benzoate (EDB), bisphenol *A*-glycidyl methacrylate (BisGMA), triethyleneglycol dimethacrylate (TEGDMA) and 2-(hydroxyethyl) acrylate (HEA) were obtained from Sigma Aldrich. 2-(Hydroxyethyl) methacrylate (HEMA) was obtained from Tokyo Chemical Industry. (3,4-Epoxy cyclohexane)methyl 3,4-

Chapter 6: Use of coumarins in photoredox polymerization processes

epoxycyclohexylcarboxylate (EPOX; Uvacure 1500) and trimethylolpropane triacrylate (TMPTA) were obtained from Allnex. TMPTA (or BisGMA/TEGDMA) and EPOX were selected as benchmarked resins for radical and cationic polymerization, respectively.

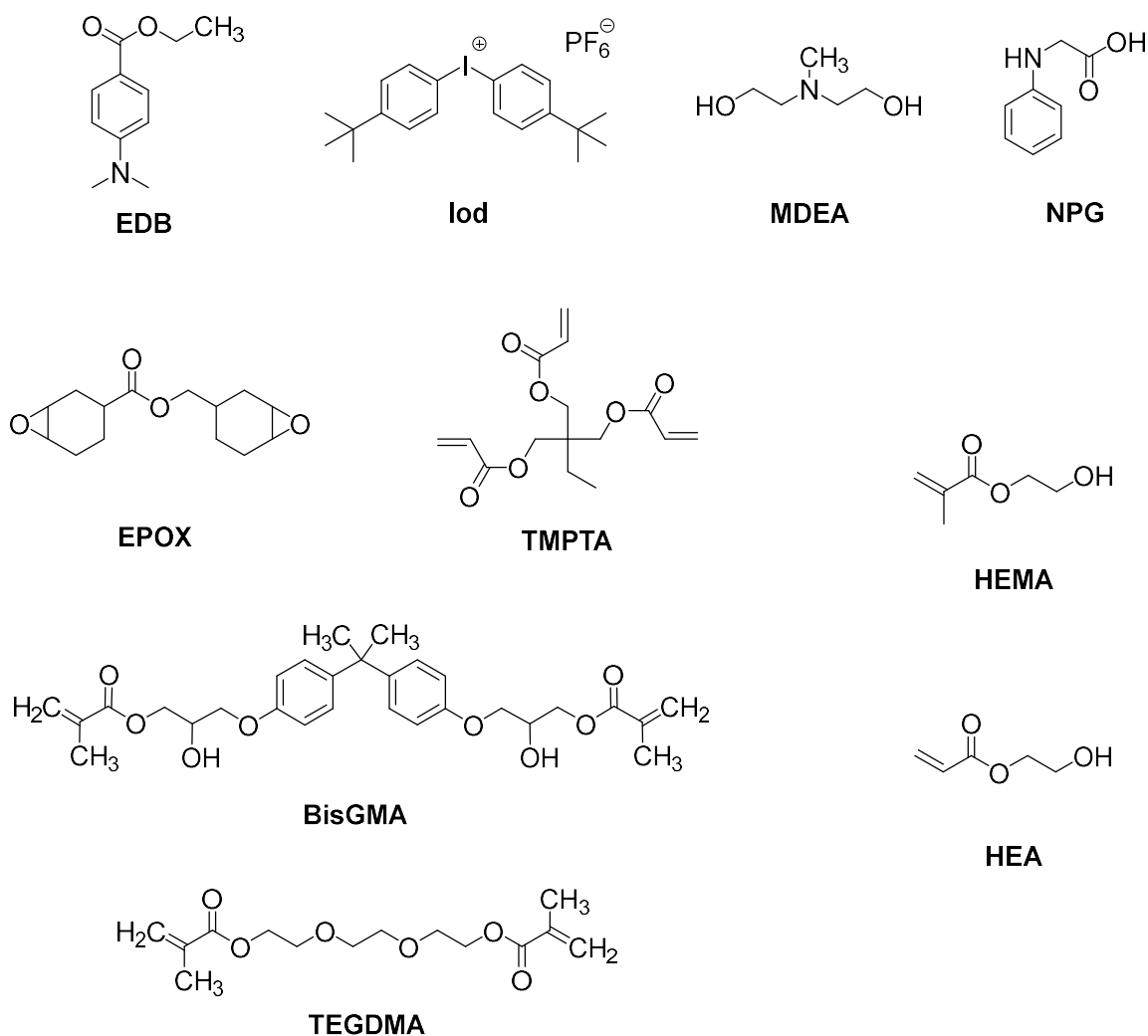


Figure 28 Other used chemical compounds.

6.4.3 Irradiation Sources

The following Light Emitting Diodes (LEDs) were used as irradiation sources: i) LED @375 nm with an incident light intensity at the sample surface: $I_0 = 40 \text{ mW}\cdot\text{cm}^{-2}$; ii) LED @405 nm; $I_0 = 110 \text{ mW}\cdot\text{cm}^{-2}$; iii) LED projector @405 nm for 3D printing; $I = 100\text{-}130 \text{ mW}\cdot\text{cm}^{-2}$.

6.4.4 Cationic Photopolymerization (CP) and Free Radical Photopolymerization (FRP)

The two-component photoinitiating systems (PISs) are mainly based on coumarin/iodonium salt or coumarin/amine (NPG or EDB) [(0.2%/1% w/w) or (0.5%/1% w/w)] for FRP and/or CP. The three-component photoinitiating systems (PISs) are mainly based on coumarin/iodonium salt/NPG [(0.2%/1%/1% w/w)] for FRP. The weight percent of the different chemical compounds of the photoinitiating system is calculated from the monomer content (w/w). The photosensitive thin formulations (~25 μm of thickness) were deposited on a BaF_2 pellet under air for the CP of EPOX, while for the FRP of TMPTA it was done in laminate (the formulation is sandwiched between two polypropylene films to reduce the O_2 inhibition). The 1.4 mm thick samples of (meth)acrylates were also polymerized under air into a rounded plastic mold of ~7 mm diameter and 1.4 mm of thickness. For thin samples, the evolution of the

Chapter 6: Use of coumarins in photoredox polymerization processes

epoxy group content of EPOX and the double bond content of acrylate functions were continuously followed by real time FTIR spectroscopy (JASCO FTIR 4100) at about 790 and 1630 cm^{-1} , respectively. The evolution of the (meth)acrylate characteristic peak for the thick samples (1.4 mm) was followed in the near-infrared range at $\sim 6160 \text{ cm}^{-1}$. The procedure used to monitor the photopolymerization profiles has been described in detail.²¹

6.4.5 Redox Potentials

The redox potentials for **1** and **2** (E_{ox} and E_{red}) were measured in acetonitrile by cyclic voltammetry with tetrabutylammonium hexafluorophosphate (0.1 M) as the supporting electrolyte (potential vs. Saturated Calomel Electrode). The free energy change ΔG_{et} for an electron transfer reaction was calculated from equation (Equation 1)²² where E_{ox} , E_{red} , E_{S} , and C are the oxidation potential of the electron donor, the reduction potential of the electron acceptor, the excited state energy level (determined from luminescence experiments) and the Coulombic term for the initially formed ion pair, respectively. C is neglected as usually done in polar solvents (Equation 1).

$$\Delta G_{\text{et}} = E_{\text{ox}} - E_{\text{red}} - E_{\text{S}} + C$$

6.4.6 ESR Spin-Trapping (ESR-ST) Experiments

The ESR-ST experiments were carried out using an X-Band spectrometer (Magnettech MS400). A 405 nm LEDs was used as irradiation source for triggering the production of radicals at room temperature (RT) under N_2 in *tert*-butylbenzene and trapped by phenyl-*N-tert*-butylnitron (PBN) according to a procedure described in literature.²³ The ESR spectra simulations were carried out with the PEST WINSIM program.

6.4.7 UV-Visible absorption and Photolysis Experiments

The UV-Visible absorbance properties of the compounds as well as the steady state photolysis experiments were studied using JASCO V730 UV-visible spectrometer.

6.4.8 Fluorescence Experiments

The fluorescence properties of the compounds were studied using a JASCO FP-6200 spectrofluorimeter.

6.4.9 Computational Procedure

Molecular orbital calculations were carried out with the Gaussian 03 suite of programs.²⁴ The electronic absorption spectra for the different compounds were calculated with the time-dependent density functional theory at the MPW1PW91-FC/6-31G* level of theory on the relaxed geometries calculated at the UB3LYP/6-31G* level of theory. The triplet state energy levels were calculated at this level of theory.

6.4.10 3D Printing Experiments

For 3D printing experiments, a laser diode @405 nm (spot size around 50 μm) and also a LED projector @405 nm (Thorlabs) were used for the spatially controlled irradiation. Rather similar intensities on the surface of the sample and similar emission spectrum for the laser diode or the LED used in 3D printing and the RT-FTIR kinetic experiments were used for sake of comparison. The photosensitive resin (various thickness) was polymerized under air and the generated patterns were analyzed by a numerical optical microscope (DSX-HRSU from OLYMPUS Corporation).²⁵

6.4.11 Hydrogel formation

The formation of hydrogels was carried out in 50% water/50% HEMA (or HEA) in which the water soluble photoinitiating system was added (**2** with an amine such as *N*-methyldiethanolamine MDEA). A LED @405 nm was used as irradiation source for the formation

Chapter 6: Use of coumarins in photoredox polymerization processes

of hydrogels in the absence of air, at room temperature (RT) after degassing the mixture with nitrogen. The generated hydrogels were analyzed by thermogravimetric analysis (TGA).

6.4.12 Near-UV conveyor

The Dymax-UV conveyor was used to cure composites. The glass fibers were impregnated with the organic resin (50/50 w/w%) and then irradiated. The UV conveyor is equipped with a 120 mm wide Teflon-coated belt and one UV lamp (mercury-Fe doped lamp). The distance between the lamp and the belt can be manually adjusted (fixed at 15 mm) as can the belt speed (fixed at 2 m.min⁻¹). LED@395nm is another source of light used as alternative (4W/cm²).

References

- ¹ a) P. Glöckner, *Radiation Curing: Coatings and Printing Inks ; Technical Basics, Applications and Trouble Shooting*, Vincentz Network, 2008; b) J. P. Fouassier, J. F. Rabek, *Radiation Curing in Polymer Science and Technology*, Springer Science & Business Media, 1993.
- ² Y. Tsujii, K. Ohno, S. Yamamoto, A. Goto and T. Fukuda, *Adv. Polym. Sci.*, 2006, **197**, 1.
- ³ Y.-L. Zhang, Q.-D. Chen, H. Xia and H.-B. Sun, *Nano Today*, 2010, **5**, 435.
- ⁴ a) B. D. Gates, Q. Xu, M. Stewart, D. Ryan, C. G. Willson and G. M. Whitesides, *Chem. Rev.* 2005, **105**, 1171; b) L. J. Guo, *Adv. Mater.*, 2007, **19**, 495; c) B.-J. de Gans, P. C. Duineveld, U. S. Schubert, *Adv. Mater.*, 2004, **16**, 203.
- ⁵ A. Ibrahim, L. D. Stefano, O. Tarzi, H. Tar, C. Ley and X. Allonas, *Photochem. Photobiol.*, 2013, **89**, 1283.
- ⁶ R. Bachelot, C. Ecoffet, D. Deloail, P. Royer and D.-J. Lougnot, *Appl. Opt.*, 2001, **40**, 5860.
- ⁷ N. Moszner and U. Salz, *Macromol. Mater. Eng.*, 2007, **292**, 245.
- ⁸ a) Y. Yagci, S. Jockusch and N. J. Turro, *Macromolecules*, 2010, **43**, 6245; b) J. L. Ifkovits and J. A. Burdick, *Tissue Eng.*, 2007, **13**, 2369.
- ⁹ a) J. P. Fouassier and J. Lalevée, *Photoinitiators for Polymer Synthesis*, Wiley-VCH, 2012; b) M. G. Ivan and J. C. Scaiano, *Photoimaging and lithographic processes in polymers*, John Wiley & Sons, Inc., 2010.
- ¹⁰ J.-P. Fouassier and J. Lalevée, *RSC Adv.* 2012, **2**, 2621.
- ¹¹ B. M. Monroe and G. C. Weed, *Chem. Rev.*, 1993, **93**, 435.
- ¹² H. J. Avens and C. N. Bowman, *J. Polym. Sci., Part A: Polym. Chem.*, 2009, **47**, 6083.
- ¹³ a) K. S. Padon and A. B. Scranton, *J. Polym. Sci., Part A: Polym. Chem.*, 2000, **38**, 2057; b) D. Kim, A. B. Scranton and J. W. Stansbury, *J. Appl. Polym. Sci.*, 2009, **114**, 1535.
- ¹⁴ A. Aguirre-Soto, C.-H. Lim, A. T. Hwang, C. B. Musgrave and J. W. Stansbury, *J. Am. Chem. Soc.*, 2014, **136**, 7418.
- ¹⁵ a) X. Pan, C. Fang, M. Fantin, N. Malhotra, W. Y. So, L. A. Peteanu, A. A. Isse, A. Gennaro, P. Liu and K. Matyjaszewski, *J. Am. Chem. Soc.*, 2016, **138**, 2411. b) M.-A. Tehfe, J. Lalevée, F. Morlet-Savary, B. Graff, N. Blanchard and J.-P. Fouassier, *ACS Macro Lett.*, 2012, **1**, 198. c) M.-A. Tehfe, F. Dumur, E. Contal, B. Graff, D. Gigmes, J.-P. Fouassier and J. Lalevée, *Macromol. Chem. Phys.*, 2013, **214**, 2189. d) M.-A. Tehfe, F. Dumur, B. Graff, F. Morlet-Savary, J.-P. Fouassier, D. Gigmes and J. Lalevée, *Macromolecules*, 2012, **45**, 8639. e) S. Telitel, F. Dumur, T. Faury, B. Graff, M.-A. Tehfe, D. Gigmes, J.-P. Fouassier and J. Lalevée, *Beilstein J. Org. Chem.*, 2013, **9**, 877, No. 101. f) M.-A. Tehfe, J. Lalevée, F. Morlet-Savary, B. Graff, N. Blanchard and J.-P. Fouassier, *Macromolecules*, 2012, **45**, 1746.
- ¹⁶ M.-A. Tehfe, F. Dumur, E. Contal, B. Graff, D. Gigmes, J.-P. Fouassier and J. Lalevée, *Macromol. Chem. Phys.*, 2013, **214**, 2189.
- ¹⁷ N. Zivic, M. Bouzrati-Zerelli, A. Kermagoret, F. Dumur, J.-P. Fouassier, D. Gigmes and J. Lalevée, *ChemCatChem*, 2016, **8**, 1617.
- ¹⁸ Indeed, spin trapping experiments using phenyl-N-tert-butyl nitron (PBN) is an efficient technique to characterize the generated radicals. In agreement with (r2), the irradiation of a **1** (or **2**) solution in the presence of Iod and PBN generates aryl (Ar•)/PBN radical adducts which are easily detected in ESR-ST experiments and characterized by hyperfine coupling constants (hfcs): aN = 14.3 G and aH = 2.2 G in full agreement with reported data.²⁵

- ¹⁹ J.-P. Fouassier and J. Lalevee, *Photoinitiators for Polymer Synthesis, Scope, Reactivity, and Efficiency*, Wiley-VCH Verlag GmbH & Co.KGaA, Weinheim, 2012.
- ²⁰ P. Garra, B. Graff, F. Morlet-Savary, C. Dietlin, J. M. Becht, J.-P. Fouassier and J. Lalevée, *Macromolecules*, 2018, **51**, 57.
- ²¹ a) C. Dietlin, S. Schweizer, P. Xiao, J. Zhang, F. Morlet-Savary, B. Graff, J. P. Fouassier and J. Lalevée, *Polym. Chem.*, 2015, **6**, 3895. b) J. Lalevée, N. Blanchard, M. A. Tehfe, F. Morlet-Savary and J. P. Fouassier, *Macromolecules*, 2010, **43**, 10191. c) J. Lalevée, N. Blanchard, M. A. Tehfe, M. Peter, F. Morlet-Savary, D. Gigmes and J. P. Fouassier, *Polym. Chem.*, 2011, **2**, 1986.
- ²² D. Rehm and A. Weller, *Isr. J. Chem.*, 1970, **8**, 259.
- ²³ a) J. Lalevée, N. Blanchard, M. A. Tehfe, F. Morlet-Savary and J. P. Fouassier, *Macromolecules*, 2010, **43**, 10191. b) J. Lalevée, N. Blanchard, M. A. Tehfe, M. Peter, F. Morlet-Savary, D. Gigmes and J. P. Fouassier, *Polym. Chem.*, 2011, **2**, 1986.
- ²⁴ a) J. B. Foresman and A. Frisch, *Exploring Chemistry with Electronic Structure Methods*, Gaussian Inc., Pittsburgh, PA, 2nd edn, 1996. b) M. J. Frisch, G. W. Trucks, H. B. Schlegel, G. E. Scuseria, M. A. Robb, J. R. Cheeseman, V. G. Zakrzewski, J. A. Montgomery, J. R. E. Stratmann, J. C. Burant, S. Dapprich, J. M. Millam, A. D. Daniels, K. N. Kudin, M. C. Strain, O. Farkas, J. Tomasi, V. Barone, M. Cossi, R. Cammi, B. Mennucci, C. Pomelli, C. Adamo, S. Clifford, J. Ochterski, G. A. Petersson, P. Y. Ayala, Q. Cui, K. Morokuma, P. Salvador, J. J. Dannenberg, D. K. Malick, A. D. Rabuck, K. Raghavachari, J. B. Foresman, J. Cioslowski, J. V. Ortiz, A. G. Baboul, B. B. Stefanov, G. Liu, A. Liashenko, P. Piskorz, I. Komaromi, R. Gomperts, R. L. Martin, D. J. Fox, T. Keith, M. A. Al-Laham, C. Y. Peng, A. Nanayakkara, M. Challacombe, P. M. W. Gill, B. Johnson, W. Chen, W. M. Wong, J. L. Andres, C. Gonzalez, M. Head-Gordon, E. S. Replogle and J. A. Pople, *Gaussian 03, Revision B-2*, Gaussian Inc., Pittsburgh, PA, 2003.
- ²⁵ a) J. Zhang, F. Dumur, P. Xiao, B. Graff, D. Bardelang, D. Gigmes, J.-P. Fouassier and J. Lalevee, *Macromolecules*, 2015, **48**, 2054. b) P. Xiao, F. Dumur, J. Zhang, J.-P. Fouassier, D. Gigmes and J. Lalevee, *Macromolecules*, 2014, **47**, 3837.

Use of coumarin dyes in biological applications

7.1 Introduction

7.1.1 Development of new LSS dyes for biological application

In the last years, researchers from academia and industry have driven their attention towards the synthesis of new coumarin dyes for use in bioanalytical assays. The use of fluorescent detection in immunoassays provides high reproducibility and sensitivity, allowing early and more accurate diagnosis. Furthermore, the ability of detecting multiple analytes in a single diagnostic test has become of great importance and relevance. In particular, combinations of dyes with different spectroscopic properties such as excitation and emission maxima allows the “multiplex” technology on instruments equipped with multiple excitation sources and detection channels (Table 1).

Laser source	350 nm	405 nm	488 nm	561 nm	633 nm
Fluorescent dye	Alexa Fluor 350 $\lambda_{em} = 450$ nm	V450 $\lambda_{em} = 450$ nm V500 $\lambda_{em} = 500$ nm BV605 $\lambda_{em} = 600$ nm	FITC $\lambda_{em} = 530$ nm PE $\lambda_{em} = 600$ nm PE-Cy5 $\lambda_{em} = 700$ nm	Alexa Fluor 555 $\lambda_{em} = 580$ nm Cy3 $\lambda_{em} = 570$ nm Cy3.5 $\lambda_{em} = 590$ nm	APC $\lambda_{em} = 570$ nm APC-Cy7 $\lambda_{em} = 700$ nm Cy5 $\lambda_{em} = 670$ nm

Table 1 List of laser sources and examples of commercially available dyes for multiplex assays.

Multiple fluorophores may be excited by a single excitation source and their emission can be detected in various detection channels. For example, dyes with different emission maxima such as ®V450, ®V500 and ®BV605 fit with the violet laser (405 nm) excitation source but are detected in different filter channels and can therefore be used together in a single analysis.

An interesting region of the light spectrum that has gained much attention over the last years is the low wavelength spectral region (350-500nm). Cyanagen has recently patented and commercialized a LSS coumarin dye excitable by the violet laser (405 nm) with an emission maximum at 518 nm for the labeling of antibodies¹ (Figure 1).

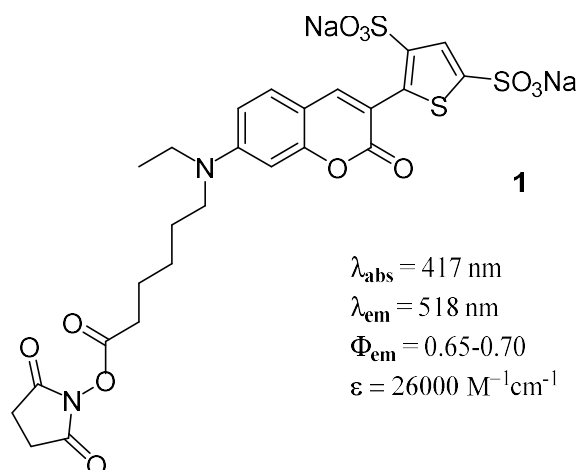


Figure 1 Molecular structure and photophysical properties of compound **1**.

The required features for use in bioconjugation techniques are the presence in coumarin **1** of an amine-reactive ester (NHS ester), linked to the coumarin in the C7 position, and high water-solubility, provided by the sulfonate groups on the thienyl ring.

Thanks to their extensive use in biological applications, the development of a library of new LSS dyes in the ultra violet/violet and blue region, has become of great interest.

The coumarin fragment is one of the most popular fluorophores used in LSS dyes excitable by the UV, violet and blue laser diode. For example, Pacific Blue™ and Alexa® Fluor 350 are notable examples (Figure 2).

Pacific Blue™ is a member of the group of Pacific dyes, which include Pacific Orange™, Green™ and Blue™, with an absorption maximum between 400 and 410 nm. The different emission spectra of 455 nm, 500 nm and 551 nm, respectively allows their use in a simultaneous analysis. Alexa® Fluor 350 shows a UV-shifted absorption and emission maxima and is largely employed in the 350 nm excitation region.

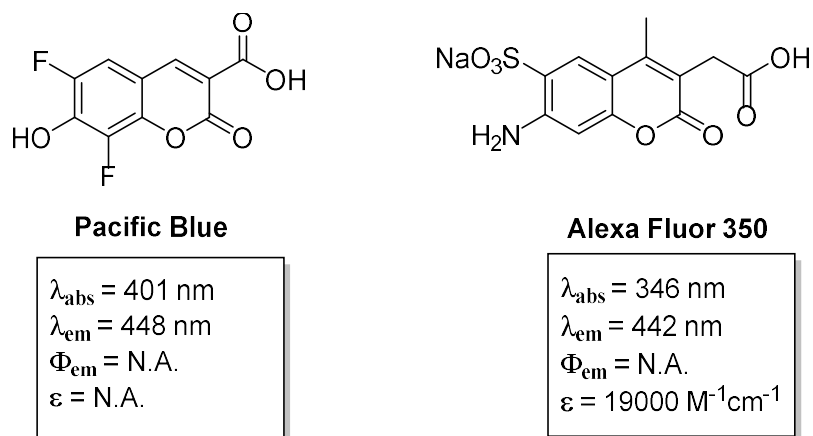


Figure 2 Molecular structure of Pacific Blue™ and Alexa® 350.

Based on literature, a general outline for the development of a new library of LSS dyes is proposed. The addition of the substituents onto the coumarin framework leads to the modification of the photophysical properties² (Figure 3).

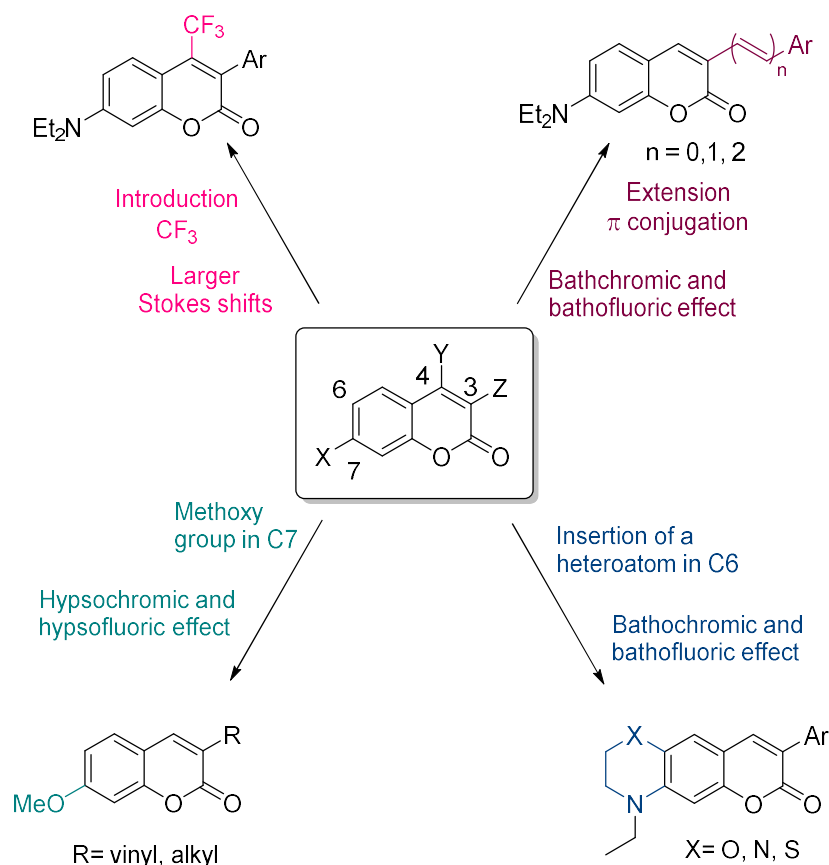


Figure 3 Guideline for the modification of the photophysical properties in coumarin dyes.

LSS coumarin dyes are mostly characterized by the presence of an electron donating group in the C7 position. The largest part of them belongs to the class of 7-amino coumarins. The presence of electron withdrawing groups, generally an aryl, in position C3 provides dyes with large Stokes shifts (>50 nm) with an absorption in the violet region (<450 nm). The extension of the π-system strongly red shifts the absorption and the emission band as in the case of DY485-XL (Figure 4) developed by Czerney *et al.*³ The same effect was obtained by the introduction in position C6 of a heteroatom as demonstrated by the compounds **2a** and **2b** (Figure 4).⁴ Furthermore, the presence of a very strong acceptor in position C4, such as a CF₃- group, increases the “push and pull” effect. The coumarin **3** exhibits a very large Stokes shift of 175 nm.⁵ Finally, the replacement of the amino group in C-7 with hydroxy- or alkoxy- groups leads to an hypso-chromic and hypso-fluoric shift of the absorption and emission bands with respect to the corresponding 7-amino substituted⁶ ones, as observed in coumarin **4** (Figure 4).

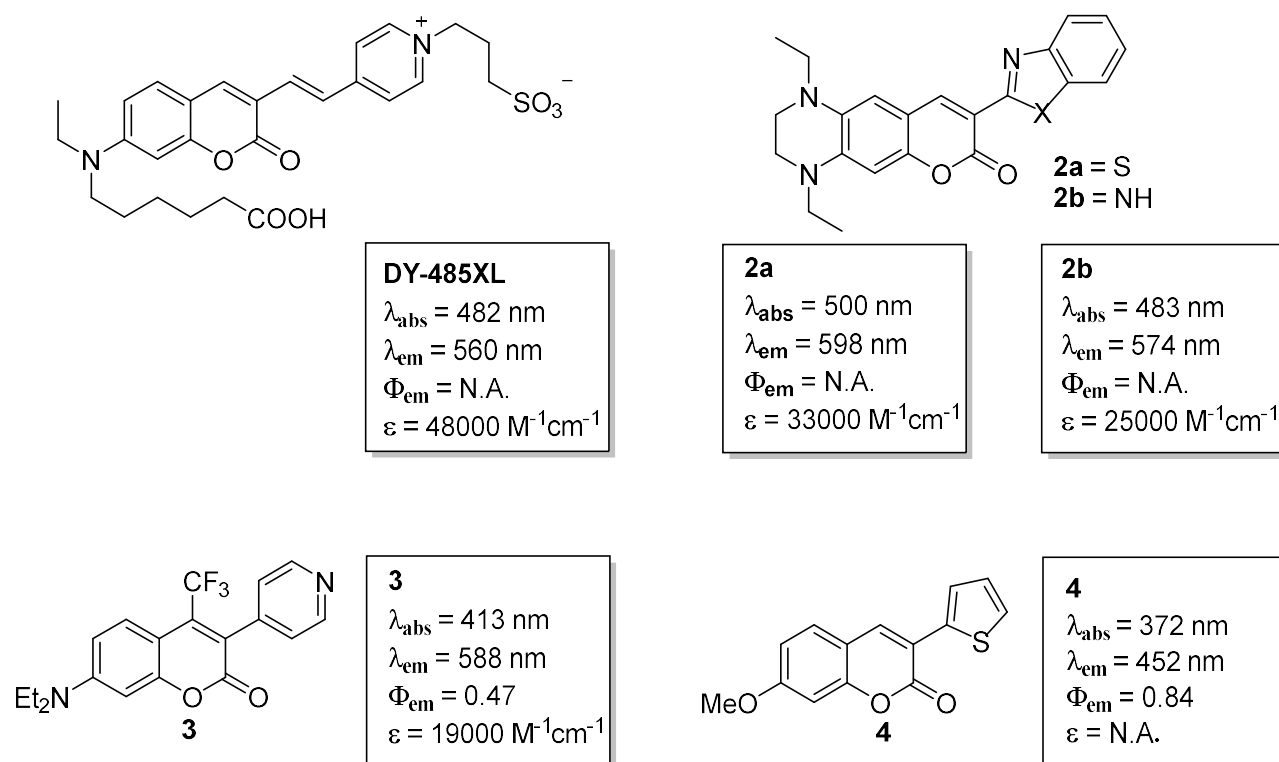


Figure 4 Molecular structures and photophysical properties of **DY-485XL** and coumarins **2**, **3** and **4**.

Within the biological applications of LSS coumarin dyes, fluorescent microscopy has been recognized as one of the most versatile optical imaging methods exploited in new innovative techniques including expansion microscopy and optical tissue clearing. Among the various uses, ranging from biology to medicine, fluorescent microscopy is employed for the visualization of cell staining, a technique which provide a wide variety of information on cells and cell components, priory stained with a fluorophore. In this view, DND 22, DND 26 and Green FM represent three examples of fluorophores used in the specific staining of lysosomes and mitochondria (Figure 5).

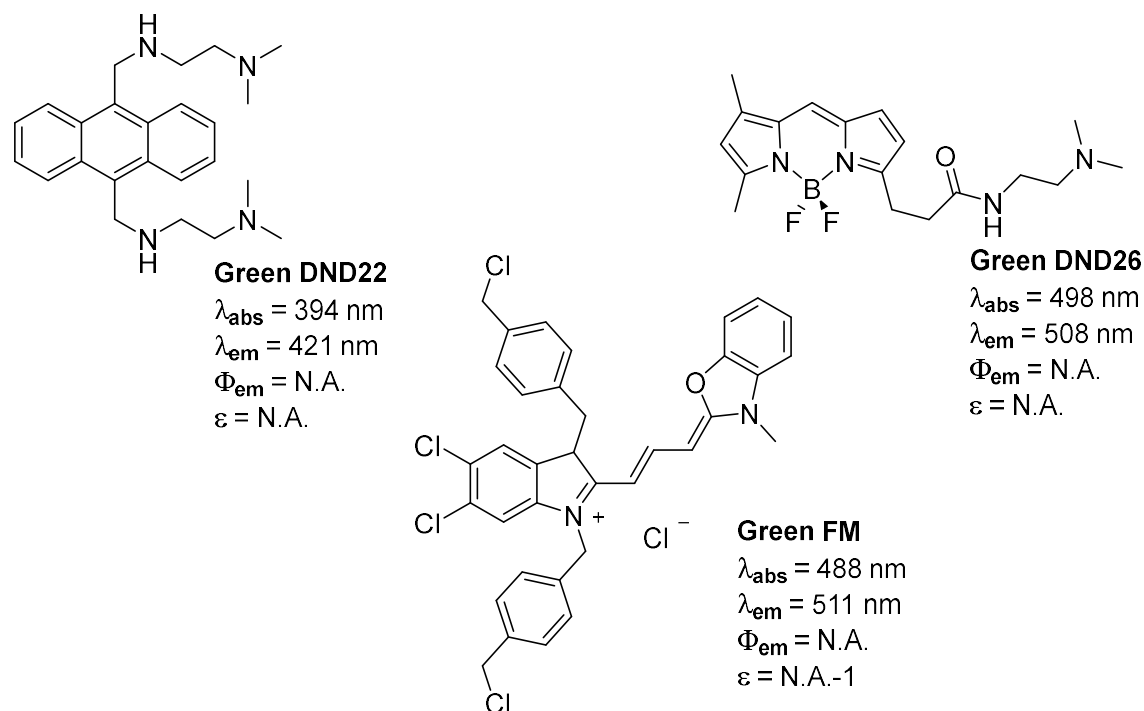


Figure 5 Molecular structures and photophysical properties of Green DND22, Green FM, Green DND26.

Lysosomal stains consist of a fluorophore linked to a weak tertiary amine base. These dyes are freely permeant to cell membranes and selectively accumulates in lysosomes probably via the lysosome pH gradient. Thanks to the pK_a of 5-6, morpholine represent a new tool for the targeting of lysosomes (pH 4-5).⁷ In case of Green FM a mitochondrial stain, which in general are mono-cationic hydrophobic dyes, exploit the mitochondrial membrane potential and permanently label a thiol reactive group on the mitochondria through reaction with the aryl halomethyl functionality. In this chapter, the selection of a library of new LSS dyes excitable by the UV, violet and blue lasers using different synthetical methodologies will be discussed. Furthermore, the design, synthesis and application in fluorescent microscopy of specific stains for lysosomes and mitochondria, based on 3-thyenyil coumarin derivatives, will be investigated.

7.2 Results and discussion

7.2.1 Development of a library of LSS coumarins

Diverse chemical strategies may be exploited towards the synthesis of LSS coumarin dyes as showed in figure 3. Some of these will be highlighted in our attempts to develop new and interesting LSS coumarins that may find application in various biological fields.

7.2.2 Extension of the π -system in the C3 position

First, extension of the π -system in the C3 position was investigated with the aim of red shifting the absorption and emission bands towards the blue/green region (480-530 nm circa).

Synthesis of new 7-dialkylamino-3-aryl coumarins (Figure 3, $n = 0$) as well as more elongated styryl systems (Figure 3, $n = 1$) with absorption profiles in the blue/green spectral region were investigated. The former may be addressed by straightforward Knoevenagel type condensations with suitable acetic acid substituted aromatic compounds, while the latter may be obtained by condensation of coumarin 3-carbaldehyde derivatives (**5**) with reactive methine compounds towards the formation of hemicyanine type dyes (Figure 6).

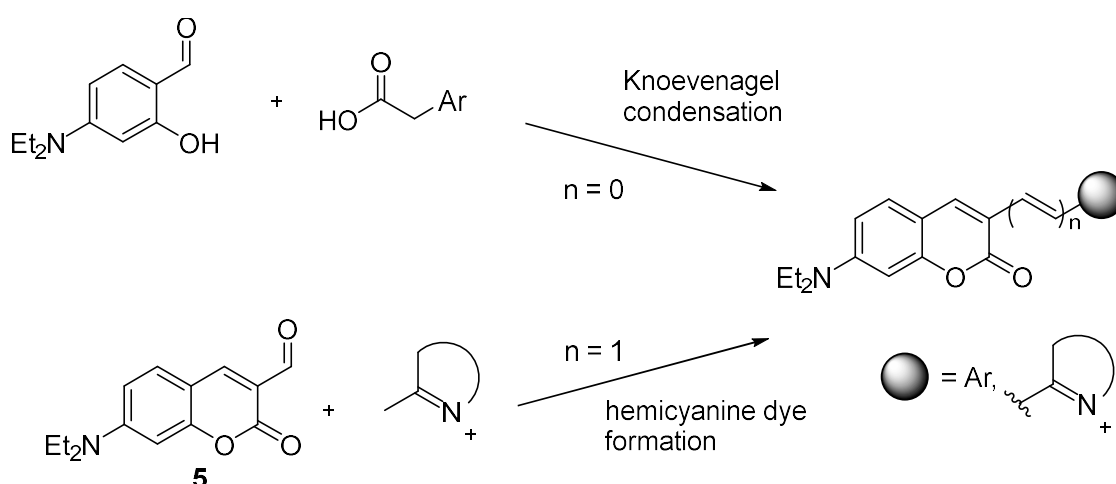


Figure 6 Different approaches for the synthesis of 3-substituted 7-amino coumarins derivatives.

Direct C3-Aryl substituted coumarins were obtained by the Knoevenagel condensation of (4-diethylamino) salicylaldehyde and inexpensive or readily available acetic acid derivatives. Patent literature describes vast amounts of compounds obtained through this approach. Two interesting motifs, quinoxalinone- and pyrimidine derivatives, common building blocks in agricultural^{8,9} and pharma chemicals^{10,11} have not been exploited.

Commercially available 5-pyrimidineacetic acid **6a** and readily synthesized quinoxalinone derivative **6b** obtained through the condensation of 1,2-phenyldiamine and oxalacetic acid in a 72% yield, were chosen (Figure 7).

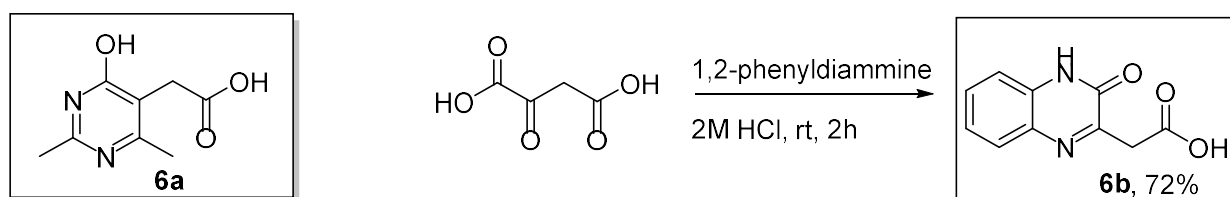


Figure 7 Molecular structures of compounds **6a** and **6b**.

Condensation of acetic acid derivatives **6a** and **6b** with 4-(diethylamino)salicylaldehyde in the presence of TEA was performed (Figure 8).

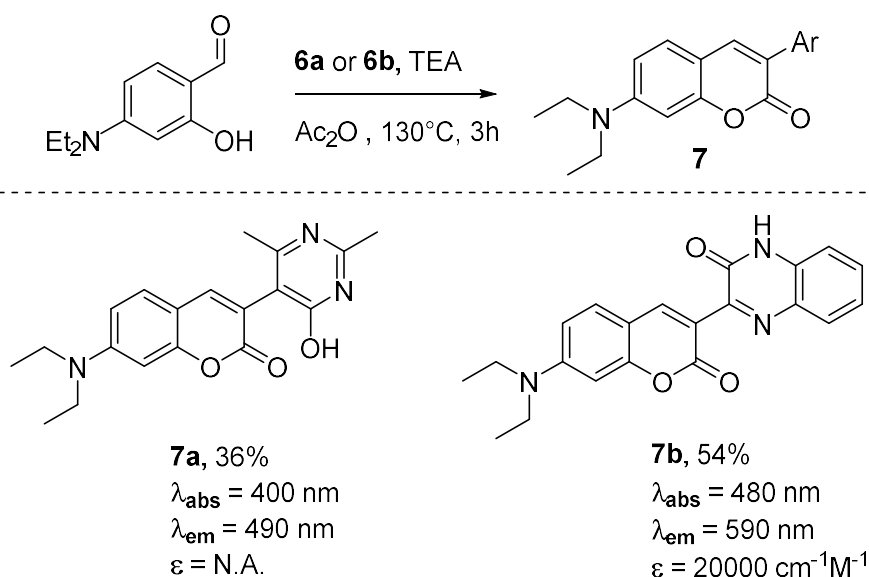


Figure 8 Synthesis of compounds **7a** and **7b**.

The products **7a** and **7b** were successfully synthesized and isolated in 36% and 54% yield, respectively. Interestingly, in the case of coumarin **7b**, a batho -chromic and -fluoric shift of the absorption and emission bands was observed due to the presence of the fused benzene. The absorption at 480 nm allows a perfect fit with a blue laser and, thanks to the Stokes shift of 110 nm, it could be used in combination with FITC ($\lambda_{\text{em}} = 530 \text{ nm}$, Stokes shift = 50 nm), one of the most popular dye for biological application.

In a diverse approach the synthesis of an LSS hemicyanine dye through the condensation of aldehyde **5** and a pyrazolium derivative was attempted. The pyrazolium building block has found application in the synthesis of fluorescent dyes such as azamethines and cyanines.¹² Surprisingly, the synthesis of such hemicyanines has not been reported in literature.

The required pyrazolium derivative was synthesized in two steps. Pyrazole **8** was obtained through a condensation between 3-dimethyl-2,4-pentanedione and hydrazine in a 50% yield. The subsequent alkylation with 1,3-propan sultone gave the pyrazole derivative **9** (Figure 9).

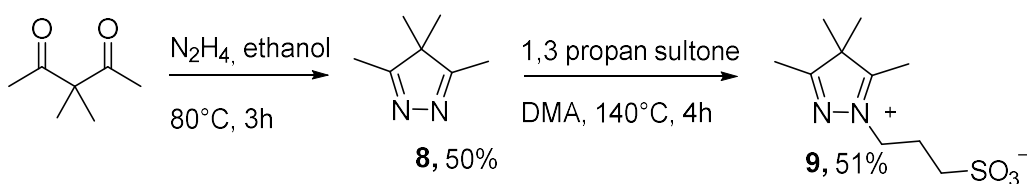


Figure 9 Synthesis of compound **9**

Aldehyde **5** was readily synthesized by Vilsmeier-Haack formylation of coumarin **10** (the preparation of compound **10** was discussed in section 4.2.2) in a 74% yield (Figure 10).

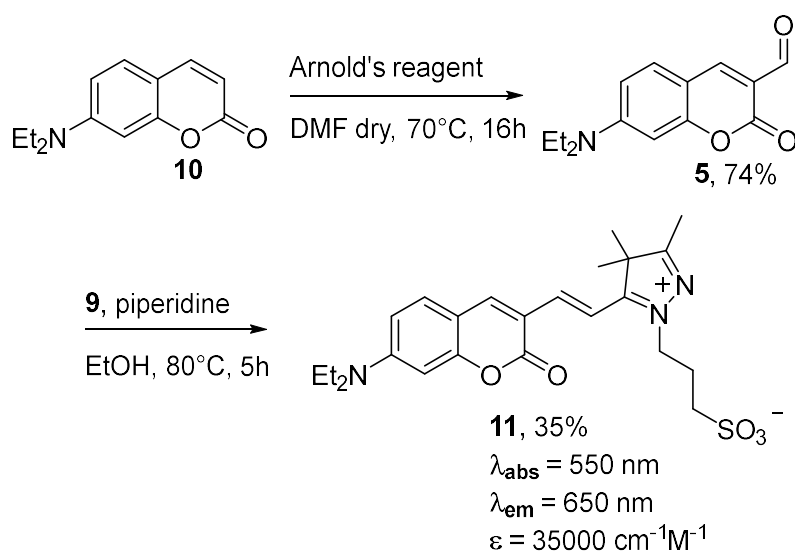


Figure 10 Synthesis of compound **11**.

The subsequent condensation reaction with the pyrazole derivative **9** gave the final product **11** in a modest 35% yield. As expected, extension of the π -system lead to a bathochromic and a bathofluoric shift of the absorption and emission bands. Coumarin **11** shows an absorption and emission maxima at 550 nm and 650 nm, respectively. The observed absorption/emission profile is well suited for multiplex applications as strong absorption in the common Cy3/Cy3.5 (530-580nm) region with emission in the Cy5 (645nm) region (as reported in table 1) was demonstrated. Furthermore, feasible introduction of the sulfonate group provides water solubility for bioconjugation applications.

7.2.3 Insertion of a heteroatom in position C6

Another method to generate a shift to the blue region of the absorption and the emission bands is the introduction of electron donating group in C6 of the coumarin core. 3-aryl-coumarin with C6-C7 fused heterocyclic rings including phenothiazine or a tetrahydroquinoxaline ring were briefly investigated in literature.¹³ Due to their interesting photophysical properties, addition of these structural features into the 3-thylenil coumarin core was evaluated. Several C6-C7 fused heterocyclic ring fused structures including tetrahydroquinoxaline, phenothiazine and benzoxazine derivatives were addressed (Figure 11).

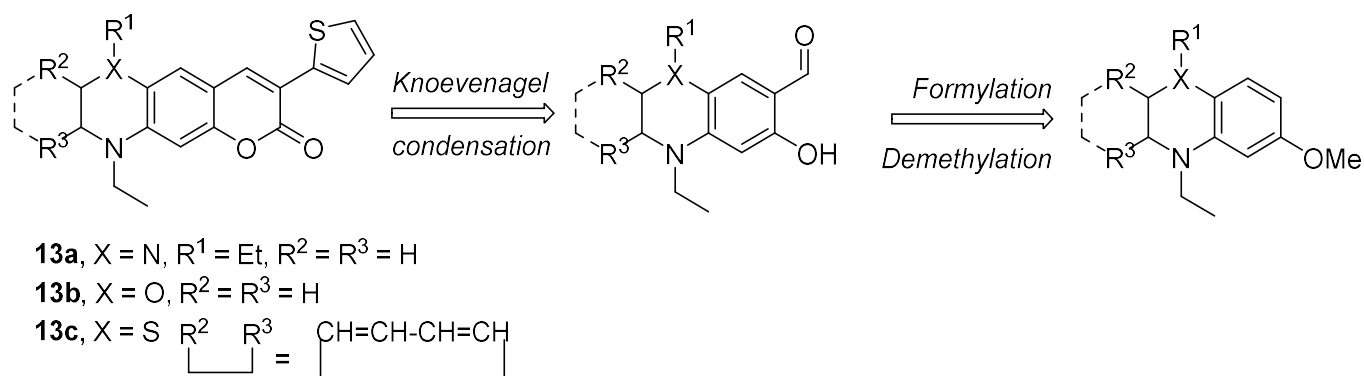


Figure 11 Synthetical approach for the introduction of a heteroatom in C6.

Target products could be obtained from suitable precursors **13a**, **13b** and **13c** through formylation, subsequent demethylation and final condensation. Even though precursors **13a**, **13b** and **13c** were not commercially available, they could be easily obtained (Figure 12).

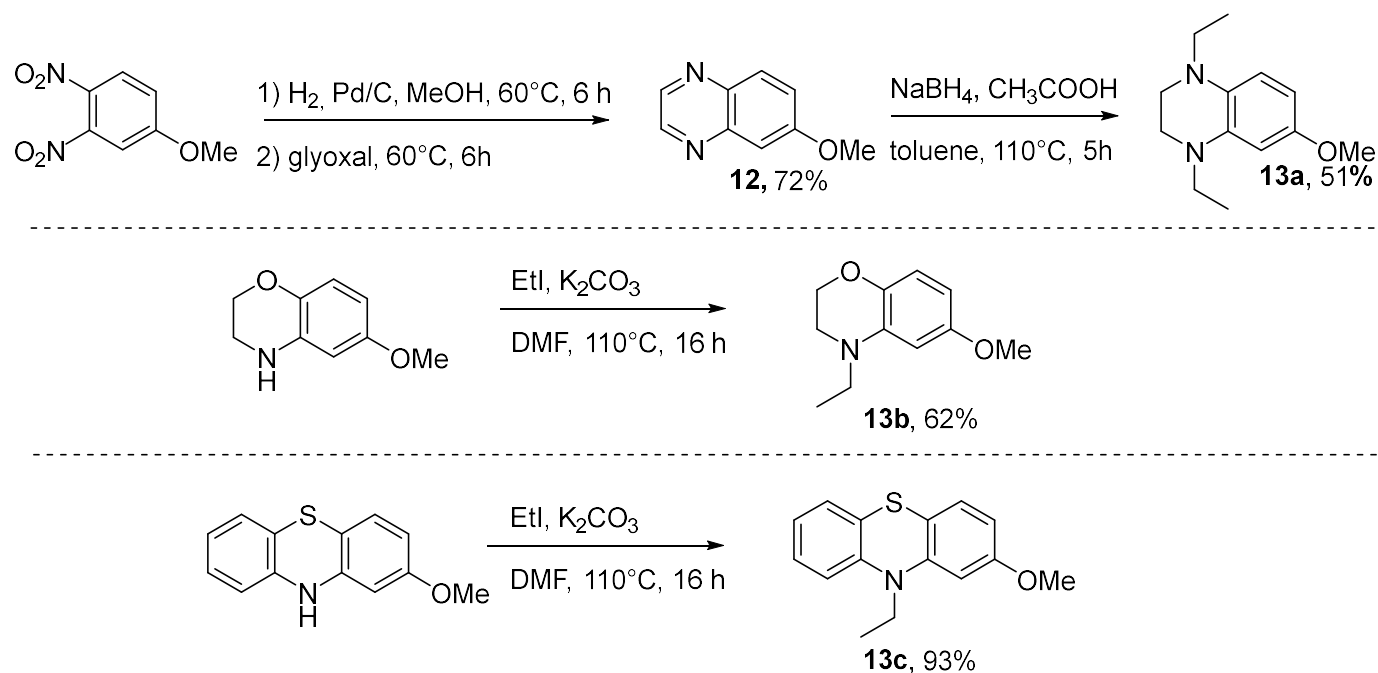


Figure 12 Synthesis of compounds **13a**, **13b** and **13c**.

Compound **13a** was prepared in three steps. Hydrogenation of the commercially available 4-methoxy-2-nitroaniline and subsequent condensation with glyoxal gave the quinoxaline derivative **13** in a 72% yield. Reductive alkylation of **13** yielded the tetrahydroquinoxaline derivative **13a** in a yield of 51%. The commercially available 3,4-dihydro-6-methoxy-2H-1,4-benzoxazine and 2-methoxyphenothiazine were straightforward alkylated with ethyl iodide to give compounds **13b** and **13c** in yield of 62% and 93%, respectively.

With precursors **13a**, **13b** and **13c** in hand, the synthesis of the 3-thienyl coumarin derivatives was attempted using the synthetical approach as outlined in figure 13.

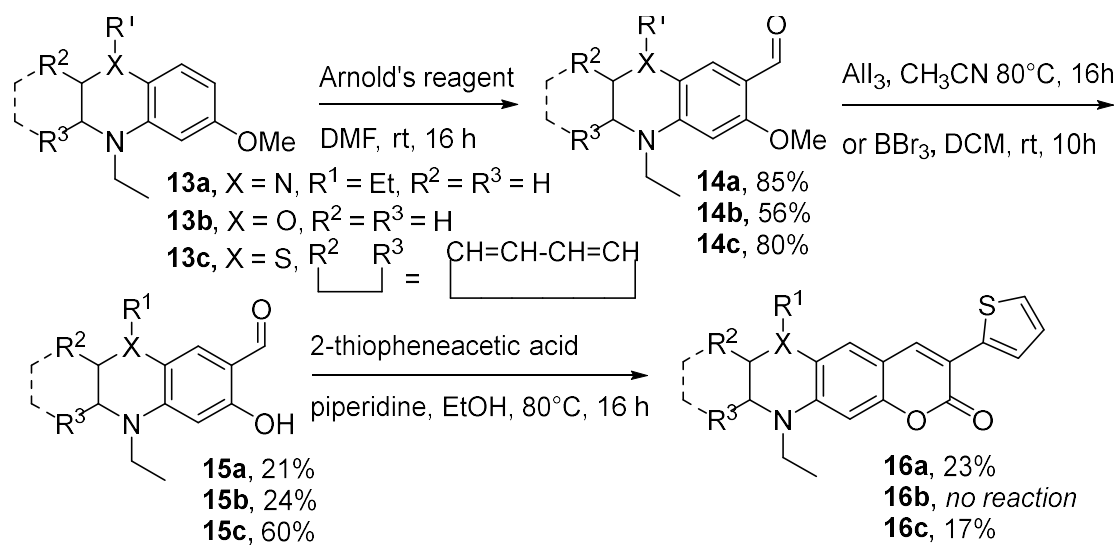


Figure 13 Synthesis of compounds **16a** and **16c**.

Formylation of compounds **13a**, **13b** and **13c** gave the corresponding aldehydes **14a**, **14b** and **14c** in yields from good to excellent. In the case of **14a** and **14b**, demethylation of the methoxy group was performed by treatment with AlI_3 , providing poor yields of 21% and 24%, respectively. In view of these disappointing results, the use of BBr_3 to give the hydroxy aldehyde **15c** was attempted observing an improvement of the yield to 60%. The prepared hydroxy aldehydes were employed in a Knoevenagel condensation with 2-thiophene acetic acid in the presence of piperidine and ethanol as solvent. Unfortunately, because of the poor yields and the tedious purifications, it was not possible to isolate the compounds **16a** and **16c** in pure form. In the case of product **16b**, no product formation was observed. Notably, performing the reaction in the presence of TEA and acetic anhydride as the solvent, also did not provide any trace of product. Although the compounds **16a** and **16c** were isolated impure, the introduction of water-solubilising sulfonate groups onto thienyl ring was attempted with the aim of simplifying the purification step (Figure 14).

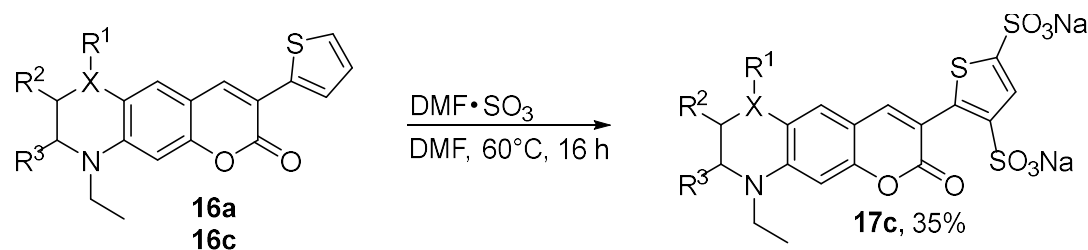


Figure 14 Synthesis of coumarin **17c**.

Unfortunately, it proved impossible to recover the product **17a** from the reaction mixture. In the case of **17c**, the reaction was carried out yielding the final dye in a yield of 35%. Photophysical studies showed an absorption maxima at 450 nm but, disappointingly, any emission was observed in aqueous media indicating a very low quantum yield under these conditions.

7.2.4 Synthesis of 7-methoxy coumarins

7-methoxy coumarins exhibit a pronounced hypso- and fluoric chromic shift with respect to the corresponding 7-amino coumarins. The development of new LSS dyes with absorption in the UV region (350 nm) was attempted through the synthesis of several 7-methoxy coumarin derivatives. In particular, the synthesis of aryl and vinyl derivative in position C3 was investigated (Figure 15).

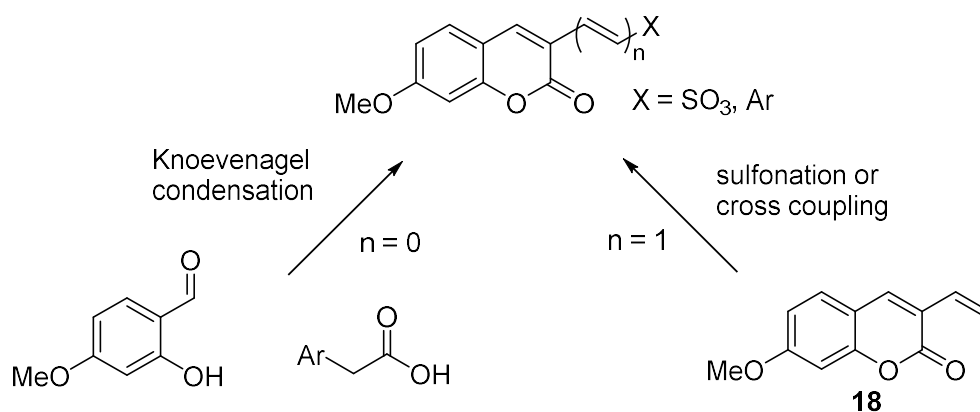


Figure 15 Synthetical approach for the synthesis of 7-methoxy coumarin derivatives.

As previously reported (**4**, Figure 4), 7-methoxy-3-thylenil coumarin **4** shows excellent photophysical properties which include a large stokes shift of 90 nm and an excellent quant yield of 0.87. However, the synthesis of a sulfonated water soluble version has not been reported (Figure 16).

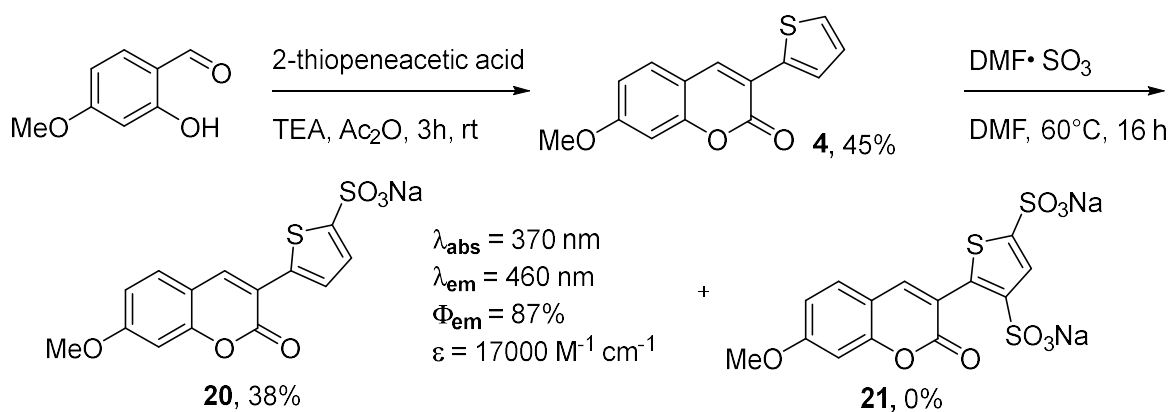


Figure 16 Synthesis of 7-methoxy-3-thylenil coumarin derivative.

The coumarin derivative **20** was readily synthesized in two steps which include a Knoevenagel condensation between 2-hydroxy-*p*-anisaldehyde and thienyl acetic acid, to give compound **4** in 45%, and the subsequent treatment with sulfur trioxide dimethylformamide complex ($\gamma = 38\%$). In the last step, only the mono-sulfonated product was achieved with a complete regioselectivity. Notably, the formation of product **21** derived from disulfonation on the aromatic ring, as in the case of 7-amino-thienyl coumarin, was not observed. Despite several attempts using large excess of sulfur trioxide dimethylformamide and harsh reaction conditions, the formation of coumarin **21** was not observed. As expected, the dye showed an absorption in the UV region, Although the absorption band does not perfectly fit with the 350nm UV laser excitation, the emission maxima at 460 nm and a reasonable extinction coefficient make the dye a plausible alternative to $\text{\textcircled{R}}$ Alexa Fluor 350. Furthermore, thanks to these promising photophysical properties, the quantum yield of the dye was measured, using AMCA (7-amino 4-methylcoumarin acetate) as reference, showing an excellent value of 0.87 with respect to the quantum yield of AMCA (not reported). Next, the introduction of vinyl derivatives in C3 of the 7-methoxy coumarin was investigated. At first, the synthesis of 7-methoxy-3-vinyl coumarin was performed using a procedure reported in literature (Figure 17).¹⁴

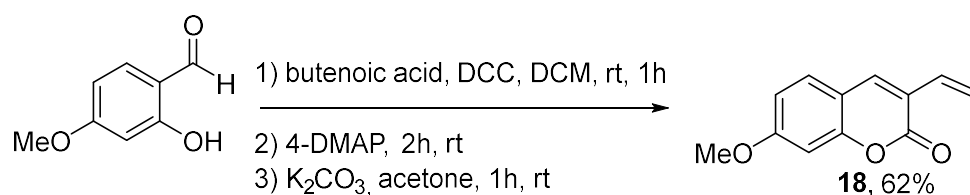


Figure 17 Synthesis of compounds **18**.

Activation of 3-butenoic acid with *N*'- dicyclohexylcarbodiimide (DCC) and the subsequent coupling with 4-methoxy-2-hydroxy benzaldehyde in the presence of DMAP generated the (*E*)-2-formyl-5-methoxyphenyl but-2-enoate. The final ring-closure performed in basic conditions provided coumarin **18** in 62% yield.

Introduction of an SO₃ group on the 7-methoxy-3vinyl coumarin **18** was carried out through the sulfonation with sulfur trioxide dimethylformamide complex (Figure 18).

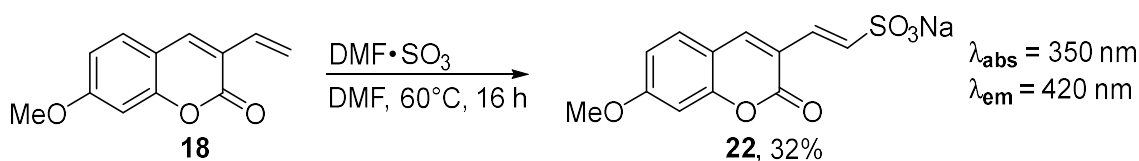


Figure 18 Synthesis of coumarin **22**.

The coumarin **22** was obtained in 32% of yield as the only product of the reaction. Unfortunately, only a modest Stokes shift of 70 nm was observed. However, it is comparable with the previously discussed Pacific Blue.

Coumarin **23** showed comparable photophysical properties coumarin **4** (Figure 4) as reported in literature.¹⁵ The development of a water-soluble version was attempted by the introduction of a phenyl onto the vinyl chain of coumarin **18** using a reported procedure and subsequent sulfonation (Figure 19).

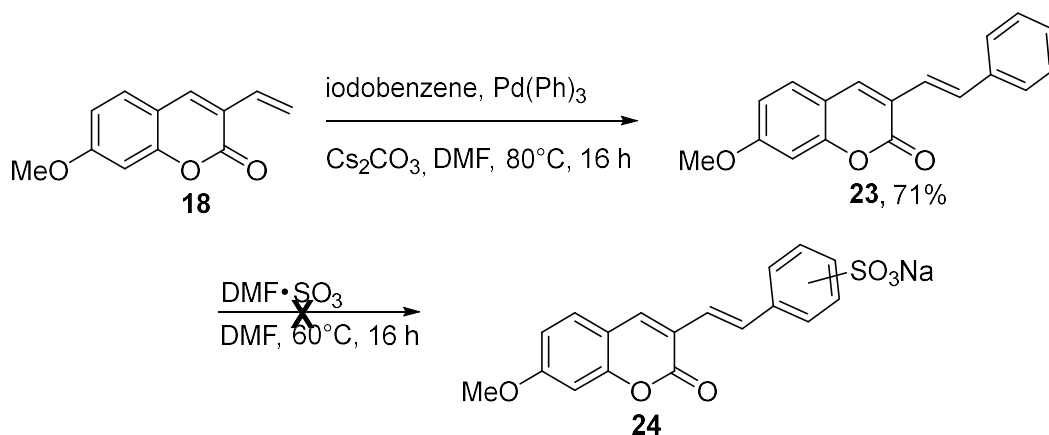


Figure 19 Synthesis of compound **24**.

Coumarin **23** was obtained by a palladium catalysed coupling between coumarin **18** and iodobenzene in a 71% yield. Unfortunately, sulfonation, using the usual procedure, did not give any of product **24** and only starting material was observed.

In view of the problem obtained in the last step of the synthesis, a new approach was adopted (Figure 20).

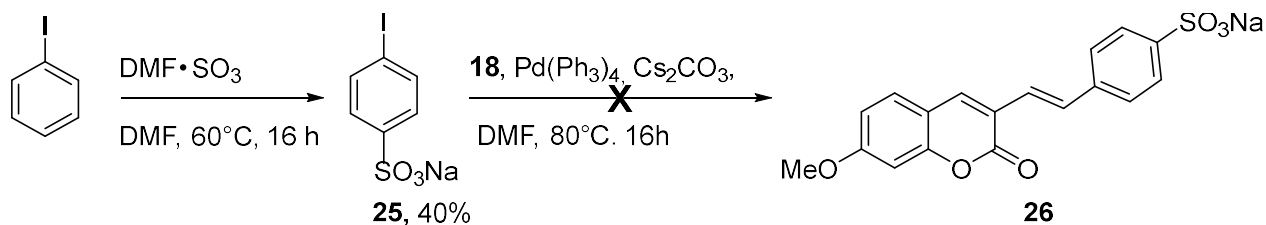


Figure 20 Attempted synthesis of coumarin **26**.

Iodobenzene derivative **25** was readily obtained by the treatment of iodobenzene with sulfur trioxide dimethylformamide complex. Disappointingly, the presence of the sulfonate group was not

tolerated during the coupling between coumarin **18** and iodobenzene derivative **25** and only starting material was recovered. The reaction was not further investigated.

In view of the screening of the synthesized dyes, coumarins **7b** and **11**, **20** and **22** showed interesting photophysical properties which may allow a future employment in multiplex technology (Table 2).

Laser source	350 nm	488 nm	561 nm
Fluorescent dye	20 $\lambda_{em} = 460$ nm	7b $\lambda_{em} = 590$ nm	11 $\lambda_{em} = 650$ nm
	22 $\lambda_{em} = 420$ nm		

Table 2 Dyes **7b**, **11**, **20**, **22** and their suitable laser excitation source.

Coumarin **20** and **22** may be used in the UV channel. In particular, **20** may represent an alternative to Alexa®Fluor 350. With the absorption maxima at 480 nm, coumarin **7b** perfectly fits with a blue laser and the Stokes shift of 110 nm allows the use of coumarin **7b** in combination with FITC ($\lambda_{em} = 530$ nm). Finally, coumarin **11** matches with a green laser and the use in multiplex applications in combination with Cy3 and Cy3.5 may be attempted.

7.2.5 Synthesis of LSS dyes for fluorescent microscopy

The development of new LSS dyes excitable by the 405 nm laser, with Stokes shifts of 100 nm, for the staining of lysosomes and mitochondria was next investigated. Thanks to the demonstrated photophysical properties, 3-thienyl coumarin was employed as the model for our investigations. As previously discussed, lysosomal and mitochondrial markers stain the corresponding organelle through a tertiary amine base and a reactive halo methyl group, respectively. The introduction of these moieties in the 3-thienyl coumarin derivative was attempted (Figure 21).

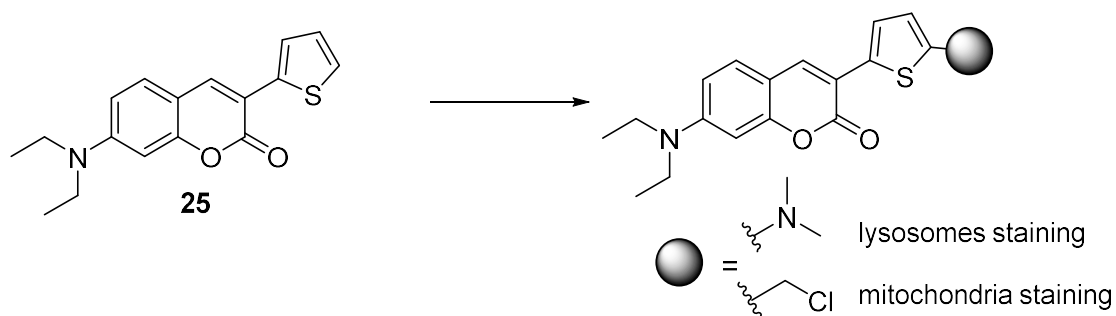


Figure 21 Introduction of the suitable moieties for the lysosome and mitochondria staining in the 7-amino-3-thienyl coumarin.

Introduction of the suitable moiety was performed on the aldehyde **28** which was obtained by the formylation of the coumarin **27** (synthesis of coumarin **27** was reported in section 2.2.2) (Figure 22).

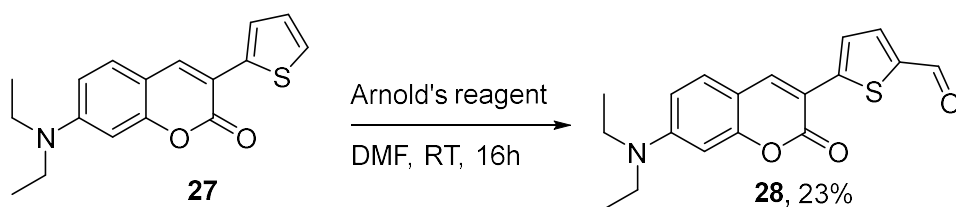


Figure 22 Synthesis of coumarin **28**.

The coumarin **27** was formylated by treatment with Arnold's reagents giving the aldehyde **28** in a 23% yield. The poor yield step was attributed to the formation of a by-product presumably due to a second formylation on the coumarin ring, but unfortunately the precise structure of this by-product could not be identified.

In case of the lysosome stains, three different moieties were introduced into the aldehyde **28** through a straightforward reductive amination strategy. Commercially available N^1,N^1 -dimethyl-1,3-propanediamine **29a** and N^3 -[3-(dimethylamino)propyl]- N^1,N^1 -dimethyl-1,3-propanediamine **9b**, as well as morpholine **30c** were used (Figure 23).

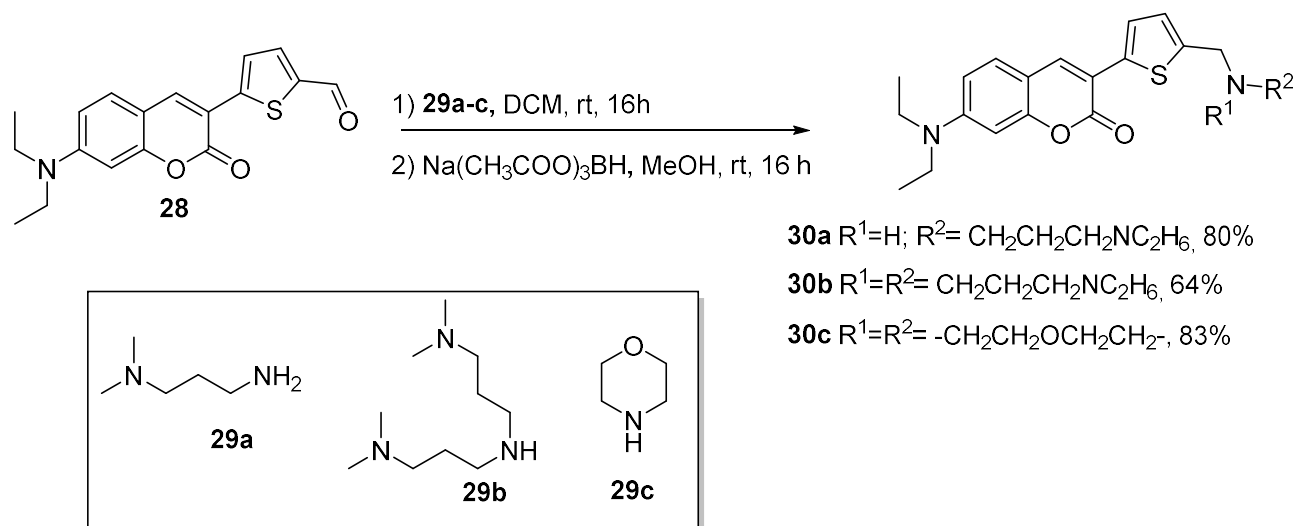


Figure 23 Synthesis of coumarins **30a**, **30b** and **30c**.

Reductive amination of aldehyde **28** through imine formation with the alkyl amines **29a**, **29b** and **29c** followed by treatment with sodium triacetoxyborohydride afforded the final compounds **30a**, **30b** and **30c** in good yields. The dyes exhibit a small red-shift of the absorption maxima towards 430 nm, but should still be excitable by a 405 nm excitation source.

Next, the development of a dye for mitochondrial staining was carried out in two steps starting again from aldehyde **28** (Figure 24).

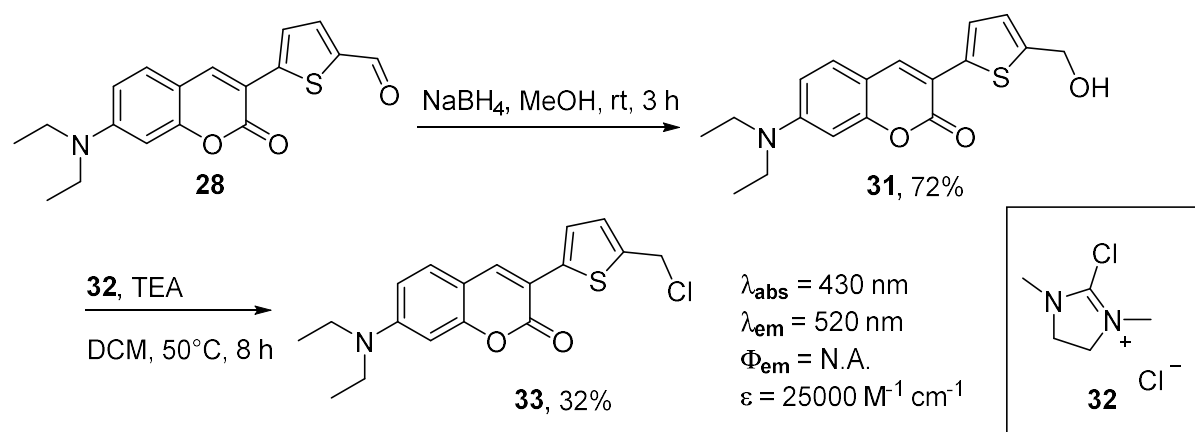


Figure 24 Synthesis of coumarin **33**.

First, reduction of the aldehyde **28** by treatment with NaBH₄ gave the alcohol **31** in a 72% yield. Conversion of the alcohol to the corresponding chloride with thionyl chloride did not give any results. Therefore, 2-chloro-1,3-dimethylimidazolium chloride **32** was used. In this case, the final compound **33** was obtained in a modest yield of 32%.

With the coumarins **30a**, **30b** and **30c**, **33** in hand, next staining of lysosomes and mitochondria could be tested.

7.2.6 Cell staining of lysosomes and mitochondria

In collaboration with Prof. Gretz and co-workers of the University of Heidelberg, preliminary investigations on the use of coumarins **30b** and **33**, in the lysosome and mitochondria staining respectively, of different cells were attempted.

To evaluate the capacity to stain lysosomes, compound **30b** was employed in the staining of live normal human dermal fibroblast (NHDF) at different concentrations (from 50 nM to 5 μ M) with an incubation time of 45'. Imaging was performed using a confocal microscope Leica sp8 with a 400 nm excitation source and the microsoft software platform Las X for the acquisition of the images (Figure 25).

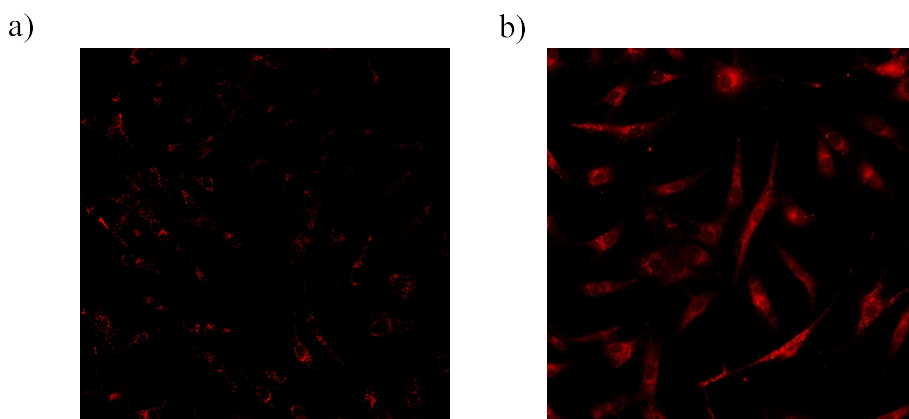


Figure 25 Labelling of NHDF using coumarin **30b** at a) 500 nM and b) 2 μ M.

The optimal staining concentrations is >500 nM. Figure 25b shows specific staining but it remained unclear if actual lysosomal staining was observed. Supposedly, these data may demonstrate good cell permeability and low cytotoxicity of coumarin **30b**. The high concentration used with respect to recommended values of commercially available Lyso-trackers may be due to the low brightness of coumarin **30b**. In order to verify specific lysosomal staining, further investigations should be performed. In particular, co-localization experiments, in combination with commercially available lyso-trackers with different λ_{abs} and λ_{em} , may demonstrate the specific staining of the lysosome by the coumarin dye. Furthermore, additional experiments to verify the cytotoxicity of the analysed dyes should be carried out. Unfortunately, it was not possible to verify the performance of

coumarins **30a** and **30c** due to the availability of suitable live cells, and mostly time limitations and instrument access.

Coumarin **33** was used for the staining of mitochondria in normal human dermal fibroblast (NHDF) and adipose stem cell. Solutions at different concentrations (from 50 nM to 200 nM) of the stain were used. The cells were incubated for 45' and washed before final imaging was performed using a Zeiss microscope. Unfortunately, in the case of coumarin **33** no staining was observed. These disappointing results may be attributed to the different position of the chloromethyl moiety, on the thienyl ring in the case of **33**. Most commercially available mitochondrial stains bear a phenyl substituted halomethyl function (for example, see Green FM in Figure 6). This different position could alter the reactivity of the moiety towards thiols. Further, an inadequate filter set (DAPI, 350nm) of the used Zeiss microscope prevents proper excitation of the coumarin dye (max abs 430nm). Unfortunately, a confocal microscope with proper excitation source at 405nm was not available at the time.

In order to demonstrate mitochondrial staining, commercially available Mito Tracker Deep Red ($\lambda_{\text{abs}} = 644 \text{ nm}$ $\lambda_{\text{em}} = 655 \text{ nm}$) was used in combination with a DAPI ($\lambda_{\text{abs}} = 348 \text{ nm}$ $\lambda_{\text{em}} = 461 \text{ nm}$) nucleus stain. Here a proper image of correct mitochondrial and nucleo staining was obtained (Figure 26).

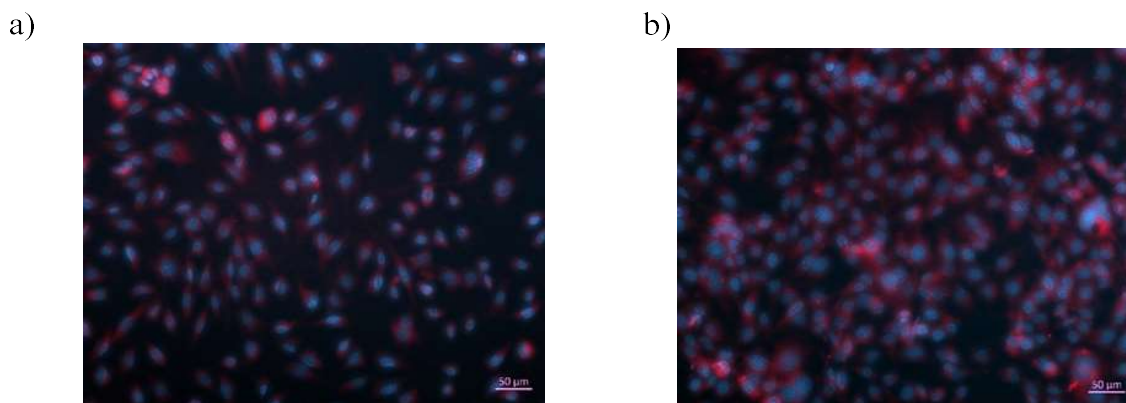


Figure 26 Labelling of NHDF using Mito Tracker Deep Red at a) 50 nM and b) 150 nM.

The images demonstrated the correct staining of mitochondria by the Mitotracker Deep Red in combination with nucleo staining of DAPI may exclude experimental error in case of coumarin **33**.

7.3 Conclusions

In this chapter, the development of new LSS dyes was carried out. Firstly, through different synthetical approaches, several dyes were successfully prepared. Some of them exhibit interesting photophysical properties including large Stokes shift, high quantum yield and molar extinction coefficient as well as excitability by the common available lasers. These characteristics make them suitable for multiplex biological assays. The development of a version for bioconjugation of **7b**, **11**, **20**, **22** may be performed. Secondly, different 3-thyrenyl coumarin derivatives were developed for the fluorescent microscopy applications. In particular, dyes **30b** and **33** were employed in the staining of lysosomes and mitochondria, respectively. The developed coumarins were preliminarily tested in the labelling of the lysosomes and mitochondria on live normal human dermal fibroblast (NHDF) and adipose stem cells. Unfortunately, disappointing results were obtained. In the case of coumarin **30b**, a possible staining of lysosomes was observed but at high concentrations. Coumarin **33** did not provide any signal in the labelling of mitochondria. Further investigations will be performed. In particular, the cytotoxicity of coumarin **30b** will be verified and co-localization experiments will ensure the specific stain of the coumarin to the lysosomes. In the case of mitochondria staining, new dyes which contain a phenylchloromethyl moiety will be designed.

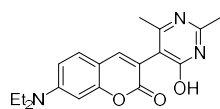
7.4 Experimental procedures

7.4.1 General methods and materials

¹H NMR spectra were recorded on Varian Mercury 400 spectrometer. Chemical shifts are reported in ppm from TMS with the solvent resonance as the internal standard (deuteriochloroform: $\delta = 7.27$ ppm; dimethyl sulfoxide-d₆: $\delta = 2.50$ ppm). Data are reported as follows: chemical shift, multiplicity (s = singlet, d = duplet, t = triplet, q = quartet, dd = double duplet, dt = double triplet, bs = broad signal, m = multiplet, quint = quintet), coupling constants (Hz). ¹³C NMR spectra were recorded on Varian MR400 spectrometer. Chemical shifts are reported in ppm from TMS with the solvent as the internal standard (deuteriochloroform: $\delta = 77.0$ ppm; dimethyl sulfoxide-d₆: $\delta = 39.5$ ppm). LC-electrospray ionization mass spectra (ESI-MS) were obtained with Agilent Technologies MSD1100 single-quadrupole mass spectrometer. Chromatographic purification was done with 240-400 mesh silica gel. Purification on preparative thin layer chromatography was done on Merck TLC silica gel 60 F₂₅₄.

7.4.2 Synthesis and characterization of substrates

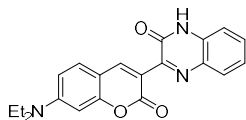
Synthesis of dyes **7a** and **7b**



Coumarin **7a** was prepared using the following procedure. In a one necked round bottom flask equipped with magnetic stirring bar, condenser and glass stoppers, 5-pyrimidineacetic acid (5.5 mmol, 1.12 g), 4-(diethylamino)-salicylaldehyde (8.5 mmol, 1.64 g) were dissolved in acetic anhydride (20 mL). Triethylamine (10.5 mmol, 1.46 mL) was added and the mixture was stirred at reflux for three hours. The reaction was cooled down at room temperature, water was added, the organic material was extracted with AcOEt (3 x 50 mL) and the organic layers were dried over Na₂SO₄. Solvent was removed under reduced pressure and the residue was purified by flash column chromatography (SiO₂, cyclohexane to cyclohexane/ethyl acetate, 7/3) to afford **7a** as reddish solid (36%, 2.0 mmol, 0.670 g). ¹H-NMR (400 MHz, CDCl₃) δ :

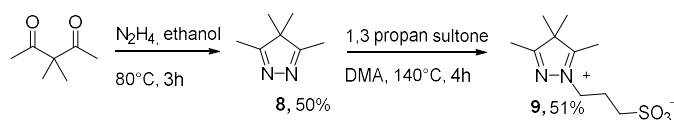
Chapter 7: Use of coumarin dyes in biological applications

7.48 (s, 1H), 7.28 (d, 1H), 6.62 (dd, $J = 2.3 - 8.9$ Hz, 1H), 6.54 (d, $J = 2.7$ Hz, 1H), 3.45 (q, $J = 7.1$ Hz, 4H), 2.47 (s, 3H), 2.17 (s, 3H), 1.23 (t, 7.1 Hz, 6H).



(7b): The general procedure reported for 7a was applied; yield 54% (2.9 mmol, 1.07 g); red solid: $^1\text{H-NMR}$ (400 MHz, CDCl_3) δ : 7.51 (m, 1H), 8.10 (s, 1H), 7.96 (s, 1H), 7.51 (m, 1H), 7.09 (dd, $J = 2.4 - 8.9$ Hz, 1H), 6.76 (d, $J = 2.5$ Hz, 1H), 6.40 (m, 1H), 6.30 (m, 1H), 3.31 (q, $J = 7.1$ Hz, 4H), 1.12 (t, 7.1 Hz, 6H).

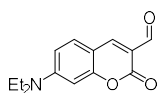
Synthesis of pyrazole derivative 9



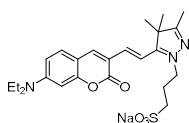
A mixture of 3,3-dimethyl-2,4-pentanedione (8.4 mmol, 1.00 g) and hydrazine monohydrate (8.4 mmol, 0.42 g) in ethanol (EtOH, 30 mL) was stirred at 80°C for 3 hours. The mixture was cooled down and the solvent was removed under reduced pressure. The crude material was subjected to purification by flash chromatography (SiO_2 , Cy/EtOAc 8/2) to give **8** as a brownish solid (500 mg; $y=50\%$). A mixture of **8** (2.41 mmol, 0.30 g) and 1,3-propane sultone (2.65 mmol, 0.32 g) in dimethylacetamide (3 mL), were stirred at 140°C for 4 hours. After completion of the reaction, the mixture was cooled down. Ethyl acetate (50 mL) was added to deposit a crystal, which was filtered, dissolved in water and purified by C18 flash chromatography to give **9** as a brownish solid (300 mg, $y=51\%$). $^1\text{H NMR}$ (400 MHz, DMSO) δ 4.34 (t, $J = 7.1$ Hz, 2H), 2.64 (s, 3H), 2.28 (s, 3H), 2.19 – 2.11 (m, 2H), 1.4 (s, 6H).

Synthesis of coumarin dye 11

Coumarin **10** was prepared using the procedure reported in section 4.4.3

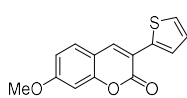


Coumarin **5** was prepared using the following procedure. Under inert atmosphere, a solution of Arnold's reagent (39 mmol, 5.0 g) in anhydrous DMF (200 mL) and stirred for 30 minutes. 7-diethylaminocoumarin (7.8 mmol, 1.7 g) was added to yield a red solution. The mixture was stirred at 70°C for 16 hours and then cooled down at room temperature and poured into 300 mL of ice water. Organic material was extracted in DCM (3x100 ml) and purified by flash chromatography (Cy/EtOAc 8/2) to give **5** as red solid (1.0 g; $y=52\%$). $^1\text{H NMR}$ corresponds to the literature.¹⁶



Coumarin **11** was prepared using the following procedure. Under inert atmosphere, a mixture of **5** (0.081, 0.020 g), **9** (0.082, 0.020 g) and piperidine (one drop) in absolute ethanol (5 mL) was stirred at 80°C for 5 hours. The mixture was cooled down at room temperature and the solvent was evaporated. The crude material was purified by flash chromatography (SiO_2 , Cy/EtOAc 8/2) to give **5** as dark solid (0.013 g; $y=35\%$). $^1\text{H-NMR}$ (400 MHz, DMSO) δ : 8.82 (s, 1H); 8.07 (d, 1H, $J = 16$ Hz); 7.67 (d, 1H, $J = 16$ Hz); 7.54 (d, 1H, $J=9.4$ Hz); 6.90 (dd, 1H, $J = 2.3 - 9.4$ Hz); 6.70 (d, 1H, $J = 2.0$ Hz); 4.43 (t, 2H, $J = 7.0$ Hz); 3.55 (q, 4H, $J = 7.4$ Hz); 2.53 (t, 2H, $J = 7.0$ Hz); 2.32 (s, 3H); 2.29 (m, 2H); 1.64 (s, 6H); 1.17 (t, 6H, $J = 6.6$).

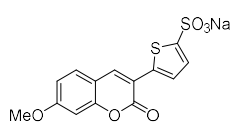
Synthesis of coumarin dye 20



Coumarin **4** was prepared using the following procedure. In a one necked round bottom flask equipped with magnetic stirring bar, condenser and glass stoppers, 2-thiophene acetic acid (2.1 mmol, 1.2 g), 4-(diethylamino)-salicylaldehyde (3.3 mmol, 1.98 g) were dissolved in acetic anhydride (120 mL). Triethylamine (4.0 mmol, 2.24 mL) was added and the mixture was stirred at reflux for three hours. The reaction was cooled down at room temperature, water was added, the organic material was extracted with AcOEt (3 x 50 mL) and the organic layers were dried over Na_2SO_4 . Solvent was removed

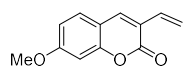
Chapter 7: Use of coumarin dyes in biological applications

under reduced pressure and the residue was purified by flash column chromatography (SiO₂, cyclohexane to cyclohexane/ethyl acetate, 7/3) to afford **4** as dark solid (0.24 g, $y=45\%$). ¹H NMR corresponds to the literature.¹⁷

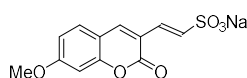


Coumarin **20** was prepared using the following procedure. A two necked round bottom flask equipped with stirring bar, glass stopper and vacuum adapter was flame dried under an Argon atmosphere. The flask was charged with **4** (2.3 mmol, 0.600 g) and dissolved in anhydrous N,N-dimethylformamide (100 mL). Sulfur trioxide N,N-dimethylformamide complex (70 mmol, 10.6 g) was added and the reaction mixture was stirred overnight at 60°C under Argon, then cooled to room temperature. Diethyl ether (400 mL) was slowly added under stirring. Two phases were formed: the viscous oil was decanted, and the upper layer was removed. The viscous oil was taken up in aqueous saturated NaHCO₃ (10 mL) and purified by reverse phase chromatography (elution gradient: water to water/acetonitrile 8/2) to give **20** as a yellowish solid (38%, 0.9 mmol, 0.328 g). ¹H-NMR (400 MHz, DMSO) δ : 8.5 (s, 1H), 7.69 (1H, d, $J=9.0$ Hz), 7.55 (1H, d, $J=3.5$ Hz;), 7.1 (1H, d $J=3.9$ Hz), 7.05 (1H, d, $J=2.3$ Hz), 6.99 (1H, dd, $J=2.7, 9.0$ Hz), 3.86 (3H, s).

Synthesis of coumarin dye **21**



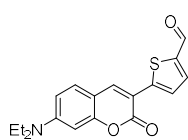
Coumarin **18** was prepared using the following procedure. To a solution of 3-butenic acid (2.2 mmol, 187 μ L) in DCM (3 mL), DCC (2.2 mmol, 0.45 g) was added. After 1 h, 2-hydroxy-*p*-anisaldehyde (1.75 mmol 278 μ L) and DMAP (0.20 mmol, 0.025 g,) were added. The mixture was stirred for 2 h and subsequently cooled down. The solid was filtered and to the solution K₂CO₃ (1.75 mmol 0.25 g) was added. The mixture was stirred for 1 h. The mixture was washed with H₂O. The organic layer was dried, filtered, and concentrated under reduced pressure. The crude product was purified by flash chromatography yellow solid (62%, 0.28 g). ¹H NMR corresponds to the literature.¹⁸



Coumarin **22** was prepared using the following procedure. A two necked round bottom flask equipped with stirring bar, glass stopper and vacuum adapter was flame dried under an Argon atmosphere. The flask was charged with **18** (0.5 mmol, 0.100 g) and dissolved in anhydrous N,N-dimethylformamide (20 mL). Sulfur trioxide N,N-dimethylformamide complex (10 mmol, 1.5 g) was added and the reaction mixture was stirred overnight at 60°C under Argon, then cooled to room temperature. Diethyl ether (200 mL) was slowly added under stirring. Two phases were formed: the viscous oil was decanted, and the upper layer was removed. The viscous oil was taken up in aqueous saturated NaHCO₃ (10 mL) and purified by reverse phase chromatography (elution gradient: water to water/acetonitrile 8/2) to give **22** as a yellowish solid (32%, 0.9 mmol, 0.048 g). ¹H-NMR (400 MHz, DMSO) δ : 8.05 (s, 1H), 7.57 (d, 1H, $J=9.0$ Hz), 7.34 (d, 1H, $J=15.0$ Hz), 7.15 (d, 1H, $J=14.8$ Hz); 6.99 (dd, 1H, $J=2.3-8.5$ Hz), 6.93 (d, 1H, $J=2.3$ Hz), 3.93 (s, 3H).

Synthesis of the aldehyde **28**

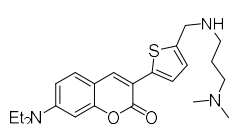
Coumarin **27** was prepared using the procedure reported in section 2.4.2



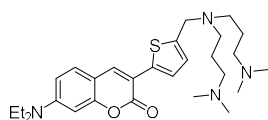
Coumarin **28** was prepared using the following procedure. Under inert atmosphere, a solution of Arnold's reagent (8.4 mmol, 1.0 g) in anhydrous DMF (30 mL) and stirred for 30 minutes. The solution was cooled at 0°C then **27** (1.67 mmol, 0.50 g) was added. The mixture was stirred at room temperature for 16 hours and poured into 300 mL of ice water. Organic material was extracted in DCM (3x100 ml) and purified by flash chromatography (Cy/EtOAc 8/2) to give **28** as red solid (0.11 g; $y=23\%$). ¹H NMR (400 MHz, CDCl₃) δ : 9.90 (s, 1H), 8.03 (s, 1H), 7.76 (dd, $J=14.1, 4.1$ Hz, 2H), 7.38 (d, $J=8.9$ Hz, 1H), 6.65 (dd, $J=8.8, 2.5$ Hz, 1H), 6.54 (d, $J=2.2$ Hz, 1H), 3.47 (q, $J=7.1$ Hz, 4H), 1.25 (t, $J=7.1$ Hz, 6H).

Chapter 7: Use of coumarin dyes in biological applications

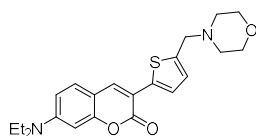
Synthesis of coumarin dyes **30a**, **30b** and **30c**



Coumarin **30a** was prepared using the following procedure. A two necked round bottom flask equipped with stirring bar, glass stopper and vacuum adapter was flame dried under an Argon atmosphere. **28** (0.24 mmol, 0.08 g), **29a** (0.6, 0.056 g) were dissolved in DCM (5 mL). The reaction mixture was stirred overnight at room temperature. Sodium triacetoxyborohydride (1.2 mmol, 0.254 g) was added and the mixture was stirred overnight at room temperature. Water was dropwise added and the organic material was extracted with DCM (3x20 mL). The organic layers were dried over Na₂SO₄ and the solvent was removed under reduced pressure and the residue was purified by flash column chromatography (SiO₂, DCM/MeOH 85/15) to give **29a** a reddish solid (80 mg, y=80%). ¹H NMR (600 MHz, CDCl₃) δ 7.78 (s, 1H), 7.53 (s, 1H), 7.26 (d, 1H), 6.88 (s, 1H), 6.64 (m, 1H), 6.48 (s, 1H), 4.7 (s, 2H), 3.47 (q, J = 7.1 Hz, 4H), 2.62 – 2.43 (m, 4H), 2.33 (s, 6H), 1.93 (m, 2H), 1.25 (t, 6H, J=6.6).

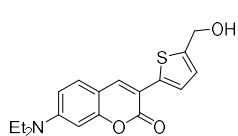


(30b): The general procedure reported for **30a** was applied; yield 64% ¹H NMR (600 MHz, CDCl₃) δ 7.66 (s, 1H), 7.53 (s, 1H), 7.26 (d, 1H), 6.78 (s, 1H), 6.64 (m, 1H), 6.44 (s, 1H), 3.72 (s, 2H), 3.47 (q, J = 7.1 Hz, 4H), 2.62 – 2.43 (m, 8H), 2.33 (s, 12H), 1.93 (m, 4H), 1.25 (t, 6H, J=6.6).

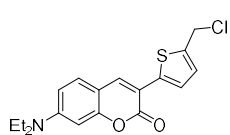


(30c): The general procedure reported for **30a** was applied; yield 83% ¹H NMR (600 MHz, CDCl₃) δ 7.86 (s, 1H), 7.56 (d, J = 3.7 Hz, 1H), 7.33 (d, J = 8.8 Hz, 1H), 6.95 (bs, 1H), 6.63 (dd, J = 8.8, 2.5 Hz, 1H), 6.56 (d, J = 2.4 Hz, 1H), 3.76 (bs, 6H), 3.45 (q, J = 7.1 Hz, 4H), 2.55 (bs, 4H), 1.24 (t, J = 7.1 Hz, 6H).

Synthesis of coumarin dye **33**



Coumarin **31** was prepared using the following procedure. A two necked round bottom flask equipped with stirring bar, glass stopper and vacuum adapter was flame dried under an Argon atmosphere. **28** (0.03 mmol, 0.05 g) was dissolved in a mixture EtOH/DCM 1/1 (5 mL). NaBH₄ (0.06 mmol, 0.025 g) was portion-wise added. The reaction mixture was stirred overnight at room temperature. Mixture was quenched with water and the organic material was extracted with DCM (3x20 mL). The organic layers were dried over Na₂SO₄ and the solvent was removed under reduced pressure and the residue was purified by flash column chromatography (SiO₂, PE/EtOAc 7/3) to give **31** a reddish solid (35 mg, y=70%). ¹H NMR (400 MHz, CDCl₃) δ 7.75 (s, 1H), 7.46 (d, J = 3.9 Hz, 1H), 7.28 (d, J = 8.9 Hz, 1H), 6.92 (d, J = 3.5 Hz, 1H), 6.54 (dd, J = 8.9 - 2.7 Hz, 1H), 6.46 (d, J = 2.7 Hz, 1H), 4.82 (s, 2H), 3.36 (q, J = 7.1 Hz, 4H), 1.28 (t, J = 7.1 Hz, 6H).



Coumarin **33** was prepared using the following procedure. A two necked round bottom flask equipped with stirring bar, glass stopper, condenser and vacuum adapter was flame dried under an Argon atmosphere. **31** (0.01 mmol, 0.03 g), was dissolved in a mixture DCM (5 mL). 2-Chloro-1,3-dimethylimidazoliumchloride (0.10 mmol, 0.02 g) was added. The reaction mixture was stirred for 8 h at 50°C. Mixture was washed with water and the organic material was extracted with DCM (3x10 mL). The organic layers were dried over Na₂SO₄ and the solvent was removed under reduced pressure and the residue was purified by flash column chromatography (SiO₂, PE/EtOAc 8/2) to give **33** a reddish solid (0.01 mg, y=32%). ¹H NMR (400 MHz, CDCl₃) δ 7.75 (s, 1H), 7.46 (d, J = 3.9 Hz, 1H), 7.28 (d, J = 8.9 Hz, 1H), 6.92 (d, J = 3.5 Hz, 1H), 6.54 (dd, J = 8.9 - 2.7 Hz, 1H), 6.46 (d, J = 2.7 Hz, 1H), 5.26 (s, 2H), 3.36 (q, J = 7.1 Hz, 4H), 1.28 (t, J = 7.1 Hz, 6H).

References

- ¹ T. P. Jansen; G. Rodeghiero, D. Foglietta, R. Perciaccante and L. Della Ciana, 2017, EP 3219712.
- ² X. Liu, Z. Xu and J. M. Cole, *J. Phys. Chem.*, 2013, **117**, 16584.
- ³ P. Czerney, M. Wenzel, B. Schweder and F. Lehmann, 2004. US 20040260093.
- ⁴ A. R. Jagtap, V. S. Satam, R. N. Rajule and V. R. Kanetkar, *Dyes Pigm.*, 2009, **82**, 84.
- ⁵ V. N. Belov, M. L. Bossi, J. Fölling, V. P. Boyarskiy and S. W. Hell, *Chem.: Eur. J.*, 2009, **15**, 10762.
- ⁶ J. Gordo, J. Avo, A. J. Parola, J. C. Lima, A. Pereira and P. S. Branco, *Org. Lett.*, 2011, **13**, 5113.
- ⁷ X. -Q. Hong, X. -H. Yu, K. Zhang and W. -H. Chen, *Org. Biomol. Chem.*, 2018, **16**, 8025.
- ⁸ K. Ataka and K. Omori, 1989, EP 326389 A2 19890802.
- ⁹ W. Schaper, L. Willms, C. Rosinger, E. Hacker, E. Rose and D. Schmutzler, 2005, US 20050256000 A1 20051117.
- ¹⁰ M. Amin and M. Youssef, *Pharma Chemica*, 2012, **4**, 1323.
- ¹¹ G. W. Miller and F. L. Rose, *J. Chem. Soc.* 1963, 5642.
- ¹² a) N. Yamamoto, T. Kurosawa, S. Hasaba, M. Date, 2010, WO 2010126045; b) J. Nishigaki, K. Takeuchi, H. Inomata and M. Kojima, 2003, JP 2003034697.
- ¹³ a) A. R. Jagtap, V. S. Satam, R. N. Rajule and V. R. Kanetkar, *Dyes Pigm.*, 2009, **82**, 84 b) J. Sheng, W. Shen, X. Yue and C. Huang, *Faming Zhuanli Shenqing*, 2018, CN108250220 A 2018706.
- ¹⁴ J. Gordo, J. Avo, A. J. Parola, J. C. Lima, A. Pereira and P. S. Branco, *Org. Lett.*, 2011, **13**, 5113.
- ¹⁵ J. Gordo, J. Avo, A. J. Parola, J. C. Lima, A. Pereira and P. S. Branco, *Org. Lett.*, 2011, **13**, 5113.3
- ¹⁶ T. -K. Kim, D. -N. Lee and H. -J. Kim, *Tetra. Lett.*, 2008, **49**, 4879.
- ¹⁷ G. Delogu, C. Picciau, G. Ferino, E. Quezada, G. Podda, E. Uriarte and D. Vina, *Eur. J. Med. Chem.*, 2011, **46**, 1147.
- ¹⁸ J. Gordo, J. Avo, A. J. Parola, J. C. Lima, A. Pereira and P. S. Branco, *Org. Lett.*, 2011, **13**, 5113.

Summary

Coumarin dyes have proven to possess unique photophysical properties thanks to the high quantum yield, and stability and an absorption and emission which cover the most part of the visible spectrum.

Thanks to these exceptional photophysical properties, coumarin dyes are widespread used in different applications including fluorescent bio-label, emitting materials in OLED and dyes in solar cells as example. To the best of our knowledge their systematic use in photoredox catalysis has not been explored yet.

This research aimed at the design, the synthesis, the photophysical characterization of new LSS coumarin dyes and their use in different fields such as photoredox catalysis, photopolymerization and biological applications (bioconjugation and fluorescent microscopy).

Chapter 1 provides an introduction into the photoredox catalysis. The principles of photoredox catalysis and the use of the most common inorganic and organic photocatalysts in particular are highlighted. Furthermore, coumarin derivatives and their property as LSS dyes are presented.

Chapter 2 describes the successful use of 3-thienyl- and 3-phenyl 7-amino coumarin derivatives as powerful photoreductants in photoredox pinacol coupling reaction of several aromatic and aliphatic aldehydes, ketones and imine. To the best of our knowledge, it represents the first reported example of coumarin as photocatalyst (Figure 1).

In **Chapter 3**, the use of coumarins as photocatalysts was extended to the photoredox generation of alkylradicals and their subsequent employment in various organic transformations was described. Photoredox atom transfer radical reactions (ATRA) mediated by coumarins showed a broad scope and good tolerance to several functional groups. Also, a 3-thienyl coumarin derivative was successfully applied in other reactions including enantioselective α -alkylations of tetrahydrocinnamaldehyde, the reductive dehalogenation of bromoacetophenone and, finally the generation of trifluoromethyl radical generation for the oxytrifluoromethylation of stilbene (Figure 1).

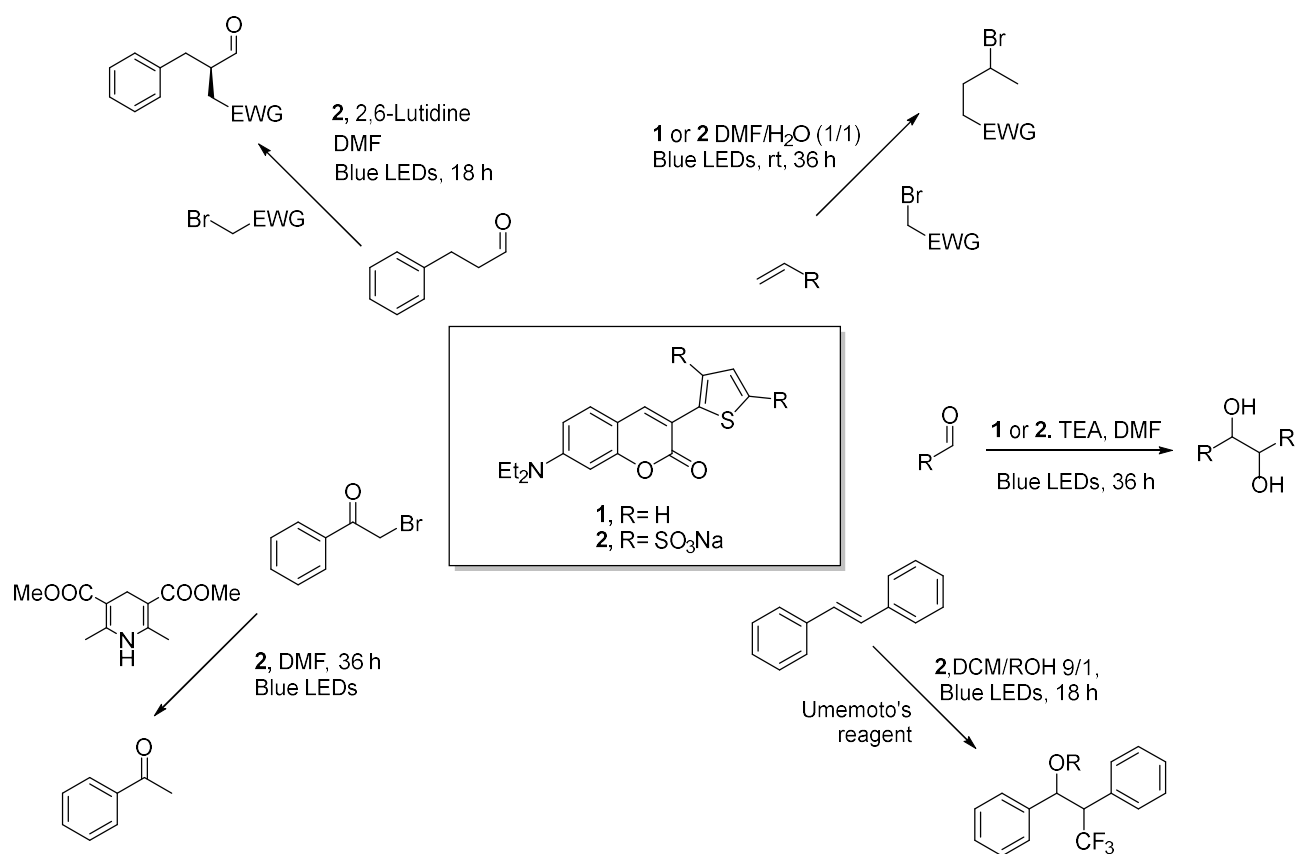


Figure 1 Use of 3-thienyl coumarin derivatives as photocatalysts of several organic reactions

In **Chapter 4**, the design and the synthesis of new more efficient coumarin core photocatalysts was investigated through either a computation as well as a rational approach. Several coumarins were successfully synthesized and applied as photocatalysts in the photoredox pinacol coupling of 4-chlorobenzaldehyde giving conversions from excellent too good in most cases. Furthermore, the use of BIH as reducing reagent provided an almost total conversion of the aldehyde to the corresponding diol.

Chapter 5 was focused on the development of a new route for the allylation of aldehydes through a dual photoredox and nickel catalysis. A combination of Ni(II) complex and $[\text{Ir}(\text{ppy})_2(\text{dtbbpy})](\text{PF}_6)$ or $[\text{Ru}(\text{bpy})_3]^{2+}$, in the presence of inexpensive reagents, provided a broad scope for the allylation of several aliphatic and aromatic aldehydes (Figure 2).

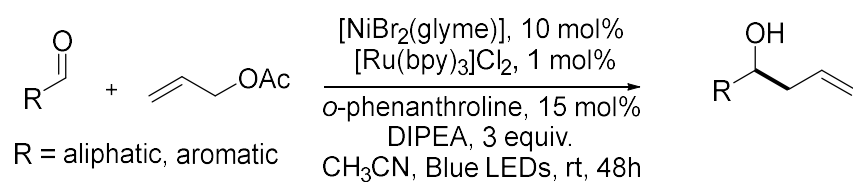


Figure 2 Allylation of aldehydes by dual nickel and photoredox catalysis

In **Chapter 6**, in collaboration with Prof. J. Lalavèe and co-workers of the Institut de Science des Matériaux de Mulhouse, the employment as organic photocatalysts of 3-thienyl coumarin derivatives in photo polymerization applications was described. In particular, the coumarins provided high performances for the photoinitiation of both the cationic polymerization of epoxides and the free radical polymerization of (meth)acrylates. The high performance of these coumarin derivatives in initiating systems is also shown for new photosensitive 3D printing resins upon exposure to a laser diode. A water-soluble 3-thienyl coumarin derivative was also successfully employed for the preparation of hydrogels.

Chapter 7 concerned the use of LSS dyes in biological applications. Firstly, the development of a library of new LSS coumarin core dyes was investigated. Through different synthetical approaches, several dyes were successfully prepared. Some of them exhibit interesting photophysical properties including large Stokes shift, high quantum yield and molar extinction coefficient as well as excitability by the common available lasers. These characteristics make them suitable for multiplex biological assays (Figure 3).

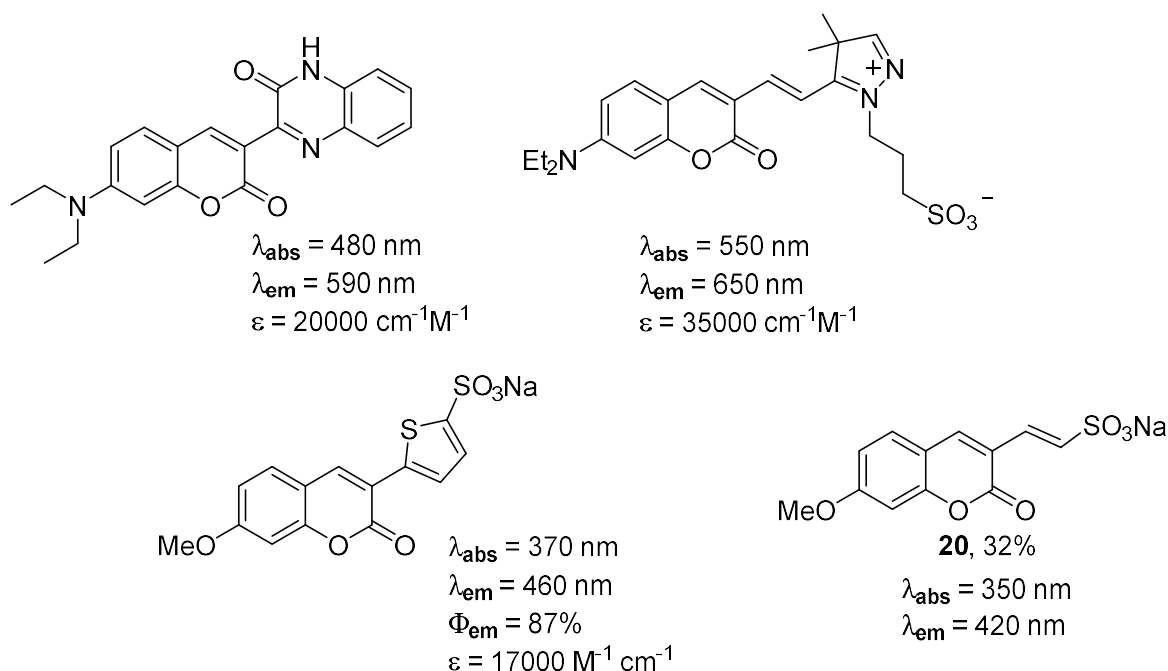


Figure 3 Molecular structure and photophysical properties of the most promising LSS dyes for multiplex biological assays.

Secondly, using 3-thienyl coumarin as model, the development of new dyes excitable by a violet lasers and with the emission at 500 nm for fluorescent microscopy was investigated. In particular,

the synthesis of several dyes for the labelling of lysosomes and mitochondria was carried out (Figure 4).

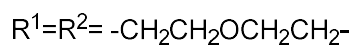
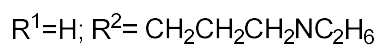
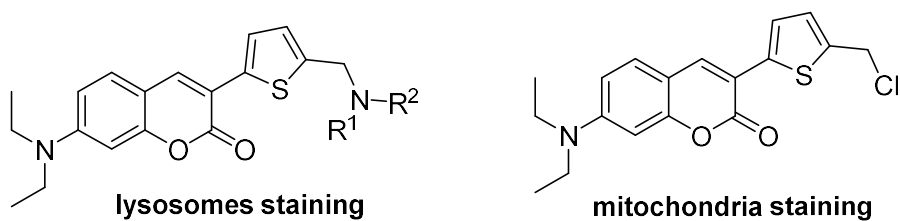


Figure 4 Developed LSS coumarins for lysosomes and mitochondria staining

The employment of the developed dyes in the labelling of lysosomes and mitochondria and the subsequent visualization by confocal microscopy concludes this thesis.

Acknowledgment

The completion of my PhD project would not been possible without the support of all the members of Cyanagen s.r.l. . In particular, a special thanks goes to Gabriele and Giuseppe Gabrielli for giving me the golden opportunity to embark on this path and my supervisor Dott. Paul Jansen who helped me in the research and writing of the thesis.

I would like to express my deep gratitude to my supervisor from University of Bologna Prof. Pier Giorgio Cozzi for offering me the opportunity to work in his research group. My appreciation also extends to the rest of the research group and in particular to Dott. Andrea Gualandi who was extremely helpful during my study period.

Finally, I am also grateful to Prof. P. Ceroni, Prof. A. Garavelli and Prof. J. Lalaveè who provided important data for the accomplishment of my research and Prof. N. Gretz for having me in his research group during the time I spent in Mannheim.